FRET-based biophysical characterization of bacterial divisome transmembrane proteins

By

Ambalika Sagarika Khadria

A dissertation submitted in partial fulfillment of

the requirements for the degree of

Doctor of Philosophy

(Biochemistry)

at the

UNIVERSITY OF WISCONSIN – MADISON

2015

Date of final oral examination: 11/24/14

The dissertation is approved by the following members of the Final Oral Committee:

Alessandro Senes, Associate Professor, Biochemistry
Brian G. Fox, Professor, Biochemistry
Aaron Hoskins, Assistant Professor, Biochemistry
Ronald T. Raines, Professor, Biochemistry
M. Thomas Record, Professor, Biochemistry and Chemistry
Martin T. Zanni, Professor, Chemistry

DEDICATION

The path leading to this PhD is a result of the constant guidance, support, encouragement and inspiration from my parents,

Nandita and Binod Khadria.

I write this thesis in their name.

Acknowledgements

The last five years as a graduate student in the Senes lab have been extremely enriching. I would like to express my gratitude to my advisor, Dr. Alessandro Senes, for giving me not just the opportunity to work on a project in his lab, but also for providing me with the experience of a wonderful student-mentor relationship to learn from. I learnt a lot of things from him on many different levels: how to critically think about a project, how to implement one's thoughts productively towards an experimental design, and how to illustrate a concept in a simple coherent fashion. Alessandro is a very effective teacher, is extremely patient and most importantly, is always approachable and available. Throughout these years, I have been given the right balance of independence and guidance from him. I thank him for letting me work on some very interesting projects and allowing me to grow as a scientist. I am also very grateful to Alessandro for providing me with so many opportunities to write. Scientific writing is quite an art, and I thank him for allowing me to write the papers and learn from my mistakes, as well as for patiently providing constructive criticism. Apart from being my advisor in graduate school, Alessandro has also guided me in the different aspects of adjusting to life in a different country, and provided me with immense support during some very difficult times I faced in these years. I could not have asked for a better experience for my PhD, and I thank Alessandro for being a source of inspiration to me regarding his motivation for science, his excellent mentoring capabilities, and his ever-positive personality.

I thank Loren, Ben and Sab for a memorable experience in lab together. Thanks to Loren for inspiring me with her hard working nature and organized manner of working. I thank Ben for his occasional comic timing and his hilarious sense of humor, which would often lighten-up the environment. Thanks to Sab for being a good friend in lab, and for helping me out during many computational crisis situations. I am happy to have Sam-n-Sam as our new lab members and thank them for enriching the lab environment with their amicable personalities. I look forward to working more with you guys, and thank you for your help in proofreading my thesis.

For all the peptide synthesis and labeling work, I am extremely grateful to Dr. Melissa Boersma, who helped me optimize the reactions for the hydrophobic TM peptides, and let me work in the facility for days, nights and weeks together. I thank you so much for all your help and guidance. I would also like to thank Dr. Darrel McCaslin for training me on the use of different instruments at the Bioinstrumentation facility, for the AUC experiments, and Dr. Martha Vestling for training me on the mass spectrometry facility at the Chemistry department.

I thank my undergraduate students, Nawaraj, Jennifer, Chin and Ashley, for sharing all the mutagenesis, HPLC and sample preparation work for the FRET experiments with me and for making graduate school more enjoyable for me. I also thank Pragya for an enjoyable summer working on the FRET project together.

I am grateful for the opportunity to have had various collaborations in these years. I thank Dr. Aaron Hoskins for the single molecule collaboration: for facilitating the use of single molecule fluorescence for my divisome project and letting me use the CoSMoS setup in his lab for my experiments. I thank Sarah, Maggie and Josh for all their help in teaching me how to make the microfluidic chambers, to use the TIRF microscope, and analyze my data in MATLAB. I really look forward to working more with you all and everyone else in the Hoskins lab. I also thank Dr. David Pagliarini for facilitating the collaboration on the ADCK3 project. Thanks to Jon Stefely for providing me with the WT constructs and for discussions on the *in vivo* aspect, and to Adam for help with cloning some of the constructs. Thanks also to Ben for sharing the project and performing the computational analyses for the study.

I thank my committee members, Dr. Brian Fox, Dr. Tom Record, Dr. Ron Raines, Dr. Martin Zanni, and Dr. Aaron Hoskins for their time and valuable feedback on my project on a yearly basis. I also thank Dr. Kim Chu Young, my advisor in NUS, Singapore, for all his support, encouragement, and valuable guidance before I started my graduate school in UW Madison.

Life in Madison would not have been the same, had it not been for my family away from home. Muffi, Adi, Ghule, Namita, Ananya, Raashi, Jatin and Aditi – I am very happy to have met you all and made some of the closest friends in my life. Thank you all so much for being there through all the good and bad times, professionally and personally, and making this journey an extremely memorable one.

I can't thank my family enough for everything that is, today. I dedicate this PhD to my parents, without whose guidance I would not be here today. I thank my father for setting the example of a principled professor and for helping me build my scientific experiences to reach this goal; and my mother, for being not just an academic advisor to me, but also a constant source of support and guidance to everyone in our entire family. Thanks to my little sister Kuku for just being the way she is, and to all three of them for visiting me in Madison frequently and making the distance seem shorter. I also thank my late grandfather for always believing in me, and my grandmother for motivating me throughout.

Finally, I thank Ranga, my best friend, for being there in my life, and for being a perfect companion to me in every sense: for all the help with the Pchem course, for the endless discussions on concepts of fluorescence and microscopy, for help with the FRET experiments, for proof-reading all my manuscripts and thesis, and for your unconditional support and encouragement throughout all the phases of graduate school. I also thank Amma, Appa and ZAG for their good wishes and love for the last two years of graduate school.

Table of Contents

List of Figures

Chapter One

Chapter Two

Chapter Three

Chapter Four

Chapter Five

List of Schemes

List of Tables

Summary

Integral membrane proteins (IMPs) in cell membranes play significant roles in a wide array of physiological processes – cell signaling, cell division, material transport and defense. IMPs are also implicated in many diseases and cover more than half of the targets for drug development. However, structural and biophysical investigations of these proteins are not straightforward due to the difficulty of mimicking their complex natural habitat, the cell membrane. Thus, the rate of solving IMP structures has lagged behind that of soluble proteins. In an effort to better understand the structure-function relationship of IMPs, a combination of *in vivo, in vitro and in silico* methods are used in tandem to characterize their structures, domain organizations, and oligomerization properties.

In our lab, we approach the subject of studying IMPs by focusing on a more tractable system – that of single-pass transmembrane (TM) proteins, which traverse the membrane once. We screen TM alpha helices and their sequence variants in bacterial membranes to test their oligomerization tendencies, use biophysical techniques to study their associations in artificial environments like lipid and detergent, and develop computational techniques to model the structures of the TM helices.

For my dissertation, I have characterized the oligomeric organization of two TM proteins of the *E.coli* divisome, and found that they interact in the form of a complex that may act as a structural hub required for other divisome proteins to facilitate cell division. To achieve this, I optimized and utilized FRET measurements of TM oligomerization in detergents and lipid bilayers. In *Chapter 1*, I discuss the wide applicability of FRET toward studying TM helix interactions in membrane mimetic systems, and present a comprehensive

literature review of the significant contributions in this field, highlighting the different parameters important for these studies. In *Chapter 2*, (published in *Methods in Molecular Biology*, *2013*) I present a protocol that I optimized for measurement of FRET between TM helices in liposomes. I also enlist the challenges associated with sample preparation and discuss the ways I adopted to circumvent them. In *Chapter 3* (published in *Biochemistry, 2013*), I demonstrate for the first time, that the FtsB and FtsL TM domains interact in lipid bilayers, that the FtsB-FtsL complex is a higher-order oligomer as opposed to a FtsB-FtsL hetero-dimer, and that the complex comprises a 1:1 stoichiometry of the proteins. This finding hypothesizes that the FtsB-FtsL complex may serve as a hub for other divisome proteins (FtsQ and FtsW) to bind and continue the division process. In order to understand how many molecules of each protein are present in the FtsB-FtsL complex, I propose the use of three different techniques in *Chapter 4* - FRET, analytical ultracentrifugation, and single molecule fluorescence - to elucidate the precise oligomeric state of the FtsB-FtsL complex. I present the experimental design, some preliminary data and future directions to carry out these experiments. Finally in *Chapter 5*, (published in *JACS, 2014*), I present a different project: the structural characterization of ADCK3, a mitochondrial kinase, predicted to dimerize via its TM domain. Using CATM, a computational program developed in our lab, we modeled the dimeric structure of the ADCK3 TM domain. Simultaneously, I used a biological screening assay, TOXCAT, to test the oligomerization of ADCK3-TM and its sequence variants in bacterial membranes, identifying an interaction interface for the oligomer. We found that the experimental and computational mutagenesis data were in agreement, making this report not only an investigation of the ADCK3 structure, but also a first validation of the CATM program.

In *Appendix I*, I attach the first structural study on a bacterial divisome protein, FtsB, generated by our lab, which laid the foundation for biophysical analysis of the heterologous FtsB-FtsL complex (described in Chapter 2). The report demonstrated that FtsB-TM self associates in bacterial membranes, that the FtsB periplasmic domain forms a weak coiled coil structure (as observed in the crystal structure), and that the two domains are linked together by a flexible linker. These findings led to the hypothesis that FtsL may be required to stabilize the FtsB, which was later demonstrated by my FRET data in lipid bilayer (Chapter 3).

CHAPTER ONE

Introduction

Abbreviations

IMP: Integral Membrane Protein, TM: Transmembrane, SE-AUC: Sedimentation Equilibrium – Analytical Ultracentifugation. FRET: Forster Resonance Energy Transfer, AMCA: 6-((6-Amino-4-methylcoumarin-3-acetyl)amino) hexanoic acid. DANS-Cl: 5-Dimethylamino-1-naphthalenesulfonyl chloride, Pyr: Pyrene, NBD: 2-(4-nitro-2,1,3-benzoxadiazol-7-yl)aminoethyl]trimethylammonium, FITC: Fluorescein Isothiocyanate, FAM: Fluorescein amidite, Coum: Coumarin, BODIPY: Boron-dipyrromethene, EYFP: Enhanced Yellow Fluorescent Protein, DABS-Cl: 4-(Dimethylamino)azobenzene-4-sulfonyl chloride, TAMRA: 5-Carboxytetramethylrhodamine, DPBS: 4-(Diethylamino)phenylazobenzene-4-sulfonyl chloride, SDS: Sodium Dodecyl sulfate, C12EB: Octaethyleneglycol mono-n-dodecylether (non-ionic detergent), OG: Octyl-glucoside, DOPC: 1,2 – Dioleoylphosphatidylcholine, DDMAB: N-Dodecyl-N,N-(dimethylammonio)butyrate, DDM: Dodecylmaltoside, DMPC: Dimyristoylphosphatidylcholine, PFO: Perfluorooctanoate, DHPC: Dihexanoylphosphatidylcholine, DLPC: Dilauroylphosphatidylcholine, DPC: Dodecylphosphocholine, POPC: Phosphatidylcholine, POPG: Phosphatidylglycerol, POPS: Phosphatidylserine, CHO: Chinese hamster ovary, HEK293T: Human Embryonic Kidney 293 cells expressing the SV40 large T antigen, MHC: Major Histocompatibility Complex, OPM database: Orientations of Proteins in Membranes database, MLV: Multi-lamellar vesicle, LUV: Large unilamellar vesicle, SUV: Small unilamellar vesicle, FCS: Fluorescence Correlation Spectroscopy

Part 1: Membrane Proteins

Integral membrane proteins (IMPs) are highly represented in the proteome; they comprise a third of all genomes, perform multiple important biological functions like signaling, material transport and defense. They are also the target for more than half of the current drugs(Overington et al. 2006). Structurally, there are two main classes of IMPs. The more common class contains transmembrane (TM) helices, which typically comprise 20-30 apolar amino acids that span the membrane bilayer. These proteins are either designated as bitopic when they have a single TM helix, or as polytopic when multiple TM helices fold in a bundle to form the functional protein. Bitopic proteins often associate to form oligomers; an example is one of the most extensively studied model systems for membrane protein association, Glycophorin A (GpA), an erythrocytic sialoglycoprotein, which self associates through its single TM helix to form homodimers (Adair & Engelman 1994; Fisher et al. 1999; Fisher et al. 2003; Fleming et al. 2004; Lemmon, Flanagan, Hunt, et al. 1992; MacKenzie et al. 1997). A widely studied polytopic membrane protein is bacteriorhodopsin (bR) (Luecke et al. 1999), where seven transmembrane helices oligomerize to form the functional light induced proton pump (Booth et al. 1995; Huang et al. 1981; Kahn et al. 1992; Krishnamani & Lanyi 2012). The second structural class is the transmembrane beta barrel, which commonly reside in the outer membrane of bacteria. Beta barrels, such as the outer mitochondrial membrane voltage dependent anion channel (VDAC) (Shoshan-Barmatz et al. 2010), typically form channels and pores, with hydrophobic residues pointing toward the lipid region and more polar residues toward the hydrated pore of the barrel.

Structural information serves as a nucleation point to understand the functional organization of any macromolecular system, but since these structures are embedded

in a chemically heterogeneous lipid bilayer, reproducing the natural habitat of these macromolecules is very challenging. Standard over-expression techniques needed to prepare samples for these structural studies often prove toxic to host cells, thereby making it difficult to produce a substantial amount of pure working sample for structural studies. Thus the rate at which IMP structures have been solved lags behind that of soluble proteins (White 2004). In spite of the challenges faced, significant advances are being made towards elucidating the structures of membrane proteins. Ever since the first membrane protein structure reported in 1985 (Deisenhofer et al. 1985), over 500 unique membrane protein structures have been documented as of September 2014 (http://blanco.biomol.uci.edu/mpstruc/, Stephen White lab at UC Irvine). The advances in the structural database of membrane proteins is now considered to be in the 'log phase', and numerous developments in the overexpression of proteins, development of new detergents and lipids, and ways of increasing protein stability are making structural investigation of membrane proteins more feasible (Bill et al. 2011; Moraes et al. 2014).

Along with structural studies, a lot of research has focused on understanding oligomerization, which is increasingly seen as a common occurrence in the case of membrane proteins (Engelman 2005). An important foundation for these studies has been laid two decades ago by the Two-Stage Model (Popot & Engelman 1990), which frames the membrane protein folding problem into two thermodynamically independent sub-stages **(Figure 1.1)** –

1. The insertion of individual trans-membrane helices into the bilayer to form stable independent helices
2. The association between these individual helices to form the final folded oligomeric tertiary structures.

This model suggests that in the case of membrane proteins, both the folding and

the oligomerization processes share a common central event – the lateral association of individual TM domains. Thus, study of the oligomerization of these TM domains is a way to understand the folding principles of membrane proteins. Even though this model may be oversimplified and not take into account the complexity of biological insertion and potential transitional states during insertion or post-insertion, much of the existing structural and functional data provide general support for the basic thermodynamic assumptions in this model (Engelman et al. 2003). With this basis, a significant progress has been made in studying the principles and motifs involved in the oligomerization and thus the formation of the native folds of IMPs (MacKenzie & Fleming 2008).

Techniques to study helix-helix association energies

Ever since the two-stage model was formulated, various biological and biophysical methods have been optimized and have complemented each other to investigate TM helix interactions *in vivo* and *in vitro*. Biological assays can serve as a means of high throughput screening for TM helix-helix interactions in a natural membrane, and enable studying the effects of large-scale mutagenesis to identify key residues involved in oligomerization. Biophysical assays on the other hand are not high throughput and are carried out *in vitro*, but can yield the precise energetic contributions involved in these interactions in various environments.

Two biological assays, TOXCAT (Russ & Engelman 1999) and GALLEX (Schneider & Engelman 2003), have provided a wealth of information on the TM domain interactions in native bilayers. Both techniques rely on transcriptional activators that trigger the expression of a reporter gene upon association of the TM helix in question; TOXCAT yields increased reporter gene expression upon self-association of TM domains, whereas GALLEX works in the opposite manner, resulting in repression of

reporter gene. TOXCAT is limited to self-association, whereas GALLEX can also be used to determine hetero-oligomerization of the different proteins. These assays are economical and provide a fast and effective means for screening relative TM interaction strengths. Attempts to provide quantitative inferences from these assays have been reported (Duong et al. 2007; Finger et al. 2006), which found that the rank order of the association free energies of sequence variants of Glycophorin A, obtained with the biological assay, is similar to the rank obtained with the biophysical analytical ultracentrifugation (AUC) data in detergents (MacKenzie & Fleming 2008). However, the magnitudes of apparent association free energy values were variable; the TOXCAT data was closer to the AUC data, whereas the GALLEX data showed that mutations had a more modest impact on the association energies of Glycophorin A. Despite these promising observations, due to the stochastic behavior of cells, these biological assays contain an appreciable amount of variability, making quantitative analyses very difficult.

For more investigation of the thermodynamics of association of TM helices *in vitro*, it is preferrable to use biophysical methods, which have significantly contributed to understanding the energetics of TM helix-helix interactions. The two most widely used methods for these studies are Sedimentation Equilibrium Analytical Ultracentrifugation (SE-AUC) and Förster Resonance Energy Transfer (FRET).

SE-AUC is directly sensitive to the oligomeric mass of an associated complex and is a rigorous technique to study the stoichiometry as well as the equilibrium constants of an interaction (Fleming 2002). One limitation of SE-AUC, however, is that measurements are limited to detergent micelles and cannot be made in lipid vesicles. Lipid vesicles will contain multiple copies of the helices, in equilibrium between the monomeric and oligomeric state. Since the helices do not exchange between individual vesicles, the sum of all the helices residing in a vesicle will contribute to its

sedimentation, irrespective of the association state.

FRET is a biophysical technique that overcomes this caveat of SE-AUC as it uses proximity as a means to look at TM domain interactions, and is thus compatible with both detergent and lipid milieus. A disadvantage of FRET is that it requires labeling the TM helices with fluorophores. The incorporation of an artificial label can potentially alter the natural course of the interaction, but labeling efficiency and effect of the labels can be accounted for with proper controls. In spite of the challenges associated with using these techniques, they have been used in tandem to make remarkable progress in understanding the thermodynamics of membrane protein interactions.

FRET has been very useful in studying the interactions between TM helices using synthetic peptides labeled with organic dyes **(Figure 1.2a)** in artificial bilayer mimetics, as well as between proteins in live cells using fluorescent protein fusion constructs. Ranging from qualitative and quantitative ensemble average spectroscopic data, to kinetic time-lapse FRET measurements, all the way to FRET under the microscope with sophisticated spatial and temporal resolution data, an extensive body of studies have been developed to studying a variety of different interactions within a membrane (Luís M S Loura 2011)– interactions within lipids, between lipids and membrane proteins, and within membrane proteins.

In this chapter I will review the use of steady state FRET in the literature to investigate TM helical interactions in various membrane proteins will be reviewed. A brief introduction to fluorescence and FRET will begin the discussion. The following sections will review various FRET studies of TM helix associations in different membrane mimetic environments. Further, the different ways of calculating FRET efficiency, and their correlation to the energetics of associations will be discussed. Finally, the challenges faced in interpreting FRET data of membrane proteins, examples

of ways employed to tackle them, and various formalisms developed to elucidate the protein oligomeric state using FRET will be presented.

FRET: A tool to investigate membrane protein interactions

FRET to study macromolecular association

Förster resonance energy transfer (FRET) is a photophysical process that is related to the phenomenon of fluorescence (described in **Scheme 1.1**). FRET occurs when an electronically excited donor (D) fluorophore doesn't emit its energy in the form of fluorescence, but instead gets quenched by non radiatively transferring its excitation energy to an acceptor (A) chromophore in its vicinity. The acceptor is often fluorescent but does not need to be. This phenomenon is possible if the D-A pair has a dipolar overlap, the emission spectrum of D overlaps with the excitation spectrum of A **(Figure 1.2b)** and if the two fluorophores are within 1-10 nm apart. This range depends on a specific distance parameter called the Förster radius or R_0, which is defined as the distance between D and A at which the FRET efficiency is 50%. For a certain D-A FRET pair, the FRET efficiency E is given as:

$$E = \left[\frac{R_0}{(R_0 + r)}\right]^6$$

where *r* is the actual distance between the pair. Thus FRET measurements can in principle yield distance measurements between two fluorophores. R_0 can be calculated using:

$$R_0 = \left[\left(Q_0 J n^{-4} K^2\right)^{1/6} \times 9.7 \times 10^3\right]$$

where Q_0 is the quantum yield of the donor in the absence of the acceptor, J is

the spectral overlap integral, n is the refractive index of the medium and K^2 is the dipole-dipole orientation factor. The calculated R_0 values assuming random fluorophore orientation typically lie within the 15-60 Å range, which is comparable in size to biological macromolecules (30-50 Å), and thus FRET has been used as a proximity calculator to elucidate macromolecular structures. Assuming dipolar overlap, FRET is most sensitive between 0.5 to $2R_0$, making the measurable distances vary from 10-100 Å, well within the range of the spatial separation in typical macromolecular interactions.

FRET in TM helix-helix interactions

FRET has been used extensively to study numerous biomolecular processes such as the folding, conformational changes and interactions of proteins, nucleic acids and lipids. These dynamic studies can complement structural information to understand the structure-function relationships of macromolecules. An area where the utility of FRET has especially shown surmount importance is the study of membrane proteins and their interactions. Since the structures of membrane proteins are hard to elucidate using conventional X-ray crystallography and NMR techniques, FRET has widely been used to ‘divide and conquer’ individual domain interaction information to map the structures and folding signatures of membrane proteins. Steady state FRET efficiency measurements as well as time resolved fluorescence microscopy have been applied to study not only membrane protein interactions but also other protein-lipid and lipid-lipid interactions within the membrane. A recent review (Luís M S Loura 2011) delved into the formalisms behind these studies, describing their complexities and covering also the use of sophisticated FRET microscopy techniques to study membrane systems *in vitro* and *in vivo*.

In this current review, I focus on the past and recent literature for biophysical

characterization of membrane protein association, specifically that of single TM helices. I will cover the numerous fluorophores and the different model membranes and detergents used in these studies. I will also discuss the important contributions to this field made by different research groups to investigate specific proteins or protein families, or to improve upon existing FRET methodologies and formalisms, or both. The goal of this review is to provide a comprehensive summary and analysis these studies for the reader to have a comparative reference of the literature while planning and designing FRET experiments for transmembrane helix-helix interactions.

FRET in TM proteins: progress over the years

Characterization of membrane protein interactions using FRET between labeled proteins or peptides has been already in use for more than three decades. The earlier studies show examples of both qualitative and quantitative measurements. In 1977, a quantitative approach by Veatch and Stryer looked at the dimerization of Gramicidin A (Veatch & Stryer 1977) and postulated the distinguishing formalisms for different oligomeric schemes. In 1982, Morris et. al., qualitatively used FRET to show that Chromaffin granule membrane proteins form aggregates upon addition of calcium ion (Morris et al. 1982). These early studies paved the platform for use and improvement of FRET techniques to study membrane proteins. In 1994, Adair and Engelman derived a model for the energy transfer within oligomers and used it to show that the Glycophorin A TM domain formed a dimer, as opposed to a higher order oligomer (Adair & Engelman 1994). This formalism has since then been used in almost all quantitative FRET measurements to confirm dimerization of TM helices. Further progress in assessing the oligomeric state was made by Li et. al. in 1999, who were able to not just distinguish between a dimer and a higher oligomer but also elucidate the precise order of a higher-

oligomer of Phospholamban, which changes based on the environment it is in (Li et al. 1999). This formalism has not been used as widely as the dimer formalism, but has been extended to other systems as well, e.g., the proton channel M2 tetramer in 2010 (Schick et al. 2010). These earlier studies enabled quantification of the energetics of oligomerization, but did not account for an important parameter, the FRET contribution due to random proximity. Simulated by Wolber and Hudson in 1979 (Wolber & Hudson 1979) and later by Wimley and White in 2000 (Wimley & White 2000), the proximity FRET term was for the first time included in membrane protein FRET efficiency calculation by Hristova and coworkers in 2005 (You et al. 2005), and then further improved upon and extended to larger oligomers in 2014 (King et al. 2014). A different formalism was also developed by Fernandes et. al. in 2008 (Fernandes et al. 2008).

Using these different formalisms, FRET using synthetic labeled peptides or fluorescent protein fusion constructs has been used over the years to investigate many different systems and problems of TM helical interactions. The Engelman group (Fisher et al. 2003; Fisher et al. 1999; Adair & Engelman 1994), and the Schneider group (Anbazhagan et al. 2010; Anbazhagan & Schneider 2010; Stangl et al. 2014; Stangl et al. 2012), have have used FRET to study the dimerization of the model system Glycophorin A and its sequence variants in different membrane mimetic environments. The Hristova group has contributed significantly to the field of FRET in membrane proteins by developing new experimental methodologies (Stahl et al. 2012; Merzlyakov et al. 2007; Merzlyakov et al. 2007; Li et al. 2008), testing different bilayer environments (Merzlyakov, Li & Hristova 2006; Merzlyakov, Li, Casas, et al. 2006; Merzlyakov, Li, Gitsov, et al. 2006; Merzlyakov et al. 2008; You et al. 2005; Sarabipour & Hristova 2013), and improving on existing formalisms for FRET calculations (You et al. 2005; King et al. 2014; Chen et al. 2010). Using their tools, they have widely investigated the

dimerization of the receptor tyrosine kinase family proteins and their sequence variants for about ten years (Li et al. 2005; Li & Hristova 2006; Li et al. 2006; You et al. 2006; You et al. 2007; Merzlyakov, You, Li, et al. 2006; Placone & Hristova 2012; Placone et al. 2014). Other groups have used FRET to investigate different biological systems or different membrane protein folding questions. For example, Deber and coworkers studied the oligomerization of biological systems such as receptors (Go et al. 2006), and ion pumps (Therien & Deber 2002), to name a few, as well as worked on model peptides to understand membrane protein folding (Johnson et al. 2004). All these investigations over the years have proved FRET to be one of the most important tools to characterize the folding of membrane proteins, and yielded invaluable understanding of the folding, association and structure of membrane proteins. A comprehensive list of selected significant work in the area is provided in **(Table 1.1)**.

The solvent for membrane proteins

Membrane proteins are highly hydrophobic and are generally not soluble in aqueous solutions. Thus, in order to investigate the structure and thermodynamic of properties of these proteins *in vitro*, using any technique, they first need to be reconstituted into environments that mimic natural membranes. Considering the complex constitution of the membrane, it is difficult to replicate the exact conditions for these proteins in an artificial milieu. Nonetheless, tremendous progress has been made to design membrane mimics that solubilize membrane proteins *in vitro* for their structural and functional characterization **(Figure 1.3)**(Hein et al. 2014; Seddon et al. 2004).

The most widely used membrane mimics for studying membrane protein

oligomerization are lipid bilayers and detergent micelles. The lipid bilayer is a more native-like membrane mimic. Bilayers can be synthetically prepared by different methods: in the form of supported bilayers (Merzlyakov et al. 2008), multilamellar liposomes (You et al. 2005) or extruded to form giant (~500 nm), large (~100 nm) or small (~30-50 nm) unilamellar liposomes, which are alternative forms that may suit different experimental requirements (Hein et al. 2014; Seddon et al. 2004). Another alternative are the nanodiscs (Lyukmanova et al. 2012), Nanodiscs are more stable bilayer mimics compared to liposomes because they are encased by a membrane scaffold protein (MSP) that holds together the lipids. They can be prepared between 6-30 nm in size based on the MSP derivative used. Finally, bilayers used for studying TM domain interactions can also be prepared from natural membranes, such as rough endoplasmic reticulum microsomes (Jaud et al. 2009) and plasma membrane derived vesicles (Sarabipour & Hristova 2013). These natural bilayers contain all the natural components of a natural membrane.

A bilayer mimetic is an ideal environment for FRET studies of membrane proteins. Unfortunately, however, challenges with achieving proper equilibration of the samples, along with light scattering artifacts generated during fluorescence measurements, makes lipid bilayers at times difficult or impossible to use. A less ideal but more convenient system for TM protein interactions are the detergents. Like lipids, detergents are amphipathic molecules consisting of a polar head group and a hydrophobic tail; however, instead of bilayers, detergents form spherical micellar structures in aqueous solutions. Because of their smaller size, detergents do not produce scattering artifacts and are in general easier to handle. As long as their concentration in solution is above its critical micellar concentration (CMC), detergents can generally solubilize a membrane protein and serve as a hydrophobic solvent.

A wide array of detergents with distinct physical-chemical properties can be chosen from to optimize conditions for a specific protein and application (Garavito & Ferguson-Miller 2001; Gohon & Popot 2003; le Maire et al. 2000; Seddon et al. 2004). Although detergents can conveniently solubilize membrane proteins, they can also destabilize the proteins over time. In an effort to design less destabilizing solvents, compounds called tripod amphiphiles (McQuade et al. 2000; Yu et al. 2000) and amphipols (Tribet et al. 1996; Stangl et al. 2014) have been developed and used for solubilizing membrane proteins. These compounds have been targeted at keeping membrane proteins active over periods of time and have been useful in structural investigations using NMR and X-ray crystallography. In certain situations, a combination of detergents and lipids to form mixed micelles (Anbazhagan et al. 2010) and bicelles (Ujwal & Bowie 2011) can be employed and has been useful in many structural investigations of membrane proteins.

All the mentioned solvents have pros depending on a variety of factors, such as whether the protein in question is a full-length polytopic protein or a single TM domain, whether the investigation is structural or biophysical, and whether the technique used can effectively deal with any background effect generated by the solvent used.

FRET studies of TM interactions in lipid and detergent

In a classical paper, FRET was used to characterize the association of a linear peptide antibiotic Gramicidin A, forming transmembrane conductance channels for alkali cations and hydrogen ions. Dansyl and DPBS labeled synthetic Gramicidin A peptides were reconstituted in multilamellar DHPC vesicles **(Table 1.1)** and the FRET signatures as a function of acceptor concentration indicated formation of a homodimer (Veatch & Stryer 1977). In a later pioneering study, 'RET' was used to investigate the dimerization of Glycophorin A in lipid bilayers using dansyl and non-fluorescent dabsyl labeled peptides in DMPC multilamellar vesicles (Adair & Engelman 1994). Similarly, FRET studies in detergents have yielded information about membrane protein association as long as the type of detergent used was able to preserve the overall structure and fold of the protein (Franzin et al. 2007; Melnyk et al. 2001). These investigations in detergent and lipid have enabled identifying key residues involved in helix-helix associations, understanding membrane protein folding properties, and obtaining the energetics of association and factors that influence the interactions.

Hydrophobic environment properties affect helix-helix dimerization

Glycophorin A (GpA) has been a paradigm in understanding the second stage of the two-stage model of membrane protein folding (Popot & Engelman 1990). Numerous FRET studies in lipid and detergent have followed the initial study in DMPC vesicles (Adair & Engelman 1994) to better understand both GpA dimerization as well as the various parameters that influence membrane protein interactions. Based on previous information on GpA-TM dimerization using other biophysical techniques, FRET was used to investigate the effect of different types of detergents on the GpA-TM association

(Fisher et al. 1999; Fisher et al. 2003) **(Table 1.1)**. The first set of experiments relied on the dilution of the peptide in its effective solvent volume, which is the detergent concentration. The GpA dimer was observed to be two orders of magnitude less stable in SDS than in zwitterionic detergents DDMAB and DPC, demonstrating that environment has an important role to play in the association of GpA. The time taken to reach steady state equilibrium also depended on the type and concentration of the detergents used. A follow up paper expanded on the previous study by studying GpA dimerization in a series of detergents **(Table 1.1)** with varying alkyl chain lengths, combined with ionic, nonionic, and zwitterionic headgroups (Fisher et al. 2003). The results suggested that the helix dimerization of GpA in detergents is influenced by two opposing effects - an enthalpic effect, which drives association with increasing detergent concentration and which is sensitive to the detergent headgroup chemistry, opposed by an entropic effect, which drives peptide dissociation with increasing detergent concentration. Thus this study begun shedding light on the importance of detergent selection and how they can influence the association equilibrium of helical dimers.

While these studies focused on the effect of detergents having different head group chemistry, a clear relationship between the alkyl chain length and strength of dimerization was not observed. A much later study investigated the effect of aggregation number, or number of detergent monomers per micelle, on TM helix dimerization. FRET measurements using labeled GpA TM peptides were carried out on lyso-PC micelles of varying acyl-chain lengths **(Table 1.1)** to investigate the effect of detergent concentration, aggregation number and the micelle's hydrodynamic radius on TM association (Stangl et al. 2012). It was observed that the dissociation of the GpA TM dimer did not correlate to dilution in detergent, indicating an influence of the detergent properties on dimerization. Further, GpA TM dimerization did not depend on the

similarity of the detergent's hydrodynamic radius to the hydrophobic length of the TM domain; in fact the oligomerization was destabilized with increasing chain length, opposing the assumption that longer chains render the detergents milder. Moreover, the detergent molecules in a micelle seemed to be able to stretch to match the hydrophobic length of the peptide, suggesting that the concept of hydrophobic match/mismatch of TM helices to lipid membrane systems (Killian 1998) may not be translated to detergent systems. One the other hand, the effect of acyl chain length of lipid vesicles had a direct correlation with GpA dimerization in different lipid vesicles with varying (2-12) carbon chain lengths (Anbazhagan & Schneider 2010) **(Table 1.1)**. Dimerization efficiency was highest in the C20 (30.5 Å) and C22 (34 Å) chain length lipids, comparable to the hydrophobic length of GpA (31-32.2 Å) according to the NMR structure of the TM dimer (MacKenzie et al. 1997) and the OPM database (Lomize et al. 2006). Unlike the observation for the lyso-PC detergents, the acyl chain length was found to severely influence the dimerization of the TM domain, being most efficient under hydrophobic length matching conditions. This again demonstrated how different environments play a role in the association of a TM protein.

FRET used to study 'unfolding' of TM proteins

In the case of membrane proteins, folding often refers to the formation of an oligomeric complex. The 'unfolded' state of a TM protein is one that retains its helicity (Popot & Engelman 1990) and thus the unfolding cannot be measured by conventional methods like circular dichroism. To study reversible folding of these systems, conditions are required that push the equilibrium to the dissociated state. This can be achieved by diluting peptide concentration in the hydrophobic volume as performed in typical FRET experiments. Apart from dilution in the same detergent or lipid, unfolding studies of TM

helix association using FRET have also been attempted by changing the hydrophobic environment from a more stable to a less stable state. A first report of the utility of mixed micelles using GpA as a dimerization standard (Anbazhagan et al. 2010) provided evidence of the second stage of membrane protein folding (Popot & Engelman 1990). Labeled GpA TM peptides **(Table 1.1)**, were reconstituted in the mild non-ionic DDM micelles, where they were helical as well as dimeric as observed by FRET. Keeping the total peptide:detergent ratio constant, SDS was added such that the mole fraction of SDS relative to DDM increased. SDS is a harsh, negatively-charged detergent shown to denature most polytopic membrane proteins, but it retains the oligomeric states of some TM helices in the low mM concentrations (Tulumello & Deber 2009; Zhou et al. 2001; Volkmer et al. 2006; Prodöhl et al. 2007; Lemmon, Flanagan, Treutlein, et al. 1992) and even in high concentrations as in the case of bacteriorhodopsin (bR) (Valluru et al. 2006; Nannepaga et al. 2004). It was observed that with increasing mole fraction of SDS, there was a decrease in FRET but not helicity of the sample (observed by CD experiments), indicating dissociation of the dimer to form helical monomers in mixed micelles.

A similar unfolding study using FRET has also been investigated using reconstitution from lipid to detergent systems. Two peptide fragments of the seven-transmembrane protein bacteriorhodopsin (Renthal et al. 2011), structurally known to associate, were reconstituted from DOPC bilayers to SDS micelles. This study involved the use of intrinsic FRET from Tyr on one peptide to two Trp residues on the other peptide **(Table 1.1)**. FRET efficiency was reduced from transferring the peptides from DOPC to SDS micelles, suggesting a loss of association, interpreted as unfolding of the peptides from DOPC bilayers to SDS micelles. However, MD simulations in the same study indicated that a small rearrangement of the peptide backbone in the SDS

micelles. This resulted in easier access of water molecules into the micelles, forming H bonds with the donor (Tyr) and decreasing its quantum yield, which contributed to a decrease in the calculated FRET efficiency. Thus it was speculated whether SDS causes unfolding or just spectroscopic perturbations due to protein-detergent interactions. The authors also argued that the validation of the use of mixed micelles in TM helix unfolding (Anbazhagan et al. 2010) might be overlooking the effects of increased surface charge density of the negatively charged SDS micelles that might affect the properties of the environmentally sensitive fluorescein and TAMRA (Packard et al. 1996) dyes. These studies highlight one of the complexities of using FRET to study membrane proteins (discussed in a later section) where changes in the hydrophobic environment can affect the chromophores and simulate a change in the FRET efficiency. In such situations, use of a few different fluorophores for FRET, or performing additional biophysical characterization can supplement the FRET data to obtain more accurate inferences about the unfolding of membrane protein complexes.

FRET shows higher TM oligomeric stability in lipid than in detergent

As the lipid bilayer is closer to the natural membrane in comparison to detergent, it is expectable that the oligomeric complexes may be better behaved and more stable in the former. This has been demonstrated using FRET in different systems. The oligomeric state of phospholamban (PLB), a 52 amino acid protein in the cardiac sarcoplasmic reticulum that regulates the cardiac calcium pump through a phosphorylation dependent mechanism, was investigated both in detergent and in lipid bilayers (Li et al. 1999; Reddy et al. 1999). It was previously shown that PLB forms homopentamers in SDS micelles (Watanabe et al. 1991; Wegener & Jones 1984). An electron plasmon resonance (EPR) study (Cornea et al. 1997) showed that the average

oligomeric size of PLB changed from 3.5 to 5.3 upon its phoshorylation, suggesting a dynamic equilibrium between PLB subunits in lipid bilayers. This suggested that there might be oligomeric changes involved in the regulation of the pump, but the EPR method could not resolve the multiple oligomeric species. Using fluorescent donors (AMCA and DANS), and a non-fluorescent DABS acceptor attached to recombinant PLB protein, this study analyzed the PLB oligomeric states in various detergents **(Table 1.1)**. The different detergents showed a varying extent of oligomerization, oligomeric size and proximity of adjacent subunits, again demonstrating how the environment can play a role in the folding of TM helices. However, the samples needed to be boiled in order to observe FRET, without which there was no FRET observed in the detergents, indicating an absence of reversible equilibrium. The DOPC data on the other hand showed FRET without the need for boiling the samples, indicating reversible equilibrium between the monomers and oligomers, and thus demonstrating that the samples were well equilibrated and better behaved in lipid than in detergent.

Other membrane protein oligomeric studies using FRET have demonstrated the higher stability of the interactions in the more native lipid bilayer. Dimerization of the TMA1 peptide from EphA1-receptor in SDS micelles and DOPC bilayers showed a ten-fold weaker free energy of association than GpA (Artemenko et al. 2008). The FRET efficiency values indicated a more stable dimerization propensity in the lipid bilayer. Similarly, the homo and hetero association FRET data of bacterial divisome proteins FtsB and FtsL, agreed on the formation of a 1:1 higher order complex in both POPC vesicles and DPC micelles (A. S. Khadria & Senes 2013)**(Table 1.1)**. However, the data showed that the self-association of FtsB and the hetero association of FtsB and FtsL were both stronger in POPC bilayers than in DPC micelles. The weaker oligomerizing tendency of the FtsB TM peptide in DPC micelles, previously shown to associate in

bacterial membranes (LaPointe et al. 2013), suggested that the contribution of a hydrogen bond formed by a Glutamine residue at the FtsB interface may be weakened by water molecules that may be more accessible to the micelles, thus favoring the monomeric structure of the peptide.

FRET in detergent as a complementary assay

In spite of the higher stability of TM peptide oligomers in lipid, detergents pose a very convenient means for these experiments. FRET in detergent micelles has aided the study of the interaction of many TM helix systems. These studies have often been performed along with other techniques such as coimmunoprecipitation, PAGE, Western blot, TOXCAT, and SE-AUC.

A variety of membrane protein systems have been investigated using FRET in detergents along with the aforementioned techniques, for example, by Deber and coworkers: the homodimerization of the TM domain of the *E.coli* single span major coat protein (MCP) of Ff bacteriophage in SDS micelles (Melnyk et al. 2002), the oligomerization of the Na, K ATPase (sodium pump) TM domain in PFO micelles (a detergent that retains association for weakly interacting helices) (Therien & Deber 2002), and the TM self association of the anthrax toxin receptor ANTRX1 in SDS micelles (Go et al. 2006). In addition to these biological systems, they also studied a model helix-loop-helix peptide made of Ala and Ile residues in SDS micelles to investigate the nature of packing interactions including van der Waal's and side-chain hydrogen bonding networks of TM peptide interactions (Johnson et al. 2004).

FRET in detergent micelles has not only aided other experimental techniques but also computational techniques. An example is in the design of computed helical anti membrane protein (CHAMP) peptides as a means to obtain specific anti-TM peptides,

which are capable of binding to TM-helices, similar to antibodies of water soluble proteins (Yin et al. 2007). A list of the fluorophores used in all these studies is provided in **(Table 1.1)**.

FRET in different lipid bilayer environments

Artificial lipid bilayers can be assembled into different forms for TM helix-helix interactions: multilamellar, or unilamellar vesicles, of varying sizes, and planar supported bilayers.

Multilamellar vesicles (MLVs) are prepared by hydration, vigorous agitation and freeze-thawing of the hydrated peptide/lipid films, which are obtained by evaporation of the solvents from their organic solutions (A. S. Khadria & Senes 2013; You et al. 2005; A. Khadria & Senes 2013). It was observed that the presence of TM peptides decreases the turbidity of MLVs after just one freeze thaw cycle. This change was not observed for free lipids (You et al. 2005), indicating that the presence of peptides facilitates formation of smaller MLVs in the 1:100 to 1:10000 peptide:lipid relative molar range, making FRET experiments feasible. Extrusion of MLV's using a 100 nm diameter membrane (Avanti) produces large unilamellar vesicles (LUVs), which in theory have the advantage to rule out any FRET contributions arising from TM peptides in consecutive leaflets of an MLV. It has been shown, however, that there is no statistically significant difference in FRET efficiencies between MLVs and LUVs. Extrusion can also cause a loss of peptide as well as lipid, but this loss is to a similar extent, and thus the FRET efficiency (which is a function of the peptide:lipid ratio) remains the same as in MLVs (You et al. 2005). Sonication of the extruded LUVs creates 30-50 nm small unilamellar vesicles (SUVs). As opposed to MLVs, in which the fluorescence of the TM peptides remains constant over a long period of time, fluorescence of SUVs decreases over time indicating

aggregation of the TM peptide over time. Thus the short preparation time and similar FRET efficiencies of MLVs compared to LUVs renders MLVs a good hydrophobic environment to investigate TM helix-heix interactions (A. S. Khadria & Senes 2013; You et al. 2005).

Another synthetic bilayer platform developed and extensively used by the Hristova group is the surface supported bilayer, where peptides are reconstituted into a single leaflet of lipid at the air/water interface, transferred onto glass substrates, fused with lipid vesicles to form the second leaflet of the supported bilayer, and imaged under the microscope (Merzlyakov, Li & Hristova 2006; Merzlyakov, Li, Casas, et al. 2006; Merzlyakov, Li, Gitsov, et al. 2006; Merzlyakov, You, Li, et al. 2006). This ‘directed assembly’ of the peptides into the bilayers is different from the previously designed 'self assembly' of peptide containing liposomes on glass surface (Li & Hristova 2004), and offers several advantages over it. First, it requires 1/100th the amount of peptide needed for reconstituting in bilayer vesicles, reducing the cost of the experiments. Secondly, it allows control over achieving unidirectional orientation of the peptides. The peptides are deposited on a single lipid monolayer first, and can be oriented according to a certain topology by ensuring that the TM region is flanked on one side by charged water soluble residues, and on the other side by neutral hydrophillic residues (Merzlyakov, Li & Hristova 2006). Moreover, the instrumentation was adapted to allow for supported bilayers to be assessed by the 'spectral FRET' method using a fluorimeter instead of 'imaging FRET' method using a microscope (Li & Hristova 2004). The imaging FRET technique relied on fluorescence recovery after photobleaching (FRAP) using acceptor photobleaching as the observed parameter, and thus required the peptides in the bilayer to be diffusing slowly as well as the fluorophores to be photostable. Use of the spectral FRET technique does not require these stringent

conditions, and records the entire spectra instead of just fluorescence intensities, enabling the use of FRET pairs like fluorescein/rhodamine with greater spectral bleedthrough and lower photostability (Merzlyakov, Li, Casas, et al. 2006);(Merzlyakov & Hristova 2008). The Hristova group has utilized the above methods to study TM interactions of the receptor tyrosine kinase (RTK) family of fibroblast growth factor FGFR3 and its sequence variants in all these different bilayers (LUVs, MLVs and surface supported bilayers) (Li et al. 2006);(Li & Hristova 2006; Li et al. 2006; Merzlyakov et al. 2007; You et al. 2006; You et al. 2007);(Merzlyakov, You, Li, et al. 2006; Meyers et al. 1995) **(Table 1.1)**.

Although artificial bilayers have enabled thorough investigations of membrane protein association energetics using FRET, one caveat of using artificial bilayers in the scheme of quantitative measurements is that the interactions are assayed in a non-native 'dilute' system. In the cell membrane, protein-protein interactions occur in a crowded environment, with a high local concentration of other proteins. *In vitro* experiments with artificial bilayers ignore the 'excluded volume effect' described for soluble proteins, which explains how macromolecules inside a cell occupy 20-30% of the cell volume (Ellis 2001a; Ellis 2001b), exerting non specific effects on the interactions. This type of crowding also occurs in the membrane with other proteins in the vicinity and could either increase the probability of association or prevent specific associations of membrane proteins in the local membrane environment. This supports an argument that working in artificial dilute conditions, for any macromolecular interaction study, could be physiologically irrelevant (Minton 2000). To account for this crowding factor, Hristova and coworkers developed a quantitative FRET imaging technique, 'QI-FRET' (Li et al. 2008) that used microscopy to measure TM interactions in cell-derived vesicles containing the native cytoplasmic milieu as well. Using this

technique, they found that the GpA dimer is in fact weaker in mammalian membranes (Chen et al. 2010) than previously established using various techniques (Adair & Engelman 1994; Finger et al. 2006; Fisher et al. 1999; Fisher et al. 2003; Fleming et al. 1997; Lemmon, Flanagan, Treutlein, et al. 1992; Lemmon, Flanagan, Hunt, et al. 1992; Lemmon et al. 1994; Russ & Engelman 1999), suggesting that molecular crowding indeed plays a role in the energetics of protein-protein interactions. They then established that six different plasma membrane derived vesicles **(Table 1.1)**, prepared from different cell lines using different methods, did not introduce any statistically significant changes in GpA dimerization (Sarabipour & Hristova 2013), reporting that any of these cell lines can be used for TM domain interaction studies using this method. Mainly, the Hristova group performed investigations of the RTK family oligomerization using plasma membrane derived vesicles using QI-FRET: a difference in dimerization of the achondroplasia-linked mutant of the FGFR3 TM domain was observed compared to WT in HEK293 cells, suggested a link to structural changes in the mutant (Placone & Hristova 2012), and investigation of the ErbB2 TM domain showed the highest dimerization strength amongst the RTKs in mammalian membranes (Placone et al. 2014). A list of the various fluorophores used in the different mammalian membranes in these studies is provided in **(Table 1.1)**.

The difficulty of reproducing the native environment of membrane proteins makes quantitative FRET measurements challenging. However, with the design of these different model membranes closer to the native system, more information is now available about the precise energetics of TM protein interactions. Based on the nature of the query, FRET has been extensively used to study TM helix-helix interactions in different model membranes to provide phenomenological, or quantitative comparisons.

Calculation of FRET Efficiency

To obtain the energetics of TM helix-helix associations, FRET efficiencies are calculated as a function of the protein concentration. The concentration of a TM peptide in these measurements is its effective concentration in its hydrophobic solvent, and not in the aqueous medium in which the hydrophobic solvent is suspended. For this reason, the use of molarity as a concentration unit has been an issue for TM domain energetic measurements (MacKenzie & Fleming 2008). The use of 'mole fraction' or 'mole ratio' has been commonly used to define membrane protein concentrations, although the term molarity, where the volume considered is the hydrophobic volume, has also been arguably used (Lomize et al. 2004). To measure association equilibria with FRET, it is important to achieve a range of [protein to hydrophobic solvent] ratios in which the equilibrium can be pushed from very concentrated to very dilute conditions. Once a system that allows for reversible equilibrium of the peptides is optimized, the FRET measurements are then used to calculate FRET efficiency of membrane proteins using the following parameters:

Calculation of FRET efficiency: The simple formalisms

Accurate measurement of FRET efficiency requires at least three different samples for every peptide concentration used; the 'donor only' sample, the 'acceptor only' sample, and the 'FRET sample', containing a mixture of donor and acceptor labeled peptides **(Figure 1.4)**. FRET pairs are chosen such that there is maximum overlap between donor emission and acceptor excitation, and minimal direct excitation of the acceptor at the donor's excitation wavelength. Even with minimal direct excitation or bleed through of the acceptor in the donor excitation channel, incorporation of the

fluorophores on a peptide and subsequently in lipid bilayers can change the spectrum of the fluorophore. Thus it is necessary to account for the direct excitation of the acceptor while measuring FRET. Primarily there are four different ways that have been used to measure the FRET efficiency of TM helix-helix oligomerization:

(i) Donor Quenching

Utilizing the 'donor only' and the 'FRET sample', the apparent FRET efficiency E_{app} is calculated from the intensity of donor emission in the presence (I_{DA}) and absence of the acceptor (I_D) according to:

$$E_{app} = \frac{(I_D - I_{DA})}{I_D}$$

…Eqn 1

at the emission maximum wavelength λ_{max} of the donor **(Figure 1.5)**. In the simple case of using FRET qualitatively to study relative phenomenon changes, the FRET efficiency is then used to calculate the apparent association constant and subsequently the apparent free energy of association [e.g., (A. S. Khadria & Senes 2013)].

(ii) Acceptor Sensitization

Another way of measuring FRET is through acceptor emission sensitization. Since in most cases there is always some direct excitation of the acceptor I_A when excited at the donor excitation wavelength **(Figure 1.5)**, it needs to be subtracted from the acceptor emission I_{AD} measured from the 'FRET sample', and the FRET efficiency is then given by

$$E_{app} = \left(\frac{(I_{AD} - I_A)}{I_A} \right) \frac{\varepsilon_A}{\varepsilon_D}$$

…Eqn 2

where ε_D and ε_A are the molar extinction coefficients of the donor and the acceptor at the donor's excitation wavelength (Hildebrandt 2013).

(iii) Sensitized Emission

In this less frequently used method, the sensitized emission is calculated by scanning the excitation spectra of the 'donor only', 'acceptor only', and the 'FRET sample' at a fixed emission wavelength of the acceptor. This is useful when using a FRET pair like pyrene and coumarin, where the excitation spectrum of the donor has narrow bands compared to that of the acceptor **(Figure 1.6 a,b)**. The 'donor only' sample would give a minimal excitation spectrum at the acceptor emission wavelength, and the 'FRET sample' will yield a measurable excitation spectrum of the donor due to FRET. The difference between the two spectra in the donor's excitation spectrum provides the sensitized emission. This can be observed in **Figure 1.6c** where the excitation spectra of pyrene and coumarin labeled Glycophorin A peptides were measured at a fixed emission wavelength of 500 nm (Fisher et al. 1999). An advantage of using this FRET pair with this method is that the excitation spectrum of the acceptor, coumarin, does not get affected by the presence or absence of the donor, pyrene **(Figure 1.6c)**, and thus the 378 nm excitation maximum intensity can be used to monitor the relative acceptor concentration of each measured sample.

(iv) EmEx-FRET

One of the uncertainties associated with FRET measurements is the variation in the effective peptide concentration from one sample to another due to low solubility of the hydrophobic TM peptides. To circumvent this problem, the EmEx-FRET technique was developed to reduce the uncertainties by reporting concentrations of the donor and acceptor labeled peptides (Merzlyakov et al. 2007). This technique relies on measurement of the excitation as well as the emission spectra for the 'FRET sample', as well as the excitation and emission spectra of 'donor only' and 'acceptor only' samples of known concentrations, serving as the 'standards'. The spectra of the standards are normalized to the spectra of the 'FRET sample' using a scaling coefficient factor, and this coefficient factor is multiplied by the known standard concentrations to get the donor and acceptor concentrations in the 'FRET sample' (Merzlyakov & Hristova 2008; Merzlyakov et al. 2007).

Use of the acceptor sensitized emission technique (ii) is a more direct measurement of FRET compared to donor quenching (i), because any increase in acceptor emission, when excited at the donor's excitation wavelength, would be only due to energy transfer. Donor quenching, on the other hand, can also occur due to dye stacking or other environmental effects and needs to be separated from the FRET signal. Nonetheless, donor quenching has been the most commonly used technique (as observed from **(Table 1.1)**) as it is more straightforward. Other quenching effects of the donor can also be controlled for by testing an increasing amount of donor peptide:lipid ratios; if the fluorescence intensity of the donor follows a linear relationship as a function of peptide concentration, then self quenching effects can be ruled out (You et al. 2005). Moreover, it does not require knowledge of the extinction coefficients of the fluorophores (comparing Equations 1 and 2), which the acceptor sensitization method would require

as an added step of characterizing environmentally sensitive dye extinction coefficients in detergent or lipid (Adair & Engelman 1994). The sensitized emission technique (iii) can be used to detect the FRET signal even when environmental effects can alter the donor quantum yield between the monomeric and oligomeric states. This method is useful especially with the pyr-cou FRET pair because the acceptor excitation near 380 nm is unaffected by FRET and may be used as an internal control to monitor acceptor concentration **(Figure 1.6c)**. The more recently developed EmEx-FRET method (iv) is the most thorough method that not only accounts for the donor quenching effects and the concentration uncertainties, but can also be used in cellular studies where the donor and acceptor concentrations are unknown. This technique was developed using the FGFR3-TM peptides in POPC vesicles (Merzlyakov et al. 2007), where the free energy of association was calculated to be −2.78 ± 0.04 kcal/mol as opposed to donor quenching that gave a free energy of association of −2.9 ± 0.7 kcal/mol, reducing the uncertainty in the free energy calculation from ±0.7 to ±0.04 kcal/mol. This method was subsequently extended to FRET microscopy to yield the quantitative imaging or 'QI-FRET' method that allows the determination of the donor and acceptor concentrations as well as FRET efficiency in cell-derived vesicles (Chen et al. 2010; Li et al. 2008; Placone & Hristova 2012; Sarabipour & Hristova 2013).

To accurately account for sequence specific FRET, two more controls to the experiment are required; competition with (a) unlabeled peptide of the same sequence and (b) an unrelated unlabeled peptide. Decrease in the observed FRET efficiency upon addition of (a) but no change in FRET upon addition of (b) confirms sequence specific oligomerization of the TM peptides.

Calculation of FRET efficiency: Challenges in the bilayer

The above basic formalisms can be used to calculate FRET, or E_{app} qualitatively and provide relative behavioral results. But to get quantitative energetics of TM helix-helix association, a number of additional factors need to be accounted for at every stage of the experimental process. The hydrophobic nature of the TM helices makes the synthesis, labeling and purification difficult and special strategies are required to maximize the yield obtained. The low aqueous solubility of these peptides requires addition of positively charged residues like Lys flanking the TM sequences (Rath & Deber 2013; A. Khadria & Senes 2013) Solid phase synthesis of these 'sticky' peptides makes the coupling reaction slow and less efficient, and thus higher equivalents of reagents and multiple coupling steps are required to push the synthesis to completion (A. S. Khadria & Senes 2013). High labeling yield is necessary for FRET experiments, and the high hydrophobicity of the unlabeled peptides renders separation of unlabeled and labeled peptides using HPLC to be tricky. Thus, achieving maximum labeling efficiency is very important at the labeling stage and can be achieved by using large molar excesses of the dyes and longer reaction times (A. Khadria & Senes 2013; Stahl et al. 2012).

Attaching dyes to peptides can have a two-way effect; the dye can affect the helicity and oligomerization of the peptides, and the peptide attachment can modify the spectroscopic properties of the dye. In the study of the oligomeric state of phospholamban (Li et al. 1999), the use of two different FRET pairs (AMCA-DABS and DANS-DABS) demonstrated that the oligomeric state of PLB differed based on the dye used. When the protein was phosphorylated, the oligomeric state decreased in the AMCA-labeled samples, and did not change for the DANS-labeled samples. This was

contrary to the EPR study (Cornea et al. 1997), where phosphorylation had led to an increase in the average oligomeric state. This finding demonstrated that the attachment of dyes altered the net electrostatic charge on PLB, which had separate effects on its oligomerization. Effect of the dye on the helicity and oligomerization can be tested by CD and SDS-PAGE experiments, and if the dye is attached to the termini, or close to the termini, it likely does not affect the oligomerization or helicity of the peptide (Iwamoto et al. 2005). Properties of the dyes, on the other hand, need to be tested each time as environmental changes due to the peptide attachment, the organic solvent they are dissolved in, and the presence of detergent or lipid can alter the extinction coefficient and cause spectral shifts in the dyes (Adair & Engelman 1994; Renthal et al. 2011; A. Khadria & Senes 2013), which can cause problems while carrying out spectroscopic measurements. Moreover, the calculated Förster radius R_0 of the same FRET pair can vary between different peptides in different environments as seen for the DANS and DABS fluorophores in **(Table 1.1)**, (Adair & Engelman 1994; Li et al. 1999), and thus needs to be accounted for each time.

Once these difficulties are overcome, the reconstitution of these peptides with low solubility into detergents and especially lipids, is the next challenge, and requires additional steps to tackle them. TM peptides and lipids are dissolved in separate organic solvents, mixed together, lyophilized and then hydrated, following freeze thaw cycles for equilibration. Unlike detergents, lipid bilayers do not exchange peptide molecules between themselves, and thus a new sample needs to be prepared for every peptide:lipid ratio. And for every ratio, there needs to be a ‘donor only’, an ‘acceptor only’, a ‘FRET sample’, an unlabeled peptide control and an unrelated peptide control. This makes the sample set large for preparing replicates for a range of peptide:lipid ratios. Further, for lipid bilayers, an additional ‘no peptide’ sample is always necessary

to serve as a light scattering control (You et al. 2005), and needs to subtracted from the fluorescent signal (Adair & Engelman 1994). Additionally, phase separation problems between the peptide and lipid solutions can cause irreversible aggregation of the TM peptides, and thus needs to be tested using X-ray diffraction or calculation of FRET efficiency as a function of the acceptor mole fraction (Li & Hristova 2006; You et al. 2005; You et al. 2006). Moreover, the orientation of the TM helices relative to the plane of bilayer may not always be perpendicular, and could be just associated with the bilayer instead of being inserted it in. This requires an additional step of characterizing every sample by oriented circular dichroism (You et al. 2005). Once all these parameters - high labeling efficiency, dye behavior in the environment, proper insertion and orientation in the bilayers, and effective peptide concentration in the bilayers - have been accounted for, the observed FRET efficiency, E_{obs} (Eqn. 4), can then be measured.

Calculation of FRET efficiency: The proximity contribution

FRET experiments for TM helix-helix interactions in bilayers are performed in low peptide:lipid ratios, such that the distances between individual peptide molecules are greater than the Förster radii of the dyes they are attached to, so that interactions between the peptides are primarily sequence-specific. However, the lipid bilayer is fluid, allowing peptides to diffuse freely and resulting in FRET arising from random colocalization of donor and acceptor molecules. Thus the observed FRET E_{obs} will always contain a contribution of proximity FRET, $E_{proximity}$. One way to ensure that the observed FRET is primarily due to sequence specific dimerization is by adding unlabeled peptides to the 'FRET sample' (assuming that unlabeled and labeled peptides have the same propensity to dimerize) and expecting a decrease in FRET (A. S. Khadria & Senes 2013; You et al. 2005). If the observed FRET is primarily due to

random colocalization, addition of unlabeled peptide will not result in a decrease in FRET. Moreover, if the addition of an equimolar amount of unlabeled peptide results in a 50% decrease in FRET for a dimer, it suggests that the observed FRET contains minimal amounts of other effects like donor self quenching, improper equilibration, and interference from labels (Fisher et al. 1999; Johnson et al. 2004).

The earlier quantitative FRET models (Adair & Engelman 1994; Li et al. 1999; Veatch & Stryer 1977) did not account for this proximity contribution. This contribution factor had been simulated for randomly distributed peptides, whose donor quenching by different acceptors in various acceptor configurations was averaged for different Förster radii (Wimley & White 2000; Wolber & Hudson 1979). The proximity term is given by:

$$E_{proximity} = \frac{1}{1 + \sum_{i} \left(R_0 / r \right)^6}$$

…Eqn 3

where r_i is the distance between the donor and the *i*th acceptor, and R_0 is the Förster radius for the FRET pair. This proximity FRET term was, for the first time, separated from the FRET due to sequence specific interaction, E_{FRET} in the formalism for observed FRET in lipid bilayers (You et al. 2005), given by:

$$E_{obs} = E_{FRET} + E_{proximity}$$

…Eqn 4

The simulation data demonstrated that there is a marked contribution of proximity FRET to the observed FRET, with higher contribution for FRET pairs having higher R_0

values, even at low acceptor mole fractions (You et al. 2005). It was also observed that FRET due to donors and acceptors between two consecutive leaflets of an MLV is relatively small, even for higher R_0 values, indicating that use of MLVs does not increase the contribution of proximity FRET by a lot. The simulations by (Wolber & Hudson 1979) calculated proximity FRET as a function of acceptor concentration. However, these simulations considered the fluorophores to be point structures negligible in size, and did not work when the fluorophores used were not small organic dyes but large (3-4 nm) fluorescent proteins with a limited distance of closest approach. A model that took the size factor into account, developed the proximity contributions for monomeric fluorophores of a finite size (Snyder & Freire 1982), but not for those attached to oligomeric membrane protein complexes. For cellular studies, large fluorescent proteins as fusion constructs are primarily used as donors and acceptors. These fluorophores participate in oligomeric structures where the probability of 'background FRET' (de Souza 2014) from a 'bystander protein'(Clayton & Chattopadhyay 2014) in a crowded environment is quite high. (King et al. 2014) predicted the proximity FRET over a wide range of exclusion radii of fluorophores and a more thorough range of acceptor concentrations. They also simulated the proximity FRET for monomers (which they also verified experimentally using plasma membrane derived vesicles), dimers, trimers and tetramers for the first time; and generated a model for the proximity FRET contribution as a function of oligomeric state and geometry of membrane protein complexes in a cellular scenario.

A different and formalism of separating the $E_{proximity}$ and E_{FRET} terms, argued to be more accurate (Luís M S Loura 2011), has been used as well where the both the FRET and proximity contributions are multiplied and integrated to obtain the donor fluorescence decay, instead of the proximity contributions being subtracted while using

the steady state donor quenching (Fernandes et al. 2008).

Calculation of FRET efficiency: The energetics of association

When performing qualitative comparisons, the apparent equilibrium constant K_{app} is calculated by plotting the apparent FRET efficiency E_{app} (equation 2) as a function of the total peptide concentration. This then yields the apparent free energy change of association using:

$$\Delta G^{o}_{app} = -RT \ln\left(K_{app}\right)$$

…Eqn 5

Quantifying the FRET efficiency to obtain the free energy of oligomerization requires a more elaborate understanding of the various possible oligomeric species in the sample. In the case of a TM homodimer, for instance, there are various types of dimers formed with equal probability – donor-donor pairs, donor-acceptor or FRET pairs, and acceptor-acceptor pairs. It is only the donor-acceptor pair that is observable by FRET, whereas the other pairs are 'dark', decreasing the expected FRET efficiency from 100%. Additionally, the presence of unlabeled peptide also participates equally in the dimerization, competing with the observable donor-acceptor pair and decreasing the FRET efficiency. Therefore these two parameters have to be accounted for to have an understanding of the amount of expected FRET, without which obtaining quantitative thermodynamics of dimerization is not possible. Considering a homodimeric system labeled with donor (D) and acceptor (D) dyes:

$$[D] = D_{total}\, L_D$$

$$[A] = A_{total}\, L_A$$

$$[U] = D_{total}(1 - L_D) + A_{total}(1 - L_A)$$

where [D] is the labeled donor concentration, $[D]_{total}$ is a total donor concentration, L_D is a labeling efficiency of the donor, [A] is the labeled acceptor concentration, $[A]_{total}$ is a total acceptor concentration, L_A is a labeling efficiency of the acceptor, and [U] is the total unlabeled peptide concentration. If the possible pairs in the case of completely dimeric system are DD, DA, DU, AA, AU and UU, then according to the donor quenching formalism, the theoretical FRET, $E_{theoretical}$ will be the amount of DA relative to the total amount of pairs containing donors:

$$E_{theoretical} = \frac{DA}{DA + DD + DU}$$

…Eqn 6

Thus, if labeling efficiency was 100%, then the maximum FRET due to sequence specific dimerization will be 50% for a completely dimeric system. Using equations 4 and 5, the fraction dimer can be calculated as

$$\frac{Dim}{Total} = \frac{E_{observed} - E_{proximity}}{E_{theoretical}} = \frac{2[X_{Dim}]}{2[X_{Dim}] + [X_{Mon}]}$$

…Eqn 7

where $2[X_{Dim}]$ is concentration of monomers in a dimer and $[X_{Mon}]$ is concentration of monomers. Using the $2[X_{Dim}]$ concentration obtained from equation 7, the association constant of a monomer-dimer equilibrium can be calculated according to

$$K_D = \frac{[X_{Dim}]}{[X_{Mon}]^2}$$

for

$$2\,Mon \Leftrightarrow Dim$$

…Eqn 8

Using the equilibrium constant from equation 8, the free energy of association of TM dimerization can be calculated according to

$$\Delta G^{o} = -RT \ln\left(K_{D}\right)$$

…Eqn 9

FRET to yield Oligomeric state

A number of models have utilized FRET for the measurement of not only the energy of association but also the order of the oligomeric complex. Using the fluorescence quantum yield of the donor as a function of the mole fraction of acceptor (keeping the total peptide:lipid ratio constant), (Veatch & Stryer 1977) were the first ones to postulate the different signature curves for different oligomeric schemes (dimer, trimer, tetramer) of membrane proteins in lipid. They also demonstrated the dependency of the equilibrium constant on the oligomeric state, and whether there is a preference for donor-donor (homo-pair) and acceptor-acceptor (hetero-pair) pairs over the productive donor-acceptor 'FRET sample'. The FRET data alone seemed to fit best to a dimer model for Gramicidin A transmembrane channel in DHPC vesicles, although it could not completely rule out the trimer and tetramer models. The dimeric nature of these channels was further supported by conductance measurements, and using that confirmation, it was reported that gramicidin A channels fit better to a dimeric model than a trimeric or a tetrameric model. A few years later, (Adair & Engelman 1994) derived a dependency of the donor quenching on the acceptor mole fraction showing that a linear relationship between the two suggests a dimer mode for Glycophorin A in DMPC vesiclesl. Working under assumptions that there was no preference between homo-pairs, hetero-pairs and pairs with unlabeled peptides, they obtained a much better fit to a dimer with a 0.97 R^2 value as opposed to that of a trimer with a 0.68 R^2 value. This relationship has since been widely used to elucidate the oligomeric state of many membrane protein complexes in lipid and detergent, most of which have shown a linear relationship suggestive of dimer formation (Anbazhagan & Schneider 2010; Artemenko et al. 2008; Johnson et al. 2004; Li et al. 2005; Melnyk et al. 2002). It is important to

note that the dimer models obtained by these FRET experiments were, in all cases, complemented by other techniques like SDS-PAGE, conductance, Western blot, TOXCAT etc. These two formalisms (Adair & Engelman 1994; Veatch & Stryer 1977), which worked under the approximation of equal energy transfer to all subunits in an oligomer, have been very useful in distinguishing between a dimer and a higher order oligomer; because the relationship between FRET efficiency and acceptor mole fraction is linear only in the case of a dimer.

Analysis of higher order oligomers using these models, however, is not possible using these models; the possibility of a biologically irrelevant but detergent induced (Challou et al. 1994) ‘head to tail’ tetrameric aggregate of GpA was inconclusive on the basis of FRET data (Fisher et al. 1999) and included previous structural and SDS-PAGE data to confirm the dimeric model. Similarly, a non-linear dependency of FRET on the acceptor mole fraction of the IRE1 TM domain approximated a tetramer formation, but was again backed up by SDS-PAGE data (Cho et al. 2012). To account for higher order oligomers, FRET within a ring shaped oligomer was simulated without the assumption of equal energy transfer to all subunits. The FRET efficiency of each donor-subunit to each acceptor-subunit was calculated explicitly and the dependency of FRET on acceptor mole fraction was simulated for 2 to 11 subunits (Li et al. 1999). This calculation was initially extended to phospholamban, which showed a different size, extent of oligomerization, and adjacent subunit distances in SDS micelles and POPC vesicles, and later used to obtain oligomeric states of other membrane proteins, such as the M2 tetramer in DLPC vesicles (Schick et al. 2010).

In addition to eludicating the oligomeric state, FRET can also be qualitatively used to obtain the stoichiometry of a heteromeric complex. This has been demonstrated by different experiments involving donor and acceptor labeled peptides in fixed

donor:acceptor and fixed peptide:lipid/detergent ratios, and competition experiments on those samples using unlabeled peptides. The stoichiometry of the heterodimeric Class II major histocompatibility complex (MHC) chains, MHC-donor and MHC-acceptor TM peptides, was found to be 1:1 by competing with unlabeled MHC TM peptides (King & Dixon 2010). Similarly, the higher order oligomer of FtsB and FtsL TM peptides of the bacterial divisome was found to have a 1:1 stoichiometry by adding unlabeled FtsL to donor and acceptor labeled FtsB peptides (A. S. Khadria & Senes 2013).

Conclusion

FRET has widely been used as a probe to assess structural and biophysical questions about macromolecules and their interactions. For membrane proteins, the use of traditional structural tools like NMR and X-ray crystallography is limited because of the difficulty of preparing stable working samples of these proteins. Thus, the structural database of membrane proteins lags behind that of soluble proteins. To understand the structure-function relationships and folding mechanisms of membrane proteins, FRET has been especially useful in transmembrane domain interaction studies, which have enabled understanding these highly represented proteins in the cell membrane.

Over the last 30 years, a lot of progress has been made in understanding membrane protein structure and folding using FRET. Different methods of performing FRET in various membrane mimetic environments have been developed, improved upon and utilized to understand the structural and functional organization of receptors, ion channels, and regulators of key physiological process that occur in the cell membrane. Various research groups have contributed to this field by establishing different techniques and formalisms to calculate FRET efficiency, use the calculated FRET to establish the oligomeric state of a complex, and compute and compare the free energies of their association between different solvent conditions. This review emphasizes on the utility of FRET to study membrane protein interactions, and discusses the challenges associated with it. It enlists the different combinations of fluorophores and membrane mimetics used, and aims to bring together the significant contributions in the field to provide the reader with a comprehensive analysis of the different parameters involved in using FRET to study membrane proteins.

Part 2: The Divisome

Cell division is one of the most fundamental processes in the life cycle of bacteria. Most types of bacteria carry out this process of cell division through a similar mechanism, with much of the same machinery. During the time of cell division, a set of essential and nonessential proteins assemble at the cell septum, to complete (at least) three major steps:

a) DNA replication, segregation of chromosomes between two dividing cells and induction of cell membrane constriction

b) Assembly of the complex of essential and nonessential proteins, and

c) Reconstruction of the cell wall and synthesis of the new peptidoglycan layer.

Apart from these three main steps, a number of minor cell division events also occur in conjunction which aid the process of cell division.

Escherichia coli has served as the model organism for studying cell division in prokaryotes. It contains an inner membrane, an outer membrane, and a cell wall. It is a rod shaped gram-negative bacterium, with the cell wall made up of one layer of peptidoglycan, unlike its gram-positive counterparts which contain several layers of peptidoglycan. The peptidoglycan, a complex polymer consisting of various sugars and amino acids, surrounds the inner membrane of bacteria to protect the cell from the surrounding environment. The cell membrane is a fluid structure composed of many different types of lipids with proteins embedded throughout. Specifically *E. coli* contains an outer membrane and an inner membrane separated by the periplasmic space, which together hold the inside of the cell containing the cytoplasm, which carries all the components of the cell. During cell division, this complex cellular structure needs to be modified; the cell membranes and peptidoglycan layers must each constrict, separate,

and rebuild in order for a cycle of cell division to be complete, and this process is carried out and completed by a complex of proteins called the “divisome.”

At least ten essential proteins in the divisome, most of them being integral membrane proteins, work together to complete the major events of cell division. These proteins localize to midcell in a linear fashion (FtsZ, FtsA, ZipA, FtsK, FtsQ, FtsB, FtsL, FtsW, FtsI, FtsN. This “hierarchy” will be revisited later in Appendix I, when a discussion on which proteins play a role in each of the aforementioned steps of cell division is provided. The proteins are categorized into the early, intermediate, and late proteins based on their timing of recruitment in cell division. Additionally, several nonessential proteins play a role in cell division and likely many more left to be discovered. In our lab we focus on elucidating the molecular structure of this divisome complex. Starting with the FtsB and FtsL subcomplex, we have begun elucidating the structure function relationships of individual divisome proteins in the context of cell-division. FtsB and FtsL are central to the bacterial divisome, participating in the intermediate stage of assembly of the divisome. Their presence is required to link together the early and late proteins of the divisome. From our work using FRET (Chapter 3), TOXCAT, computational modeling and X-ray crystallography (Appendix I), we hypothesize that the transmembrane domain of FtsB self associates and forms a stable core for its association with FtsL, which in turn is required to stabilize the periplasmic domain of FtsB. Together the FtsB-FtsL complex, we believe, is competent for binding to FtsQ and in turn, for their recruitment to the division septum to carry out cell division. This structural analysis not only serves as the first of its kind for the membane regions of divisiome proteins, but also creates a foundation for functional studies *in vivo*.

References

Adair, B.D. & Engelman, D.M., 1994. Glycophorin A helical transmembrane domains dimerize in phospholipid bilayers: a resonance energy transfer study. *Biochemistry*, 33(18), pp.5539–5544.

Anbazhagan, V., Cymer, F. & Schneider, D., 2010. Unfolding a transmembrane helix dimer: A FRET study in mixed micelles. *Archives of Biochemistry and Biophysics*, 495(2), pp.159–164.

Anbazhagan, V. & Schneider, D., 2010. The membrane environment modulates self-association of the human GpA TM domain—Implications for membrane protein folding and transmembrane signaling. *Biochimica et Biophysica Acta (BBA) - Biomembranes*, 1798(10), pp.1899–1907.

Artemenko, E.O. et al., 2008. Transmembrane domain of EphA1 receptor forms dimers in membrane-like environment. *Biochimica et Biophysica Acta (BBA) - Biomembranes*, 1778(10), pp.2361–2367.

Bill, R.M. et al., 2011. Overcoming barriers to membrane protein structure determination. *Nature Biotechnology*, 29(4), pp.335–340.

Booth, P.J. et al., 1995. Intermediates in the folding of the membrane protein bacteriorhodopsin. *Nature Structural & Molecular Biology*, 2(2), pp.139–143.

Challou, N. et al., 1994. Sequence and Structure of the Membrane-Associated Peptide of Glycophorin A. *Biochemistry*, 33(22), pp.6902–6910.

Chen, L. et al., 2010. Measuring the Energetics of Membrane Protein Dimerization in Mammalian Membranes. *Journal of the American Chemical Society*, 132(10), pp.3628–3635.

Cho, H., LaMarca, R. & Chan, C., 2012. Oligomerization of the transmembrane domain of IRE1α in SDS micelles. *Biochemical and Biophysical Research Communications*, 427(4), pp.764–767.

Clayton, A.H.A. & Chattopadhyay, A., 2014. Taking Care of Bystander FRET in a Crowded Cell Membrane Environment. *Biophysical Journal*, 106(6), pp.1227–1228.

Cornea, R.L. et al., 1997. Mutation and phosphorylation change the oligomeric structure of phospholamban in lipid bilayers. *Biochemistry*, 36(10), pp.2960–2967.

Deisenhofer, J. et al., 1985. Structure of the protein subunits in the photosynthetic reaction centre of Rhodopseudomonas viridis at 3|[angst]| resolution. *Nature*, 318(6047), pp.618–624.

Duong, M.T. et al., 2007. Changes in Apparent Free Energy of Helix–Helix Dimerization in a Biological Membrane Due to Point Mutations. *Journal of Molecular Biology*, 371(2), pp.422–434.

Ellis, R.J., 2001a. Macromolecular crowding: an important but neglected aspect of the intracellular environment. *Current Opinion in Structural Biology*, 11(1), pp.114–119.

Ellis, R.J., 2001b. Macromolecular crowding: obvious but underappreciated. *Trends in Biochemical Sciences*, 26(10), pp.597–604.

Engelman, D.M. et al., 2003. Membrane protein folding: beyond the two stage model. *FEBS Letters*, 555(1), pp.122–125.

Engelman, D.M., 2005. Membranes are more mosaic than fluid. *Nature*, 438(7068), pp.578–580.

Fernandes, F. et al., 2008. Role of Helix 0 of the N-BAR Domain in Membrane Curvature Generation. *Biophysical Journal*, 94(8), pp.3065–3073.

Finger, C. et al., 2006. The Stability of Transmembrane Helix Interactions Measured in a Biological Membrane. *Journal of Molecular Biology*, 358(5), pp.1221–1228.

Fisher, L.E., Engelman, D.M. & Sturgis, J.N., 1999. Detergents modulate dimerization, but not helicity, of the Glycophorin A transmembrane domain. *Journal of Molecular Biology*, 293(3), pp.639–651.

Fisher, L.E., Engelman, D.M. & Sturgis, J.N., 2003. Effect of detergents on the association of the Glycophorin a transmembrane helix. *Biophysical Journal*, 85(5), pp.3097–3105.

Fleming, K.G., 2002. Standardizing the Free Energy Change of Transmembrane Helix-Helix Interactions. *Journal of Molecular Biology*, 323(3), pp.563–571.

Fleming, K.G. et al., 2004. Thermodynamics of Glycophorin A transmembrane helix dimerization in C14 betaine micelles. *Biophysical Chemistry*, 108(1–3), pp.43–49.

Fleming, K.G., Ackerman, A.L. & Engelman, D.M., 1997. The effect of point mutations on the free energy of transmembrane alpha-helix dimerization. *Journal of Molecular Biology*, 272(2), pp.266–275.

Franzin, C.M., Teriete, P. & Marassi, F.M., 2007. Structural Similarity of a Membrane Protein in Micelles and Membranes. *Journal of the American Chemical Society*, 129(26), pp.8078–8079.

Garavito, R.M. & Ferguson-Miller, S., 2001. Detergents as Tools in Membrane Biochemistry. *Journal of Biological Chemistry*, 276(35), pp.32403–32406.

Gohon, Y. & Popot, J.-L., 2003. Membrane protein–surfactant complexes. *Current Opinion in Colloid & Interface Science*, 8(1), pp.15–22.

Go, M.Y. et al., 2006. Self-association of the Transmembrane Domain of an Anthrax Toxin Receptor. *Journal of Molecular Biology*, 360(1), pp.145–156.

Hein, C. et al., 2014. Hydrophobic supplements in cell-free systems: Designing artificial environments for membrane proteins. *Engineering in Life Sciences*, 14(4), pp.365–379.

Hildebrandt, N., 2013. How to Apply FRET: From Experimental Design to Data Analysis. In I. Medintz & N. Hildebrandt, eds. *FRET – Förster Resonance Energy Transfer*. Wiley-VCH Verlag GmbH & Co. KGaA, pp. 105–163. Available at: http://onlinelibrary.wiley.com/doi/10.1002/9783527656028.ch05/summary [Accessed October 19, 2014].

Huang, K.S. et al., 1981. Refolding of an integral membrane protein. Denaturation, renaturation, and reconstitution of intact bacteriorhodopsin and two proteolytic fragments. *The Journal of Biological Chemistry*, 256(8), pp.3802–3809.

Iwamoto, T. et al., 2005. Synthesis and initial characterization of FGFR3 transmembrane domain: consequences of sequence modifications. *Biochimica Et Biophysica Acta*, 1668(2), pp.240–247.

Jaud, S. et al., 2009. Insertion of short transmembrane helices by the Sec61 translocon. *Proceedings of the National Academy of Sciences*, 106(28), pp.11588–11593.

Johnson, R.M., Heslop, C.L. & Deber, C.M., 2004. Hydrophobic Helical Hairpins: Design and Packing Interactions in Membrane Environments†. *Biochemistry*, 43(45), pp.14361–14369.

Kahn, T.W., Sturtevant, J.M. & Engelman, D.M., 1992. Thermodynamic measurements of the contributions of helix-connecting loops and of retinal to the stability of bacteriorhodopsin. *Biochemistry*, 31(37), pp.8829–8839.

Khadria, A. & Senes, A., 2013. Measurement of transmembrane peptide interactions in liposomes using Förster resonance energy transfer (FRET). *Methods in Molecular Biology (Clifton, N.J.)*, 1063, pp.19–36.

Khadria, A.S. & Senes, A., 2013. The Transmembrane Domains of the Bacterial Cell Division Proteins FtsB and FtsL Form a Stable High-Order Oligomer. *Biochemistry*, 52(43), pp.7542–7550.

Killian, J.A., 1998. Hydrophobic mismatch between proteins and lipids in membranes. *Biochimica Et Biophysica Acta*, 1376(3), pp.401–415.

King, C. et al., 2014. The FRET Signatures of Noninteracting Proteins in Membranes: Simulations and Experiments. *Biophysical Journal*, 106(6), pp.1309–1317.

King, G. & Dixon, A.M., 2010. Evidence for role of transmembrane helix-helix interactions in the assembly of the Class II major histocompatibility complex. *Molecular bioSystems*, 6(9), pp.1650–1661.

Krishnamani, V. & Lanyi, J.K., 2012. Molecular dynamics simulation of the unfolding of individual bacteriorhodopsin helices in sodium dodecyl sulfate micelles. *Biochemistry*, 51(6), pp.1061–1069.

LaPointe, L.M. et al., 2013. Structural organization of FtsB, a transmembrane protein of the bacterial divisome. *Biochemistry*, 52(15), pp.2574–2585.

Lemmon, M.A. et al., 1994. A dimerization motif for transmembrane [alpha]-helices. *Nat Struct Mol Biol*, 1(3), pp.157–163.

Lemmon, M.A., Flanagan, J.M., Hunt, J.F., et al., 1992. Glycophorin A dimerization is driven by specific interactions between transmembrane alpha-helices. *The Journal of Biological Chemistry*, 267(11), pp.7683–7689.

Lemmon, M.A., Flanagan, J.M., Treutlein, H.R., et al., 1992. Sequence specificity in the dimerization of transmembrane alpha-helices. *Biochemistry*, 31(51), pp.12719–12725.

Li, E. et al., 2008. Quantitative Measurements of Protein Interactions in a Crowded Cellular Environment. *Analytical Chemistry*, 80(15), pp.5976–5985.

Li, E. & Hristova, K., 2004. Imaging Förster resonance energy transfer measurements of transmembrane helix interactions in lipid bilayers on a solid support. *Langmuir: the ACS journal of surfaces and colloids*, 20(21), pp.9053–9060.

Li, E. & Hristova, K., 2006. Role of receptor tyrosine kinase transmembrane domains in cell signaling and human pathologies. *Biochemistry*, 45(20), pp.6241–6251.

Li, E., You, M. & Hristova, K., 2006. FGFR3 Dimer Stabilization Due to a Single Amino Acid Pathogenic Mutation. *Journal of Molecular Biology*, 356(3), pp.600–612.

Li, E., You, M. & Hristova, K., 2005. Sodium Dodecyl Sulfate−Polyacrylamide Gel Electrophoresis and Förster Resonance Energy Transfer Suggest Weak Interactions between Fibroblast Growth Factor Receptor 3 (FGFR3) Transmembrane Domains in the Absence of Extracellular Domains and Ligands†. *Biochemistry*, 44(1), pp.352–360.

Li, M. et al., 1999. A fluorescence energy transfer method for analyzing protein oligomeric structure: application to phospholamban. *Biophysical Journal*, 76(5), pp.2587–2599.

Lomize, A.L., Pogozheva, I.D. & Mosberg, H.I., 2004. Quantification of helix-helix binding affinities in micelles and lipid bilayers. *Protein Science: A Publication of the Protein Society*, 13(10), pp.2600–2612.

Lomize, M.A. et al., 2006. OPM: Orientations of Proteins in Membranes database. *Bioinformatics*, 22(5), pp.623–625.

Luecke, H. et al., 1999. Structure of bacteriorhodopsin at 1.55 Å resolution. *Journal of Molecular Biology*, 291(4), pp.899–911.

Luís M S Loura, M.P., 2011. FRET in Membrane Biophysics: An Overview. *Frontiers in physiology*, 2, p.82.

Lyukmanova, E.N. et al., 2012. Lipid–protein nanodiscs for cell-free production of integral membrane proteins in a soluble and folded state: Comparison with detergent micelles, bicelles and liposomes. *Biochimica et Biophysica Acta (BBA) - Biomembranes*, 1818(3), pp.349–358.

MacKenzie, K.R. & Fleming, K.G., 2008. Association energetics of membrane spanning α-helices. *Current Opinion in Structural Biology*, 18(4), pp.412–419.

MacKenzie, K.R., Prestegard, J.H. & Engelman, D.M., 1997. A transmembrane helix dimer: structure and implications. *Science (New York, N.Y.)*, 276(5309), pp.131–133.

Le Maire, M., Champeil, P. & Moller, J.V., 2000. Interaction of membrane proteins and lipids with solubilizing detergents. *Biochimica Et Biophysica Acta*, 1508(1-2), pp.86–111.

McQuade, D.T. et al., 2000. Rigid Amphiphiles for Membrane Protein Manipulation. *Angewandte Chemie International Edition*, 39(4), pp.758–761.

Melnyk, R.A., Partridge, A.W. & Deber, C.M., 2001. Retention of Native-like Oligomerization States in Transmembrane Segment Peptides: Application to the Escherichia coli Aspartate Receptor†. *Biochemistry*, 40(37), pp.11106–11113.

Melnyk, R.A., Partridge, A.W. & Deber, C.M., 2002. Transmembrane domain mediated self-assembly of major coat protein subunits from Ff bacteriophage. *Journal of Molecular Biology*, 315(1), pp.63–72.

Merzlyakov, M., Li, E., Casas, R., et al., 2006. Spectral Förster Resonance Energy Transfer Detection of Protein Interactions in Surface-Supported Bilayers. *Langmuir*, 22(16), pp.6986–6992.

Merzlyakov, M., Li, E., Gitsov, I., et al., 2006. Surface-Supported Bilayers with Transmembrane Proteins: Role of the Polymer Cushion Revisited. *Langmuir*, 22(24), pp.10145–10151.

Merzlyakov, M., You, M., Li, E., et al., 2006. Transmembrane Helix Heterodimerization in Lipid Bilayers: Probing the Energetics behind Autosomal Dominant Growth Disorders. *Journal of Molecular Biology*, 358(1), pp.1–7.

Merzlyakov, M., Chen, L. & Hristova, K., 2007. Studies of receptor tyrosine kinase transmembrane domain interactions: the EmEx-FRET method. *The Journal of Membrane Biology*, 215(2-3), pp.93–103.

Merzlyakov, M. & Hristova, K., 2008. Forster Resonance Energy Transfer Measurements of Transmembrane Helix Dimerization Energetics. *Methods in enzymology*, 450, pp.107–127.

Merzlyakov, M., Li, E. & Hristova, K., 2006. Directed Assembly of Surface-Supported Bilayers with Transmembrane Helices. *Langmuir*, 22(3), pp.1247–1253.

Merzlyakov, M., Li, E. & Hristova, K., 2008. Surface supported bilayer platform for studies of lateral association of proteins in membranes (Mini Review). *Biointerphases*, 3(2), pp.FA80–FA84.

Meyers, G.A. et al., 1995. Fibroblast growth factor receptor 3 (FGFR3) transmembrane mutation in Crouzon syndrome with acanthosis nigricans. *Nature Genetics*, 11(4), pp.462–464.

Minton, A.P., 2000. Implications of macromolecular crowding for protein assembly. *Current Opinion in Structural Biology*, 10(1), pp.34–39.

Moraes, I. et al., 2014. Membrane protein structure determination — The next generation. *Biochimica et Biophysica Acta (BBA) - Biomembranes*, 1838(1, Part A), pp.78–87.

Morris, S.J., C.Südhof, T. & Haynes, D.H., 1982. Calcium-promoted resonance energy transfer between fluorescently labeled proteins during aggregation of chromaffin granule membranes. *Biochimica et Biophysica Acta (BBA) - Biomembranes*, 693(2), pp.425–436.

Nannepaga, S.J. et al., 2004. Estimation of Helix–Helix Association Free Energy from Partial Unfolding of Bacterioopsin†. *Biochemistry*, 43(2), pp.550–559.

Overington, J.P., Al-Lazikani, B. & Hopkins, A.L., 2006. How many drug targets are there? *Nature Reviews Drug Discovery*, 5(12), pp.993–996.

Packard, B.Z. et al., 1996. Profluorescent protease substrates: intramolecular dimers described by the exciton model. *Proceedings of the National Academy of Sciences*, 93(21), pp.11640–11645.

Placone, J. et al., 2014. Strong dimerization of wild-type ErbB2/Neu transmembrane domain and the oncogenic Val664Glu mutant in mammalian plasma membranes. *Biochimica et Biophysica Acta (BBA) - Biomembranes*, 1838(9), pp.2326–2330.

Placone, J. & Hristova, K., 2012. Direct Assessment of the Effect of the Gly380Arg Achondroplasia Mutation on FGFR3 Dimerization Using Quantitative Imaging FRET. *PLoS ONE*, 7(10), p.e46678.

Popot, J.L. & Engelman, D.M., 1990. Membrane protein folding and oligomerization: the two-stage model. *Biochemistry*, 29(17), pp.4031–4037.

Prodöhl, A. et al., 2007. A mutational study of transmembrane helix–helix interactions. *Biochimie*, 89(11), pp.1433–1437.

Rath, A. & Deber, C.M., 2013. Design of transmembrane peptides: coping with sticky situations. *Methods in Molecular Biology (Clifton, N.J.)*, 1063, pp.197–210.

Reddy, L.G., Jones, L.R. & Thomas, D.D., 1999. Depolymerization of phospholamban in the presence of calcium pump: a fluorescence energy transfer study. *Biochemistry*, 38(13), pp.3954–3962.

Renthal, R. et al., 2011. Interaction of a two-transmembrane-helix peptide with lipid bilayers and dodecyl sulfate micelles. *Biophysical chemistry*, 159(2-3), pp.321–327.

Russ, W.P. & Engelman, D.M., 1999. TOXCAT: a measure of transmembrane helix association in a biological membrane. *Proceedings of the National Academy of Sciences of the United States of America*, 96(3), pp.863–868.

Sarabipour, S. & Hristova, K., 2013. Glycophorin A transmembrane domain dimerization in plasma membrane vesicles derived from CHO, HEK 293T, and A431 cells. *Biochimica Et Biophysica Acta*, 1828(8), pp.1829–1833.

Schick, S. et al., 2010. Assembly of the M2 Tetramer Is Strongly Modulated by Lipid Chain Length. *Biophysical Journal*, 99(6), pp.1810–1817.

Schneider, D. & Engelman, D.M., 2003. GALLEX, a Measurement of Heterologous Association of Transmembrane Helices in a Biological Membrane. *Journal of Biological Chemistry*, 278(5), pp.3105–3111.

Seddon, A.M., Curnow, P. & Booth, P.J., 2004. Membrane proteins, lipids and detergents: not just a soap opera. *Biochimica et biophysica acta*, 1666(1-2), pp.105–117.

Shoshan-Barmatz, V. et al., 2010. VDAC, a multi-functional mitochondrial protein regulating cell life and death. *Molecular Aspects of Medicine*, 31(3), pp.227–285.

Snyder, B. & Freire, E., 1982. Fluorescence energy transfer in two dimensions. A numeric solution for random and nonrandom distributions. *Biophysical Journal*, 40(2), pp.137–148.

De Souza, N., 2014. Biophysics: Background FRET. *Nature Methods*, 11(5), pp.477–477.

Stahl, P.J. et al., 2012. On-the-resin N-terminal modification of long synthetic peptides. *Analytical Biochemistry*, 424(2), pp.137–139.

Stangl, M. et al., 2012. Detergent Properties Influence the Stability of the Glycophorin A Transmembrane Helix Dimer in Lysophosphatidylcholine Micelles. *Biophysical Journal*, 103(12), pp.2455–2464.

Stangl, M. et al., 2014. Sequence-Specific Dimerization of a Transmembrane Helix in Amphipol A8-35. *PLoS ONE*, 9(10), p.e110970.

Therien, A.G. & Deber, C.M., 2002. Oligomerization of a Peptide Derived from the Transmembrane Region of the Sodium Pump γ Subunit: Effect of the Pathological Mutation G41R. *Journal of Molecular Biology*, 322(3), pp.583–590.

Tribet, C., Audebert, R. & Popot, J.-L., 1996. Amphipols: Polymers that keep membrane proteins soluble in aqueous solutions. *Proceedings of the National Academy of Sciences*, 93(26), pp.15047–15050.

Tulumello, D.V. & Deber, C.M., 2009. SDS Micelles as a Membrane-Mimetic Environment for Transmembrane Segments. *Biochemistry*, 48(51), pp.12096–12103.

Ujwal, R. & Bowie, J.U., 2011. Crystallizing membrane proteins using lipidic bicelles. *Methods (San Diego, Calif.)*, 55(4), pp.337–341.

Valluru, N. et al., 2006. Transmembrane Helix–Helix Association: Relative Stabilities at Low pH†. *Biochemistry*, 45(14), pp.4371–4377.

Veatch, W. & Stryer, L., 1977. The dimeric nature of the gramicidin A transmembrane channel: Conductance and fluorescence energy transfer studies of hybrid channels. *Journal of Molecular Biology*, 113(1), pp.89–102.

Volkmer, T. et al., 2006. Assembly of a transmembrane b-Type cytochrome is mainly driven by transmembrane helix interactions. *Biochimica et Biophysica Acta (BBA) - Biomembranes*, 1758(11), pp.1815–1822.

Watanabe, Y. et al., 1991. Molecular weight determination of phospholamban oligomer in the presence of sodium dodecyl sulfate: application of low-angle laser light scattering photometry. *Journal of Biochemistry*, 110(1), pp.40–45.

Wegener, A.D. & Jones, L.R., 1984. Phosphorylation-induced mobility shift in phospholamban in sodium dodecyl sulfate-polyacrylamide gels. Evidence for a protein structure consisting of multiple identical phosphorylatable subunits. *The Journal of Biological Chemistry*, 259(3), pp.1834–1841.

White, S.H., 2004. The progress of membrane protein structure determination. *Protein Science*, 13(7), pp.1948–1949.

Wimley, W.C. & White, S.H., 2000. Determining the Membrane Topology of Peptides by Fluorescence Quenching†. *Biochemistry*, 39(1), pp.161–170.

Wolber, P.K. & Hudson, B.S., 1979. An analytic solution to the Förster energy transfer problem in two dimensions. *Biophysical Journal*, 28(2), pp.197–210.

Yin, H. et al., 2007. Computational Design of Peptides That Target Transmembrane Helices. *Science*, 315(5820), pp.1817–1822.

You, M. et al., 2007. Effect of Pathogenic Cysteine Mutations on FGFR3 Transmembrane Domain Dimerization in Detergents and Lipid Bilayers†. *Biochemistry*, 46(39), pp.11039–11046.

You, M. et al., 2005. Förster resonance energy transfer in liposomes: Measurements of transmembrane helix dimerization in the native bilayer environment. *Analytical Biochemistry*, 340(1), pp.154–164.

You, M., Li, E. & Hristova, K., 2006. The achondroplasia mutation does not alter the dimerization energetics of the fibroblast growth factor receptor 3 transmembrane domain. *Biochemistry*, 45(17), pp.5551–5556.

Yu, S.M. et al., 2000. An improved tripod amphiphile for membrane protein solubilization. *Protein Science: A Publication of the Protein Society*, 9(12), pp.2518–2527.

Zhou, F.X. et al., 2001. Polar residues drive association of polyleucine transmembrane helices. *Proceedings of the National Academy of Sciences*, 98(5), pp.2250–2255.

Scheme 1.1 Fluorescence

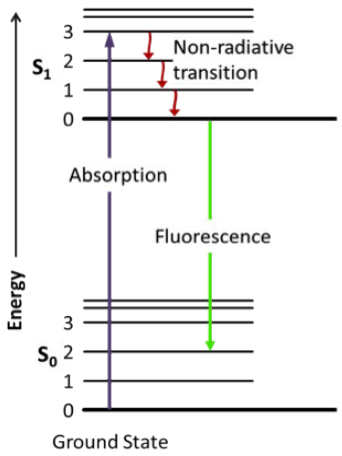

Figure S1.1: A simplified Jablonski diagram showing the possible electronic and vibrational transitions involved in Fluorescence

Fluorescence is a form of luminescence in which light is emitted from an electronically excited state. If the electron in a singlet excited state has an opposite spin to the electron in the ground state (and is thus paired), then return to the ground state is 'spin allowed' and occurs very fast (~10^8 per second). This phenomenon is termed fluorescence, and can be typically illustrated using a **Jablonski diagram (Figure S1.1)**. Energy absorbed by a molecule results in excitation of its electrons from the S_0 ground electronic state to the S_1 excited electronic state. Within these electronic states are different vibrational energy levels (0,1,2…), and following light absorption, electrons usually get excited to some vibrational energy level **(level 3 in Fig. S1.1**) in S_1. Relaxation from a vibrational excited state 3 to a vibrational ground state 0 in the electronic excited state S_1 occurs through a rapid (~10^{-12}s) non radiative transition process termed as '**internal conversion'**. Thus fluorescence emission occurs after thermal equilibration of the vibrational energy states, from the lowest energy vibrational state 0 of an excited electronic state S_1. Due to this loss in energy, the emission spectrum of a fluorophore is always shifted to a longer wavelength, and is termed the '**Stokes shift' (Figure S1.2)**.

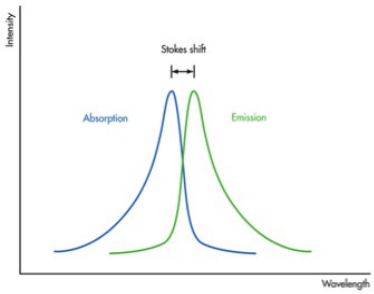

Figure S1.2: Stokes shift or loss of energy by fluorophore upon excitation by light.

Fluorophores are generally aromatic compounds that have distinct spectral properties like **quantum yield** that distinguish them for various applications. Quantum yield refers to the ratio of the emitted photons to the number of absorbed photons, and approaches unity for the brightest fluorophores. A phenomenon that can decrease the intensity of fluorescence is termed **quenching**, in which the excited state fluorophore can be deactivated by collisions due to other molecules, solvent effects etc. Quenching does not alter the chemical structure of the molecule, which is different from **photobleaching**, where the electrons move from a singlet to a triplet excited state and reside longer to form irreversible covalent modifications with another molecule. A fluorophore can photobleach after a few or a million excitation and emission cycles. This is dependent on the chemical structure of the fluorophore as well as its local environment. These fluorophores range from small organic molecules like Dansyl Chloride and Fluorescein to large fluorescent proteins like GFP and its variants. Considering the various properties, fluorophores are specifically chosen for appropriate spectroscopic techniques. **Fluorescence Anisotropy** uses photoselective excitation of polarized light to yield answers about size, shape and rigidity of macromolecules. Forster resonance energy transfer or **FRET** utilizes proximity based fluorescent energy transfer as a means to measure macromolecular interactions, and shed light on spatial distances within molecules. Fluorescence correlation spectroscopy or **FCS** and **single molecule detection** methods are more sensitive techniques that work with very dilute solutions and thus avoid the errors associated with ensemble averaging of information. Steady state and time resolved experiments are combined to piece all the information together to get a clearer picture underlying natural processes. **Live cell imaging** is being used and microscopy techniques are becoming more and more sophisticated to track processes in their natural environment. Together all these advances in the field of fluorescence are being and will continue to answer questions in the life sciences.

Table 1.1 Various FRET pairs used for TM interactions in detergents and lipids

Donor	Acceptor	Hydrophobic Solvent	Forster radius	Biological system	FRET method
[6 - ((7 - Amino - 4 - methylcoumarin - 3 - acetyl)amino)hexanoic acid] (AMCA)	DABS-chloride	SDS micelles C12E8 micelles OG micelles	49 ± 1 A°	Phospolamban (Li et al. 1999)	Donor Quenching
		DOPC vesicles	48 ± 1 A°		
DANS-chloride	DABS-chloride	SDS micelles C12E8 micelles OG micelles	33 ± 1 A°	Phospolamban (Li et al. 1999)	Donor Quenching
		DOPC vesicles	32 ± 1 A°		
Pyrene (Pyr)	7-dimethylaminocoumarin (Cou)	SDS micelles DDMAB micelles DPC micelles	60 A°	Glycophorin A (Fisher et al. 1999)	Sensitized Emission
Pyrene (Pyr)	7-dimethylaminocoumarin (Cou)	C_{12}Sulfate, C_{12}DMAB, C_{10},C_{11} Maltoside , C_{10},C_{11},C_{12}DAO	Not used	Glycophorin A (Fisher et al. 2003)	Sensitized Emission
Fluorescein	Carboxytetramethyl-rhodamine (TAMRA)	DDM+SDS mixed micelles	54 A°	Glycophorin A (Anbazhagan et al. 2010)	Donor Quenching
Tyrosine57	Tryptophan10 Tryptophan12	DOPC vesicles and SDS micelles	13.2 A° 9 A°	Bacteriorhodopsin (Renthal et al. 2011)	
4-chloro-7-nitrobenzofurazan (NBD)	Rhodamine	SDS micelles DMPC vesicles	50 A°	EphA1 receptor (Artemenko et al. 2008)	Donor Quenching
Fluorescein Isothiocyanate (FITC)	Rhodamine	SDS micelles	55 A°	IRE1α (Cho et al. 2012)	Donor Quenching
DANS-chloride	DABS-chloride	SDS micelles	Not used	Major coat protein (Melnyk et al. 2002)	Donor Quenching
DANS-chloride	DABS-chloride	SDS micelles	Not used	ANTRX1 (Go et al. 2006)	Donor Quenching
Carboxyfluorescein (FAM)	TAMRA	SDS micelles PFO micelles	Not used	Na,K-ATPase (Therien & Deber 2002)	Donor Quenching
7-hydroxycoumarin (Coum)	FAM/FITC	DPC micelles POPC vesicles	Not used	FtsB, FtsL (Khadria & Senes 2013)	Donor Quenching
7-hydroxycoumarin (Coum)	FITC	C_{14}Betaine micelles	Not used	CHAMP peptides (Yin et al. 2007)	Donor Quenching
DANS-chloride	DABS-chloride	SDS micelles	Not used	Model Ai_{pep} (Johnson et al. 2004)	Donor Quenching
DANS-chloride	4-(diethylamino)-phenylazobenzene-4-sulfonyl (DPBS) chloride	DHPC vesicles	39 A°	Gramicidin A (Veatch & Stryer 1977)	Donor Quenching
DANS-chloride	DABS chloride	DMPC vesicles	40 A°	Glycophorin A (Adair & Engelman 1994)	Donor Quenching
Fluorescein	TAMRA	DMPC, diC(14:1)PC, diC(16:1)PC, diC(18:1)PC, diC(20:1)PC, diC(22:1)PC	49-54 A°	Glycophorin A (Anbazhagan & Schneider 2010)	Donor Quenching
Fluorescein	Rhodamine	POPC vesicles	55 A°	Fibroblast growth factor receptor (FGFR3)-TM (You et al. 2005)	Donor Quenching
Cy3	Cy5	POPC vesicles	55 A°	FGFR3-TM (You et al. 2005)	Donor Quenching
Fluorescein	Rhodamine	POPC,POPG,POPS vesicles	56.1 A°	FGFR3-TM mutants (Li et al. 2006; You et al. 2006)	Donor Quenching
BODIPY-fluorescein	Rhodamine	POPC,POPG,POPS vesicles	56.3 A°	FGFR3-TM ACH mutant (Li et al. 2006; You et al. 2006; Merzlyakov et al. 2006)	Donor Quenching
Fluorescein	Rhodamine	POPC vesicles	56 A°	FGFR3-TM, Pathogenic Cys mutants (Merzlyakov et al. 2007; You et al. 2007)	EmEx-FRET (Merzlyakov et al. 2007), Donor Quenching(You et al. 2007)
EYFP	mCherry	CHO cell membrane derived vesicles	53 A°	Glycophorin A (Chen et al. 2010)	EmEx-FRET (QI-FRET)
EYFP	mCherry	CHO, HEK293T and A431 cell membrane derived vesicles	Not used	Glycophorin A (Sarabipour & Hristova 2013)	EmEx-FRET (QI-FRET)
EYFP	mCherry	HEK293T cell membrane derived vesicles	Not used	FGFR3-TM & ACH mutant (Placone & Hristova 2012)	EmEx-FRET (QI-FRET)
EYFP	mCherry	CHO cell membrane derived vesicles	53 A°	ErbB2 TM & oncogenic mutant (Placone et al. 2014)	EmEx-FRET (QI-FRET)
Fluorescein	Rhodamine	DLPC, POPC vesicles	55 A°	M2 (Schick et al. 2010)	Donor quenching
Fluorescein	Rhodamine	DPC micells	~50 A°	major histocompatibility complex chains MHC and MHC (King & Dixon 2010)	Donor quenching

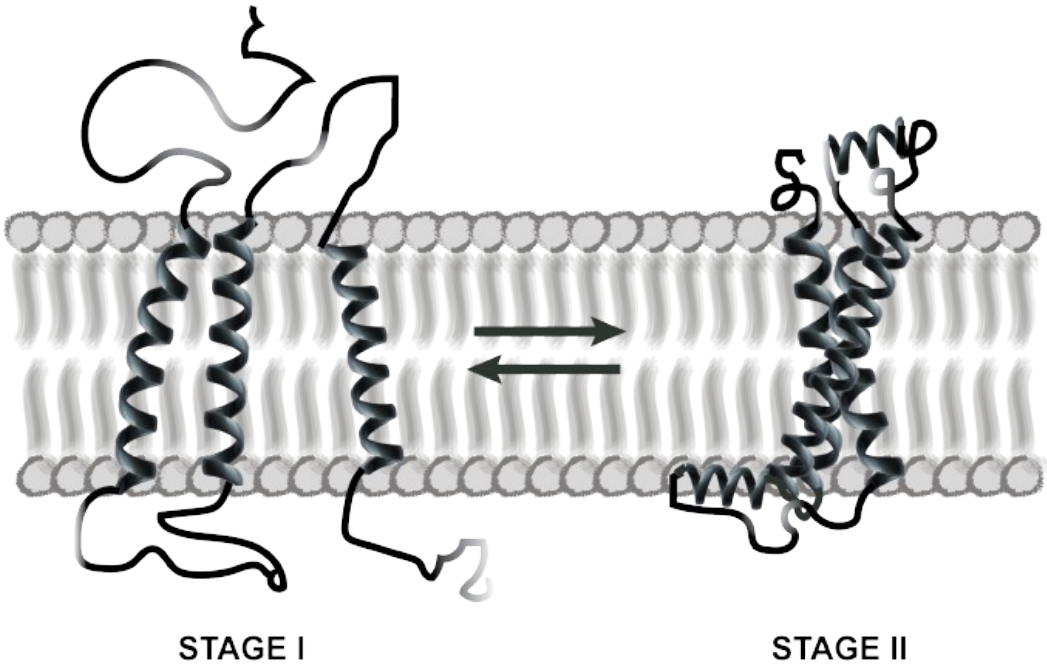

Figure 1.1. The Two Stage Model of membrane protein folding. Stage I represents insertion of individual transmembrane helices into the lipid bilayer, and Stage II represents association of the individual helices to form the final folded tertiary structure. (Figure inspired from (Popot & Engelman 1990))

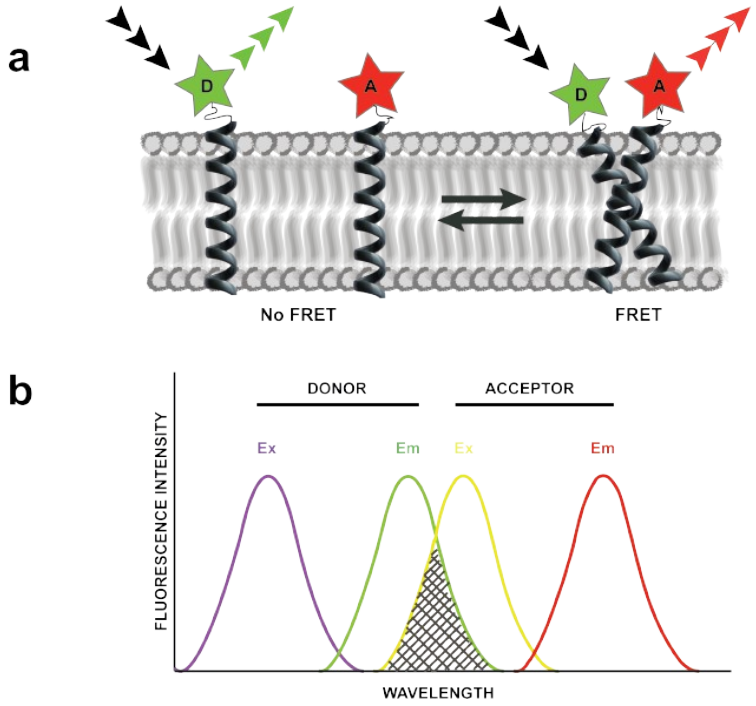

Figure 1.2. FRET as a tool to study transmembrane protein interactions. (a) *TM helices in a lipid bilayer, labeled with donor (green) and acceptor (red) fluorophores*. The fluorophores exhibit FRET upon TM helix-helix association, as observed by acceptor emission (red arrows) upon exciting the donor (black arrows). If the TM helices do not associate, then excitation of the donor yields donor emission (green arrows). (b) *Depiction of the excitation and emission spectra of a FRET pair*. FRET occurs when the emission spectrum of the donor (green curve) overlaps with the excitation spectrum of the acceptor (yellow curve) with a good overlap integral denoted by the gray shaded area. A good FRET pair has a notable spectral overlap with minimal bleedthrough of the acceptor's excitation into the donor excitation wavelength (overlap of the violet and yellow spectra), and minimal emission of the donor in the acceptor emission wavelength (overlap of the green and red spectra). Colors of the spectrum are a depiction of the increasing wavelength of light.

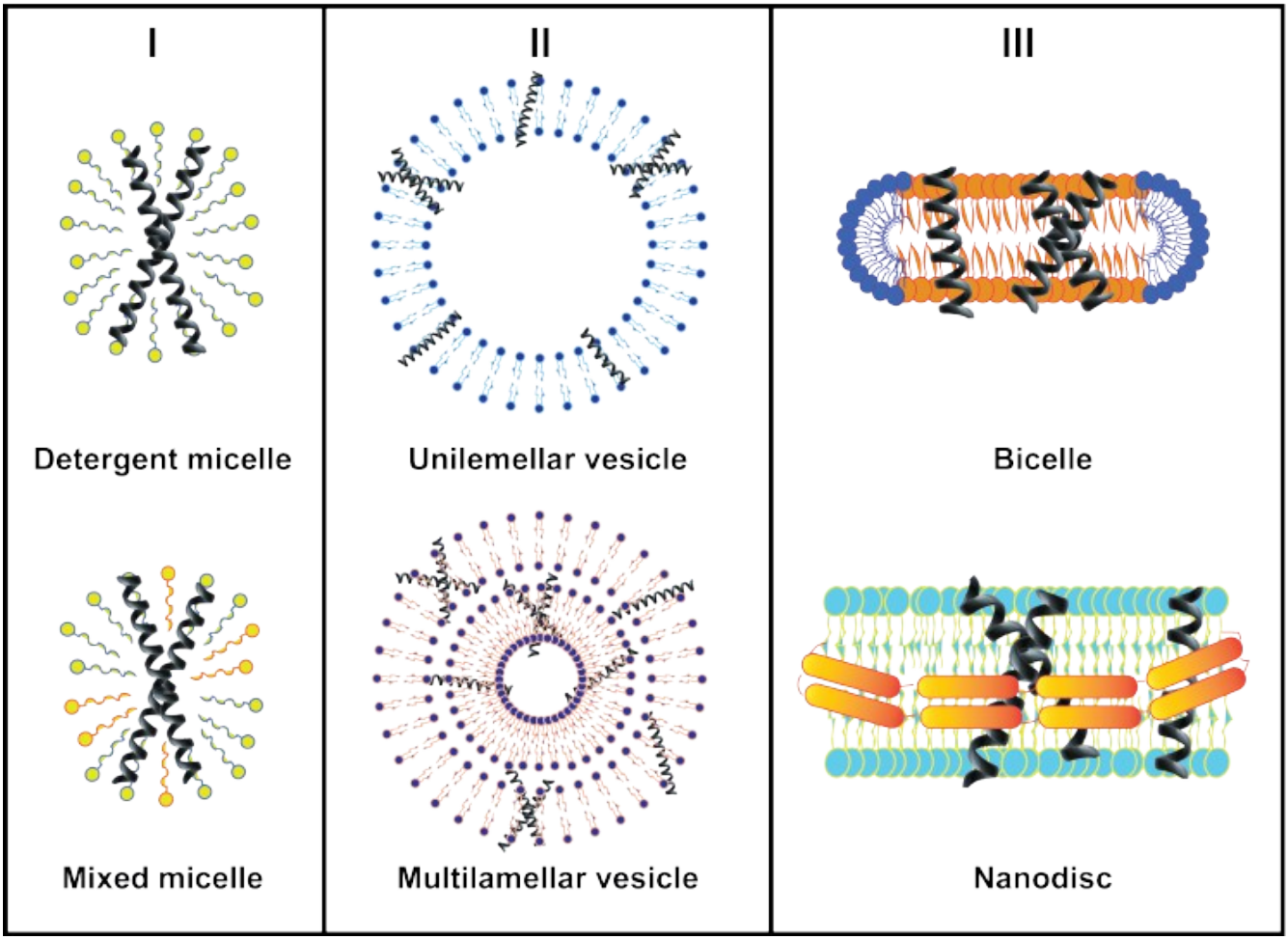

Figure 1.3. Artificial environment representations for membrane protein solubilization. (I) TM helices incorporated in detergent micelles made of the same (top) or different detergents to form mixed micelles (bottom). (II) Lipid bilayers in the form of unilamellar (top) or multilamellar (vesicles) demonstrating equilibrium between monomeric and associated TM peptides. (III) Hybrid environments made of different types of lipids to form smaller structures like bicelles (top) and lipids with membrane scaffolding protein (bottom) to form nanodiscs. *Figures not drawn to scale.*

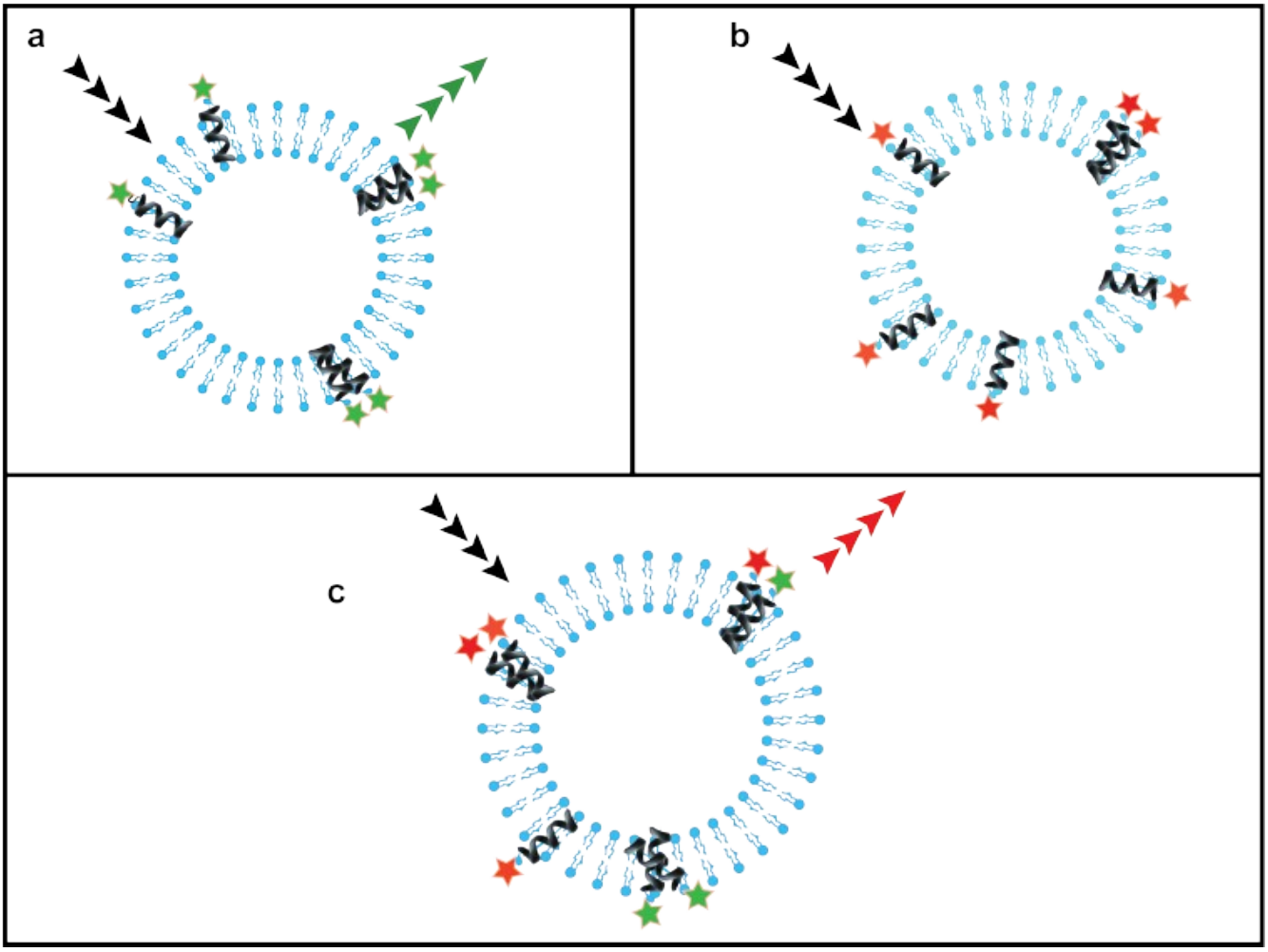

Figure 1.4. Representative vesicles with labeled TM peptides in samples of a FRET experiment. Peptides exist in a monomer-dimer (in this figure) equilibrium (a) '*Donor Only' sample*: Peptides labeled with donor fluorophores are excited with donor excitation wavelength (black arrow) and exhibit donor fluorescence (green arrow). (b) *'Acceptor Only' sample*: Peptides labeled with acceptor fluorophores are excited with donor excitation wavelength (black arrow) and show no red fluorescence (minimal spectral bleedthrough). (c) *'FRET sample'*: Peptides with equilmolar donor:acceptor peptide ratio, with the same total peptide:lipid ratio are excited with donor excitation wavelength (black arrow), and exhibit acceptor fluorescence (red arrow) due to FRET arising from TM peptide association. Also shown are the different possible 'no-FRET' dimers.

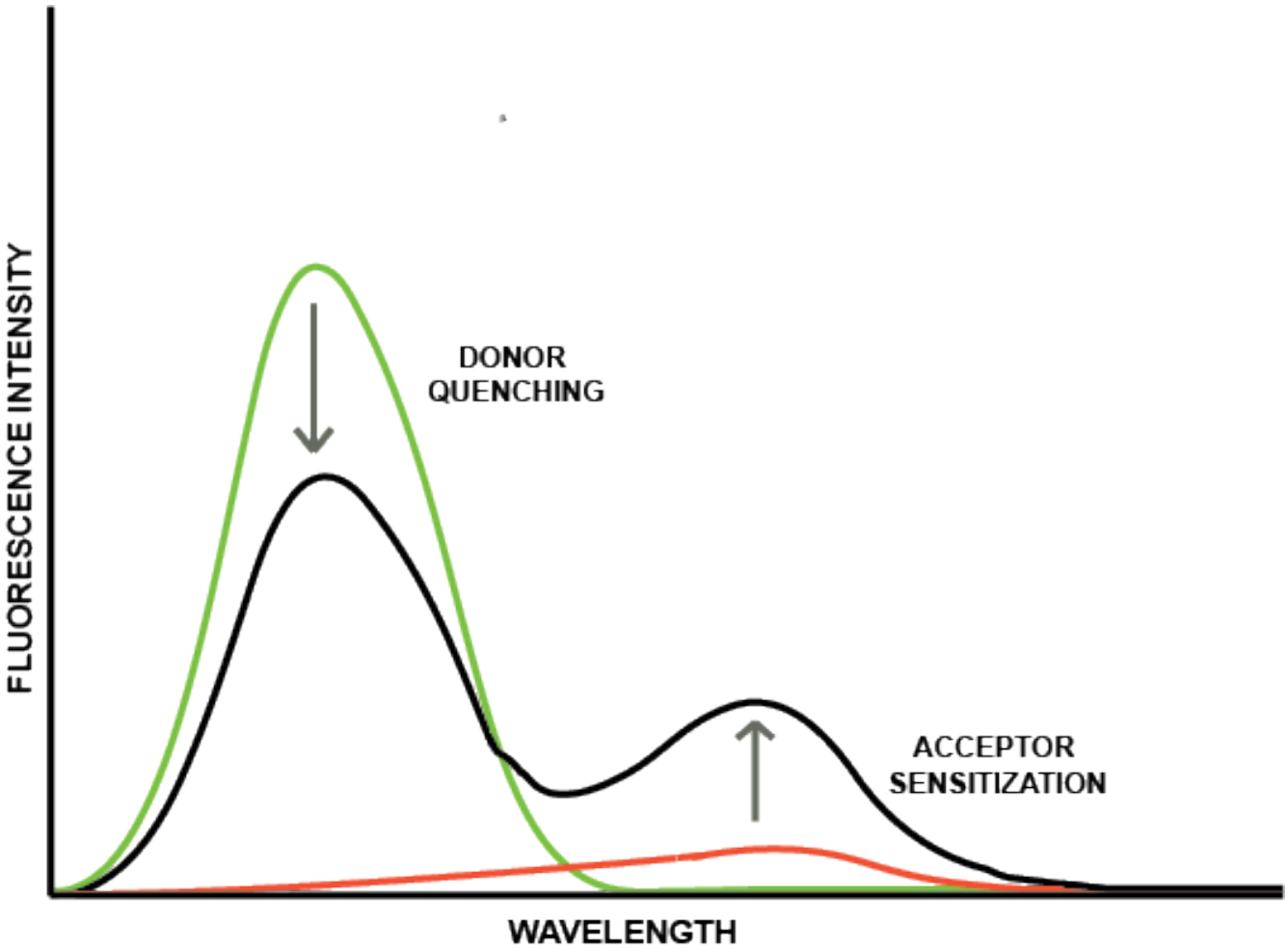

Figure 1.5. Representation of different ways to calculate FRET efficiency. Green curve is a spectrum of the 'donor only' sample, representing the donor emission spectrum at the donor's excitation wavelength. Red curve is a spectrum of the 'acceptor only' sample, representing the acceptor emission spectrum from direct excitation of the acceptor at the donor's excitation wavelength (due to spectral bleed-through of the acceptor's excitation spectrum into the donor's excitation spectrum). Black curve is an emission spectrum of the 'FRET sample' containing a mixture donor and acceptor samples, excited at the donor's excitation wavelength. FRET efficiency can be calculated either by monitoring the decrease in the donor's emission intensity (indicated by downward arrow) or by monitoring the increase in the acceptor's emission intensity (indicated by the upward arrow).

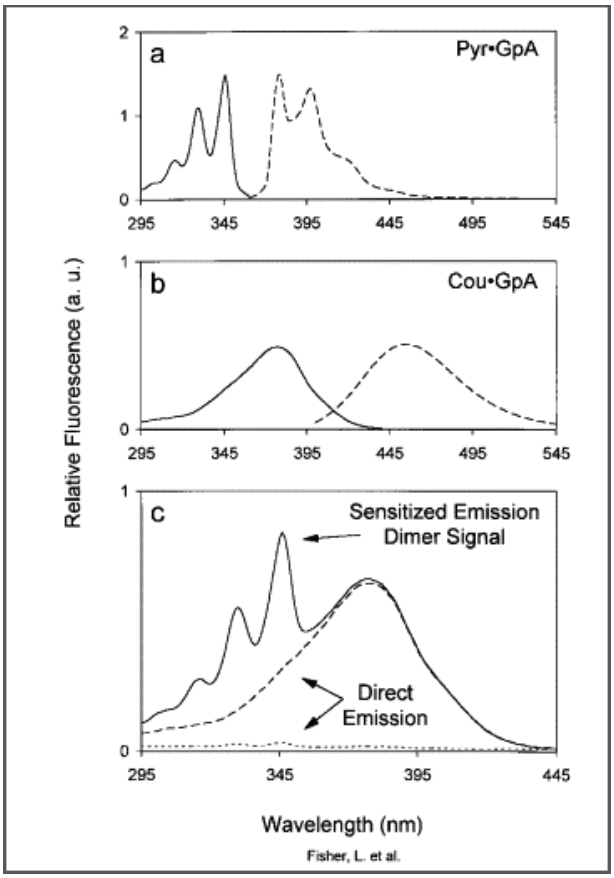

Figure 1.6. Demonstration of Sensitized Emission using pyrene and coumarin labeled peptides (Fisher et al. 1999)**.** Fluorescence spectra shown are that of Glycophorin A (GpA) peptides labeled with pyrene (donor) and coumarin (acceptor), in DDMAB detergent. (a) Pyr-GpA: Excitation spectra (—) at 378 nm emission wavelength and emission spectra (– – –) at 345 nm excitation wavelength. (b) Cou-GpA: Excitation spectra (—) at 460 nm emission wavelength and emission spectra (– – –) at 378 nm excitation wavelength. (c) At 500 nm emission wavelength, the excitation spectrum of a 'Donor only' sample (- - -), an 'acceptor only' sample (– – –), and a 1:1 donor:acceptor 'FRET sample' (—) was recorded. Sensitized emission was observed by an increased intensity of the Pyr-GpA (donor) excitation spectrum in the 'FRET sample' compared to that in the 'donor only' sample. Cou-GpA (acceptor) spectrum was unaltered between the 'acceptor only' and the 'FRET sample'.

CHAPTER TWO

Measurement of transmembrane peptide interactions in liposomes using Förster Resonance Energy Transfer (FRET)

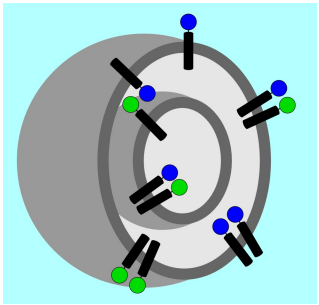

Based on:

Khadria, A. & Senes, A., 2013. Measurement of transmembrane peptide interactions in liposomes using Förster resonance energy transfer (FRET). Methods in Molecular Biology, 1063, pp.19–36

Summary

Present day understanding of the thermodynamic properties of integral membrane proteins (IMPs) lags behind that of water-soluble proteins due to difficulties in mimicking the physiological environment of the IMPs in order to obtain a reversible folded system. Despite such challenges faced in studying these systems, significant progress has been made in the study of the oligomerization of single span transmembrane helices. One of the primary methods available to characterize these systems is based on Förster Resonance Energy Transfer (FRET). FRET is a widely used spectroscopic tool that provides proximity data that can be fitted to obtain the energetics of a system. Here we discuss various technical aspects related to the application of FRET to study transmembrane peptide oligomerization in liposomes. The analysis is based on FRET efficiency relative to the concentration of the peptides in the bilayer (peptide:lipid ratio). Some important parameters that will be discussed include labeling efficiency, sample homogeneity and equilibration. Furthermore, data analysis has to be performed keeping in mind random colocalization of donors and acceptors in liposome vesicles.

Introduction

Free energy measurements of transmembrane (TM) helix association in single and multispan membrane proteins are important to understand the mechanisms behind vital cellular processes such as membrane protein folding and signal processing (Popot & Engelman 1990). However, research in the field of integral membrane proteins has considerably lagged behind in comparison to that of soluble proteins (MacKenzie & Fleming 2008). This is due to the difficulty in obtaining experimental systems that match the nature of the complex native environment, the bilayer, and conditions in which reversible association/unfolding can be established. Moreover, since the unfolded state of membrane proteins retains considerable amount of helical component (Popot & Engelman 1990) (in opposition to soluble proteins where the unfolded state largely lacks a secondary structure), monitoring unfolding is a significant challenge.

To overcome these challenges, a strong focus has been applied toward a more approachable folding problem – the oligomerization of single-pass TM domains – a problem that retains the core process that is important for the folding of membrane proteins, the association of the transmembrane helices. Several biophysical tools have been developed to measure TM helix associations in a number of environments, from detergent micelles to lipid vesicles and even biological membranes. Analytical ultracentrifugation (AUC) , Förster Resonance Energy Transfer (FRET) and Thiol Disulfide Exchange (MacKenzie & Fleming 2008; You et al. 2005; DeGrado et al. 2003) are biophysical methods that are suitable for measuring the association of TM peptides in artificial environments. Genetic methods based on the conditional expression of a reporter gene such as TOXCAT (Russ & Engelman 1999) and GALLEX (Schneider & Engelman

2003), are useful for measuring homo and hetero-association of TM helices in the natural inner membrane of *Escherichia coli*.

In this chapter we focus on FRET-based studies of TM association in artificial liposomes. FRET involves excitation of the ground electronic state of a donor molecule followed by non-radiative transfer of energy from the excited state of the donor to an appropriate acceptor. Since FRET occurs only when two suitable fluorophores (a donor and and acceptor molecule) are located within ~10 nm of each other, it can be used as a measure of molecular proximity (Popot & Engelman 1990; DeGrado et al. 2003; Li et al. 2005). The two fluorophores must have a significant spectral overlap between the emission spectrum of the donor and the excitation spectrum of the acceptor, a sufficiently high quantum yield, and a favorable dipole–dipole orientation **(Figure 2.1)**. When the fluorophores come in close proximity, energy is transferred non radiatively, resulting in quenching of donor fluorescence and increase (sensitization) in acceptor fluorescence.

In the case of TM helix-helix interactions, each peptide is labeled with either a donor or an acceptor molecule, and they are solubilized in artificial hydrophobic environments like detergents and lipids. Because TM peptides are insoluble in water and only experience the 'hydrophobic volume' of the solution, their concentration is expressed as mole fraction, i.e. the number of moles of peptide relative to number of moles of the “true solvent” (detergent or lipid), yielding a peptide:detergent or peptide:lipid ratio. In addition to mole fractions, the second parameter that is often varied in a typical FRET experiment is the relative percentage of the donor and acceptor labeled peptides, which can help determining the of specific oligomeric state (i.e. dimer, trimer, etc.) of the system being studied (Li et al. 1999). Once a donor/acceptor system has been equilibrated, the FRET efficiency can be calculated by monitoring the degree of donor quenching in the presence of acceptor (as

discussed in this chapter), or by monitoring the increase in acceptor emission. Spectral overlap between the donor and acceptor also causes contamination of the FRET signal due to Acceptor Spectral Bleedthrough, which refers to direct excitation of the acceptor by radiation at the donor excitation wavelength **(Figure 2.2).** This must be subtracted from the acceptor emission intensity in the FRET samples while calculating FRET efficiency using acceptor sensitization (not used in this chapter).

FRET has been shown to yield association energetics in TM peptides in detergents (Fisher et al. 1999) as well as lipids (You et al. 2005; Li et al. 2005). It can also be used for studying hetero-oligomers in which cases the calculations are applied taking into account the various possible equilibria present in the system. This chapter discusses the experimental procedure to measure helix-helix *self* association in lipid vesicles and the relationship between mole fraction and FRET efficiency to calculate the association of affinity. An outline of the sample preparation techniques, including solid phase peptide synthesis, labeling technique, HPLC purification and MS characterization, is presented. This is followed by a detailed description of the FRET experimental layout and data collection. In addition, there is a discussion of possible challenges faced in data interpretation due to false positives and false negatives that can arise from adventitious interactions in vesicles (Popot & Engelman 1990; Li et al. 2005; Yevgen O. Posokhov n.d.), inefficient labeling efficiency of the molecules (Posokhov et al. 2008), or light scattering.

Materials

- ***Solid-phase peptide synthesis***

- Automated peptide synthesizer
- Amino acids
- Resin : Fmoc-PAL-PEG
- Activator : 2-(1H-7-Azabenzotriazol-1-yl)--1,1,3,3-tetramethyl uronium hexafluorophosphate methanaminium (HATU)
- Base : N-methylmorpholine (NMM)
- Deprotecting agent : 20% Piperidine
- Solvent : Dimethylformamide (DMF), Dichloromethane (DCM), 1-methyl-2-pyrrolidone (NMP)

- ***N-terminal labeling with fluorophores.***

- Fluorophore for solid phase coupling
- Solvent : DMF, NMP
- Base : N,N-Diisopropylethylamine (DIPEA)
- Activator : Benzotriazol-1-yl-oxytripyrrolidinophosphonium hexafluorophosphate (PyBOP) or 7-Azabenzotriazol-1-yloxy)tripyrrolidinophosphonium hexafluorophosphate (PyAOP)

- ***HPLC purification and Mass Spectrometry (MS)***

- Reversed phase semi-preparative and analytical column

- HPLC instrument
- Solvents: Acetonitirile, Isopropanol, water, Trifluoroacetic acid (TFA)
- Lyophilizer maintained below -80 ºC
- Glassware: glass screw cap vials, pear-shaped glass flask
- Compressed N_2 gas
- Mass spectrometry facility

- ***Solubilization of TM peptides in lipids and FRET measurements***

- Solvents: Hexafluoroisopropanol (HFIP), Chloroform, Trifluoroethanol (TFE)
- 1-palmitoyl-2-oleoyl-sn-glycero-3-phosphocholine (POPC) lipid (Avanti Polar Lipids)
- Purified TM peptides
- Compressed N_2 gas
- Liposome buffer (10 mM Sodium Phosphate Buffer, 500 mM NaCl, pH 7.0)
- Dry ice, acetone, 37 ºC water bath
- Glass screw cap vials
- UV/Vis spectrophotometer, quartz cuvettes
- Plate reader or Fluorimeter (If using a plate reader, the plate reader should contain a monochromator, such as the Tecan M1000 which provides for a Fluorescence intensity scan instead of point measurements from fixed emission wavelength filters).

Methods

- ***Fmoc solid-phase peptide synthesis***

1. Review the amino acid sequence of the peptide/peptides of interest, adding positively charged Lys residues to increase aqueous solubility of the highly hydrophobic sequence (See Note 1) (Rath & Deber n.d.)
2. Decide the scale of synthesis and the resin to be used (See Note 2). Weigh the calculated amount of resin, use the appropriate solvent (DMF/NMP) and activator (HATU) and set up the automated synthesis. A review of solid-phase peptide synthesis should be consulted for standard protocols and optimizations (See Note 2) (Amblard et al. 2005)
3. Take the resin containing the completed peptide, check for correct sequence by MS (See Note 3), and then proceed with on-resin N-terminal labeling of the peptide with the fluorescent dye (See Note 4).

THIS STEP ONWARD, PERFORM ALL EXPERIMENTS PROTECTED FROM LIGHT, TILL THE END OF THE CHAPTER.

- ***N-terminal labeling with fluorescent dye***

1. Divide the resin with peptide in half and proceed with two separate manual N-terminal couplings using donor and acceptor fluorescent dyes comprising a good FRET pair. If the dye is not carboxylic acid derviatized to enable Fmoc chemistry on a deprotected amine group, then an appropriate linker is attached to the amine group first (e.g, aminohexanoic acid, mini-PEG etc), followed by attachment of the fluorescent dye.

2. Use DMF and NMP as solvents, and PyBOP/PyAOP as activators using the protocol optimized for hydrophobic sequences (Stahl et al. 2012). (See Note 5)
3. Cleave the labeled peptide, precipitate using cold ether and dry it under a stream of compressed N_2 gas with agitation by a glass rod.
4. Blanket the peptide with a stream of N_2 or Ar, seal the cap with parafilm and store it at -20 ºC.

- ***Reversed phase HPLC purification***

1. Solubilize a small amount of the peptide in the appropriate solvent for HPLC purification. (See Note 6). Blanket the rest of the peptide with a stream of N_2 or Ar, seal the cap with teflon and store it in -20 ºC.
2. Filter the sample with a 0.22 um filter.
3. Using the appropriate column for use, inject the sample, and follow a gradient of 2% to 100% Buffer B in 98 minutes (1% per minute). Monitor the chromatogram at 280 nm if Trp or Tyr is present and at the wavelength of the fluorescent dye. (See Note 7)
4. Collect the various fractions, and analyze them using MS to identify the peak of interest. (See Note 7)
5. Optimize the gradient to achieve better separation and collection of individual peaks. (See Note 8)
6. Perform multiple HPLC runs using the same method, and pool in the desired fractions from the various runs in a glass pear-shaped flask of appropriate volume such that the total volume doesn't exceed a third of the flask.

7. Flash-freeze the sample in the flask, rotating it over liquid N_2 with a tilt to increase the surface:volume ratio for better lyophilization. Attach it to the lyophilizer, cover it with foil and leave it overnight till it forms a dry powder.
8. Take the flask out of the lyophilizer, and empty its contents into a pre-weighed glass vial with screw cap. Weigh the vial with the sample in it and note the weight of the final sample.

- ***Solubilization of peptides and lipids to make stock solutions***

1. Dissolve 1 mg of powdered POPC lipid (Avanti Polar lipids) in 1 ml of 1:1:1 HFIP:Chloroform:TFE in a screw cap glass vial and keep it tightly sealed. Calculate the number of moles/ µL according to **Scheme 2.1**.
2. Turn on the spectrophotometer, and set up the method for protein concentration scan including the absorbance wavelength of Trp (280 nm) and that of the fluorescent dyes.
3. Perform a blank scan with 1:1:1 HFIP: Chloroform: TFE (solvent).
4. Scoop out a tiny amount of donor labeled peptide and add it to 100 µL of the solvent. Label this as 'stock 1'.
5. Make a 1:10 dilution of stock 1 (call it stock 2) and add it to the appropriate cuvette for protein concentration scan. (See Note 9)
6. Calculate concentration of the peptides and the labeling efficiency according to **Scheme 2.2**. (See also *Discussion* section).
7. Repeat steps 4 to 6 for the acceptor labeled peptide.

- ***Setup of the peptide:lipid ratios for FRET***

  The goal of this experimental setup is to achieve a large concentration range of peptide, or a range of peptide:lipid ratios which spans the spectrum from a 'no FRET' sample to a 'maximum FRET' sample. Since liposomes, unlike detergent micelles, do not 'communicate' with other liposomes to exchange peptide molecules, titrating the solution with more lipid will not change the effective mole fraction of the peptides in the liposomes. Thus to obtain sufficient number of data points for an accurate curve fitting to obtain the energetics of the system, samples spanning a wide range of peptide:lipid ratios have to be prepared in separate tubes. Lipids can be equilibrated to form multilamellar vesicles (MLVs) as described later. It has been shown that FRET efficiencies for helix-helix interactions in large unilamellar vesciles (LUVs) are comparable to that of MLVs, and thus this protocol follows setting up FRET interactions in MLVs (You et al. 2005).

1. Once the peptide stocks for donor and acceptor labeled peptides and the lipid stocks are ready, start labeling small 12x35 mm screw cap vials for the FRET experiments.
2. Cover the labeling on the tubes with a tape to prevent the labels from being washed away by acetone in the dry-ice bath used in future steps.
3. From the peptide stock solutions, calculate the volume required for 50 pmoles of the donor and acceptor labeled peptides. (See Note 10).
4. Take a corning black 96 well plate, and add the required volume for 50 pmoles of the donor peptide, say 8.9 µL, into one well. If the well volume is

75 µL, add 75 – 8.9 = 66.1 µL of liposome buffer into it and mix by pipetting up and down a few times. In another well, do the same for the acceptor peptide. In a third well, add 75 µL of liposome buffer only.

5. Take the plate to the plate reader, and run two separate fluorescence scans – one spanning the absorbance spectrum of the donor and another of the acceptor (See Note 11).
6. For the 'donor only' well, set the excitation maximum wavelength of the donor such that there is maximum overlap between the donor emission and acceptor excitation spectrum. If the emission spectrum looks noisy, try changing the parameters of the instrument (gain, PMT voltage, slit width etc.), or increase the amount of peptide to get a smooth signal. The goal is to achieve a high enough concentration of the peptide for good signal to noise ratio (See Note 12).
7. Again, for the 'acceptor only' well, set the same excitation wavelength used in step 6. This step is to test for spectral bleedthrough between the donor and acceptor pairs. A minimal emission peak at the acceptor emission maxima on being excited by the donor excitation maxima is a sign of a good FRET pair.
8. Perform both steps 5 and 6 for the 'liposome buffer' well. This sample serves as a blank for data analysis.
9. At this point, start making the peptide:lipid ratio calculations. An example of the volumes is given in **Table 2.1**, based on the example in the section '***Solubilization of peptides and lipids to make stock solutions****, step 4*.
10. Pipette these solutions into the small glass screw cap vials arranged in

increasing peptide:lipid ratio on a vial rack and briefly pipette up and down to mix them **(Figure 2.3a).**

11. Take each vial in a fume hood and slowly evaporate the solvent using a light stream of compressed N_2 gas till all the solvent has evaporated, leaving a thin whitish lipid film at the bottom/sides of the vial **(Figure 2.3b)**. (See Note 13)
12. Don't screw the caps on the vials. Cover the tray with vials with aluminium foil to protect it from light, and pierce holes on the foil at the mouth of each vial.
13. Place the covered tray inside a vacuum dessicator overnight. (See Note 14)
14. The next day, add 75 µL (or 100 µL depending on the volume of the wells in the plate, or the cuvette of the fluorimeter) of liposome buffer into each vial, screw its cap on tightly and vortex vigorously for about a minute **(Figure 2.3c)**. The samples with higher lipid will turn more turbid. Note the extent of turbidity in these samples.

- ***Preparation of Multilamellar lipid vesicles (MLVs) using freeze-thaw cycles***

1. Prepare a dry ice/acetone bath and a water bath set at 37 ºC
2. Place the tray with vials on the dry ice/acetone bath for about 1 minute. Make sure all the samples are frozen, and the labels aren't getting washed off.
3. Now place the tray on the water bath, shaking them mildly. A crackling sound will signify thawing of the liquids. Continue thawing till the sound subsides.
4. Repeat steps 2-3 alternately for 2-3 cycles.

5. Now note the turbidity of the samples again. Decrease in turbidity signifies formation of multilamellar vesicles (Note 15). At this point, the donor and acceptor peptides should have equilibrated with the lipid and with each other based on their affinity and the peptide-to-lipid ratio **(Figure 2.3d)**.
6. Pipette out the samples from the vials into a 96 well corning plate according to **Table 2.1**. Do not pipette up and down to avoid formation of air bubbles in the sample as they can lead to light scattering effects.

- ***Measurement of FRET and data analysis***

1. Take the plate to the plate reader, insert the plate and adjust the settings for the plate (or alternatively use a fluorimeter).
2. Set the excitation wavelength as the excitation maxima for maximum spectral overlap for the pair, and collect the fluorescence emission scans spanning the emission wavelengths of both the donor and acceptor fluorophores. Maintain the same scan for each sample.
3. The 'Control' samples in **Table 2.1** serve as the “no FRET' controls for their corresponding sample row. For instance, Row 1 in **Table 2.1** has a 1:100 peptide-to-lipid ratio where there are 50 pmoles of donor and acceptor each. Control 1 therefore has 50 pmoles of the donor only, with the same amount of lipid as Row 1 sample.
4. Calculate percent FRET, *E(%)*, by the wavelength of the emission maximum of the donor in the absence and presence of the acceptor according to **Scheme 2.3**.

Discussion

A lot of factors need to be taken into account for accurate FRET intensity measurements. One of the most important factors is the labeling efficiency of peptides. Hydrophobic peptides pose a greater level of difficulty for their labeling and purification, and alternative methods for labeling have been discussed (Stahl et al. 2012). Once this step has been optimized, the next level of difficulty arises in accurate quantification of these peptides. An unlabeled peptide is commonly quantified using uv/vis spectrophotometry where the Trp and Tyr absorbance at 280 nm is measured and protein concentration determined using Beer's law. In the case of a labeled peptide, the absorbance of the peptide sample at 280 nm comprises of three components -

1. Trp/Tyr absorbance of labeled peptide.
2. Trp/Tyr absorbance of unlabeled peptide.
3. Absorbance of the dye at 280 nm.

Thus its important to differentiate the individual components for accurate quantification. This is done using the 'Correction Factor of the dye', and the labeling efficiency of the peptide **(Scheme 2.2)**. However, to be able to use the calculations in **Scheme 2.2**, another important parameter needs to be established, the molar extinction coefficient, $\varepsilon_{Fluorophore}$ *in the given solvent system*. Vendors selling dyes usually provide the molar extinction coefficient values of dyes at their A_{max} in an aqueous buffer at a particular pH. But these values of $\varepsilon_{Fluorophore}$ and A_{max} significantly change (**Figure 2.4)**. For accurate determination of equimolar ratios of the peptides, it is very important to characterize the behavior of the fluorophores in the solvent system being used. This can be done by plotting a calibration curve of the A_{max} of the dye in the given solvent versus concentration.

Sometimes it is difficult to dissolve a known amount of dye in the organic solvent at a measurable concentration. In that case it is advisable to make the stock solution in a buffer that it has been characterized in, and then use the provided molar extinction coefficient and λ_{max} values to calculate the stock concentration. One should make this concentration high enough such that a very small volume can be used to dilute into the organic solvent to obtain the calibration curve. Then serial dilutions should be made to obtain samples of known concentration in organic solvent, absorbance scans should be taken **(Figure 2.5**) and A_{max} of the dye in that solvent versus concentration should be plotted **(Figure 2.5 inset**). The slope of the curve will provide for the $\varepsilon_{Fluorophore}$ at the new λ_{max} of the dye in the organic solvent. Once the behavior of the dye has been characterized in the given solvent in this manner, the concentration and labeling efficiency of the peptide can be calculated according t**o Scheme 2.2** and utilized in **Scheme 2.3** to calculate the FRET efficiency values.

Apart from labeling efficiency, another contributor towards the observed FRET intensity is random colocalization due to proximity of donors and acceptors, which needs to be subtracted from the steady state FRET observed. Depending on the level of quantification necessary for the experiment at hand, there are several ways by which this can be taken into account (Wolber & Hudson 1979; Wimley & White 2000). The peptide pairs that will be forming in a self-associating system of TM peptides will be the random proximity pairs, *DA*, *DD*, *AA*, *DU*, *AU* and *UU* (where *D* is donor labeled peptide, *A* is acceptor labeled peptide and *U* is unlabeled peptide). **Figure 2.3e** shows a schematic representation of the possible pairs. Finally, once all these parameters have been characterized, the FRET efficiency can be calculated according to **Scheme 2.3**. Contributions of proximity and sequence dependent association to FRET efficiency can be distinguished by spiking the

existing donor-acceptor labeled samples with unlabeled peptide at the time of preparation. If the FRET efficiency is primarily due to sequence dependent association, then addition of unlabeled peptides will lead to a decrease in the FRET efficiency (You et al. 2005; Li et al. 2005).

For a homodimer, the FRET efficiency, a measure of association, **(Scheme 2.3, Eq. (2))** is calculated according to **Scheme 2.3, Eq. (1)**, and the data is fitted to a curve using **Scheme 2.3, Eq. (3)** to yield the association constant and the free energy values (You et al. 2005; Li et al. 2005).

Notes

Lysine tags increase solubility and decrease peptide aggregation in hydrophobic sequences by providing for unfavorable electrostatic interactions (Rath & Deber n.d.). The number of Lys residues incorporated and their positioning varies depending on the TM peptide sequence, and a detailed description of this optimization can be found in (Rath & Deber n.d.). Addition of extra amino acids will also provide for a flexible linker between the peptide and the dye with which it will be labeled. It is important, however, to make sure that the linker length keeps the fluorophores within the limit of their Förster radius in all orientations.

1. It is advised to begin with a smaller scale of synthesis as hydrophobic peptides usually need some optimization of the protocol for synthesis. A 25 μmole scale is a good starting point, and is enough for preliminary experiments. Choice of resin is important – a low load resin (e.g. Fmoc PAL-PEG resin from Applied Biosystems, with a 0.18 mmol/g loading capacity) will decrease aggregation potential of the peptides on the resin. After an assessment of the hydrophobicity of the final sequence, a 'brute force' method can be applied for the preliminary trial. For instance, in a Val-Val- Thr- Ala-His sequence, the difficult couplings are Val-Val, Val-Thr and Thr-Ala. For these couplings, one could use double or triple coupling and extended coupling times, whereas for the Ala-His coupling, a single coupling should suffice. This approach has been utilized before (Fisher & Engelman 2001) and is found to be effective for particularly hydrophobic sequences.

2. CHCA (4-Chloro-α-Cyanocinnamic Acid) is one of the best universal matrices for performing MALDI-TOF in peptides (Leszyk 2010). Typically a barely visible amount of peptide is dissolved in about 100 µL of Acetonitrile in water (percentage depending on solubility). The matrix is prepared as follows: 10 mg of CHCA matrix in 1 ml of 50:50 Acetonitrile:water with 0.1% TFA. Then various ratios of the matrix:peptide solutions are made and 1-2 µL of the final samples are spotted on the target for MALDI-TOF analysis.
3. For FRET, the peptide has to be labeled with a donor or acceptor molecule. In this procedure, the labeling will be done on the N terminus manually, on-resin, using commercially available carboxylated fluorescent dyes. An important point is to program the automated synthesis to terminate the the last coupling step before deprotection. This will keep the final N-terminal residue Fmoc protected and prevent unwanted reactions till the peptide is ready for labeling. Also, it is advisable that the peptide on resin remains solvated till the next step to reduce aggregation. Before proceeding with the labeling process, it is better to take out a tiny amount of the resin (a touch with the spatula), deprotect it and cleave it using standard procedures (Amblard et al. 2005), and then analyze it using MS. If the peptide has been synthesized correctly, deprotect the last amino acid on the enitre resin manually, and proceed with the labeling.
4. For quantitative FRET experiments, it is important to obtain high labeling yields of peptides, as the separation of the labeled from the unlabeled species in the case of hydrophobic peptides is difficult by HPLC (You et al. 2005; Li et al. 2005; Schick et al. 2010, p.2; Chen et al. 2009; Merzlyakov & Hristova 2008; You et al. 2007). Standard on resin N-terminal labeling yields have been found to be very

low for hydrophobic peptides, and thus a method for higher labeling efficiency of hydrophobic peptides was developed, utilizing larger amounts of dyes and coupling agents (Stahl et al. 2012).

5. Dissolve minimum amount of peptide (~0.5 mg) in minimum amount of DMF. If the peptide does not readily dissolve, try other solvents like HFIP, THF, TFE. Then slowly add water drop-wise, till the peptide just starts precipitating, turning slightly murky. It is important to have a high enough percentage of water in the solution (≥ 60%) for the peptide to bind the reverse phase column, but also maintain solubility of the peptide a the same time. If using TFA for solubilization, do not exceed the final TFA concentration to be above 5%.
6. The Reversed Phase HPLC system usually consists of an *n*-alkylsilica-based sorbent from which the solutes are eluted. The most commonly used *n*-alkyl ligand is C-18, but for hydrophobic peptides, C4, C8, phenyl and cyanopropyl ligands provide better separation (Aguilar 2012). It is good practice to first perform a blank run with 100% Buffer A till a stable baseline is obtained and then a blank run with the solvent the sample is dissolved in, before injecting the sample. Choice of columns for hydrophobic peptides varies and there are various parameters that can be changed for optimization. Usually a small volume (~10 µL) of the sample is injected into an analytical column first, and analyzed for the retention time of the sample elution with a linear gradient from 2% to 100% Buffer B (Acetonitrile with 0.1% TFA) over 30 minutes. For hydrophobic peptides which do not elute easily, sometimes using 60% Isopropanol in Acetonitrile with 0.1% TFA can be used for Buffer B.
7. If LC-MS facilities are available, it is better to perform a run on an analytical

column and monitor the masses of the peaks as the elute. The conditions can then be transferred to a semi-prep column having the same n-alkyl silica group for fraction collection.

8. Sometimes it is necessary to make higher dilutions of the initial stock solution of the peptide for accurate concentration determination. In that case, make serial dilutions till you get an absorbance value between 0 and 1, use the most diluted stock for concentration determination, and calculate the concentrations of the original stock by scaling up. Later in the experiment this stock will be used for solubilization with lipid and then involve evaporation of the solvents, and thus its easier to have a higher stock concentration to minimize the volume of solvent to be evaporated.
9. If the stock concentration of the peptide is 0.2 mg/ml and you have 500 µL of that solution, the concentration in terms of number of moles is 5.6 pmoles/ µL.Thus, to use 50 pmoles of peptide, use 50/5.6 = 8.9 µL of the stock solution. Calculate the stock concentration of each donor and acceptor labeled peptide in number of moles per microliter and start with a total of 100 pmoles of 1:1 peptide (donor:acceptor) to begin the peptide:lipid molar ratios.
10. A fluorimeter can also be used in place of a plate reader, and the sample volumes in that case have to be according to the the volume of the fluorimeter cuvette *(*~10-20 µL higher) than the cuvette volume to prevent the beam from hitting the meniscus of the solution leading to scattering. It has been shown that volume of the sample does not change the FRET efficiency as long as the amounts of lipid and peptide are the same (You et al. 2005)
11. It should be kept in mind that increasing the peptide amount will also mean

increasing the amount of lipid to maintain a peptide:lipid ratio. If the lipid concentration is too high, light scattering by the lipid will interfere with the FRET results, so a balance has to be achieved. For a true scattering control, use the same amount of unlabeled peptide in the highest amount of lipid being used in the experiment to check for any scattering.

12. It may take ~20 minutes for vials with higher volumes of solvent to evaporate. The higher the lipid content, the longer will it take to evaporate and the more visible will the lipid film be.
13. This step can also be substituted by adding the samples in a lyophilizer for 2-3 hours if the experiment has to be finished on the same day.
14. Freeze-thaw cycles are generally required for equilibration of buffers, salts, etc. MLVs, prepared by premixing the proteins and lipids in organic solvent and hydrating the mixture, are in equilibrium after a single freeze–thaw cycle (You et al. 2005). When thin lipid films are hydrated, stacks of liquid crystalline bilayers become fluid and swell as shown in **Figure 2.3c**. The hydrated lipid sheets detach during agitation and self-close to form MLVs preventing interaction of the hydrocarbon core of the bilayer from interacting with water at the edges. It has been shown that presence of unlabeled peptide helps in equilibration of the peptides in the lipids and leads to a faster decrease in turbidity upon just one freeze-thaw cycle .

References

Aguilar, M.-I., Reversed-Phase High-Performance Liquid Chromatography. In *HPLC of Peptides and Proteins*. New Jersey: Humana Press, pp. 9–22. Available at: http://www.springerprotocols.com/Abstract/doi/10.1385/1-59259-742-4:9 [Accessed December 15, 2012].

Amblard, M. et al., 2005. Fundamentals of modern peptide synthesis. *Methods in molecular biology (Clifton, N.J.)*, 298, pp.3–24.

Chen, L. et al., 2009. Energetics of ErbB1 Transmembrane Domain Dimerization in Lipid Bilayers. *Biophysical Journal*, 96(11), pp.4622–4630.

DeGrado, W.F., Gratkowski, H. & Lear, J.D., 2003. How do helix-helix interactions help determine the folds of membrane proteins? Perspectives from the study of homo-oligomeric helical bundles. *Protein science: a publication of the Protein Society*, 12(4), pp.647–665.

Fisher, L.E. & Engelman, D.M., 2001. High-Yield Synthesis and Purification of an α-Helical Transmembrane Domain. *Analytical Biochemistry*, 293(1), pp.102–108.

Fisher, L.E., Engelman, D.M. & Sturgis, J.N., 1999. Detergents modulate dimerization, but not helicity, of the glycophorin A transmembrane domain. *Journal of Molecular Biology*, 293(3), pp.639–651.

Leszyk, J.D., 2010. Evaluation of the New MALDI Matrix 4-Chloro-α-Cyanocinnamic Acid. *Journal of Biomolecular Techniques: JBT*, 21(2), pp.81–91.

Li, E., You, M. & Hristova, K., 2005. Sodium Dodecyl Sulfate−Polyacrylamide Gel Electrophoresis and Förster Resonance Energy Transfer Suggest Weak Interactions between Fibroblast Growth Factor Receptor 3 (FGFR3) Transmembrane Domains in the Absence of Extracellular Domains and Ligands†. *Biochemistry*, 44(1), pp.352–360.

Li, M. et al., 1999. A fluorescence energy transfer method for analyzing protein oligomeric structure: application to phospholamban. *Biophysical Journal*, 76(5), pp.2587–2599.

MacKenzie, K.R. & Fleming, K.G., 2008. Association energetics of membrane spanning alpha-helices. *Current opinion in structural biology*, 18(4), pp.412–419.

Merzlyakov, M. & Hristova, K., 2008. Forster Resonance Energy Transfer Measurements of Transmembrane Helix Dimerization Energetics. *Methods in enzymology*, 450, pp.107–127.

Popot, J.L. & Engelman, D.M., 1990. Membrane protein folding and oligomerization: the two-stage model. *Biochemistry*, 29(17), pp.4031–4037.

Posokhov, Y.O. et al., 2008. A SIMPLE “PROXIMITY” CORRECTION FOR FRET EFFICIENCY DETERMINATION IN MEMBRANES USING LIFETIME MEASUREMENTS. *Analytical biochemistry*, 380(1), pp.134–136.

Rath, A. & Deber, C., M., *Design of transmembrane peptides:Coping with sticky situations*,

Russ, W.P. & Engelman, D.M., 1999. TOXCAT: A measure of transmembrane helix association in a biological membrane. *Proceedings of the National Academy of Sciences*, 96(3), pp.863–868.

Schick, S. et al., 2010. Assembly of the M2 Tetramer Is Strongly Modulated by Lipid Chain Length. *Biophysical Journal*, 99(6), pp.1810–1817.

Schneider, D. & Engelman, D.M., 2003. GALLEX, a Measurement of Heterologous Association of Transmembrane Helices in a Biological Membrane. *Journal of Biological Chemistry*, 278(5), pp.3105–3111.

Stahl, P.J. et al., 2012. On-the-resin N-terminal modification of long synthetic peptides. *Analytical Biochemistry*, 424(2), pp.137–139.

Wimley, W.C. & White, S.H., 2000. Determining the Membrane Topology of Peptides by Fluorescence Quenching†. *Biochemistry*, 39(1), pp.161–170.

Wolber, P.K. & Hudson, B.S., 1979. An analytic solution to the Förster energy transfer problem in two dimensions. *Biophysical Journal*, 28(2), pp.197–210.

Yevgen O. Posokhov, M.M., A simple “proximity” correction for Förster resonance energy transfer efficiency determination in membranes using lifetime measurements. *Analytical Biochemistry*, (1), pp.134–136.

You, M. et al., 2007. Effect of Pathogenic Cysteine Mutations on FGFR3 Transmembrane Domain Dimerization in Detergents and Lipid Bilayers†. *Biochemistry*, 46(39), pp.11039–11046.

You, M. et al., 2005. Förster resonance energy transfer in liposomes: Measurements of transmembrane helix dimerization in the native bilayer environment. *Analytical biochemistry*, 340(1), pp.154–164.

Scheme 2.1: Calculation for number of moles for 1 mg/ml POPC lipid stock.

Molecular weight = 760.10 g/mol

No. of moles = weight/molecular weight

$$= \frac{1\text{mg}}{760.1\text{mg/mol}}$$

= 1.31 umol in 1 ml, or 1.31 nmol/ µL

Scheme 2.2: Calculation of protein concentration and labeling efficiency.

Concentration of the fluorescent label on peptide:

$$\textbf{[Fluorophore]} = A_{max}/\varepsilon_{Fluorophore}\, l$$

where A_{max} is absorbance at λ_{max} of the dye
$\varepsilon_{Fluorophore}$ is extinction coefficient of the dye at that absorbance
l is path length of the cuvette (usually 1 cm)

Concentration of the peptide based on Trp absorbance (λ=280nm)

$$\textbf{[Peptide]} = A_{280} - (A_{max} * CF)/\varepsilon\, l$$

where A_{280} is absorbance at 280nm
CF is the correction factor that adjusts for absorbance at 280 nm by the fluorophore, and is given by A_{280} / A_{max}
ε is extinction coefficient of the peptide (calculated based on no. of Trp, Tyr and Phe)

After calculating the concentration in terms of Molarity, calculate the number of moles in the stock solutions of the peptides similar to Scheme 2.1.

Calculating the labeling efficiency

$$\textbf{Percent labeling} = \textbf{[Fluorophore]/[Peptide]} * 100$$

Note: For peptides that do not have a Trp or Tyr to get accurate concentration from UV/VIS Spectrophotometry, CD can also be used to determine peptide concentration ***(3)***

Scheme 2.3: Calculation of percent FRET efficiency:

$$E_{observed} = [\,(I_D - I_{DA})/ I_D\,] \qquad \text{...Eq. (1)}$$

where I_D and I_{DA} are the donor emission maximum intensities of samples containing only donor-labeled proteins (controls)and samples with both donor- and acceptor-labeled proteins, respectively.

$$E_{expected} = \frac{[D][A]}{[D][D]+[D][U]+[D][A]}$$

where $[D] = [D]^{total} \times L_D$

$[A] = [A]^{total} \times L_A$

and $[U] = [D]^{total}(1-L_D) + [A]^{total}(1-L_A)$

($[D]$ is concentration of labeled donor-peptide, L_D is labeling efficiency of donor-peptide and $[D]^{total}$ is total donor-peptide, $[A]$ is concentration of labeled acceptor-peptide, L_A is labeling efficiency of donor-peptide and $[A]^{total}$ is total donor-peptide, and $[U]$ is concentration of unlabeled peptide)

$$\textbf{Fraction Dimer} = E_{observed} / E_{expected}$$

$$\textbf{= Dimer / Total}$$

$$= 2X_{dimer} / (2X_{dimer} + X_{monomer}) \qquad \text{…Eq. (2)}$$

where X is the mole fraction of the peptide.

Finally, mole fraction concentrations can be used to calculate a partition coefficient by

$$K_x = [X_{dimer}] / [\,X_{monomer}]^2 \qquad \text{...Eq. (3)}$$

which is an equilibrium constant, and the free energy of association is calculated by

$$\Delta G_x = -RT\, ln\, (K_x)$$

	Mole Fraction (peptide:lipid ratio)	Volume of donor stock (µL)	Volume of acceptor stock (µL)	Volume of 1mg/ml POPC Lipid stock (µL)
1	1:100	Calculate for 50 pmol (8.9ul)	Calculate for 50 pmol	Calculate for 10 nmol (= 7.7)
2	1:200	Ditto	Ditto	20 nmole = 15.4
3	1:500	Ditto	Ditto	50 nmol = 38.5
4	1:1000	Ditto	Ditto	100 nmol = 77
5	1:2000	Ditto	Ditto	200 nmol = 154
6	1:5000	Ditto	Ditto	500 nmol = 385
7	1:10000	Ditto	Ditto	1 mmol = 770
8	Control 1	Ditto	x	10 nmol = 7.7
9	Control 2	Ditto	x	20 nmole = 15.4
10	Control 3	Ditto	x	50 nmol = 38.5
11	Control 4	Ditto	x	100 nmol = 77
12	Control 5	Ditto	x	200 nmol = 154
13	Control 6	Ditto	x	500 nmol = 385
14	Control 7	Ditto	x	1 mmol = 770
15	No fluorophore control (contains 100 pmoles unlabeled peptide)	x	x	1 mmol = 770
16	No liposome control	Ditto	Ditto	x

Table 2.1 : Table for typical FRET sample preparation calculations in liposomes. Rows 1 to 7 show calculations for 'FRET samples' with decreasing peptide to lipid ratio. Rows 8 to 14 are the 'donor only' controls for each 'FRET sample', with 'Control 1' being the control for the '1:100' sample, and so on. Row 15 with the highest amount of lipid and same amount of unlabeled peptides serves as a scattering control to subtract any background scattering from the lipids alone. Row 16 serves as a control for any FRET arising out of peptide aggregates in solution in the case of incomplete incorporation of peptides into vesicles.

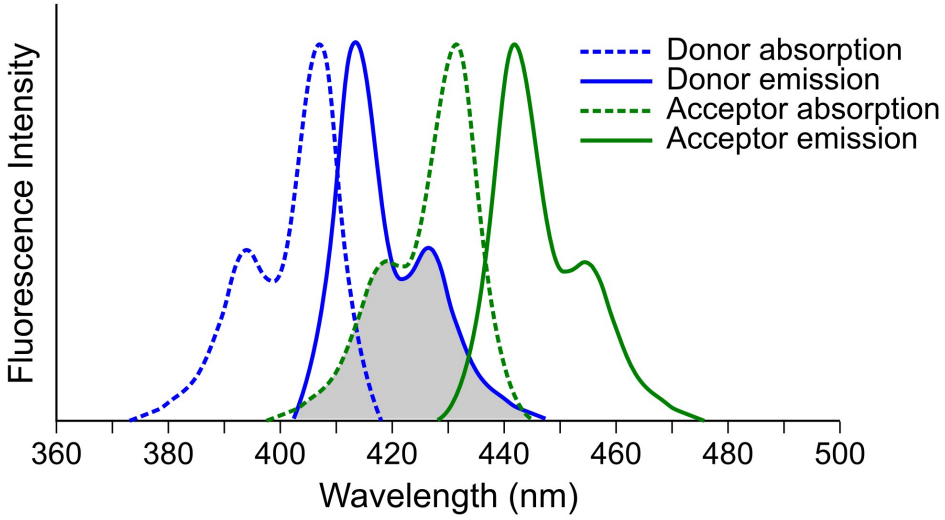

Figure 2.1 : Spectral overlap between a FRET pair. Blue curves depict the donor excitation and emission spectra and green curves depict the acceptor excitation and emission spectra. Note significant overlap (shaded region) between the donor emission and the acceptor excitation, leading to a good spectral overlap, one of the requirements for a FRET pair.

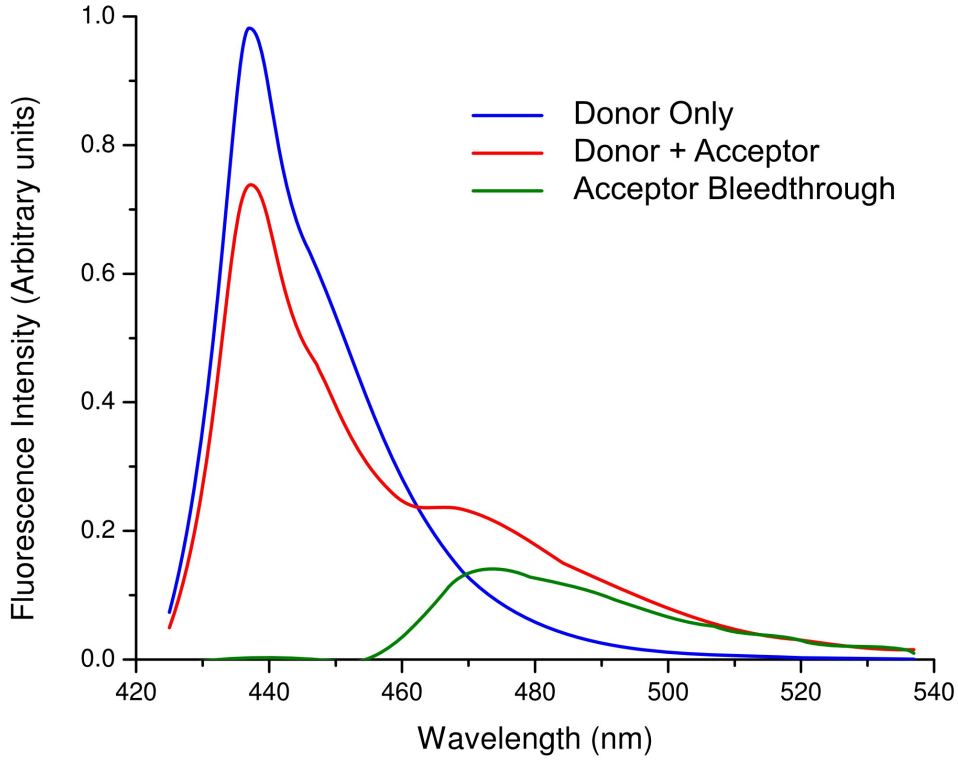

Figure 2.2 : Donor quenching and acceptor sensitization due to FRET. The decrease in the donor emission intensity is used to calculate the FRET efficiency. The sensitization of acceptor emission (FRET) is evident from the increased fluorescence intensity compared to direct excitation (acceptor bleedthrough) of the acceptor at the donor excitation wavelength.

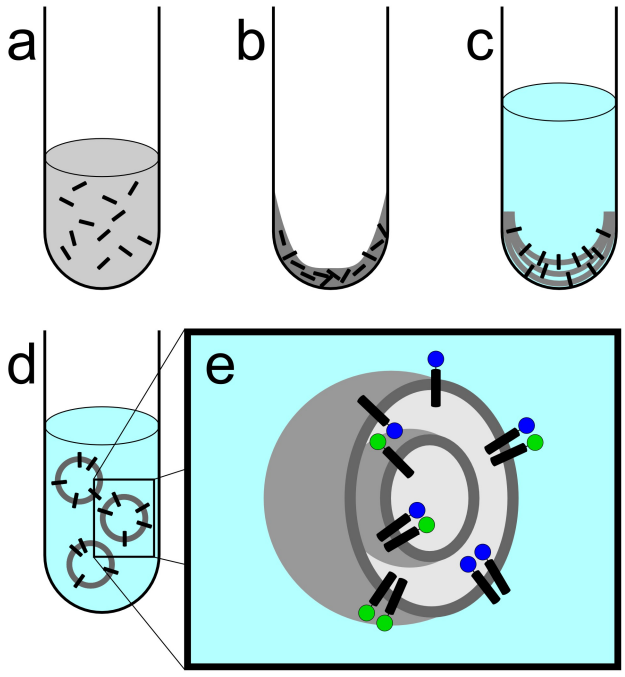

Figure 2.3 : Setup of FRET in liposomes. (a) Peptides and lipids dissolved in solvent and mixed together in a glass vial. (b) The solvent is evaporated using a stream of Nitrogen gas to leave behind a thin lipid film containing the peptide molecules. (c) The lipid film is hydrated using aqueous buffer, vortexed, and freeze-thawed to achieve proper equilibration and (d) formation of multilamellar vesicles containing the peptides. (e) The various pairs that will be contributing to FRET efficiency due to association of peptides and just colocalization, as well as 'dark pairs' formed by donor-donor, acceptor-acceptor associations.

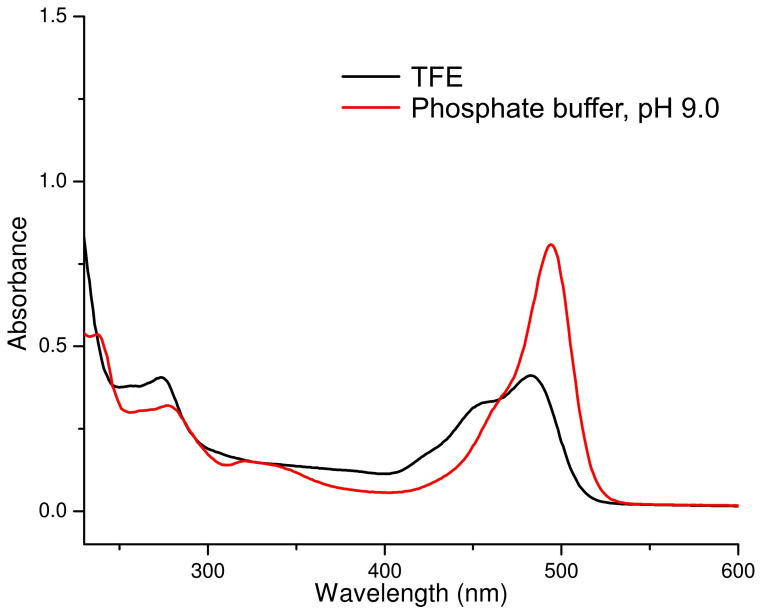

Figure 2.4 : Absorbance spectra of FITC in Phosphate Buffer, pH 9.0 and in TFE. The solvent has an effect on the λ_{max} and its molar extinction coefficient ε

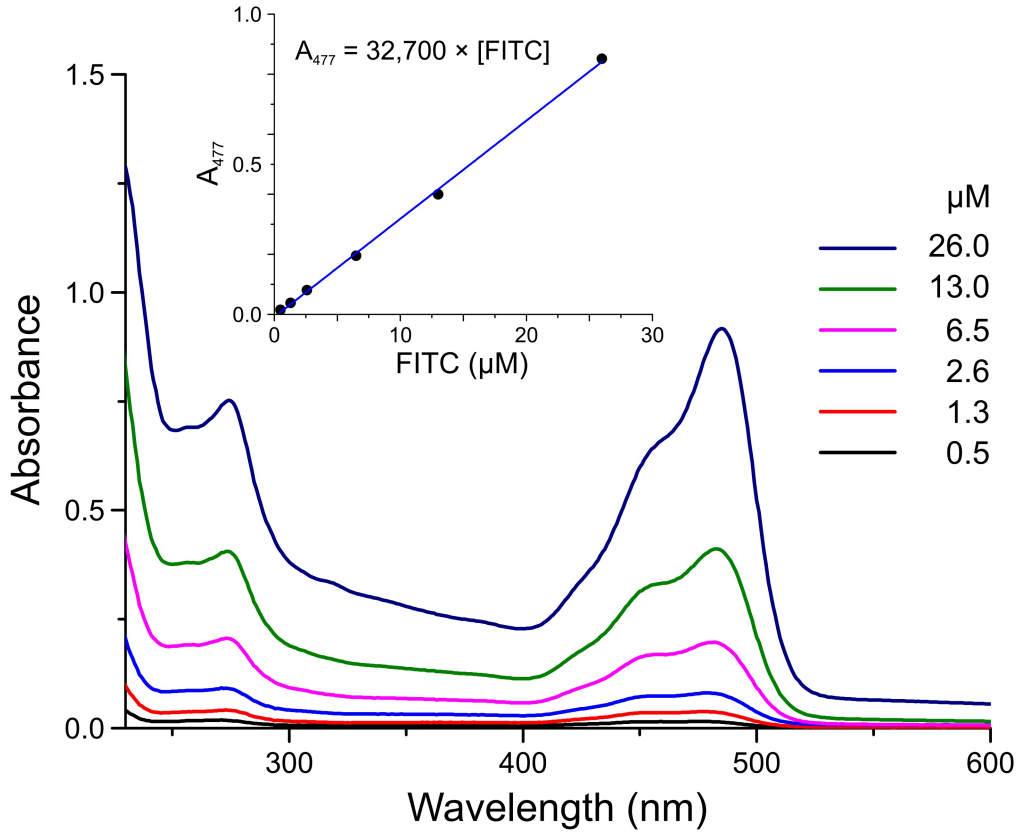

Figure 2.5: Calculating the molar extinction coefficient $\varepsilon_{Fluorophore}$ of FITC in TFE. Absorbance scans of increasing concentrations of FITC dye in organic solvent. A_{max} (477nm) is plotted versus concentration and the slope of the curve yields the new molar extinction coefficient $\varepsilon_{Fluorophore}$ of FITC (32,700 M^{-1} cm^{-1}) in TFE (inset). The ratio of A_{280} to A_{max} yields the new correction factor for FITC in TFE required for calculating the degree of labeling. Note that the wavelength of maximum absorbance shifts and that the molar extinction coefficient at A_{max} decreases more than two-fold compared to that in Phosphate bufffer pH 9.0.

CHAPTER THREE

The transmembrane domains of the bacterial cell division proteins FtsB and FtsL form a stable high-order oligomer

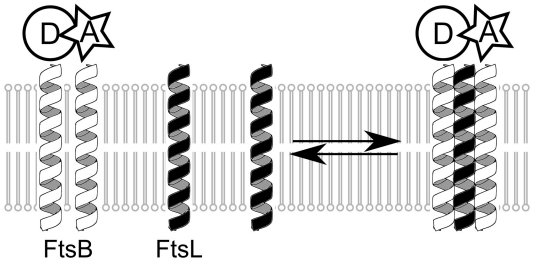

Based on:

Khadria, A.S. & Senes, A., 2013. The Transmembrane Domains of the Bacterial Cell Division Proteins FtsB and FtsL Form a Stable High-Order Oligomer. *Biochemistry*, 52(43), pp.7542–7550.

Abbreviations

TM: transmembrane; FtsB-TM: transmembembrane domain of FtsB; FtsL-TM: transmembembrane domain of FtsL; FRET: Förster Resonance Energy Transfer; POPC: 1-palmitoyl-2-oleoyl-sn-glycero-3-phosphocholine; DPC: dodecylphosphocholine; FITC: fluorescein isothiocyanate; 5-FAM: 5-carboxyfluorescein; TFE: trifluoroethanol.

Abstract

FtsB and FtsL are two essential integral membrane proteins of the bacterial division complex or “divisome”, both characterized by a single transmembrane helix and a juxta-membrane coiled coil domain. The two domains are important for the association of FtsB and FtsL, a key event for their recruitment to the divisome, that in turn enables recruitment of the late divisomal components to the Z-ring and subsequent completion of the division process. Here we present a biophysical analysis performed *in vitro* that shows that the transmembrane domains of FtsB and FtsL associate strongly in isolation. Using FRET, we have measured the oligomerization of fluorophore-labeled transmembrane domains of FtsB and FtsL in both detergent and lipid. The data indicates that the transmembrane helices are likely a major contributor to the stability of the FtsB-FtsL complex. Our analyses show that FtsB and FtsL form a 1:1 higher-order oligomeric complex, possibly a tetramer. This finding suggests that the FtsB-FtsL complex is capable of multi-valent binding to FtsQ and other divisome components, a hypothesis that is consistent with the possibility that the FtsB-FtsL complex has a structural role in the stabilization of the Z-ring.

Introduction

I n *Escherichia coli,* the multiprotein cell-division mediating complex, or "divisome", comprises at least ten essential proteins, most of which are integral membrane proteins. The proteins are recruited at mid-cell over a scaffold formed by the polymeric FtsZ (the Z-ring) (Adams & Errington 2009; Mingorance et al. 2010; Erickson et al. 2010) where they assemble according to a defined stepwise pathway(Goehring & Beckwith 2005). Two such essential components, FtsB and FtsL, occupy a place mid-way into this hierarchy(Goehring et al. 2006; Gonzalez & Beckwith 2009); they are preceded by the early components (FtsZ, FtsA, ZipA, FtsK and FtsQ); in turn, they are required for the recruitment of the late divisome components (FtsW, FtsI, FtsN), which are important for the reconstruction of the cell wall.

The specific role of FtsB and FtsL is still not well understood. It has been suggested that they have a structural role in the assembly of the divisome(Gonzalez & Beckwith 2009; Robichon et al. 2011) and that they are important for the stabilization of the Z-ring(Geissler & Margolin 2005). It is clear, however, that FtsB and FtsL form a stable sub-complex *in vivo* prior to their association with the divisome(Buddelmeijer et al. 2002; Daniel & Errington 2000; Ghigo et al. 1999; Katis et al. 2000) and that their mutual interaction is central to their role in bacterial division.

The recruitment of FtsB and FtsL depends on their interaction with FtsQ. However, even when FtsQ is depleted these two proteins still associate with each other, and as long as they are artificially targeted to the division septum, they are still able to recruit the downstream proteins(Gonzalez & Beckwith 2009). Evidence for the formation of a stable FtsB-FtsL complex is also provided by the fact that their *B. subtilis* homologs form a complex when co-

expressed in *E. coli*, even though they are unlikely to interact with the significantly divergent division proteins of the host(Robichon et al. 2008). Moreover, FtsB and FtsL are quickly depleted from the cell when the proteins are not co-expressed, suggesting that they are functionally dependent on each other(Buddelmeijer et al. 2002; Daniel & Errington 2000; Daniel et al. 1998; Daniel et al. 2006; Bramkamp et al. 2006).

Determining the structural organization of the FtsB-FtsL complex, its stoichiometry, and its stability, is critical to understanding its role in division. Topologically, FtsB and FtsL are similar to each other, being small single-pass integral membrane proteins consisting of an N-terminal transmembrane (TM) helix, a juxta-membrane periplasmic coiled coil and a short C-terminal domain **(Figure 3.1a)**. Previous studies indicate that both the transmembrane and the coiled coil domains are involved in their mutual association(Gonzalez & Beckwith 2009; Robichon et al. 2011; Rowland et al. 2010). To investigate this we recently studied the structural organization of the individual domains of FtsB in isolation(LaPointe et al. 2013). Using an *in vivo* interaction assay, we showed that the TM domain of FtsB self-associates in *E. coli* membranes. We performed extensive mutagenesis and computed a structural model of FtsB-TM that is in excellent agreement with the experimental data, showing a left-handed homo-dimer mediated by an inter-helical hydrogen bond **(Figure 3.1b)**. We also solved the crystal structure of the coiled coil domain of FtsB in homo-dimeric form, solubilized as a fusion construct with the viral coiled coil protein Gp7. From this evidence, we hypothesized that the FtsB-TM homodimer forms a core for the lateral association of FtsL-TM **(Figure 3.1c)**.

Here we present a Förster Resonance Energy Transfer (FRET) based study performed *in vitro* that shows for the first time that FtsB and FtsL TM domains interact and provides new insight into the structural organization of the FtsB-FtsL complex. The data shows that the TM

region of the FtsB-FtsL complex is stably folded and that the TM helices are likely a major determinant for the association of the complex. We also show that FtsL and FtsB forms a 1:1 higher-order oligomeric complex, which is consistent with our previous hypothesis that the FtsB-FtsL complex is likely a tetramer(LaPointe et al. 2013) **(Figure 3.1c).** From these results, we hypothesize that the FtsB-FtsL complex may form a multi-valent binding hub that is important for the stabilization of the Z-ring.

Materials and Methods

Peptide sequences. The predicted TM regions of *E. coli* FtsB and FtsL (underlined sequence) were synthesized flanked by Gly amino acids on the N terminus to provide a linker between the peptide and the N-terminal fluorophore. Lys residues were added on the C terminus to improve the solubility of the peptide in aqueous media to facilitate purification of the hydrophobic TM peptides(Rath & Deber 2013; Liu & Deber 1998; Melnyk et al. 2001). A Trp residue (in bold) was introduced in place of a native His residue in the C-terminus of FtsL-TM to facilitate absorbance monitoring at 280nm.

FtsB-TM: GGKLTLLLLAILVWLQYSLWFGKKKK

FtsL-TM: GGGKLPLCLFICIILTAVTVVTTA**W**HKK

Fmoc Solid Phase Peptide synthesis. Peptides were synthesized at 25 µmole scale on a Protein Technologies Symphony peptide synthesizer, over a low substitution (0.16mmol/g) Fmoc amide resin (Applied Biosystems) using DMF (dimethylformamide) as the solvent, 20% Piperidine with 2% DBU (1,8-diazabicyclo[5.4.0]undec-7-ene) for deprotection and HATU (*O*-(7-azabenzotriazol-1-yl)-*N*,*N*,*N*′,*N*′-tetramethyluronium hexafluorophosphate) for activation (0.40 M in DMF). Unlabeled peptides were N-terminally acetylated using standard procedures . Side chain deprotection and final cleavage from the resin was achieved using a mixture of 95:2.5:2.5 v/v of TFA (trifluoroacetic acid)/EDT(1,2-ethanedithiol)/water at room temperature for 4 hours. The cleaved peptide was precipitated using 1:10 v/v of cleavage mix:cold MTBE (methyl tertiary butyl ether) and dried in a vacuum dessicator.

On-resin N-terminal labeling of peptides. Labeling of the peptides was carried out on the peptide-resin prior to cleavage using variations of a protocol for labeling hydrophobic

peptides(Stahl et al. 2012). Briefly, excess of a linker, N-ε-Fmoc-aminohexanoic acid (Fmoc-ε-Ahx-OH, AnaSpec) was coupled to the peptide-resin using standard coupling procedures at room temperature overnight. Following thorough washing and deprotection of the Ahx labeled peptide-resin, FITC (Fluorescein isothiocyanate) 'isomer 1' (Sigma Aldrich) was coupled with repeated washing and recoupling for ~4 days to achieve efficient labeling. For FtsL, successful coupling was obtained for the 5-FAM (5-carboxyfluorescein) version of the fluorophore in the same manner. Coupling of 7-hydroxycoumarin-3-carboxylic acid (Anaspec) was performed in a similar fashion without prior coupling of the Ahx linker. A detailed labeling procedure is provided in the Supplementary Information.

Purification of peptides. The peptides were purified on a reversed phase HPLC system (Varian ProStar 335) with a Zorbax SB-CN semi-preparative column, 5µm, 9.4 x 250mm (Agilent) for FtsB and a VP 250/10 NUCLEOSIL 100-7 C2 semi-preparative column (Macherey-Nagel) for FtsL, using a linear gradient of water and acetonitrile in the presence of 0.1% TFA. Collected fractions were lyophilized and the masses of the peptides were confirmed by a Bruker REFLEX II MALDI-TOF system using CHCA as the matrix.

Quantification of peptides. Quantification and preparation of peptide stocks in TFE (trifluoroethanol) was carried out by absorbance measurements using a Cary 50 scan UV/Vis spectrophotometer. Accurate quantification and calculation of labeling efficiencies was performed using a detailed procedure(Khadria & Senes 2013) described in Supplementary Information. The fluorophores were characterized in TFE as described in **Figure S3.1**. The calculated labeling efficiencies of the purified FITC-FtsB, coumarin-FtsB, 5-FAM-FtsL and coumarin-FtsL peptides used were >95%. In spite of numerous efforts, the maximum labeling efficiency obtained for FITC-FtsL was <15%. For this reason the 5-FAM version of the

fluorophore was used for the FtsL homo-FRET studies.

FRET assay. Peptides were mixed in the desired molar ratios and added to PTFE lined screw cap glass vials containing the calculated amounts of DPC (Dodecylphosphocholine) and POPC (1-palmitoyl-2-oleoyl-sn-glycero-3-phosphocholine) (Avanti Polar Lipids) in chloroform. The mixture was vigorously vortexed, and solvents were dried using a stream of nitrogen gas and dessicated overnight in a vacuum dessciator to remove residual organic solvents. Samples were hydrated in 10 mM HEPES, pH 7.5. Lipid samples were vortexed vigorously and equilibrated using three freeze-thaw cycles for lipid samples. Detergent samples were equilibrated by incubating them at room temperature for 4 hours.

For the donor+acceptor (FRET) samples, total peptide amount used was 0.5 nmoles containing 1:1 donor to acceptor molar ratios, and amount of detergent or lipid was varied to span a range of peptide:lipid/detergent molar ratios from 1:10000 to 1:300. Donor only (for 'no FRET' control) and acceptor only (for bleed-through correction) samples contained 0.25 nmoles of donor peptides and acceptor peptides, respectively, in the same range of peptide:detergent/lipid molar ratios. A sample with unlabeled FtsB:lipid ratio of 1:10000 was used as a scattering control for the lipid experiments. Triton-x 100 (0.5%) was added to coumarin-FtsB-lipid samples and fluorescence intensity measurements were taken before and after the detergent addition to account for effect of scattering on fluorescence intensity values. Fluorescence readings were taken in a HITACHI F-4500 Fluorescence Spectrophotometer. Samples were excited at 415 nm and emission scans were recorded from 425 to 650 nm at 25°C. **Supplementary Figure S3.2** shows a characteristic FRET curve between donor and acceptor labeled FtsB peptides. FRET efficiency (E%) values were calculated using donor-quenching of coumarin emission λ_{max} at 450nm, using the formula E%

= $[(I_D-I_{DA})/I_D]*100$, where I_D is the fluorescence intensity of the donor only sample, and I_{DA} is the fluorescence intensity of the donor in the presence of the acceptor(Li et al. 2005; You et al. 2005). Alternatively, 0.5% Triton X-100 was added to the FRET samples and incubated for 10 minutes to disrupt the liposomes and the peptide complexes, and yield a 'no FRET' control. In these cases, FRET efficiency was measured as E% = $[(I_T-I_{DA})/I_T]*100$, where I_T is the donor emission at 450nm after Triton addition and $I_{D\ A}$ is the donor emission before Triton addition(Schick et al. 2010). For the competition experiment **(Figure 3.4)**, equimolar amounts of unlabeled FtsL were added to 1:1 donor:acceptor ratios of FtsB in a range of [total FtsB peptide]:[lipid/detergent] values of 1:10000 to 1:300. For the stoichiometric experiment **(Figure 3.5)**, increasing amounts of FtsL were added to 1:1 donor:acceptor ratios of FtsB in a fixed [total FtsB peptide]:[lipid] ratio of 1:1000. Experiments were performed at least in triplicate.

Results

The TM domain of FtsB homo-oligomerizes *in vitro*. Using a biological assay (TOXCAT), we previously established that FtsB-TM self-associates in *E. coli* membranes, while FtsL-TM appeared to be largely monomeric(LaPointe et al. 2013). To confirm these observations *in vitro*, we measured FRET between coumarin/FITC or coumarin/5-FAM labeled peptides as a function of peptide concentration **(Figure 3.2)**. Fluorescence measurements were taken by maintaining the concentration of the peptides constant while increasing the amount of detergent or lipid to vary the available "hydrophobic volume", and for this reason peptide concentrations are expressed as peptide:detergent or peptide:lipid molar ratios(Fleming et al. 2004). FRET efficiency values were calculated using donor quenching at coumarin emission maxima (450 nm).

A concentration dependent increase in FRET is observed for FtsB-TM in lipid **(Figure 3.2b)**, confirming that it self-associates. Fit to a monomer-dimer equilibrium, the FRET data in lipid yield an estimated dissociation constant of 9.4×10^{-4}, corresponding to a free energy of association of approximately -4 kcal/mol. A small increase in FRET is also observable in detergent **(Figure 3.2a)**, but the apparent association energy appears to be very low. Consistent with our previous TOXCAT analysis(LaPointe et al. 2013), FtsL-TM appears to oligomerize very weakly in both detergent and lipid environments.

The TM domains of FtsB and FtsL associate. Having confirmed *in vitro* that the FtsB-TM oligomerizes, our main interest was to verify whether the TM domains of FtsB and FtsL interact, as hypothesized. **Figure 3.3** shows the FRET data for coumarin-FtsL (donor) and FITC-FtsB (acceptor) peptides, mixed in a 1:1 ratio, and equilibrated with decreasing amounts

of DPC detergent (panel a) or POPC lipid (panel b). Increase in FRET efficiency values with increasing peptide concentration demonstrates that FtsB and FtsL TM peptides indeed associate both in detergent and in lipid. In both environments, the FtsB-FtsL heterologous FRET curves grow more rapidly than the FtsB-FtsB homo-FRET, which is displayed in **Figure 3.3** in gray for direct visual comparison. The curves in **Figure 3.3** are fit to a monomer-tetramer equilibrium and provide estimated K_d values of 2.3×10^{-9} in DPC and 1.3×10^{-11} in POPC.

FtsB and FtsL form a higher-order oligomer. Once established that the TM domains of FtsB and FtsL associate, the next question was whether FtsL competes with and disrupts the FtsB homo-dimer to form an FtsB-FtsL hetero-dimer, or whether FtsL associates with the FtsB homo-dimer to form a tetramer or, potentially, another higher-order complex **(scheme in Figure 3.4a)**. To investigate this question, we performed a competition experiment in which an equimolar amount of unlabeled FtsL-TM peptide was added to samples containing labeled FtsB-TM donor and acceptor pairs. The data shows that addition of FtsL led to a significant increase in the FtsB-TM FRET both in detergent micelles **(Figure 3.4b)** as well as in lipid vesicles **(Figure 3.4c).** The apparent dissociation constant of the FtsB homo-oligomer in the presence of an equimolar amount of FtsL decreases by almost two orders of magnitude from 9.4×10^{-4} to 1.3×10^{-5}, corresponding to an apparent stabilization of an FtsB dimer of 2.5 kcal/mol. Control experiments were carried out with the addition of an equimolar amount of either an unrelated polyleucine based monomeric model TM peptide (pL-3F-dC(Pace et al. 2011)), or an equimolar amount of unlabeled FtsB **(supplementary Figure S3.3**). The unrelated peptide did not alter the FtsB homo-FRET values. Conversely, addition of unlabeled FtsB decreased FRET, as expected.

FtsB and FtsL form a 1:1 oligomer. To further investigate the stoichiometry of the FtsB-FtsL complex, we performed a titration experiment in which unlabeled FtsL was added in increasing amounts to donor and acceptor labeled FtsB in a fixed [total FtsB peptide]:[lipid] ratio, and FtsB homo-FRET was measured. **Figure 3.5** shows that addition of unlabeled FtsL leads to a linear increase in the FRET efficiency of FtsB homo-oligomer until the FtsL:FtsB molar ratio reaches a value of approximately 1, after which the signal flattens. The data clearly indicate that the oligomer has an equal number of FtsB and FtsL molecules, which is consistent with the hypothesized tetramer (2:2). A tetrameric FtsB-FtsL is also consistent with one of the hypothesized by Villanello et al. on the basis of a bioinformatic analysis of the soluble domains(Villanelo et al. 2011). The steep linear rise in the FRET efficiency until equal stoichiometry Is reached confirms that the complex is stable at the peptide:lipid ratio in which the experiment was performed (1:1000). The FRET signal compare well with **Figure 3.4c** where the FtsB-FRET increases from ~0.4 to ~0.8 FRET efficiency upon addition of equimolar amount of unlabeled FtsL.

Discussion

An important question for understanding the FtsB-FtsL complex is how their two adjacent interaction domains – the TM helix and the juxta-membrane coiled-coil region – contribute and cooperate toward the stability of the complex. We have begun addressing this question by studying the individual domains in isolation. In our previous work we reported that the TM domain of FtsB self-associates(LaPointe et al. 2013). We used extensive mutagenesis to identify the interaction interface and used computational modeling to interpret the experimental data. The analysis produced a complementary packed homo-dimer mediated by an inter-helical hydrogen bond **(Figure 3.1b)**. While a biological role for the FtsB homo-dimer is not excluded, we hypothesized that the dimer likely represents the core of an FtsB-FtsL higher oligomer. The current results provide further evidence for this hypothesis.

We have confirmed that FtsB self-associates *in vitro* in lipid bilayers **(Figure 3.2b)**. The calculated free energy of association is approximately -4 kcal/mol, a value that places FtsB as a moderately stable dimer, compared to other examples from the literature(MacKenzie & Fleming 2008). The oligomerization of FtsB is only marginal in DPC micelles **(Figure 3.2a)**: its association curve is superimposable to that of FtsL, which does not associate in lipid. The higher stability of FtsB in lipid could be in part due to the fact that a bilayer provides an environment closer to a natural membrane(Seddon et al. 2004). We note the additional possibility that the inter-helical hydrogen bonding formed by the polar Gln 16 at the FtsB dimer interface **(Figure 3.1b)** may contribute differently to the energy of oligomerization in the two environments. Polar side chains can contribute to the interaction of TM helices(Xiao Zhou et al. 2000; Choma et al. 2000). The contribution of a polar amino acid to association depends on the net balance between any gain of hydrogen bonding and electrostatic

interactions in the bound state, and any loss of favorable interactions between the polar groups of the side chain and water in the unassociated state(Hendsch & Tidor 1999). For a TM helix, however, this desolvation cost is presumably lower when, in the monomeric state, the side chain is sequestered away from water into the hydrophobic core of a lipid bilayer(Xiao Zhou et al. 2000; Choma et al. 2000). The desolvation cost may be more significant in a detergent environment, either because of the higher propensity of water molecules to penetrate deeply into a micellar environment(Renthal et al. 2011; Tulumello & Deber 2011), or because of the difference in the ability of the long Gln side chain to 'snorkel' toward the surface of a micelle than in a lipid.

The main highlight of the present work is that we have obtained for the first time experimental evidence that the TM domains of FtsB and FtsL interact in isolation **(Figure 3.3)** and narrowed down the stoichiometry of the complex **(Figure 3.5)**. The FRET results indicate that FtsB and FtsL associate strongly in both detergent and lipid. The calculated dissociation constants obtained by fitting the coumarin-FtsL/FITC-FtsB FRET data to a theoretical monomer-tetramer equilibrium are 2.3×10^{-9} and 1.3×10^{-11} in DPC and POPC respectively, and the corresponding ΔG^{o} values of association are -11.7 and -14.7 kcal/mol, respectively. It is again noteworthy that the association is more stable in lipid than in detergent. The high stability of the transmembrane region of the FtsB-FtsL complex postulates that this domain has an important structural, and potentially functional role.

While it is challenging to determine the precise oligomeric state of a heterologous TM complex by FRET analysis, we provide evidence that the FtsB-FtsL complex is a higher oligomer with a 1:1 stoichimetric ratio. The observed increase of FtsB self-association in the presence of an equimolar amount of FtsL both in lipids and in detergent clearly indicates that

FtsL has a strong effect in promoting the formation of a complex that contains more than one FtsB molecule **(Figure 3.4)**. When the relative amount of FtsL is varied compared to FtsB, we found that the apparent FtsB stabilization increases linearly until a 1:1 FtsB-FtsL molar ratio is reached, at which point the curve sharply flattens **(Figure 3.5)**.

The observed stabilization of FtsB self-association is due to a specific interaction with FtsL as opposed to non specific FRET due to crowding, as supported by two controls **(Figure S3.3)**. The addition of an unrelated unlabeled monomeric model TM peptide does not perturb the FtsB self-association equilibrium, indicating that the increase in FtsB FRET is a sequence dependent effect of FtsL. On the other hand, the addition of unlabeled FtsB results in a reduction of FtsB FRET consistent with the expected competition and thus apparent dissociation of the labeled peptide pairs.

The FRET efficiency grows very rapidly as a function of concentration in the competition experiment in **Figure 3.4**, compared to the heterologous FtsB/FtsL FRET in **Figure 3.3**. It should be noted here that the concentration in **Figure 3.3** is expressed for total peptide (FtsB+FtsL) while in **Figure 3.4** it is expressed for FtsB peptide only, to allow direct comparison with the FtsB homo-FRET. In addition, the FtsB-FtsL experiment is only sensitive to formation of hetero-oligomers, while the competition experiment reports FRET due to FtsB homo-dimer formation as well as hetero-oligomers. It is, however, possible that other factors may also influence the analysis. For example imprecision in the difficult quantification of all labeled and unlabeled species could render the peptide molar ratios inaccurate. Moreover, the calculation of the reported dissociation constants are based on FRET efficiency, which was obtained from donor quenching at its emission maximum. This quantity may contain contributions from self quenching of the donor as well as colocalization

effects due to random proximity of donors and acceptors as peptides diffuse randomly in bilayers even in low peptide concentrations. Accounting for these effects could in principle lower the actual FRET efficiency values and yield more precise thermodynamics of association. Furthermore, proximity effects due to different orientation in the opposite bilayer leaflets of multi-lamellar vesicles could also lead to spurious increased FRET efficiency values that have variable contributions for different FRET pairs(You et al. 2005; Posokhov et al. 2008). Nonetheless, it is reasonable to infer that the contribution of non specific FRET due to all these factors is comparable across experiments performed in similar experimental conditions with the same FRET pair. Therefore, while from a rigorously quantitative stand point this report is an initial thermodynamic analysis, we note that, overall, the magnitude and the consistency of the data across the different experiments provide strong evidence that the TM domains of FtsB and FtsL form a stable 1:1 higher-oligomer complex, a fact that is important toward understanding their biological function.

Further work is necessary to establish the precise oligomerization state of the FtsB-FtsL complex, using methods that are directly sensitive to the total mass of the complex, such as Analytical Ultracentrifugation(Doura & Fleming 2004; Burgess et al. 2008). The present work, however, represents a significant step toward understanding the structural organization of the FtsB-FtsL complex and its role in the assembly and function of the divisome. It provides further evidence for our previously reported hypothesis that a tetrameric TM complex is likely formed by the lateral association of FtsL-TM helix onto a FtsB-TM dimer(LaPointe et al. 2013), and it demonstrates that the TM region of FtsB-FtsL is stable and likely a major contributor to the stability of the overall complex **(Figure 3.1c)**.

The fact that FtsB-FtsL form a higher-oligomeric complex may be significant for the

functional role of the proteins. FtsB and FtsL have been hypothesized to be structural proteins that contribute to the stabilization of the Z-ring(Gonzalez & Beckwith 2009; Robichon et al. 2011; Geissler & Margolin 2005). There is indeed substantial evidence that FtsB and FtsL bind to with multiple partners: they associate with FtsQ, an interaction that is mediate by the periplasmic domains of the proteins(Gonzalez & Beckwith 2009; Gonzalez et al. 2010; Masson et al. 2009; Villanelo et al. 2011; van den Berg van Saparoea et al. 2013); the N-terminal tail of FtsL is important for the recruitment of FtsW(Gonzalez et al. 2010); moreover, two-hybrid assay have identified several potential interactions with other proteins(D'Ulisse et al. 2007; Karimova et al. 2005). This leads to the hypothesis that a tetrameric and thus multi-valent FtsB-FtsL complex may simultaneously bind multiple partners and act as an interaction hub that tethers together several complexes of the divisome. This hypothetical role is schematically illustrated in **Figure 3.6**.

Acknowledgement

We are grateful to Dr. Melissa Boersma at the Peptide Synthesis facility of the UW-Madison Biotech Center for assistance and very useful discussion in the synthesis and labeling of the peptides. We are also grateful to Dr. Kalina Hristova and Kristen Duthie for valuable inputs for labeling of peptides and the FRET assay and N. Rangarajan for assistance with characterization of the fluorophores and use of the fluorimeter. We thank Dr. Martha M. Vestling at the Mass Spectrometry facility at the Department of Chemistry and Dr. Darrel McCaslin of the Biophysical Instrumentation Facility of the Department of Biochemistry for assistance and guidance in data collection. Finally, we thank Nawaraj Subedi, Pragya Sidhwani, Jennifer Peotter and Chin Tan for assistance during sample preparation, and Loren LaPointe and Ben Mueller for useful discussion and critical reading of the manuscript.

Supporting Information

Supplementary Methods covering N-terminal labeling of peptides and quantification. Characterization of FITC in TFE **(Figure S3.1)**. Fluorescence spectra of coumarin (donor) and FITC (acceptor) labeled peptides **(Figure S3.2)**. Effect of unlabeled control peptides on FtsB homo-FRET **(Figure S3.3)**. Supporting materials may be accessed free of charge online at http://pubs.acs.org.

References

Adams, D.W. & Errington, J., 2009. Bacterial cell division: assembly, maintenance and disassembly of the Z ring. *Nature Reviews Microbiology*, 7(9), pp.642–653.

Van den Berg van Saparoea, H.B. et al., 2013. Fine-mapping the Contact Sites of the Escherichia coli Cell Division Proteins FtsB and FtsL on the FtsQ Protein. *The Journal of biological chemistry*, 288(34), pp.24340–24350.

Bramkamp, M. et al., 2006. Regulated intramembrane proteolysis of FtsL protein and the control of cell division in Bacillus subtilis. *Molecular Microbiology*, 62(2), pp.580–591.

Buddelmeijer, N. et al., 2002. YgbQ, a cell division protein in Escherichia coli and Vibrio cholerae, localizes in codependent fashion with FtsL to the division site. *Proceedings of the National Academy of Sciences*, 99(9), pp.6316–6321.

Burgess, N.K., Stanley, A.M. & Fleming, K.G., 2008. Determination of Membrane Protein Molecular Weights and Association Equilibrium Constants Using Sedimentation Equilibrium and Sedimentation Velocity. In I. Dr. John J. Correia and Dr. H. William Detrich, ed. *Methods in Cell Biology*. Academic Press, pp. 181–211. Available at: http://www.sciencedirect.com/science/article/pii/S0091679X07840076 [Accessed July 22, 2013].

Choma, C. et al., 2000. Asparagine-mediated self-association of a model transmembrane helix. *Nature Structural & Molecular Biology*, 7(2), pp.161–166.

Daniel, R.A. et al., 1998. Characterization of the essential cell division gene ftsL (yllD) of Bacillus subtilis and its role in the assembly of the division apparatus. *Molecular Microbiology*, 29(2), pp.593–604.

Daniel, R.A. et al., 2006. Multiple Interactions between the Transmembrane Division Proteins of Bacillus subtilis and the Role of FtsL Instability in Divisome Assembly. *Journal of Bacteriology*, 188(21), pp.7396–7404.

Daniel, R.A. & Errington, J., 2000. Intrinsic instability of the essential cell division protein FtsL of Bacillus subtilis and a role for DivIB protein in FtsL turnover. *Molecular Microbiology*, 36(2), pp.278–289.

Doura, A.K. & Fleming, K.G., 2004. Complex interactions at the helix-helix interface stabilize the glycophorin A transmembrane dimer. *Journal of molecular biology*, 343(5), pp.1487–1497.

D'Ulisse, V. et al., 2007. Three functional subdomains of the Escherichia coli FtsQ protein are involved in its interaction with the other division proteins. *Microbiology (Reading, England)*, 153(Pt 1), pp.124–138.

Erickson, H.P., Anderson, D.E. & Osawa, M., 2010. FtsZ in Bacterial Cytokinesis: Cytoskeleton and Force Generator All in One. *Microbiology and Molecular Biology Reviews: MMBR*, 74(4), pp.504–528.

Fleming, K.G. et al., 2004. Thermodynamics of glycophorin A transmembrane helix dimerization in C14 betaine micelles. *Biophysical Chemistry*, 108(1–3), pp.43–49.

Geissler, B. & Margolin, W., 2005. Evidence for functional overlap among multiple bacterial cell division proteins: compensating for the loss of FtsK. *Molecular Microbiology*, 58(2), pp.596–612.

Ghigo, J.-M. et al., 1999. Localization of FtsL to the Escherichia coli septal ring. *Molecular Microbiology*, 31(2), pp.725–737.

Goehring, N.W. & Beckwith, J., 2005. Diverse Paths to Midcell: Assembly of the Bacterial Cell Division Machinery. *Current Biology*, 15(13), pp.R514–R526.

Goehring, N.W., Gonzalez, M.D. & Beckwith, J., 2006. Premature targeting of cell division proteins to midcell reveals

hierarchies of protein interactions involved in divisome assembly. *Molecular Microbiology*, 61(1), pp.33–45.

Gonzalez, M.D. et al., 2010. Multiple interaction domains in FtsL, a protein component of the widely conserved bacterial FtsLBQ cell division complex. *Journal of bacteriology*, 192(11), pp.2757–2768.

Gonzalez, M.D. & Beckwith, J., 2009. Divisome under construction: distinct domains of the small membrane protein FtsB are necessary for interaction with multiple cell division proteins. *Journal of bacteriology*, 191(8), pp.2815–2825.

Hendsch, Z.S. & Tidor, B., 1999. Electrostatic interactions in the GCN4 leucine zipper: Substantial contributions arise from intramolecular interactions enhanced on binding. *Protein Science*, 8(7), pp.1381–1392.

Karimova, G., Dautin, N. & Ladant, D., 2005. Interaction network among Escherichia coli membrane proteins involved in cell division as revealed by bacterial two-hybrid analysis. *Journal of Bacteriology*, 187(7), pp.2233–2243.

Katis, V.L., Wake, R.G. & Harry, E.J., 2000. Septal Localization of the Membrane-Bound Division Proteins of Bacillus subtilis DivIB and DivIC Is Codependent Only at High Temperatures and Requires FtsZ. *Journal of Bacteriology*, 182(12), pp.3607–3611.

Khadria, A. & Senes, A., 2013. Measurement of Transmembrane Peptide Interactions in Liposomes Using Förster Resonance Energy Transfer (FRET). *Methods in molecular biology (Clifton, N.J.)*, 1063, pp.19–36.

LaPointe, L.M. et al., 2013. Structural organization of FtsB, a transmembrane protein of the bacterial divisome. *Biochemistry*, 52(15), pp.2574–2585.

Li, E., You, M. & Hristova, K., 2005. Sodium Dodecyl Sulfate−Polyacrylamide Gel Electrophoresis and Förster Resonance Energy Transfer Suggest Weak Interactions between Fibroblast Growth Factor Receptor 3 (FGFR3) Transmembrane Domains in the Absence of Extracellular Domains and Ligands†. *Biochemistry*, 44(1), pp.352–360.

Liu, L.-P. & Deber, C.M., 1998. Guidelines for membrane protein engineering derived from de novo designed model peptides. *Peptide Science*, 47(1), pp.41–62.

MacKenzie, K.R. & Fleming, K.G., 2008. Association energetics of membrane spanning α-helices. *Current Opinion in Structural Biology*, 18(4), pp.412–419.

Masson, S. et al., 2009. Central domain of DivIB caps the C-terminal regions of the FtsL/DivIC coiled-coil rod. *The Journal of Biological Chemistry*, 284(40), pp.27687–27700.

Melnyk, R.A., Partridge, A.W. & Deber, C.M., 2001. Retention of Native-like Oligomerization States in Transmembrane Segment Peptides: Application to the Escherichia coli Aspartate Receptor†. *Biochemistry*, 40(37), pp.11106–11113.

Mingorance, J. et al., 2010. Strong FtsZ is with the force: mechanisms to constrict bacteria. *Trends in Microbiology*, 18(8), pp.348–356.

Pace, C.J. et al., 2011. A FlAsH–Tetracysteine Assay for Quantifying the Association and Orientation of Transmembrane α-Helices. *ChemBioChem*, 12(7), pp.1018–1022.

Posokhov, Y.O. et al., 2008. A SIMPLE “PROXIMITY” CORRECTION FOR FRET EFFICIENCY DETERMINATION IN MEMBRANES USING LIFETIME MEASUREMENTS. *Analytical biochemistry*, 380(1), pp.134–136.

Rath, A. & Deber, C.M., 2013. Design of transmembrane peptides: Coping with sticky situations. *Methods in molecular biology (Clifton, N.J.)*, In Press.

Renthal, R. et al., 2011. Interaction of a two-transmembrane-helix peptide with lipid bilayers and dodecyl sulfate micelles. *Biophysical chemistry*, 159(2-3), pp.321–327.

Robichon, C. et al., 2008. Artificial Septal Targeting of Bacillus subtilis Cell Division Proteins in Escherichia coli: an Interspecies Approach to the Study of Protein-Protein Interactions in Multiprotein Complexes. *Journal of Bacteriology*, 190(18), pp.6048–6059.

Robichon, C. et al., 2011. Role of Leucine Zipper Motifs in Association of the Escherichia coli Cell Division Proteins FtsL and FtsB ▽. *Journal of Bacteriology*, 193(18), pp.4988–4992.

Rowland, S.L. et al., 2010. Evidence from Artificial Septal Targeting and Site-Directed Mutagenesis that Residues in the Extracytoplasmic? Domain of DivIB Mediate Its Interaction with the Divisomal Transpeptidase PBP 2B. *Journal of Bacteriology*, 192(23), pp.6116–6125.

Schick, S. et al., 2010. Assembly of the M2 Tetramer Is Strongly Modulated by Lipid Chain Length. *Biophysical Journal*, 99(6), pp.1810–1817.

Seddon, A.M., Curnow, P. & Booth, P.J., 2004. Membrane proteins, lipids and detergents: not just a soap opera. *Biochimica et biophysica acta*, 1666(1-2), pp.105–117.

Stahl, P.J. et al., 2012. On-the-resin N-terminal modification of long synthetic peptides. *Analytical Biochemistry*, 424(2), pp.137–139.

Tulumello, D.V. & Deber, C.M., 2011. Positions of Polar Amino Acids Alter Interactions between Transmembrane Segments and Detergents. *Biochemistry*, 50(19), pp.3928–3935.

Villanelo, F. et al., 2011. A model for the Escherichia coli FtsB/FtsL/FtsQ cell division complex. *BMC structural biology*, 11, p.28.

Xiao Zhou, F. et al., 2000. Interhelical hydrogen bonding drives strong interactions in membrane proteins. *Nature Structural & Molecular Biology*, 7(2), pp.154–160.

You, M. et al., 2005. Förster resonance energy transfer in liposomes: Measurements of transmembrane helix dimerization in the native bilayer environment. *Analytical Biochemistry*, 340(1), pp.154–164.

FIGURES

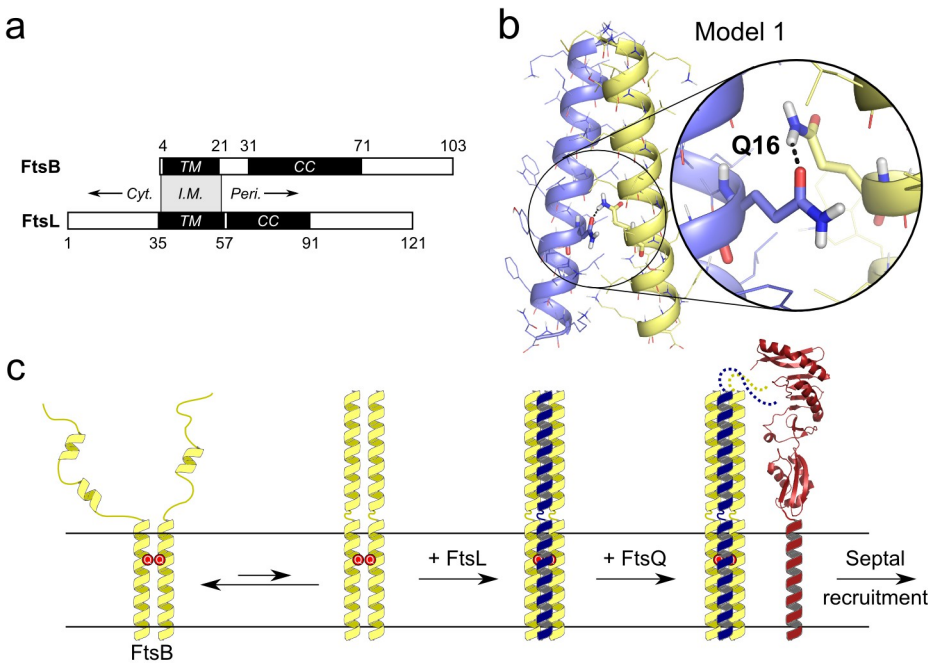

Figure 3.1. Starting hypothesis: FtsB and FtsL form a higher-order oligomer. a) FtsB and FtsL are two integral membrane proteins of the bacterial division complex. Their topology consists of a single transmembrane domain (TM) and a juxta-membrane coiled coil domain (CC). b) In previous work we determined that the transmembrane domain of FtsB homo-oligomerizes, and obtained an experimentally-supported computational model of a homo-dimer mediated by a critical hydrogen bond. c) We hypothesized that the TM dimer of FtsB (yellow) forms a core mediated by the critical Gln16 (red circles) for the lateral association of FtsL (blue). Here, we further provide support for this hypothesis by demonstrating that the TM domains of FtsB and FtsL associate stably in isolation forming a 1:1 higher-order oligomer.

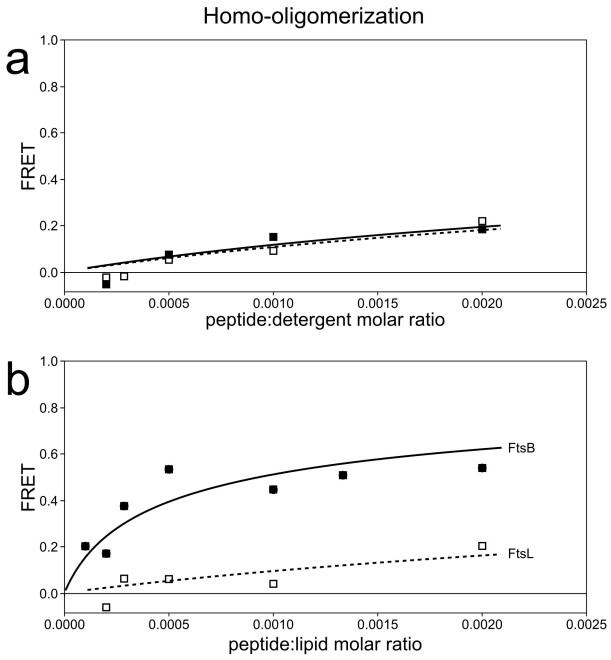

Figure 3.2. FtsB self-associates *in vitro* in lipid. Concentration-dependent FRET between a coumarin/FITC donor/acceptor pair, measured in (a) DPC micelles and (b) POPC multi-lamellar vesicles. The peptide concentration is expressed as a function of "hydrophobic volume" as peptide:detergent or peptide:lipid molar ratio. a) FtsB (filled squares) and FtsL (open squares) self-associate very weakly in detergent. b) The self-association of FtsL is not enhanced in lipid, while significant association is observed for FstB. The finding confirm the self-association of FtsB previously reported using TOXCAT(LaPointe et al. 2013). The lines correspond to fits to monomer-dimer equilibria.

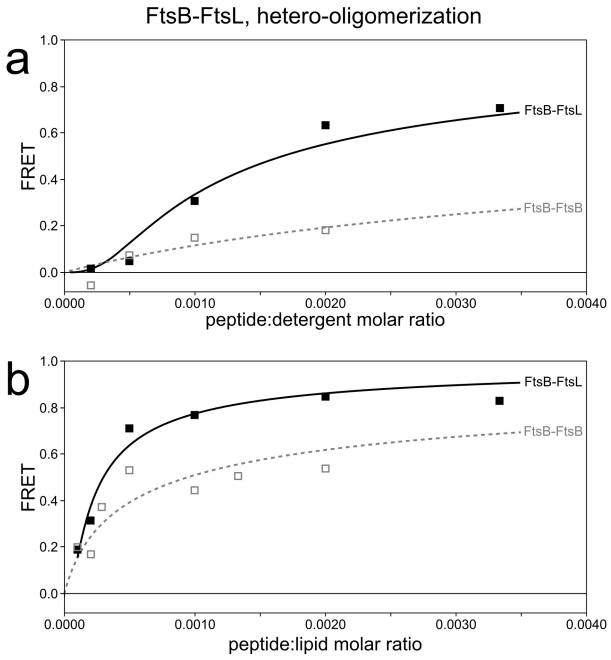

Figure 3.3. The TM domains of FtsB and FtsL form a stable oligomeric complex. Concentration-dependent FRET (black squares) between a coumarin-FtsL/FITC-FtsB pair, measured in a) DPC micelles and b) POPC multi-lamellar vesicles. The curves represent fits to monomer-tetramer equilibria. The FtsB self-association data **(Figure 3.2)** is reported as a reference (gray, dashed lines). The data indicate that FtsB and FtsL TM domains interact in both detergent and lipid environments.

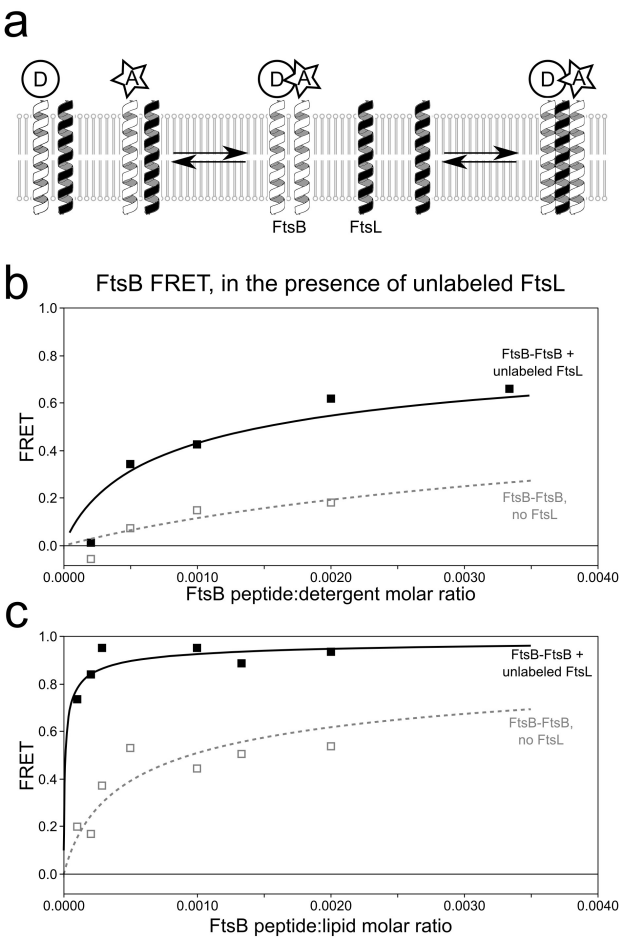

Figure 3.4. The TM domains of FtsB and FtsL form a higher-order oligomeric complex. a) Schematic view of a competition experiment in which FRET for a coumarin-FtsB/FITC-FtsB donor/acceptor pair (white helices, D: donor, A: acceptor) is measured in the presence of an equimolar amount of unlabeled FtsL (black helices). The concentration-dependent FRET in DPC detergent (b) and in POPC multi-lamellar vesicles (c) is reported as FtsB peptide concentration (not as FtsB+FtsL total peptide) as black squares. The FtsB self-association data **(Figure 3.2)** is repeated here as a reference (gray, dashed lines). The data is consistent with an FtsL-dependent stabilization of an FtsB homo-oligomer (right-most equilibrium in panel a) rather than a competing disruption (left-most equilibrium), suggesting the formation of a higher-order FtsB-FtsL oligomer.

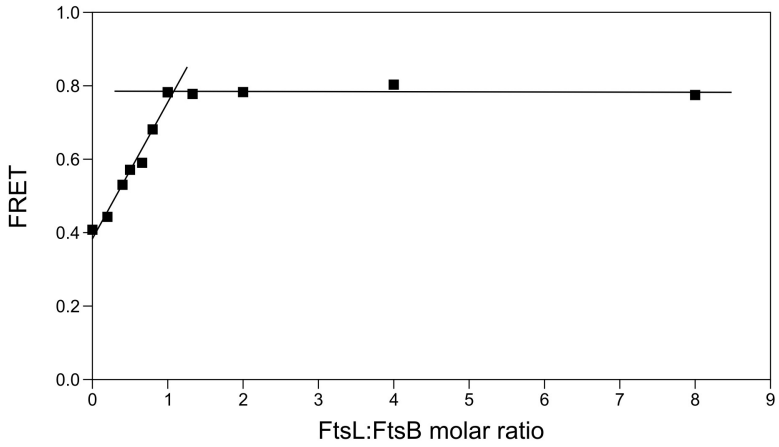

Figure 3.5. FtsB and FtsL form a 1:1 complex. Titration experiment in which unlabeled FtsL is added to donor and acceptor labeled FtsB, in a 1:1000 FtsB peptide to lipid ratio. The data shows a steep increase of FtsB homo-FRET until the stoichiometric ratio with FtsL reaches 1:1, followed by a sharp plateauing of the signal. The data is consistent with formation of a tetrameric (2:2) or hexameric (3:3) or higher complex. The lines represent two linear regressions to the set of FtsL:FtsB ratios of 0 to 1 and of 1 and higher.

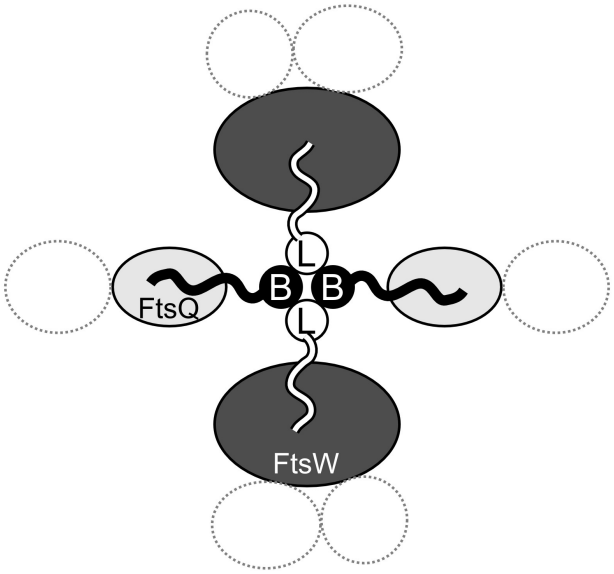

Figure 3.6. A higher-oligomeric FtsB-FtsL complex may be a multi-valent tethering structural element of the divisome. A schematic depiction of a tetrameric FtsB-FtsL complex (black and white circles marked B and L) seen from above the plane of the membrane. The FtsB-FtsL complex is bound to FtsQ with the periplasmic tail of FtsB(Gonzalez & Beckwith 2009; van den Berg van Saparoea et al. 2013) and to FtsW with the cytoplamic tail of FtsL(Gonzalez et al. 2010). Other hypothetical divisome components are depicted as dotted circles. The scheme illustrates how a tetrameric FtsB-FtsL complex could potentially bind to multiple divisome elements at the same time, therefore acting as a tethering structural element that contributes to hold together multiple sub-complexes within the Z-ring.

Supplementary Methods

N-terminal labeling of peptides

FITC labeling.

12 equivalents of N-ε-Fmoc-aminohexanoic acid (Fmoc-ε-Ahx-OH, AnaSpec) were coupled to the amino terminal of the peptide-resin overnight. After thorough washing, 20% Piperidine in DMF (Dimethylformamide) with 2% DBU (1,8-Diazabicyclo[5.4.0]undec-7-ene) was used to remove the Fmoc protecting group in two cycles in the MARS microwave at the UW Biotech center. 12 equivalents of FITC (Fluorescein isothiocyanate) 'isomer 1' (Sigma Aldrich) were mixed with 12 equivalents of PyBOP (Benzotriazol-1-yl-oxytripyrrolidinophosphonium hexafluorophosphate) and resuspended in minimal volume of DMF, and then NMP (N-Methylpyrrolidone) was added dropwise while stirring until a homogeneous solution was formed. This mixture was added to the deprotected peptide-resin while agitating the resin, and DIPEA (N,N-Diisopropylethylamine) was added dropwise. The reaction was carried out at room temperature, in dark, for 24 hours, washed thoroughly, and repeated 4 times. Efficient labeling of the peptide was achieved by this 'brute force' method of labeling the peptides. FITC, due to its high hydrophobicity, was particularly hard to label the peptides with, and required more number of repeats for efficient labeling. For the FtsL peptide, 5-carboxyfluorescein (5-FAM) was used to efficiently label the peptide using the same method as above.

Coumarin labeling.

7-hydroxycoumarin-3-carboxylic acid (Anaspec) was coupled directly to the deprotected

peptide-resin using the same technique described above, without the coupling of the Fmoc-ε-Ahx-OH linker. Addition of higher excess of DIPEA led to better labeling efficiencies for the coumarin labeled peptides. Frequent changes of reaction mixture for coumarin labeling minimized aggregation of the mixture to form an insoluble precipitate.

Quantification of peptides

Quantification and preparation of peptide stocks in TFE (Trifluoroethanol) was carried out by absorbance measurements using a Cary 50 scan UV/Vis spectrophotometer. Accurate quantification and calculation of labeling efficiencies was performed using a detailed procedure[1]. The calculations used have been listed below. It is important to note here that in the case of a labeled peptide, the absorbance of the peptide sample at 280 nm comprises of contributions from Trp and Tyr residues of both labeled and unlabeled peptides, as well as the absorbance of the fluorophore at 280 nm. To separate these components and achieve accurate quantification, 'correction factor' of the fluorophore (A_{280}/A_{max}) and accurate degree of labeling values need to be used. Correction factors for commonly used fluorophores are characterized along with their molar extinction coefficients at their λ_{max} values in aqueous buffers at a certain pH. However, these parameters change for the fluorophore in different solvent systems. **Figure S3.1(a)** shows a blue shift for the absorbance of FITC in TFE as compared to phosphate buffer, pH 9.0, where the molar extinction coefficient of FITC at 495nm is ~70,000 M^{-1} cm^{-1}. Various concentrations of FITC in TFE were scanned as shown in **Figure S3.1(b)**. **Figure S3.1(b) inset** shows a plot of the new A_{max} (477nm) of FITC in TFE versus FITC concentration. The slope of the curve provided the new $\varepsilon_{Fluorophore}$ (~32690 $M^{-1}cm^{-1}$) at the new λ_{max} (477nm) of FITC in TFE, which was used for quantification of the FITC peptides. The behavior of 5-FAM was found to be the same as FITC in TFE. The same

calculations were carried out for 7-hydroxycoumarin-3-carboxylic acid in TFE (data not shown).

Concentration of the fluorophore in the sample

$$\textbf{[Fluorophore]} = A_{max}/\varepsilon_{Fluorophore}\, l \quad \textbf{(1)}$$

where A_{max} is absorbance at λ_{max} of the dye

$\varepsilon_{Fluorophore}$ is extinction coefficient of the dye at λ_{max}

l is path length of the cuvette

Concentration of the peptide based on Trp absorbance

$$\textbf{[Peptide]} = A_{280} - (A_{max} * CF)/\varepsilon\, l \quad \textbf{(2)}$$

where A_{280} is absorbance at 280nm

CF is the correction factor that adjusts for absorbance at 280 nm by the fluorophore, and is given by A_{280} / A_{max}

ε is extinction coefficient of the peptide (calculated based on no. of Trp, and Tyr)

Calculation of the degree of labeling

$$\textbf{Percent labeling} = \textbf{[Fluorophore]/[Peptide]} * 100 \quad \textbf{(3)}$$

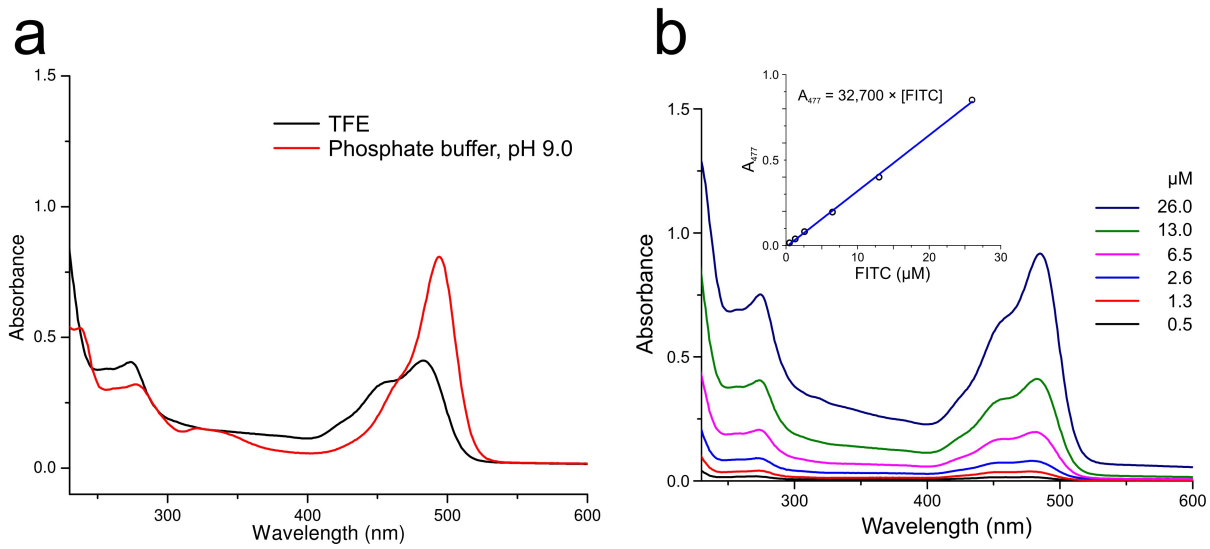

Figure S3.1. Characterization of FITC in TFE. a) Red curve shows absorbance scan of FITC in phosphate buffer pH 9.0, showing a λ_{max} of 495 nm. Black curve shows absorbance scan equal concentration of FITC in TFE, exhibiting a blue shift of the λ_{max} to 477nm. b) Absorbance scans of different concentrations of FITC in TFE. The slope of the absorbance plot at 477 nm, according to Beer's law, yielded the molar extinction coefficient of FITC in TFE.

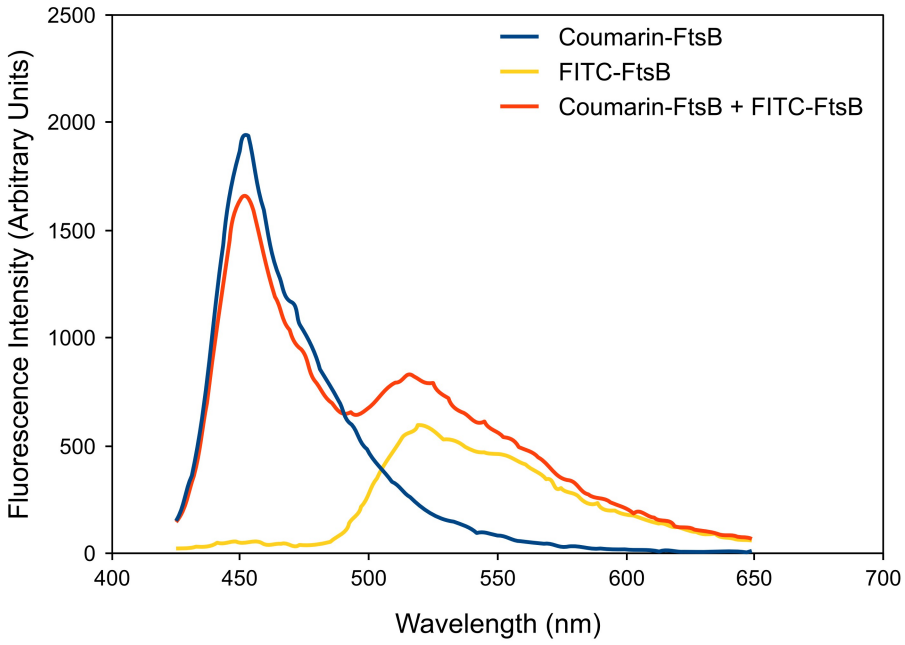

Figure S3.2. Fluorescence spectra of coumarin (donor) and FITC (acceptor) labeled peptides. Characteristic fluorescence scans of peptides in POPC in a 1:5000 peptide:lipid ratio. The excitation wavelength was fixed at 415 nm for maximum spectral overlap for the donor-acceptor pair. The emission scan was from 425 nm to 650 nm. The coumarin-FtsB+FITC-FtsB sample (orange curve) shows donor quenching compared to the coumarin-FtsB only sample (blue curve). The donor+acceptor pair also shows acceptor sensitization above the level of FITC-FtsB direct excitation at 415 nm (yellow curve), indicating FRET between the two FtsB peptides. Percentage FRET was calculated from decrease in the donor emission maxima at 450 nm.

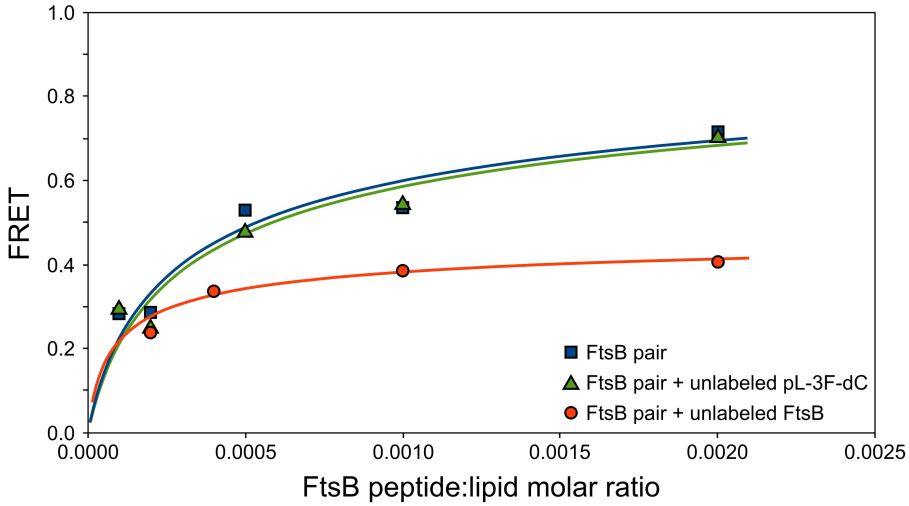

Figure S3.3. Effect of unlabeled control peptides on FtsB homo-FRET. Addition of equimolar amount of an unrelated monomeric peptide, pL-3F-dC (green triangles) to an FtsB FRET pair in POPC lipid does not shift the curve compared to the no-peptide control (blue squares). Addition of an equimolar amount of unlabeled FtsB reduces FRET in a manner that is consistent with a 50% decrease in FRET efficiency. All curves were fit assuming an FtsB monomer-dimer equilibrium. The “unlabeled FtsB” data set was fit by using total FtsB peptide (labeled + unlabeled) for concentration and a maximum FRET efficiency of 50%.

References

(1) Khadria, A., and Senes, A. (2013) Measurement of Transmembrane Peptide Interactions in Liposomes Using Förster Resonance Energy Transfer (FRET). *Methods Mol. Biol. Clifton NJ 1063*, 19–36

CHAPTER FOUR

Determination of the oligomeric state of the FtsB-FtsL complex

Introduction

The *E.coli.* divisome proteins FtsB and FtsL have been hypothesized to be structural proteins that contribute to the stabilization of the Z-ring (Gonzalez & Beckwith 2009; Robichon et al. 2011; Geissler & Margolin 2005). In previous work, we have shown that FtsB TM domain self-associates to form homo-oligomers both in bacterial membranes (LaPointe et al. 2013) and in artificial bilayers (Khadria & Senes 2013b), and that FtsL TM domain stabilizes the FtsB oligomer to form a higher order complex of 1:1 stoichiometry (Khadria & Senes 2013b).

Evidence suggests that FtsB and FtsL bind to multiple partners in the divisome. Being a part of the set of intermediate proteins in the functional hierarchy of the divisome, the formation of the FtsB-FtsL higher oligomeric complex may be crucial to the functional role of these proteins. FtsB and FtsL associate with FtsQ through their periplasmic domains (Gonzalez & Beckwith 2009; Gonzalez et al. 2010; Masson et al. 2009; Villanelo et al. 2011; van den Berg van Saparoea et al. 2013), the tail of FtsL is required for recruitment of FtsW(Gonzalez et al. 2010), a late protein, and several other potential interactions with other proteins have been postulated (D'Ulisse et al. 2007).This evidence suggests the hypothesis that a multi-valent FtsB-FtsL complex may bind multiple partners simultaneously and act as an interaction hub that tethers together several complexes of the divisome (Khadria & Senes 2013b). It is therefore important to establish the precise oligomeric state of the FtsB-FtsL complex, whether it is a tetramer, hexamer, or an even higher oligomer.

To ascertain the oligomeric state of the FtsB-FtsL complex, I propose to use three different techniques: FRET, analytical ultracentrifugation (AUC) (Doura & Fleming 2004; Burgess et al. 2008) and single molecule photobleaching. FRET efficiency as a function of

acceptor mole fraction, assuming a 1:1 stoichiometry of FtsB:FtsL, may yield an indirect measure of the number of molecules in the complex. AUC will be directly sensitive to the mass of the complex, and yield the molecular weight of the complex in detergent. Single molecule photobleaching experiments will provide a precise could on the oligomeric state of individual FtsB-FtsL complexes. Together these three techniques will allow us to determine the number of molecules of FtsB and FtsL, and shed further light on the function of these proteins in the divisome.

FRET to measure oligomeric state

As described in Chapter 1, the relationship between FRET efficiency as a function of the acceptor mole fraction can be used to predict whether a TM complex is dimeric, exhibiting a linear relationship, or a higher order oligomer (Adair & Engelman 1994; Veatch & Stryer 1977) as well as the number of subunits in a higher-oligomer (Li et al. 1999). The formalisms used in this work have been primarily used to elucidate the oligomeric state of homo-oligomers.

In the case of the FtsB-FtsL complex, FRET data was fit under the assumption that FtsB forms a homo-dimer and FtsB-FtsL form a tetramer (Khadria & Senes 2013b). It may not be straightforward to interpret the FRET data as a function of mole fraction of acceptor to elucidate the oligomeric state of the complex; due to the presence of an additional FtsB dimer species in the equilibrium. However, the establishment of a 1:1 stoichiometry of the complex provided a starting point to modify the experiment and apply it for the hetero-oligomer of FtsB and FtsL.

Experimental design

In the previous FRET experiments (Chapter 3), donor- and acceptor-labeled FtsB peptides were mixed in a 1:1 molar ratio. This mixture was equilibrated with an equimolar amount of unlabeled FtsL. Samples were prepared over a wide range of total peptide:lipid ratios. The increase in FtsB-FRET values in the presence of equimolar unlabeled FtsL showed that FtsL stabilizes the FtsB homo-oligomer. Further, addition of increasing amounts of unlabeled FtsL to a 1:1 donor:acceptor labeled FtsB in a fixed total peptide:lipid ratio

showed that increasing amounts of FtsL, beyond a 1:1 stoichiometry, did not stabilize the FtsB homo oligomer any further. Combining this knowledge with the 1:1 stoichiometry determined previously, we can estimate the number of FtsB (and FtsL) molecules in the complex. For example, tetramers or hexamers of FtsB-FtsL will have two or three molecules of FtsB, respectively.

To perform this experiment, FtsB- and FtsL-TM peptides (underlined sequence is the native TM sequence) have been synthesized, labeled on the resin, purified and quantified as previously described (Khadria & Senes 2013b). Separate batches of FtsB-TM peptides have been N-terminally labeled with 7-hydroxycoumarin and 5-carboxyfluorescein dyes, and FtsL-TM peptides have been left unlabeled.

FtsB-TM: GGKLTLLLLAILVWLQYSLWFGKKKK

FtsL-TM: GGGKLPLCLFICIILTAVTVVTTA**W**HKK

Reconstitution of peptides in detergent and lipid will be carried out as before (Chapter 2 and 3). 'FRET samples' will be prepared keeping a fixed 1:1000 peptide:lipid ratio (a concentration where FtsB was found to be associated). The total amount of FtsB peptide will remain constant, but the ratio of Coum-FtsB : FAM-FtsB (or donor:acceptor FtsB) will be varied in different samples from 1:0 to 0:1. The amount of FtsL will remain constant such that each sample will contain a 1:1 FtsB:FtsL ratio. For each sample there will be a 'donor only' sample containing the same amount of donor-FtsB as its corresponding sample and the same amount of unlabeled FtsL and lipid, but no acceptor-FtsB. Control experiments will be carried out using unlabeled FtsB in place of acceptor FtsB, corresponding to each 'FRET sample', to get the donor quantum yield values in an environment of similar crowding. FRET efficiency

will be calculated using donor quenching (described in Chapters 1,2 and 3), and will be plotted as a function of increasing mole fraction of the acceptor according to the theory developed by Adair and Engelman. A linear dependency of the FRET efficiency on the acceptor mole ratio will indicate an FtsB dimer, suggesting that the FtsB-FtsL complex is a tetramer. A non linear fit to the curve will have to be analyzed to determine whether the number of FtsB molecules in the complex is three or higher, indicating a hexamer or a higher FtsB-FtsL complex. The same experiment with labeled FtsL and unlabeled FtsB can also be carried out to validate the results. For example, if the dependency is linear in both the experiments, we can conclude that FtsL is also dimeric, and thus the complex is a tetramer.

Although this experiment will not be a direct measurement of the FtsB-FtsL proximity using FRET, the 1:1 stoichiometry (inferred from previous experiments) will indirectly yield the oligomeric state of the FtsB-FtsL complex.

AUC to measure oligomeric mass

Sedimentation equilibrium analytical ultracentrifugation (SE-AUC) is a thermodynamically rigorous method that yields the average molecular weight of any macromolecule as a function of its concentration. If a system has achieved reversible equilibrium along the opposing concentration and diffusion gradients, then AUC experiments can provide thermodynamic parameters for the reaction like the oligomeric state and the associated equilibrium constants.

In the case of FRET experiments, a monomer-dimer curve will not be distinguishable from a dimer-tetramer curve. An advantage of SE-AUC in this regard is that it provides a direct measure of the mass of the species, where a change in the oligomeric state will lead to a direct measurement of the unassociated monomer or the associated oligomer.

In the case of membrane proteins, use of AUC to determine the oligomeric mass of the complex is challenging. Because of the chemically heterogeneous environment of the native lipid bilayer that these proteins reside in, and their high hydrophobic nature, they need to be handled in the presence of a hydrophobic solvent, and then resuspended in aqueous media. The presence of this hydrophobic co-solvent introduces complexity into the analysis as it contributes to the overall mass of a membrane protein complex and needs to be accounted for in order to separate the mass contributions of the protein from those of the bound solvent. As the process of sedimentation in a centrifuge begins, the protein begins to concentrate toward the bottom of the centrifuge cell. As the concentration at the bottom starts to increase, diffusion begins to oppose sedimentation, and over a period of time, an equilibrium is obtained, with the concentration of the protein increasing exponentially towards the cell bottom. At equilibrium, this concentration gradient does not change any more and is a

function of the molecular weight of the complex. Now if the density of the detergent used is greater than the solvent, the solute will sediment toward the cell bottom. Conversely, if the density of the detergent is less than that of the solvent, then the detergent will float towards the top of the solution. When densities are equal, there will be no tendency to move in either direction. Thus one way to simplify the experiment is by matching the densities of the detergent. There are many strategies that are useful in accounting for the contribution of the bound solvent (Burgess et al. 2008; Reynolds & McCaslin 1985; Reynolds & Tanford 1976) which are very useful in determining the molecular weights of membrane protein complexes in detergent micelles.

Experimental design

In collaboration with Dr. Darrel McCaslin (Bioinstrumentation Facility, Department of Biochemistry), I aim to perform SE-AUC experiments on the FtsB-FtsL TM domain complex to determine the oligomeric mass and hence the oligomeric state of the complex. To perform this experiment, FtsB and FtsL-TM peptides (underlined sequence is the native TM sequence) have been synthesized, and purified as previously described (Khadria & Senes 2013b):

FtsB-TM: GGKLTLLLLAILVWLQYSLWFGKKKK

FtsL-TM: GGKLPLCLFICIILTAVTVVTTAHHKKK

Unlike in the case of FRET experiments, the FtsL sequence does not contain the artificially introduced Trp residue. This is because the AUC experiment will be performed using absorbance optics at 280nm wavelength, and the oligomeric mass of FtsB will be determined in the presence and absence of FtsL. Thus, FtsB will be easily distinguishable from FtsL due to the presence of two Trp and one Tyr in FtsB and none in FtsL.

Preliminary experiments

Peptides were dissolved in C12E8 (Octaethylene glycol monododecyl ether) detergent at a detergent concentration above its CMC of 80 μM. Preliminary experiments were performed using two different concentrations of FtsB, 3 3 μM and 48 μM (such that the absorbance values in the centrifuge cell at 280 nm and 1.2 cm path length, are 0.4 ad 0.6, respectively). FtsB peptides were dissolved in a 1:1000 peptide:detergent ratio, in the presence and absence of 1.2x molar concentrations of FtsL to push the equilibrium to an associated state (assuming a 1:1 stoichiomtery as observed from FRET experiments (Khadria & Senes 2013b)). The molecular weight of FtsB in the presence of FtsL was double that in the absence of FtsL, indicating that FtsL is stabilizing FtsB self association (data not shown), as observed in the FRET data. It also appeared that FtsB alone was monomeric in C12E8 in the 1:1000 ratio, suggesting weak association in detergent, possibly even weaker than observed with DPC detergent in the FRET data (Khadria & Senes 2013b). However, the absorbances recorded during the centrifugation process were also lower than measured at the time of sample preparation, indicating that the low solubility of the peptides in the detergent could be rendering the effective concentration of FtsB in C12E8 lower, and thus monomeric. These analyses are speculative, and repeated measurements need to be performed to obtain conclusive data.

Future Work

I aim to repeat these experiments, and if required, increase the solubility of the peptides in the detergent by synthesizing different versions of the peptides with greater number of positively charged Lys residues (Khadria & Senes 2013a). With the help of Dr. Darrel McCaslin, the data obtained will be fitted to obtain the oligomeric state of the FtsB-FtsL

TM complex, and eventually extended to the full length proteins as well.

Single molecule photobleaching to measure number of subunits

In contrast with traditional biochemical and biophysical experiments, single molecule techniques are free of ensemble averaging of measurements. This enables the unraveling of inherent heterogeneities in the structures and dynamics of biological systems. In particular, single molecule fluorescence microscopy allows the imaging of individual molecules of interest *in vitro* and in living cells. It provides a distribution of high resolution data from single fluorophore tagged molecules that allows high precision energetic as well as kinetic measurements (provided the reaction timescale is measurable by the technique used). Here, I describe a single molecule method, currently being developed in collaboration with Dr. Aaron Hoskins, to establish the exact number of FtsB and FtsL molecules in the FtsB-FtsL complex.

Experimental design

The goal of this project is to use single molecule photobleaching to estimate the number of fluorophore labeled FtsB-TM molecules present in a single lipid vesicle, in the presence and absence of unlabeled FtsL-TM.

Photobleaching is a process in which a fluorophore, upon exposure to light, undergoes irreversible photon-induced damage and permanently loses its ability to fluoresce. Chemically, the electrons in the excited state, when transitioning into a long lived 'dark' triplet state (shown in Scheme 1.1, Chapter 1), can react with other molecules to form irreversible covalent modifications in the fluorophores. A fluorophore undergoes many cycles of excitation and emission cycles before photobleaching, which varies between a few cycles to millions of cycles based on the fluorophore used and its local environment. While performing imaging experiments, photobleaching can be reduced by using lower laser power, reducing the

illumination time, or using oxygen scavenging systems like glucose, glucose oxidase, and catalase. If the photobleaching process can be optimized to be within the timescale of the imaging experiment, then the number of photobleaching steps observed can be used to estimate the number of fluorophores in the sample. Thus, using photobleaching, the number of labeled FtsB molecules in the presence and absence of unlabeled FtsL can be estimated in an immobilized vesicle.

The vesicles continuing labeled peptides will be immobilized directly on PEG-biotinylated glass surfaces or via supported bilayers on glass (Boukobza et al. 2001), or through non specific interactions with glass. Imaging will be performed on a Total Internal Reflection Fluorescence (TIRF) microscope in Dr. Aaron Hoskins' lab (J. Larson et al. 2014; J. D. Larson et al. 2014). This setup will enable time-lapse imaging of single immobilized vesicles and a photobleaching profile will be generated. Step-wise photobleaching will indicate the number of labeled peptides present within a single immobilized vesicle **(Figure 4.1)**. The peptide:lipid ratio will be adjusted to obtain, on average, less than one labeled FtsB molecule per lipid vesicle **(Figure 4.1a,b).** Photobleaching trajectories in the absence of FtsL will be analyzed and the number of FtsB molecules per vesicle will be determined. Next, we will introduce unlabeled FtsL into the system in a 1:1 FtsB:FtsL ratio. From our previous work (Chapter 3), we know that FtsL stabilizes the FtsB homo-dimer by forming a higher-order oligomer. Therefore, the addition of FtsL is expected to result in an increase in the average number of FtsB molecules per vesicle. We hope to observe this effect as an increase in the average number of photobleaching steps **(Figure 4.1c,d)**.

To perform this experiment, FtsB and FtsL-TM peptides (underlined sequence is the native TM sequence) were synthesized, labeled on the resin, purified and quantified as previously described (Khadria and Senes 2013b). FtsB-TM peptides were **N-terminal**ly

labeled with Cy3-NHS ester, and FtsL-TM peptides were left unlabeled.

FtsB-TM: GGKLTLLLLAILVWLQYSLWFGKKKK

FtsL-TM: GGGKLPLCLFICIILTAVTVVTTA**W**HKK

Cy3-FtsB peptides were reconstituted in POPC lipid, evaporated, hydrated using 50 mM sodium phosphate, pH 8.0, 100 mM NaCl, and freeze thawed to form multilamellar vesicles (MLVs) as described before (Khadria & Senes 2013a; Khadria & Senes 2013b). MLVs were extruded through 100 nm polycarbonate membranes using an Avanti Mini Extruder to form large unilamellar vesicles (LUVs). Dynamic light scattering was used to monitor the size distribution of the extruded vesicles.

LUVs immobilized on a glass surface were imaged on a mmTIRF microscope equipped with an oil-immersion objective (Olympus Plan Apo, 60x magnification, 1.45 numerical aperture) using an Andor EMCCD camera with 512 by 512 pixels of size 16 μm X 16 μm. Data was acquired using Glimpse software implemented in LabVIEW (National Instruments). Immobilized vesicles containing Cy3-FtsB were imaged using 488 nm excitation with laser power ~400 μW (16W/cm^2, considering a field of view 50 μm X 50 μm). Images were collected continuously at an acquisition rate of 1 frame per second for 5 minutes with no inter-frame dead time.

0.1-1% NBD-PE labeled POPC vesicles without peptides were first used for control experiments to visualize immobilization of single LUVs on microfluidic chambers on glass slides. A field of view (FOV) on the microfluidic chamber was chosen. Buffer containing labeled POPC LUVs was flowed into the chamber and image acquisition was started. 'Landing' of spots within the FOV due to non specific binding of the vesicles to glass was observed until the number of spots was constant. Buffer was flowed through the chamber

twice to wash off the unbound vesicles. Concentration of the LUV sample was optimized so that we observed 25-30 single spots in the FOV. The FOV was imaged for 5 minutes to observe unbinding of the immobilized vesicles, and minimal dissociation of the vesicles was observed in this timescale.

Typically, LUVs 100nm in diameter contain ~10,000 lipid molecules (Huwyler et al. 1996; Hansen et al. 1995). Thus, to achieve less then 1 peptide per LUV, the reconstituted peptide to lipid ratios used were 1:100,000 and 1:200,000. LUVs made of unlabeled POPC containing the Cy3-FtsB peptides were then imaged using the above imaging conditions under similar concentrations as obtained from the control experiment.

Proposed analysis

A proposed scheme for analysis of the single molecule fluorescence data is given below.

Selection of fluorescent spots

Single-molecule photobleaching analyses will be performed using custom software in MATLAB. Fluorescent spots are first selected as areas of interest (AOIs) and their intensity is integrated as a function of time. This generates a photobleaching profile for each molecule selected. The total fluorescence intensity of an AOI will be determined by integrating the intensities corresponding to all pixels within the AOI. AOIs will be analyzed only if they were well-resolved from other spots and displayed stepwise photobleaching

Defining a photobleaching step

Noise in the photobleaching time traces will be estimated at each time point as the standard deviation, S, of all preceding points since the last detected step. A threshold will be determined by multiplying the standard deviation with a user-defined factor, k. A photobleaching step will be detected when the difference in intensities between two

consecutive frames, I_{t-1} and I_t, is greater than this threshold (Das et al. 2007), i.e.

$$I_t - I_{t-1} = \Delta I \geq k * S$$

Counting the number of steps

Based on the analysis protocol mentioned above, the number of photobleaching steps associated with each single-molecule will be determined for ~100 molecules per experiment. The robustness of the results will be verified by performing each experiment in triplicate. To determine the number of subunits present, histograms of the frequency of photobleaching steps (number of molecules vs number of photobleaching steps) will be made. In the absence of unlabeled FtsL, most vesicles will be expected to have a single Cy3-FtsB peptide. Working in the same total peptide:lipid concentration regime, the presence of unlabeled FtsL is expected to stabilize the FtsB oligomer (Khadria & Senes 2013b) and thus increase the occupancy of Cy3-FtsB in single vesicles. Based on the distribution of Cy3-FtsB photobleaching steps in the presence of FtsL, the oligomeric state of the FtsB-FtsL complex will be determined.

Preliminary data

Here I present representative data and an outline of the analysis that will be performed. Cy3-FtsB peptides were reconstituted in POPC vesicles in a 1:100,000 peptide:lipid ratio, extruded, and monitored for uniform distribution by DLS. Samples were non-specifically immobilized on glass slides and imaged as described above. Fluorescent spots were analyzed **(Figure 4.2a)** and photobleaching time traces of selected AOIs were plotted. A wide variety of photobleaching profiles were observed. Some AOIs seemed to have <5 photobleaching steps **(Figure 4.2b).** However, most of the AOIs exhibited higher fluorescence

intensity (brighter and larger spots) and a slow temporal decay of the signal **(Figure 4.2c)**, indicating either clustering of lipid vesicles, or higher Cy3-FtsB occupancy per vesicle.

Future Work

Several peptide:lipid ratios will be tested and optimized to obtain photobleaching trajectories for single Cy3-FtsB molecules. Further, use of labeled FtsL peptides and colocalization experiments with labeled FtsB and FtsL molecules will be carried out. This analysis will validate a direct role of FtsL in the stabilization of the FtsB oligomer, and yield an accurate estimate of the number of FtsB and FtsL molecules in the complex.

References

Adair, B.D. & Engelman, D.M., 1994. Glycophorin A helical transmembrane domains dimerize in phospholipid bilayers: a resonance energy transfer study. *Biochemistry*, 33(18), pp.5539–5544.

Van den Berg van Saparoea, H.B. et al., 2013. Fine-mapping the Contact Sites of the Escherichia coli Cell Division Proteins FtsB and FtsL on the FtsQ Protein. *The Journal of biological chemistry*, 288(34), pp.24340–24350.

Boukobza, E., Sonnenfeld, A. & Haran, G., 2001. Immobilization in Surface-Tethered Lipid Vesicles as a New Tool for Single Biomolecule Spectroscopy. *The Journal of Physical Chemistry B*, 105(48), pp.12165–12170.

Burgess, N.K., Stanley, A.M. & Fleming, K.G., 2008. Determination of Membrane Protein Molecular Weights and Association Equilibrium Constants Using Sedimentation Equilibrium and Sedimentation Velocity. In I. Dr. John J. Correia and Dr. H. William Detrich, ed. *Methods in Cell Biology*. Academic Press, pp. 181–211. Available at: http://www.sciencedirect.com/science/article/pii/S0091679X07840076 [Accessed July 22, 2013].

Das, S.K. et al., 2007. Membrane protein stoichiometry determined from the step-wise photobleaching of dye-labelled subunits. *Chembiochem: A European Journal of Chemical Biology*, 8(9), pp.994–999.

Doura, A.K. & Fleming, K.G., 2004. Complex interactions at the helix-helix interface stabilize the Glycophorin A transmembrane dimer. *Journal of molecular biology*, 343(5), pp.1487–1497.

D'Ulisse, V. et al., 2007. Three functional subdomains of the Escherichia coli FtsQ protein are involved in its interaction with the other division proteins. *Microbiology (Reading, England)*, 153(Pt 1), pp.124–138.

Geissler, B. & Margolin, W., 2005. Evidence for functional overlap among multiple bacterial cell division proteins: compensating for the loss of FtsK. *Molecular Microbiology*, 58(2), pp.596–612.

Gonzalez, M.D. et al., 2010. Multiple interaction domains in FtsL, a protein component of the widely conserved bacterial FtsLBQ cell division complex. *Journal of bacteriology*, 192(11), pp.2757–2768.

Gonzalez, M.D. & Beckwith, J., 2009. Divisome under construction: distinct domains of the small membrane protein FtsB are necessary for interaction with multiple cell division proteins. *Journal of bacteriology*, 191(8), pp.2815–2825.

Hansen, C.B. et al., 1995. Attachment of antibodies to sterically stabilized liposomes: evaluation, comparison and optimization of coupling procedures. *Biochimica Et Biophysica Acta*, 1239(2), pp.133–144.

Huwyler, J., Wu, D. & Pardridge, W.M., 1996. Brain drug delivery of small molecules using immunoliposomes. *Proceedings of the National Academy of Sciences*, 93(24), pp.14164–14169.

Karimova, G., Dautin, N. & Ladant, D., 2005. Interaction network among Escherichia coli membrane proteins involved in cell division as revealed by bacterial two-hybrid analysis. *Journal of Bacteriology*, 187(7), pp.2233–2243.

Khadria, A.S. & Senes, A., 2013a. Measurement of Transmembrane Peptide Interactions in Liposomes Using Förster Resonance Energy Transfer (FRET). *Methods in molecular biology (Clifton, N.J.)*, In Press.

Khadria, A.S. & Senes, A., 2013b. The Transmembrane Domains of the Bacterial Cell Division Proteins FtsB and FtsL Form a Stable High-Order Oligomer. *Biochemistry*, 52(43), pp.7542–7550.

LaPointe, L.M. et al., 2013. Structural organization of FtsB, a transmembrane protein of the bacterial divisome. *Biochemistry*, 52(15), pp.2574–2585.

Larson, J. et al., 2014. Design and construction of a multiwavelength, micromirror total internal reflectance fluorescence microscope. *Nature Protocols*, 9(10), pp.2317–2328.

Larson, J.D., Rodgers, M.L. & Hoskins, A.A., 2014. Visualizing cellular machines with colocalization single molecule microscopy. *Chemical Society Reviews*, 43(4), pp.1189–1200.

Li, M. et al., 1999. A fluorescence energy transfer method for analyzing protein oligomeric structure: application to phospholamban. *Biophysical Journal*, 76(5), pp.2587–2599.

Masson, S. et al., 2009. Central domain of DivIB caps the C-terminal regions of the FtsL/DivIC coiled-coil rod. *The Journal of Biological Chemistry*, 284(40), pp.27687–27700.

McGuire, H. et al., 2012. Automating single subunit counting of membrane proteins in mammalian cells. *The Journal of Biological Chemistry*, 287(43), pp.35912–35921.

Reynolds, J.A. & McCaslin, D.R., 1985. [3] Determination of protein molecular weight in complexes with detergent without knowledge of binding. In S. N. T. C.H.W. Hirs, ed. *Methods in Enzymology*. Enzyme Structure Part J. Academic Press, pp. 41–53. Available at: http://www.sciencedirect.com/science/article/pii/S0076687985170059 [Accessed October 30, 2014].

Reynolds, J.A. & Tanford, C., 1976. Determination of molecular weight of the protein moiety in protein-detergent complexes without direct knowledge of detergent binding. *Proceedings of the National Academy of Sciences of the United States of America*, 73(12), pp.4467–4470.

Robichon, C. et al., 2011. Role of Leucine Zipper Motifs in Association of the Escherichia coli Cell Division Proteins FtsL and FtsB ▽. *Journal of Bacteriology*, 193(18), pp.4988–4992.

Veatch, W. & Stryer, L., 1977. The dimeric nature of the gramicidin A transmembrane channel: Conductance and fluorescence energy transfer studies of hybrid channels. *Journal of Molecular Biology*, 113(1), pp.89–102.

Villanelo, F. et al., 2011. A model for the Escherichia coli FtsB/FtsL/FtsQ cell division complex. *BMC structural biology*, 11, p.28.

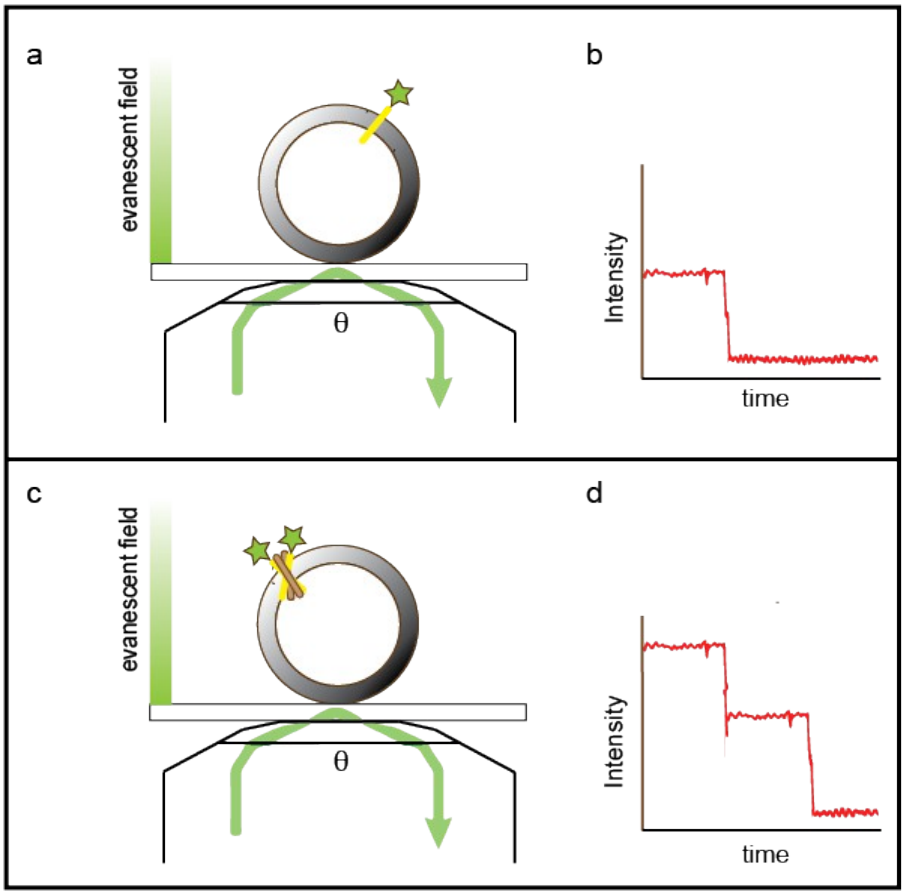

Figure 4.1. A single-molecule photobleaching study to monitor oligomeric state of FtsB-FtsL complex. Schematic depiction of the TIRF microscope. An incident beam with an angle of incidence θ (critical angle) is completely reflected by the glass slide (green arrow). Below the cover slip, an evanescent field is created with a depth of 100-150 nm, which can excite molecules present in that layer. The lipid vesicles are non specifically immobilized to the glass surface containing (a) one (average) Cy3-FtsB TM peptide (yellow) and (c) two (average) Cy3-FtsB TM peptides due to stabilization of FtsB-FtsL complex in presence of unlabeled FtsL (brown). Expected time traces of the intensity of Cy3 showing (b) one step photobleaching and (d) two step photobleaching behaviors indicating tetramer formation assuming 1:1 FtsB:FtsL stoichiometry.

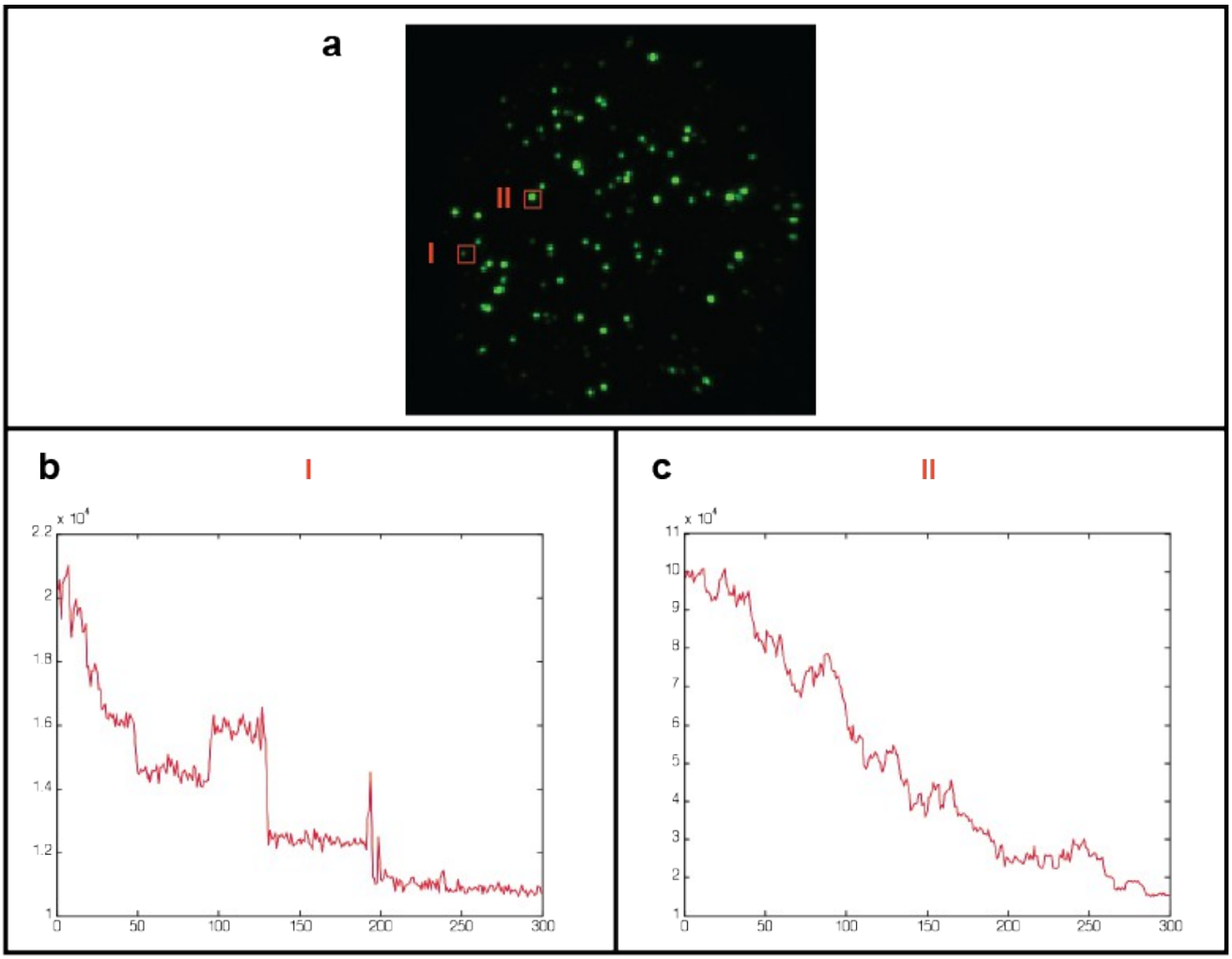

Figure 4.2. Analysis of fluorescent spots to obtain photobleaching trajectories. Cy3-FtsB in POPC LUVs on glass, imaged by excitation with the 488 nm green laser. (a) A field of view with ~50 spots (AOIs) with varying size and brightness of spots. Analysis is done in a custom MATLAB program by selecting the AOIs and drawing a rectangle around it. Two representative AOIs labeled I and II are shown. (b) Photobleaching trajectory of AOI (I) with seemingly <5 photobleaching steps. (c) Photobleaching trajectory of AOI (II) with a much higher fluorescence intensity (5 fold). Spot II photobleaches in a more gradual, continuous fashion as compared to sharp steps in spot I.

CHAPTER FIVE

A Gly-zipper motif mediates homo-dimerization of the transmembrane domain of the mitochondrial kinase ADCK3

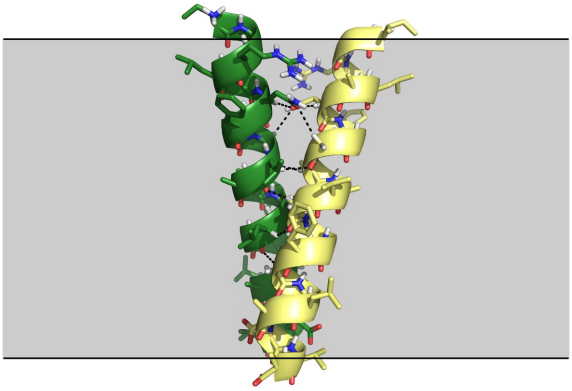

Based on:

Khadria, A.S., Mueller, B.K., Stefely, J.A., Tan C.H., Pagliarini, D.J., and Senes, A., 2014. A Gly-zipper motif mediates homo-dimerization of the transmembrane domain of the mitochondrial kinase ADCK3. *J Am Chem Soc* (2014) 136, 14068-77

(*My contribution in this paper was the experimental section, and the computational analyses were performed by B.K. Mueller)*

Abstract

Interactions between α-helices within the hydrophobic environment of lipid bilayers are integral to the folding and function of transmembrane proteins; however, the major forces that mediate these interactions remain debated, and our ability to predict these interactions is still largely untested. We recently demonstrated that the frequent transmembrane association motif GAS_{right} – the GxxxG-containing fold of the glycophorin A dimer – is optimal for the formation of extended networks of Cα–H hydrogen bonds, supporting the hypothesis that these bonds are major contributors to association. We also found that optimization of Cα–H hydrogen bonding and inter-helical packing is sufficient to computationally predict the structure of known GAS_{right} dimers at near atomic level. Here, we demonstrate that this computational method can be used to characterize the structure of a protein not previously known to dimerize, by predicting and validating the transmembrane dimer of ADCK3, a mitochondrial kinase. ADCK3 is involved in the biosynthesis of the redox active lipid, ubiquinone, and human ADCK3 mutations cause a cerebellar ataxia associated with ubiquinone deficiency, but the biochemical functions of ADCK3 remain largely undefined. Our experimental analyses show that the transmembrane helix of ADCK3 dimerizes, with an interface based on an extended Gly-zipper motif, as predicted by our models. The data provide strong evidence for the hypothesis that optimization of Cα–H hydrogen bonding is an important factor in the association of transmembrane helices. This work also provides a structural foundation for investigating the role of transmembrane association in regulating the biological activity of ADCK3.

Introduction

A fundamental event in the folding and oligomerization of membrane proteins is the association of the transmembrane (TM) helices(Popot & Engelman 1990; Engelman et al. 2003). After the TM helices have been inserted in the membrane, helix-helix association is required to achieve the final fold and oligomeric state of the protein. A favorite system for investigating the rules that govern TM helix association are the single-span membrane proteins(Rath & Deber 2012; Senes et al. 2004; Mackenzie 2006; MacKenzie & Fleming 2008; Moore et al. 2008), primarily because a variety of methods are available for measuring their oligomerization (including FRET(Fisher et al. 1999; Merzlyakov et al. 2006; You et al. 2005; Khadria & Senes 2013), sedimentation equilibrium analytical ultra-centrifugation(Fleming 2002; Choma et al. 2000), *i n vivo* assays in biological membranes(Russ & Engelman 1999; Lindner & Langosch 2006; Schneider & Engelman 2003), SDS-PAGE(Lemmon et al. 1992; Rath et al. 2009), and steric trapping(Hong et al. 2010; Hong et al. 2013)). Conversely, assessing the folding energetics of multi-span membrane proteins still represents a tremendous challenge(Bowie 2005; Chang & Bowie 2014).

In addition to being a tractable system, the single-span membrane proteins attract interest because of their biological importance. These proteins comprise the most numerous class of membrane proteins, constituting about half of the total(Wallin & von Heijne 1998; Arkin & Brunger 1998; Hubert et al. 2010). Rather than acting as mere membrane anchors for soluble domains, as it was once assumed, the oligomerization of the single TM domains actively plays roles in assembly, signal transduction, ion conduction and regulation in a wide variety of biological processes(Moore et al. 2008).

To investigate the basis of oligomerization in TM helices, our group and others have

pursued a strategy based on the analysis of frequently occurring association motifs(Cunningham et al. 2011; Walters & DeGrado 2006; Russ & Engelman 2000; Senes et al. 2000; Kim et al. 2005; Doura et al. 2004; Unterreitmeier et al. 2007). One of the most important motifs is GAS_{right}(Walters & DeGrado 2006) **(Figure 5.1)**, which is best known as the fold of a widely studied model system for TM association, the glycophorin A TM dimer(MacKenzie et al. 1997). GAS_{right} gets its name from its right-handed crossing angle **(Figure 5.1b)**, and from the characteristic small amino acids at its interface (GAS: Gly, Ala, Ser)(Walters & DeGrado 2006), which are arranged to form GxxxG and GxxxG-like patterns (GxxxA, AxxxG, etc)(Senes et al. 2000; Russ & Engelman 2000). In many ways GAS_{right} parallels the important coiled coil, a frequently occurring interaction motif and model for folding and association for soluble proteins(Harbury et al. 1993; Harbury et al. 1995; Betz et al. 1995). Like the coiled coil, GAS_{right} is characterized by a specific geometry (a short inter-helical distance and a crossing angle near −40°), it has a distinctive sequence signature (the GxxxG patterns), and is one of the most common – if not the most common – oligomerization motif(Walters & DeGrado 2006).

In a recent computational analysis of transmembrane dimer geometry, we proposed that the primary role of GxxxG in GAS_{right} is to promote the formation of networks of stabilizing hydrogen bonds between Cα–H donors and carbonyl oxygen acceptors on opposed helices(Mueller et al. 2014) **(Figure 5.1b,c)**. More specifically, we proposed that the small amino acids perform two distinct functions: the first is to create permissive steric conditions, allowing the two helices to come in backbone contact, thus bringing the Cα–H donors and carbonyl acceptors in proximity. The second function, which is performed exclusively by Gly, is to increase the number of hydrogen bonds by donating with the second Hα, which corresponds to the side chain R-group in all other amino acids. To perform these functions,

the small amino acids are required to be present at specific positions. The formation of this network of hydrogen bonds is also dependent on the specific crossing angle of GAS_{right} (−40°), which precisely aligns Cα–H donors spaced at *i*, *i*+1 on one helix against carbonyl acceptors spaced at *i*, *i*+3 on the opposing helix (see **Figure 5.4** in Mueller *et al*.(Mueller et al. 2014)). Overall, GAS_{right} appears geometrically optimized for inter-helical Cα–H formation(Mueller et al. 2014).

Cα–H hydrogen bonds are commonly observed in proteins(Horowitz & Trievel 2012). Carbons are generally weak donors, but the Cα in proteins is activated by the electron-withdrawing amide groups on both sides, and quantum calculations indicate that the energy of Cα–H hydrogen bonds may be as much as one third to half of that of canonical donors in vacuum(Vargas et al. 2000; Scheiner et al. 2001). Therefore, they are likely to be stabilizing factors in proteins embedded in the hydrophobic milieu of the membrane, particularly when they occur in multiple instances at the same interface, as in the GAS_{right} motif **(Figure 5.1)** (Senes et al. 2001). An IR-based investigation of the CD_2 stretching mode of a Cα–H donor in the transmembrane domain of glycophorin A produced an estimated contribution of −0.88 kcal/mol for the hydrogen bond(Arbely & Arkin 2004). Conversely, a folding study of the multi-span membrane protein bacteriorhodopsin in which a Cα–H···O side chain hydroxyl acceptor (Thr-24) was mutated indicated that this particular bond was not stabilizing(Yohannan et al. 2004). Subsequent computational work suggested that the orientation of the groups can determine whether an interaction may be strongly favorable or unfavorable(Mottamal & Lazaridis 2005; Park et al. 2008).

The exact contribution of hydrogen bonds – whether the donor is a Cα–H or a more “canonical” N–H or O–H group – to membrane protein folding and association is still unresolved(Bowie 2011). A governing assumption maintains that donors and acceptors

buried in the membrane would not pay a significant desolvation penalty upon helix association, and therefore the formation of hydrogen bonds should contribute appreciably to the stability of membrane proteins. Indeed, polar residues can promote interaction of transmembrane helices(Zhou et al. 2000; Choma et al. 2000; Herrmann et al. 2010). Yet, the limited number of experimental observations made to date seem to indicate that the contribution of hydrogen bonding in the membrane may be – surprisingly – of the same magnitude observed for water soluble proteins(Bowie 2011).

Despite the scarce experimental evidence regarding the contribution of Cα–H hydrogen bonds to TM interactions, the hypothesis that they drive folding and oligomerization remains compelling. In particular, the fact that the prevalent GAS_{right} motif corresponds to the only inter-helical geometry that maximizes formation of Cα–H···O=C networks, strongly suggests that these bonds are indeed a major contributor to association(Mueller et al. 2014). Under these premises, we hypothesized that a computational structural search based on the simultaneous optimization of side chain packing and Cα–H hydrogen bonding may be able to predict the structure of GAS_{right} dimers. The resulting program, named CATM, was tested against the small database of known GAS_{right} homo-dimeric structures(Mueller et al. 2014). We found that CATM predicts these known structures at near atomic precision. The finding provides further indirect support that Cα–H hydrogen bonding is likely to be a structural determinant of GAS_{right} dimers(Mueller et al. 2014). The positive result also indicates that CATM may be a powerful tool for assisting the experimental investigation of GAS_{right} homo-dimers of unknown structure.

To test the ability of our methods to predict *ab initio* the structure of unknown GAS_{right} dimers, here we investigate ADCK3, a human mitochondrial protein that is a member of the highly conserved UbiB protein kinase-like family(Leonard et al. 1998). UbiB family members

account for approximately one-quarter of microbial PKL sequences(Kannan et al. 2007), are ubiquitous among eukaryotes(Kannan et al. 2007), and are strongly associated with lipid metabolism(Tan et al. 2013; Martinis et al. 2013; Lundquist et al. 2013). Most organisms have a UbiB family member that is required for the biosynthesis of coenzyme Q (CoQ, ubiquinone). Deletion of the *E. coli* gene *ubiB(Poon et al. 2000)* or the yeast gene *coq8(Do et al. 2001)* completely halts CoQ biosynthesis. Similarly, mutations to human ADCK3 are known to cause CoQ deficiency and cerebellar ataxia(Lagier-Tourenne et al. 2008; Mollet et al. 2008; Gerards et al. 2010; Horvath et al. 2012), and mutations to human ADCK4 were recently shown to cause CoQ deficiency and a steroid-resistant nephrotic syndrome(Ashraf et al. 2013). Our knowledge of the molecular mechanism by which UbiB family proteins enable CoQ biosynthesis is limited, primarily because the endogenous substrates of UbiB proteins have not yet been discovered. However, we do know that coq8p in yeast somehow stabilizes a complex of CoQ biosynthesis enzymes(He et al. 2014). CoQ biosynthesis occurs within the context of cellular membranes — either the plasma membrane of prokaryotes or the inner mitochondrial membrane of eukaryotes — and the responsible enzymes are either integral membrane proteins or peripherally associated membrane proteins(He et al. 2014). ADCK3, which contains a predicted TM domain, is also likely to associate with membranes, but this hypothesis has not yet been tested. Biochemical characterization of the ADCK3 TM domain would provide an important foundation for understanding how it enables CoQ biosynthesis.

The potential functional importance of the ADCK3 TM region is underlined by the existence of a mutation at the putative edge of the TM domain (R213W) that disrupts CoQ biosynthesis and causes cerebellar ataxia in human patients(Mollet et al. 2008). Furthermore, dimerization of single-span TM domains is known to be central to the regulation of some kinase families, such as the receptor tyrosine kinases(Lemmon et al. 2014; Li & Hristova 2006). However, it

was unknown whether the predicted TM helix of ADCK3 could actually insert into biological membranes and whether the TM helix can self-associate to potentially drive dimerization of ADCK3.

Here, we demonstrate experimentally that the TM domain of ADCK3 inserts into membranes and self-associates. Using extensive mutagenesis, we also show that the interaction interface is consistent with the structural models predicted by CATM, which involves an extended Gly-zipper motif(Kim et al. 2005) (i.e. a series of Gly amino acids separated at *i*, *i*+4). The experimental and computational data also indicates that the Gly-zipper interface is potentially compatible with alternative conformations of the TM domain, opening the possibility that conformational changes of the TM dimer may be important for ADCK3 function.

Methods

Vectors and strains

All oligonucleotides were purchased in desalted form from Integrated DNA Technologies and used without purification. The expression vectors pccKAN, pccGpA-wt, and pccGpA-G83I, and *malE* deficient *Escherichia coli* strain MM39 were kindly provided by Dr. Donald M. Engelman(Russ & Engelman 1999). The genes encoding the TM domain of ADCK3 (214-LANFGGLAVGLGFGALA-230) and ADCK4 (92-LANFGGLAVGLGLGVLA-108) were cloned into the NheI-BamHI restriction sites of the pccKAN vector. Site directed mutations to produce single amino acid variants in the TM domain of ADCK3 were introduced with the QuikChange kit (Stratagene).

Expression of Chimeric Proteins in MM39 cells

The TOXCAT constructs were transformed into MM39 cells. A freshly streaked colony was inoculated into 3 mL of LB broth containing 100 µg/mL ampicillin and grown overnight at 37 °C. 30 µL of overnight cultures were inoculated into 3 mL of LB broth and grown to an OD_{420} of approximately 0.8-1.1 (OD_{600} of 0.4 to 0.6) at 37 ˚C. After recording the optical density, 1 mL of cells was spun down for 10 min at 17000*g* and resuspended in 500 mL of sonication buffer (25 mM Tris-HCl, 2 mM EDTA, pH 8.0). Cells were lysed by probe sonication at medium power for 8 seconds over ice. An aliquot was removed from each sample and stored in SDS-PAGE loading buffer for immunoblotting. The lysates were then cleared by centrifugation at 17000*g* and the supernatant was kept on ice for chloramphenicol acetyltransferase (CAT) activity assay.

MalE Complementation Assay

To confirm proper membrane insertion and orientation of the TOXCAT constructs, overnight

cultures were plated on M9 minimal medium plates containing 0.4% maltose as the only carbon source and grown at 37 ˚C for 48 hours(Russ & Engelman 1999).

Chloramphenicol Acetyltransferase (CAT) spectrophotometric assay

CAT activity was measured as described(Shaw 1975; LaPointe et al. 2013). Briefly, 1 mL of buffer containing 0.1 mM acetyl CoA, 0.4 mg/mL 5,5'-dithiobis-(2-nitrobenzoic acid) or Ellman's reagent, and 0.1 M Tris-HCl pH 7.8, were mixed with 40 µL of cleared cell lysates and the absorbance at 412 nm was measured for two minutes to establish basal enzyme activity rate. After addition of 40 µL of 2.5 mM chloramphenicol in 10% ethanol, the absorbance was measured for an additional two minutes to determine CAT activity. The basal CAT activity was subtracted and the value was normalized by the cell density measured as OD_{420}. All measurements were determined at least in duplicate and the experiments were repeated at least twice.

Quantification of expression by immunoblotting

Protein expression was confirmed by immunoblotting. The cell lysates (10 µL) were loaded onto a NuPAGE 4-12% Bis-Tris SDS-PAGE gel (Invitrogen) and then transferred to PVDF membranes (VWR) for 1 hour at 100 millivolts. Blots were blocked using 5% Bovine serum albumin (US Biologicals) in TBS-Tween buffer (50 mM Tris, 150 mM NaCl, 0.05% Tween 20) for two hours at 4 ˚C, incubated with biotinylated anti-Maltose Binding Protein antibodies (Vector labs) overnight at 4 ˚C, followed by peroxidase-conjugated streptavidin (Jackson ImmunoResearch) for two hours at 4 ˚C. Blots were developed with the Pierce ECL Western Blotting Substrate Kit and chemiluminescence was measured using an ImageQuant LAS 4000 (GE Healthsciences).

Computational modeling

The structure of ADCK3-TM was predicted with CATM(Mueller et al. 2014), which is distributed with the open source MSL C++ library v. 1.2(Kulp et al. 2012) at http://msl-libraries.org. The computational mutagenesis was performed on all ADCK3 models by applying the same point mutations measured experimentally in the context of a fixed backbone, followed by side chain optimization. Side chain mobility was modeled using the Energy-Based conformer library applied at the 95% level(Subramaniam & Senes 2012). Energies were determined using the CHARMM 22 van der Waals function(MacKerell et al. 1998) and the hydrogen bonding function of SCWRL 4(Krivov et al. 2009), as implemented in MSL(Kulp et al. 2012), with the following parameters for Cα donors, as reported previously: B=60.278; D_0=2.3 Å; σ_d=1.202 Å; α_{max}=74.0°; β_{max}=98.0°(Mueller et al. 2014). The relative energy of each mutant was calculated as

$$\Delta E_{mut} = (E_{mut,dimer} - E_{mut,monomer}) - (E_{WT,dimer} - E_{WT,monomer})$$

where $E_{WT,dimer}$ and $E_{mut,dimer}$ are the energies of the wild type and mutant sequence, respectively, in the dimeric state, and $E_{WT,monomer}$ and $E_{mut,monomer}$ are the energies of the wild type and mutant sequence, respectively, in a side chain optimized monomeric state with the same sequence. As reported previously(LaPointe et al. 2013), the effect of each mutation was classified in four categories (analogous to the experimental mutagenesis) using the following criterion: category 0, “WT-like”, $\Delta E_{mut} < 2$ kcal/mol; category 1, “Mild”, $2 \leq \Delta E_{mut} < 4$; category 2, “Severe”, $4 \leq \Delta E_{mut} < 8$; category 3, “Disruptive”, $\Delta E_{mut} \geq 8$. The numerical category values were averaged to calculate the average position-dependent disruption value.

Results and Discussion

ADCK3 is predicted to have a TM helix

The protein kinase-like domain of ADCK3 is preceded on the N-terminal side by a region of undefined function. A predicted TM helix within this region is annotated in UniProt for the close homolog ADCK4(UniProt Consortium 2013), providing a potential anchor for the protein at the inner mitochondrial membrane (Fig 2a). UniProt does not report a predicted TM domain for the corresponding region of ADCK3, but the sequence of the putative TM segment is highly conserved between the two proteins. The same general domain organization and function is also predicted for the yeast homolog Coq8p. Given that ADCK3 and ADCK4 are localized to the mitochondrial matrix(Rhee et al. 2013), the TM domain would position their catalytic kinase domains on the matrix face of the inner membrane, the same localization of the enzymes involved in the biosynthesis of coenzyme Q(He et al. 2014; Rhee et al. 2013). Therefore, it is important to verify the TM domain experimentally and to investigate its potential functional role.

The sequences of the putative TM domains of ADCK3 and ADCK4 are aligned in **Figure 5.2b.** As summarized in Table 5.1, these sequences have low hydrophobicity and a relative short length (17 amino acids), and thus are not well recognized by prediction servers. The TM domain of ADCK3, which contains one polar amino acid (Asn 216), is recognized as a borderline TM sequence by most servers. Specifically, the segment is not recognized by *TMHMM(Krogh et al. 2001)* and *E(z)(Senes et al. 2007)* but the segment is predicted as transmembrane by *MemBrain(Shen & Chou 2008; Yang et al. 2013)* and *HMMTOP*(Tusnády & Simon 1998; Tusnády & Simon 2001), and *Phobius*(Käll et al. 2004; Käll et al. 2007) and *ΔG prediction(Hessa et al. 2007)* recognize it with low confidence. ADCK4 shares over 50%

sequence identify with ADCK3 but their TM domains are almost identical, differing only at two positions **(Figure 5.2b)**. Because of these two substitutions (and primarily because of the A228V substitution), the hydrophobicity of the TM domain of ADCK4 is higher (as calculated with either the Wimley-White octanol scale(Wimley et al. 1996) or the “biological” scale(Hessa et al. 2007; Hessa et al. 2005)) and is sufficient to be predicted by most servers, except *E(z)*, with good confidence (Table 5.1).

In interpreting these prediction data, it is important to consider that TM prediction servers are trained against a majority of proteins that are inserted in the membrane via a translocon mediated mechanism. The sequence requirements for translocon mediated insertion in an eukaryotic system are well understood(Hessa et al. 2007; Hessa et al. 2005). A recent analysis in a bacterial system shows good overall correspondence to the mammalian system, but the hydrophobicity threshold appears to be distinctly lower(Ojemalm et al. 2013). Much less is known about the requirements for membrane insertion of mitochondrial integral membrane proteins that are encoded in the nucleus, such as ADCK3. There is, however, good indication that the hydrophobicity threshold for these proteins should be even lower, to avoid mistargeting of these proteins to the endoplasmic reticulum and to facilitate their translocation to the mitochondrion(Tong et al. 2011; Supekova et al. 2010; Horie et al. 2002; Daley et al. 2002; Horie et al. 2003; Daley & Whelan 2005). Based on the above considerations, it is highly probable that the predicted TM segments of ADCK3 and ADCK4 are indeed *bona fide* TM domains.

The TM domain of ADCK3 has conserved GxxxG-like motifs

As shown in **Figure 5.2b**, the predicted TM regions of ADCK3 and ADCK4 are very rich in small amino acids such as Gly, Ala and Ser (9 in each). The sequences contain a number of GxxxG and GxxxG-like (AxxxG) helix association patterns, which appear to be evolutionarily

conserved **(Figure 5.2c)**. In particular, they contain an extended Gly-zipper motif(Kim et al. 2005), i.e. a series of small amino acids (215-AxxxGxxxGxxxG-227) spaced at *i*, *i*+4, highlighted in red in **Figure 5.2b**. They also contain an additional AxxxG motif (magenta), which is off-frame by two positions with respect to the Gly-zipper. This spacing projects the two motifs on opposite helical faces.

CATM predicts that the TM domain of ADCK3 can form a GAS_{right} homo-dimer

GxxxG-like patterns can drive helix-helix association(Russ & Engelman 2000). They occur with high frequency in TM helices(Senes et al. 2000), both in multi-span proteins and in oligomerizing single-span membrane proteins(Senes et al. 2001), and are often important for biological function(Senes et al. 2004). The presence of GxxxG-like motifs in the putative TM sequence of ADCK3 raised the question of whether this domain oligomerizes. To investigate this question, we analyzed the sequence with CATM(Mueller et al. 2014), a program for the structural prediction of GAS_{right} motifs, an important and common class of GxxxG-mediated dimers(Walters & DeGrado 2006).

As shown in **Figure 5.3**, CATM predicts five alternative models for the TM sequence of ADCK3. The figure schematically depicts the geometrical features of the dimers. The position of the crossing point between the two helices is marked (dot), and the interfacial positions that surround this crossing point are highlighted by a green parallelogram. All the positions that are involved in inter-monomer contacts at the interface are highlighted in either yellow, or in red if they belong to the Gly-zipper motif. The scores of the top models of ADCK3 in CATM (−59.8, −50.8 and −47.7 for Models 1, 2 and 3 respectively) are comparable to the scores obtained for the five known structures of GAS_{right} motifs (which range between −56 and −38) , which CATM is able to predict at near atomic precision(Mueller et al. 2014).

Notably, the extended Gly-zipper is involved at the helix-helix interface in all models

(Figure 5.3). Model 1 and 2 are related geometries whose crossing points fall in the quadrilateral defined by Gly 219, Leu 220, Gly 223 and Leu 224 (Axxx**GL**xx**GL**xxG). These two models differ by the position of the crossing point and, most importantly, by their crossing angle, which is near the canonical −40° of GAS_{right} motifs for Model 2, and narrower for Model 1 (−27.1°). The smaller crossing angle causes Model 1 to have a more extended interface, which is reflected also by the more extensive der Waals interaction of Model 1. Both models have twelve inter-helical Cα–H hydrogen bonds, although Model 2 has a better overall hydrogen bonding score (Tables S5.1 and S5.2).

The other three predicted models cross at different sections of the Gly-zipper. Model 3 and Model 5 are variations that cross within the N-terminal side of the zipper (**AN**xx**GL**xxGxxxG). Conversely, Model 4 crosses on the C-terminal side of the zipper (AxxxGxxx**GL**xx**GA**). CATM does not produce any model mediated by the off-frame AxxxG motif of ADCK3 (magenta in **Figure 5.2b**). The coordinates of all ADCK3 models are available as Supplementary Information and for download at http://seneslab.org/ADCK3_models.

ADCK3-TM self-associates strongly in E. coli membranes.

To investigate the structural predictions of CATM, we assessed the dimerization of ADCK3-TM and ADCK4-TM experimentally using TOXCAT, a widely used assay for TM association in biological membranes(Russ & Engelman 1999). This assay involves the biological expression in the membrane of *Escherichia coli* of a chimeric construct that fuses the TM domain of interest with the ToxR transcriptional activator of *Vibrio cholera* **(Figure 5.4a)**. TM helix association leads to the dimerization of the ToxR domain, resulting in expression of the reporter gene chloramphenicol acetyltransferase (CAT). The expression level of CAT (measured by its enzymatic activity) is compared to that of a stable dimer, Glycophorin A (GpA), and to a monomeric GpA variant (GpA-G83I) as standards.

We first tested whether the constructs inserted correctly in the plasma membrane of *E. coli*, using a complementation test in the *malE* deficient strain MM39. The ADCK3-TM and ADCK4-TM TOXCAT constructs supported growth in minimal media with maltose as the sole carbon source **(Figure 5.4b)**, indicating that the fusion proteins are recognized as a TM domain and are expressed in the bacterial inner membrane in the correct orientation, with the MBP moiety positioned on the periplasmic side.

To examine whether ADCK3 oligomerizes in TOXCAT, we quantified the enzymatic activity of the reporter gene CAT, as an indirect measure of its expression. As shown in **Figure 5.4c**, the CAT activities of the ADCK3-TM and ADCK4-TM constructs are higher than the activity of the GpA standard, which is a stable homo-dimer. These results indicate that the TM domain of ADCK3 and ADCK4 form strong homo-oligomers in TOXCAT.

Large scale mutagenesis demonstrates that the Gly zipper motif is important for association

To assess experimentally the interaction interface of the ADCK3-TM oligomer and validate the computational predictions, we performed large scale mutagenesis along the entire span of the TM segment, and measured their self-association in TOXCAT. Each position was individually changed to a variety of large and small hydrophobic amino acids. The expectation is that the changes at interfacial positions are more likely to perturb oligomerization than changes at lipid exposed positions, as commonly observed (for example(Adams et al. 1995; Fleming & Engelman 2001a; Jenei et al. 2011; Lemmon et al. 1992; Li et al. 2004)). A total of 53 mutants were generated and analyzed in TOXCAT.

The TOXCAT data is shown in supplementary **Figure S5.1** and is schematically represented in **Figure 5.5a**. To compute an overall position-dependent sensitivity to mutation, we applied a classification scheme for the variants' phenotypes using four categories (dashed

lines in **Figure S5.1**), labeled as “WT-like” (>80% of wild type CAT activity), “Mild” (50-80%), “Severe” (20-50%) and “Disruptive” (0-20%). These scores were then averaged to obtain a position specific “average disruption”. Position-based averaging reduces some of the natural variability of the biological assay and the method has been reliable in identifying the most sensitive positions at the helix-helix binding interface(Sulistijo et al. 2003; Li et al. 2004; Adams et al. 1995; LaPointe et al. 2013). The position-dependent “average disruption” is also plotted in numerical form in **Figure 5.5b**.

A majority of the variants had CAT activity levels similar or higher compared to the wild type sequences **(Figure 5.5b)**. However, a number of variants showed dramatically reduced activity in a position specific fashion. In particular, all variants of the two C-terminal Gly residues of the Gly-zipper (G223 and G227) have the strongest disruptive phenotypes. Interestingly, the next most sensitive positions are L220 and L224, which are also predicted to be interfacial in almost all CATM models **(Figure 5.3)**. Conversely, the N-terminal positions of the zipper are either mildly affected by mutation (G219) or appear completely tolerant (A215).

The off-frame 221-AxxxG-225 (magenta) is also relatively insensitive to mutation. Substitution for a large Leu at these two positions has only a mild effect, and the Ile variants are completely tolerated. This is consistent with the CATM predictions, which do not identify any model in which this motif is at the interface.

A position of interest for self-association was Asn 216. Polar residues can drive TM helix oligomerization through the formation of hydrogen bonds, and have been found to be important for the association of model peptides(Choma et al. 2000; Zhou et al. 2000) and of biological systems(Fleming & Engelman 2001b; Stanley & Fleming 2007; Li et al. 2006; Lawrie et al. 2010, p.3), including in the context of GAS_{right} motifs(Sulistijo & Mackenzie 2009; Sulistijo et al. 2003). In addition, some polarity of position 216 appears to be relatively

conserved, as the main substitutions of N216 in a sequence alignment **(Figure 5.2c)** are Gly, Ser, Gln and Glu. However, neither the computational nor the experimental analysis suggest that N216 is important for self-association. Asn 216 can be mutated to Ala, Leu or Phe in TOXCAT without reduction of self-association. CATM is in agreement with the experimental data, as it does not identify any potential strong polar interaction (i.e., N–H···O hydrogen bonds) involving the side chain of N216, although the side chain carbonyl oxygen (Oδ1) acts as a Cα–H bond acceptor in most models.

Overall the data indicates that the interface of the ADCK3-TM oligomer is mediated by Gly-zipper motif and, in particular, by the C-terminal side of this interaction motif.

Computational mutagenesis suggests potential alternative conformations for ADCK3-TM

In order to identify the structure most consistent with the TOXCAT data, we performed a mutational analysis of the five models generated by CATM. Using a protocol developed previously to analyze similar mutational data(LaPointe et al. 2013), we created *in silico* the same set of variants that were tested experimentally, and computed an analogous position-dependent “average disruption” index based on the interaction energies.

The experimental and theoretical disruption patterns are compared in **Figure 5.6**. Given that all CATM structures interact through portions of the extended Gly-zipper, the computed patterns have similar periodicity across all models, with disruption peaking at position G219, G223 and/or G227. Models 1, 3 and 5 **(Figure 5.6a,c,e)** show high sensitivity to mutation on the N-terminal side of the TM domain, in disagreement with the experimental observations. In these three models, mutations to G219 are completely disruptive, whereas the position is only mildly sensitive in TOXCAT. Models 1 and 5 are also very sensitive at positions A215 and N216, which are completely tolerant experimentally.

The structures of Models 2 and 4 are compared in **Figure 5.7**. Model 2 **(Figure 5.6b)** and Model 4 **(Figure 5.6d)** are in better agreement with the experimental data and represent two possible structural solutions for the ADCK3 TM dimer. The disruption for both models peak at G223 and G227, which are also the two most disruptive positions in TOXCAT. However, Model 4 appears insensitive at position G219 (which is mildly sensitive experimentally) and it is extremely disruptive at position A228 (which is insensitive experimentally). In addition to being a better match, Model 2 also has lower energy, better packing and a larger number of hydrogen bonds (Tables S5.2 and S5.4). Therefore, Model 2 appears to be the best structural candidate for the ADCK3 TM dimer.

In a recent analysis of known GAS_{right} structures, we demonstrated that CATM is capable of capturing alternative conformations of biological importance(Mueller et al. 2014). Therefore, an additional possibility is that the TM domain of ADCK3 may be in equilibrium between two or more structures. We observed that a linear combination of the mutagenesis profiles of the two models that best fit the data, 60% of Model 2 and 40% of Model 4, improves the fit with the TOXCAT data, producing an excellent correspondence between the two experiments **(Figure 5.6f)**. This interpolation is not necessarily quantitative, but it suggests that a conformational equilibrium would be compatible with the data. If such an equilibrium occurs in the biological context, it would postulate that the TM domain of ADCK3 may be a switchable element, a trait that could be important for regulation or signaling, as observed in a number of other single-span TM proteins(Moore et al. 2008). In this framework, the Gly-zipper would provide a dynamic interface for structural changes that can potentially affect either the distance of the helical termini or the relative rotation of the helices.

Conclusions

We have presented a computational and experimental analysis of the structural organization of the TM domain of the mitochondrial kinase ADCK3. While more experiments are necessary to fully test CATM, the work provides a first practical demonstration of the applicability of the program to the characterization of a TM dimer of unknown structure. It also confirms the ability of the algorithm (which is based on optimization of van der Waals and Cα–H hydrogen bonding) to correctly predict GAS_{right} motifs.

We have experimentally demonstrated that the TM domain of ADCK3 self-associates in *E. coli* membranes. While the specific oligomeric state could not determined by TOXCAT, the evidence suggests that ADCK3-TM is likely dimeric. Although Gly-zipper motifs can be involved in the formation of higher-oligomeric complexes(Kim et al. 2005), the good agreement between the experimental and computational mutagenesis supports the homo-dimeric hypothesis. Moreover, such oligomeric state is also consistent with a large body of structural evidence which shows that kinases frequently form dimeric complexes (for example(Cobb & Goldsmith 2000; West & Stock 2001; Lemmon & Schlessinger 2010)), while higher-oligomers are rarely observed.

The analysis reveals a number of leads that may be biologically important. The helix-helix interaction interface was determined and the mutagenesis identified a number of disruptive interfacial mutations that will be useful for follow-up functional studies. The computational prediction of alternative models in which the helices adopt a different crossing point along Gly-zipper interface raises also the hypothesis that the TM domain of ADCK3 may possibly undergo conformational changes.

Indirectly, the work also provides important insight about ADCK4. All the amino acids that

participate at the dimerization interface of ADCK3 are identical in ADCK4. The two positions that differ between the two sequences (F228L and A230V, **Figure 5.2**) are insensitive to variation when they are mutated individually **(Figure 5.5)**. The computational predictions obtained for ADCK3 and ADCK4 are nearly identical and it is thus expected that both TM domains dimerize with the same structure. Because the two interfaces are compatible with each other, it also possible that the TM domains could associate to drive formation of a hetero-dimeric complex between ADCK3 and ADCK4. These hypotheses need to be investigated in a biological context; the present analysis provides the theoretical foundation necessary for testing *in vivo* the role of these TM domains.

Supporting Information

Summaries of the features of the five CATM models, PDB files of the models, TOXCAT mutagenesis data, definition of the geometric parameters, and identifiers of the sequences of ADCK3 homologues. This information is available free of charge via the internet at http://pubs.acs.org.

Acknowledgements

The work was supported by startup funds from the University of Wisconsin-Madison and by National Institutes of Health Grant R01GM099752 and National Science Foundation Grant CHE-1415910 to A.S. D.J.P. and J.A.S. were supported by a Searle Scholar Award, a Shaw Scientist Award and by National Institutes of Health Grants R01DK098672 and U01GM094622 to D.J.P. J.A.S was supported by an NIH Ruth L. Kirschstein National Research Service Award F30AG043282. B.K.M. acknowledges the support of the NLM Grant 5T15LM007359 to the CIBM Training Program. We are grateful to Sabareesh Subramaniam for assistance in the computational modeling and Jennifer Peotter for assistance in the preparation of the TOXCAT constructs.

References

Adams, P.D. et al., 1995. Computational searching and mutagenesis suggest a structure for the pentameric transmembrane domain of phospholamban. *Nature Structural Biology*, 2(2), pp.154–162.

Arbely, E. & Arkin, I.T., 2004. Experimental measurement of the strength of a C alpha-H...O bond in a lipid bilayer. *Journal of the American Chemical Society*, 126(17), pp.5362–5363.

Arkin, I.T. & Brunger, A.T., 1998. Statistical analysis of predicted transmembrane alpha-helices. *Biochimica Et Biophysica Acta*, 1429(1), pp.113–128.

Ashraf, S. et al., 2013. ADCK4 mutations promote steroid-resistant nephrotic syndrome through CoQ10 biosynthesis disruption. *The Journal of clinical investigation*, 123(12), pp.5179–5189.

Betz, S.F., Bryson, J.W. & DeGrado, W.F., 1995. Native-like and structurally characterized designed alpha-helical bundles. *Current opinion in structural biology*, 5(4), pp.457–463.

Bowie, J.U., 2011. Membrane protein folding: how important are hydrogen bonds? *Current Opinion in Structural Biology*, 21(1), pp.42–49.

Bowie, J.U., 2005. Solving the membrane protein folding problem. *Nature*, 438(7068), pp.581–9.

Chang, Y.-C. & Bowie, J.U., 2014. Measuring membrane protein stability under native conditions. *Proceedings of the National Academy of Sciences of the United States of America*, 111(1), pp.219–224.

Choma, C. et al., 2000. Asparagine-mediated self-association of a model transmembrane helix. *Nature structural biology*, 7(2), pp.161–6.

Cobb, M.H. & Goldsmith, E.J., 2000. Dimerization in MAP-kinase signaling. *Trends in Biochemical Sciences*, 25(1), pp.7–9.

Cunningham, F. et al., 2011. Beta-branched residues adjacent to GG4 motifs promote the efficient association of glycophorin A transmembrane helices. *Biopolymers*, 96(3), pp.340–347.

Daley, D.O., Clifton, R. & Whelan, J., 2002. Intracellular gene transfer: reduced hydrophobicity facilitates gene transfer for subunit 2 of cytochrome c oxidase. *Proceedings of the National Academy of Sciences of the United States of America*, 99(16), pp.10510–10515.

Daley, D.O. & Whelan, J., 2005. Why genes persist in organelle genomes. *Genome biology*, 6(5), p.110.

Do, T.Q. et al., 2001. A defect in coenzyme Q biosynthesis is responsible for the respiratory deficiency in Saccharomyces cerevisiae abc1 mutants. *The Journal of biological chemistry*, 276(21), pp.18161–18168.

Doura, A.K. et al., 2004. Sequence context modulates the stability of a GxxxG-mediated transmembrane helix-helix dimer. *Journal of Molecular Biology*, 341(4), pp.991–998.

Engelman, D.M. et al., 2003. Membrane protein folding: beyond the two stage model. *FEBS Letters*, 555(1), pp.122–125.

Fisher, L.E., Engelman, D.M. & Sturgis, J.N., 1999. Detergents modulate dimerization, but not helicity, of the glycophorin A transmembrane domain. *Journal of Molecular Biology*, 293(3), pp.639–651.

Fleming, K.G., 2002. Standardizing the free energy change of transmembrane helix-helix interactions. *Journal of*

Molecular Biology, 323(3), pp.563–571.

Fleming, K.G. & Engelman, D.M., 2001a. Computation and mutagenesis suggest a right-handed structure for the synaptobrevin transmembrane dimer. *Proteins*, 45(4), pp.313–317.

Fleming, K.G. & Engelman, D.M., 2001b. Specificity in transmembrane helix-helix interactions can define a hierarchy of stability for sequence variants. *Proceedings of the National Academy of Sciences of the United States of America*, 98(25), pp.14340–14344.

Gerards, M. et al., 2010. Nonsense mutations in CABC1/ADCK3 cause progressive cerebellar ataxia and atrophy. *Mitochondrion*, 10(5), pp.510–515.

Harbury, P.B. et al., 1993. A switch between two-, three-, and four-stranded coiled coils in GCN4 leucine zipper mutants. *Science (New York, N.Y.)*, 262(5138), pp.1401–1407.

Harbury, P.B., Tidor, B. & Kim, P.S., 1995. Repacking protein cores with backbone freedom: structure prediction for coiled coils. *Proceedings of the National Academy of Sciences of the United States of America*, 92(18), pp.8408–8412.

He, C.H. et al., 2014. Coenzyme Q supplementation or over-expression of the yeast Coq8 putative kinase stabilizes multi-subunit Coq polypeptide complexes in yeast coq null mutants. *Biochimica et biophysica acta*, 1841(4), pp.630–644.

Herrmann, J.R. et al., 2010. Ionic interactions promote transmembrane helix-helix association depending on sequence context. *Journal of molecular biology*, 396(2), pp.452–461.

Hessa, T. et al., 2007. Molecular code for transmembrane-helix recognition by the Sec61 translocon. *Nature*, 450(7172), pp.1026–30.

Hessa, T. et al., 2005. Recognition of transmembrane helices by the endoplasmic reticulum translocon. *Nature*, 433(7024), pp.377–81.

Hong, H. et al., 2010. Method to measure strong protein-protein interactions in lipid bilayers using a steric trap. *Proceedings of the National Academy of Sciences of the United States of America*, 107(46), pp.19802–19807.

Hong, H., Chang, Y.-C. & Bowie, J.U., 2013. Measuring transmembrane helix interaction strengths in lipid bilayers using steric trapping. *Methods in molecular biology (Clifton, N.J.)*, 1063, pp.37–56.

Horie, C. et al., 2002. Characterization of signal that directs C-tail-anchored proteins to mammalian mitochondrial outer membrane. *Molecular biology of the cell*, 13(5), pp.1615–1625.

Horie, C. et al., 2003. Targeting and assembly of mitochondrial tail-anchored protein Tom5 to the TOM complex depend on a signal distinct from that of tail-anchored proteins dispersed in the membrane. *The Journal of biological chemistry*, 278(42), pp.41462–41471.

Horowitz, S. & Trievel, R.C., 2012. Carbon-oxygen hydrogen bonding in biological structure and function. *The Journal of biological chemistry*, 287(50), pp.41576–41582.

Horvath, R. et al., 2012. Adult-onset cerebellar ataxia due to mutations in CABC1/ADCK3. *Journal of neurology, neurosurgery, and psychiatry*, 83(2), pp.174–178.

Hubert, P. et al., 2010. Single-spanning transmembrane domains in cell growth and cell-cell interactions: More than meets the eye? *Cell adhesion & migration*, 4(2), pp.313–324.

Jenei, Z.A. et al., 2011. Packing of transmembrane domain 2 of carnitine palmitoyltransferase-1A affects

oligomerization and malonyl-CoA sensitivity of the mitochondrial outer membrane protein. *FASEB journal: official publication of the Federation of American Societies for Experimental Biology*, 25(12), pp.4522–4530.

Käll, L., Krogh, A. & Sonnhammer, E.L.L., 2004. A combined transmembrane topology and signal peptide prediction method. *Journal of molecular biology*, 338(5), pp.1027–1036.

Käll, L., Krogh, A. & Sonnhammer, E.L.L., 2007. Advantages of combined transmembrane topology and signal peptide prediction--the Phobius web server. *Nucleic acids research*, 35(Web Server issue), pp.W429–432.

Kannan, N. et al., 2007. Structural and functional diversity of the microbial kinome. *PLoS biology*, 5(3), p.e17.

Khadria, A. & Senes, A., 2013. Measurement of Transmembrane Peptide Interactions in Liposomes Using Förster Resonance Energy Transfer (FRET). *Methods in molecular biology (Clifton, N.J.)*, 1063, pp.19–36.

Kim, S. et al., 2005. Transmembrane glycine zippers: physiological and pathological roles in membrane proteins. *Proceedings of the National Academy of Sciences of the United States of America*, 102(40), pp.14278–14283.

Krivov, G.G., Shapovalov, M.V. & Dunbrack, R.L., 2009. Improved prediction of protein side-chain conformations with SCWRL4. *Proteins*, 77(4), pp.778–795.

Krogh, A. et al., 2001. Predicting transmembrane protein topology with a hidden Markov model: application to complete genomes. *Journal of molecular biology*, 305(3), pp.567–580.

Kulp, D.W. et al., 2012. Structural informatics, modeling, and design with an open-source Molecular Software Library (MSL). *Journal of computational chemistry*, 33(20), pp.1645–1661.

Lagier-Tourenne, C. et al., 2008. ADCK3, an ancestral kinase, is mutated in a form of recessive ataxia associated with coenzyme Q10 deficiency. *American Journal of Human Genetics*, 82(3), pp.661–672.

LaPointe, L.M. et al., 2013. Structural organization of FtsB, a transmembrane protein of the bacterial divisome. *Biochemistry*, 52(15), pp.2574–2585.

Lawrie, C.M., Sulistijo, E.S. & MacKenzie, K.R., 2010. Intermonomer hydrogen bonds enhance GxxxG-driven dimerization of the BNIP3 transmembrane domain: roles for sequence context in helix-helix association in membranes. *Journal of Molecular Biology*, 396(4), pp.924–936.

Lemmon, M.A. et al., 1992. Sequence specificity in the dimerization of transmembrane alpha-helices. *Biochemistry*, 31(51), pp.12719–25.

Lemmon, M.A. & Schlessinger, J., 2010. Cell signaling by receptor tyrosine kinases. *Cell*, 141(7), pp.1117–1134.

Lemmon, M.A., Schlessinger, J. & Ferguson, K.M., 2014. The EGFR family: not so prototypical receptor tyrosine kinases. *Cold Spring Harbor perspectives in biology*, 6(4), p.a020768.

Leonard, C.J., Aravind, L. & Koonin, E.V., 1998. Novel families of putative protein kinases in bacteria and archaea: evolution of the “eukaryotic” protein kinase superfamily. *Genome research*, 8(10), pp.1038–1047.

Li, E. & Hristova, K., 2006. Role of receptor tyrosine kinase transmembrane domains in cell signaling and human pathologies. *Biochemistry*, 45(20), pp.6241–6251.

Li, E., You, M. & Hristova, K., 2006. FGFR3 dimer stabilization due to a single amino acid pathogenic mutation.

Journal of molecular biology, 356(3), pp.600–612.

Lindner, E. & Langosch, D., 2006. A ToxR-based dominant-negative system to investigate heterotypic transmembrane domain interactions. *Proteins*, 65(4), pp.803–807.

Li, R. et al., 2004. Dimerization of the transmembrane domain of Integrin alphaIIb subunit in cell membranes. *The Journal of Biological Chemistry*, 279(25), pp.26666–26673.

Lundquist, P.K. et al., 2013. Loss of plastoglobule kinases ABC1K1 and ABC1K3 causes conditional degreening, modified prenyl-lipids, and recruitment of the jasmonic acid pathway. *The Plant cell*, 25(5), pp.1818–1839.

Mackenzie, K.R., 2006. Folding and stability of alpha-helical integral membrane proteins. *Chemical Reviews*, 106(5), pp.1931–1977.

MacKenzie, K.R. & Fleming, K.G., 2008. Association energetics of membrane spanning alpha-helices. *Current opinion in structural biology*, 18(4), pp.412–419.

MacKenzie, K.R., Prestegard, J.H. & Engelman, D.M., 1997. A transmembrane helix dimer: structure and implications. *Science (New York, N.Y.)*, 276(5309), pp.131–133.

MacKerell et al., 1998. All-Atom Empirical Potential for Molecular Modeling and Dynamics Studies of Proteins†. *The Journal of Physical Chemistry B*, 102(18), pp.3586–3616.

Martinis, J. et al., 2013. A chloroplast ABC1-like kinase regulates vitamin E metabolism in Arabidopsis. *Plant physiology*, 162(2), pp.652–662.

Merzlyakov, M. et al., 2006. Transmembrane helix heterodimerization in lipid bilayers: probing the energetics behind autosomal dominant growth disorders. *Journal of Molecular Biology*, 358(1), pp.1–7.

Mollet, J. et al., 2008. CABC1 gene mutations cause ubiquinone deficiency with cerebellar ataxia and seizures. *American Journal of Human Genetics*, 82(3), pp.623–630.

Moore, D.T., Berger, B.W. & DeGrado, W.F., 2008. Protein-Protein Interactions in the Membrane: Sequence, Structural, and Biological Motifs. *Structure*, 16(7), pp.991–1001.

Mottamal, M. & Lazaridis, T., 2005. The contribution of C alpha-H...O hydrogen bonds to membrane protein stability depends on the position of the amide. *Biochemistry*, 44(5), pp.1607–1613.

Mueller, B.K., Subramaniam, S. & Senes, A., 2014. A frequent, GxxxG-mediated, transmembrane association motif is optimized for the formation of interhelical Cα-H hydrogen bonds. *Proceedings of the National Academy of Sciences of the United States of America*, 111(10), pp.E888–895.

Ojemalm, K. et al., 2013. Quantitative analysis of SecYEG-mediated insertion of transmembrane α-helices into the bacterial inner membrane. *Journal of molecular biology*, 425(15), pp.2813–2822.

Park, H., Yoon, J. & Seok, C., 2008. Strength of Calpha-H...O=C hydrogen bonds in transmembrane proteins. *The journal of physical chemistry. B*, 112(3), pp.1041–1048.

Poon, W.W. et al., 2000. Identification of Escherichia coli ubiB, a gene required for the first monooxygenase step in ubiquinone biosynthesis. *Journal of bacteriology*, 182(18), pp.5139–5146.

Popot, J.L. & Engelman, D.M., 1990. Membrane protein folding and oligomerization: the two-stage model. *Biochemistry*, 29(17), pp.4031–7.

Rath, A. et al., 2009. Detergent binding explains anomalous SDS-PAGE migration of membrane proteins.

Proceedings of the National Academy of Sciences of the United States of America. Available at: http://www.ncbi.nlm.nih.gov/pubmed/19181854 [Accessed February 10, 2009].

Rath, A. & Deber, C.M., 2012. Protein structure in membrane domains. *Annual review of biophysics*, 41, pp.135–155.

Rhee, H.-W. et al., 2013. Proteomic mapping of mitochondria in living cells via spatially restricted enzymatic tagging. *Science (New York, N.Y.)*, 339(6125), pp.1328–1331.

Russ, W.P. & Engelman, D.M., 2000. The GxxxG motif: a framework for transmembrane helix-helix association. *Journal of Molecular Biology*, 296(3), pp.911–9.

Russ, W.P. & Engelman, D.M., 1999. TOXCAT: A Measure of Transmembrane Helix Association in a Biological Membrane. *Proceedings of the National Academy of Sciences*, 96(3), pp.863–868.

Scheiner, S., Kar, T. & Gu, Y., 2001. Strength of the Calpha H..O hydrogen bond of amino acid residues. *The Journal of Biological Chemistry*, 276(13), pp.9832–9837.

Schneider, D. & Engelman, D.M., 2003. GALLEX, a measurement of heterologous association of transmembrane helices in a biological membrane. *The Journal of Biological Chemistry*, 278(5), pp.3105–3111.

Senes, A. et al., 2007. E(z), a depth-dependent potential for assessing the energies of insertion of amino acid side-chains into membranes: derivation and applications to determining the orientation of transmembrane and interfacial helices. *Journal of Molecular Biology*, 366(2), pp.436–448.

Senes, A., Engel, D.E. & DeGrado, W.F., 2004. Folding of helical membrane proteins: the role of polar, GxxxG-like and proline motifs. *Current Opinion in Structural Biology*, 14(4), pp.465–479.

Senes, A., Gerstein, M. & Engelman, D.M., 2000. Statistical analysis of amino acid patterns in transmembrane helices: the GxxxG motif occurs frequently and in association with beta-branched residues at neighboring positions. *Journal of molecular biology*, 296(3), pp.921–36.

Senes, A., Ubarretxena-Belandia, I. & Engelman, D.M., 2001. The Calpha ---H...O hydrogen bond: a determinant of stability and specificity in transmembrane helix interactions. *Proceedings of the National Academy of Sciences of the United States of America*, 98(16), pp.9056–61.

Shaw, W.V., 1975. Chloramphenicol acetyltransferase from chloramphenicol-resistant bacteria. *Methods in Enzymology*, 43, pp.737–755.

Shen, H. & Chou, J.J., 2008. MemBrain: improving the accuracy of predicting transmembrane helices. *PloS one*, 3(6), p.e2399.

Stanley, A.M. & Fleming, K.G., 2007. The role of a hydrogen bonding network in the transmembrane beta-barrel OMPLA. *Journal of molecular biology*, 370(5), pp.912–924.

Subramaniam, S. & Senes, A., 2012. An energy-based conformer library for side chain optimization: Improved prediction and adjustable sampling. *Proteins*, 80(9), pp.2218–2234.

Sulistijo, E.S., Jaszewski, T.M. & MacKenzie, K.R., 2003. Sequence-specific dimerization of the transmembrane domain of the “BH3-only” protein BNIP3 in membranes and detergent. *The Journal of Biological Chemistry*, 278(51), pp.51950–51956.

Sulistijo, E.S. & Mackenzie, K.R., 2009. Structural basis for dimerization of the BNIP3 transmembrane domain. *Biochemistry*, 48(23), pp.5106–5120.

Supekova, L. et al., 2010. A single mutation in the first transmembrane domain of yeast COX2 enables its allotopic expression. *Proceedings of the National Academy of Sciences of the United States of America*, 107(11), pp.5047–5052.

Tan, T. et al., 2013. Mcp1 and Mcp2, two novel proteins involved in mitochondrial lipid homeostasis. *Journal of cell science*, 126(Pt 16), pp.3563–3574.

Tong, J. et al., 2011. Ancestral and derived protein import pathways in the mitochondrion of Reclinomonas americana. *Molecular biology and evolution*, 28(5), pp.1581–1591.

Tusnády, G.E. & Simon, I., 1998. Principles governing amino acid composition of integral membrane proteins: application to topology prediction. *Journal of molecular biology*, 283(2), pp.489–506.

Tusnády, G.E. & Simon, I., 2001. The HMMTOP transmembrane topology prediction server. *Bioinformatics (Oxford, England)*, 17(9), pp.849–850.

UniProt Consortium, 2013. Update on activities at the Universal Protein Resource (UniProt) in 2013. *Nucleic acids research*, 41(Database issue), pp.D43–47.

Unterreitmeier, S. et al., 2007. Phenylalanine promotes interaction of transmembrane domains via GxxxG motifs. *Journal of molecular biology*, 374(3), pp.705–718.

Vargas, R. et al., 2000. How Strong Is the Cα−H···OC Hydrogen Bond? *J. Am. Chem. Soc.*, 122(19), pp.4750–4755.

Wallin, E. & von Heijne, G., 1998. Genome-wide analysis of integral membrane proteins from eubacterial, archaean, and eukaryotic organisms. *Protein Science: A Publication of the Protein Society*, 7(4), pp.1029–1038.

Walters, R.F.S. & DeGrado, W.F., 2006. Helix-packing motifs in membrane proteins. *Proceedings of the National Academy of Sciences of the United States of America*, 103(37), pp.13658–63.

West, A.H. & Stock, A.M., 2001. Histidine kinases and response regulator proteins in two-component signaling systems. *Trends in Biochemical Sciences*, 26(6), pp.369–376.

Wimley, W.C., Creamer, T.P. & White, S.H., 1996. Solvation energies of amino acid side chains and backbone in a family of host-guest pentapeptides. *Biochemistry*, 35(16), pp.5109–5124.

Yang, J. et al., 2013. High-accuracy prediction of transmembrane inter-helix contacts and application to GPCR 3D structure modeling. *Bioinformatics (Oxford, England)*, 29(20), pp.2579–2587.

Yohannan, S. et al., 2004. A C alpha-H...O hydrogen bond in a membrane protein is not stabilizing. *Journal of the American Chemical Society*, 126(8), pp.2284–2285.

You, M. et al., 2005. Forster resonance energy transfer in liposomes: measurements of transmembrane helix dimerization in the native bilayer environment. *Analytical Biochemistry*, 340(1), pp.154–164.

Zhou, F.X. et al., 2000. Interhelical hydrogen bonding drives strong interactions in membrane proteins. *Nature structural biology*, 7(2), pp.154–60.

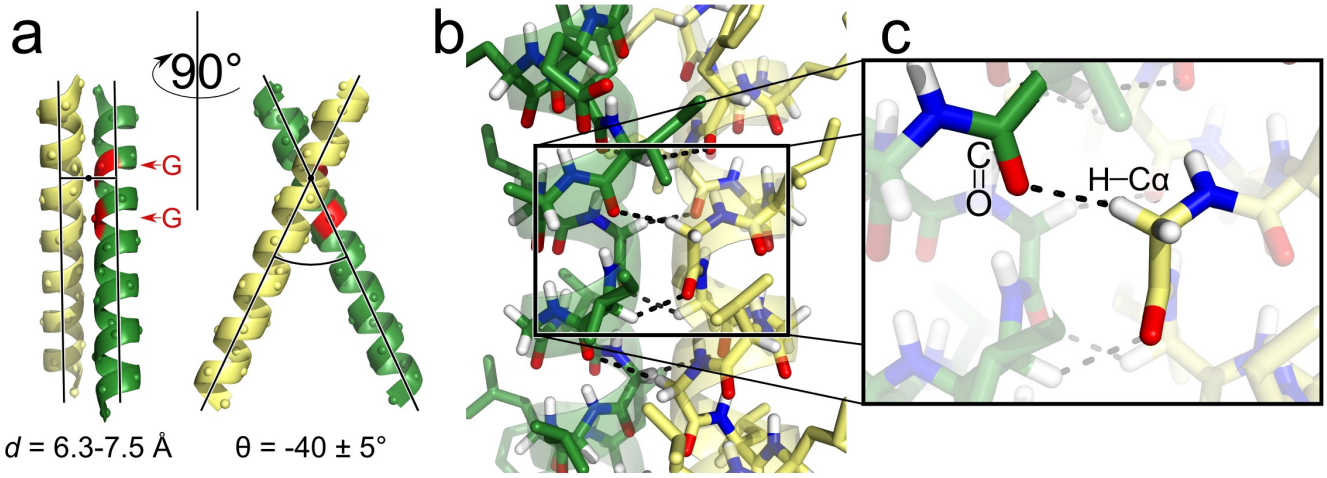

Figure 5.1. Structural features of the GAS_{right} TM association motif. a) The GAS_{right} motif (which is best known as the fold of the TM region of glycophorin A) is a right-handed helical dimer with a short inter-helical distance *d* and a right-handed crossing angle θ of approximatively −40°. The GxxxG sequence pattern near the crossing point (marked in red in the green helix) allows the backbones to come into close contact. b) The contact enables the formation of networks of inter-helical hydrogen bonds between Cα–H donors and carbonyl oxygen acceptors (shown in detail in c).

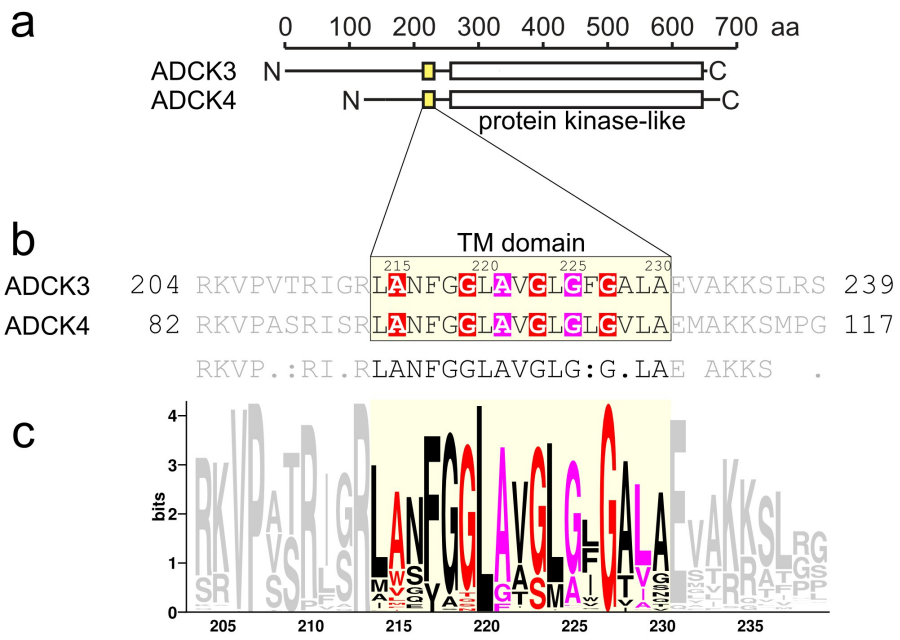

Figure 5.2. The transmembrane domain of ADCK3 has a conserved Gly-zipper motif. a) Domain organization of ADCK3 homologs, which are proteins associated with the mitochondrial inner membrane. They are predicted to contain a TM domain (yellow) and a protein kinase-like domain (white). b) The sequence alignment of the TM domains of ADCK3, ADCK4 (yellow box). The TM domains of ADCK3 and ADKC4, which differ only at two positions, contain a number of GxxxG-like motifs, including an extended Gly-zipper motif (red) and a second AxxxG motif which is off-register by two positions (magenta). c) Sequence logo of the alignment of 400 sequences homologous to ADCK3 from a broad range of eukaryotic species highlights conservation in the TM domain and in the N-terminal side of the juxta-membrane region. All Gly positions in the Gly-zipper (red) appear strongly conserved. The most conserved positions in the TM region are L220 and G227. Identifiers of the sequences used for the alignment are provided in Supplementary Text S1.

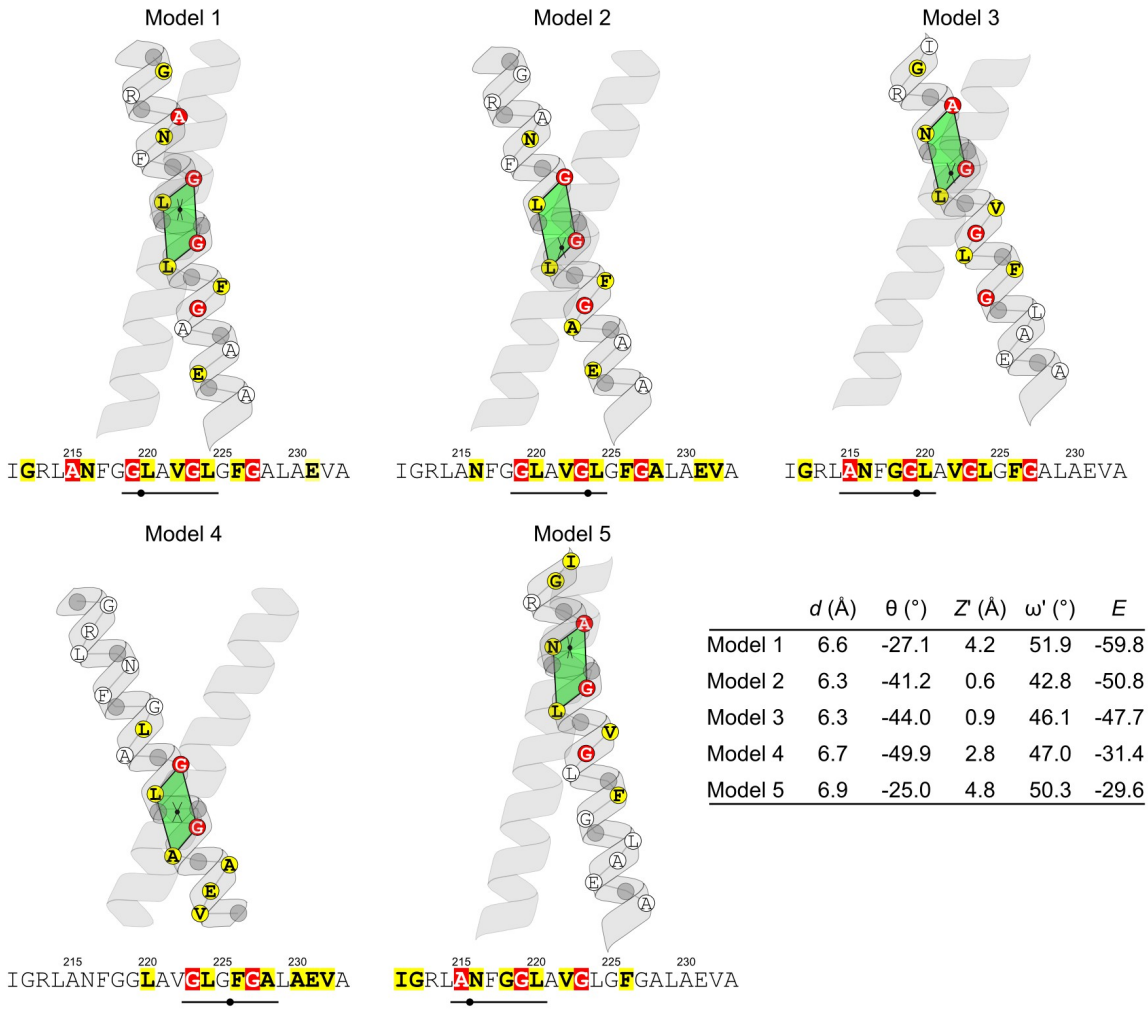

	d (Å)	θ (°)	*Z'* (Å)	ω' (°)	*E*
Model 1	6.6	-27.1	4.2	51.9	-59.8
Model 2	6.3	-41.2	0.6	42.8	-50.8
Model 3	6.3	-44.0	0.9	46.1	-47.7
Model 4	6.7	-49.9	2.8	47.0	-31.4
Model 5	6.9	-25.0	4.8	50.3	-29.6

Figure 5.3. CATM predicts multiple modes of interaction along the Gly-zipper motif of ADCK3. Schematic representation of the five models of GAS_{right} homo-dimers generated by CATM for ADCK3-TM. The crossing point is marked by a black dot. The four positions that surround the crossing point are marked by a green parallelogram and are underlined in the sequence. The positions involved in inter-helical packing at the dimer interface are highlighted: in red are the interfacial positions that belong to the extended Gly-zipper motif of ADCK3; all other interfacial positions are highlighted in yellow. The table summarizes the geometry of the five models: interhelical distance *d;* crossing angle θ; vertical (*Z*') and axial (ω') coordinates of the crossing point within the parallelogram of closest approach; and energy score *E*. For the geometric definitions see **Figure S5.2** and Mueller *et al*.(Mueller et al. 2014).

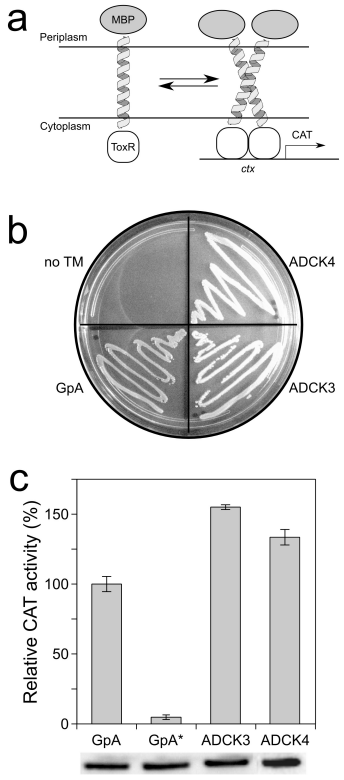

Figure 5.4. ADCK3-TM and ADCK4-TM associate strongly in TOXCAT. a) TOXCAT is an in vivo assay based on a construct in which the transmembrane domain under investigation is fused to the ToxR transcriptional activator of *V. cholerae*. Transmembrane association results in the expression of a reporter gene in *E. coli* cells, which can be quantified. b) *malE* complementation assay. The TOXCAT construct containing the TM domain of ADCK3 and ADCK4 can use maltose as a carbon source, demonstrating correct insertion. GpA: Glycophorin A positive control; no TM: pcckan plasmid without TM insert, negative control. c) TOXCAT assay of ADCK3 and ADCK4. ADCK3 shows approximately 150% of the CAT activity of the strong transmembrane dimer of Glycophorin A (GpA). The monomeric G83I mutant (GpA*) is used as a negative control. Data reported as average and standard deviation over four replicate experiments. Expression levels were controlled by immunoblotting.

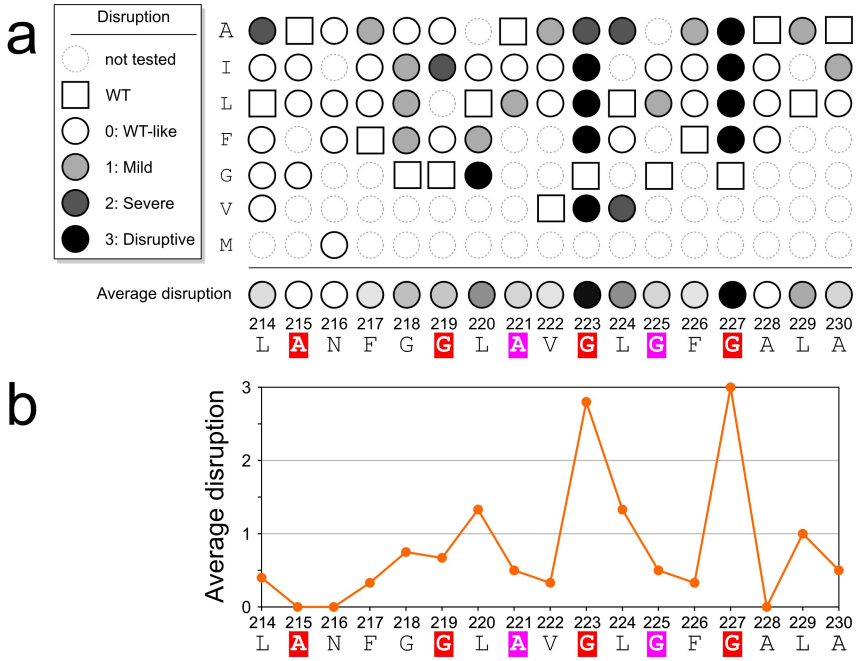

Figure 5.5. Position specific "average disruption" suggests that the Gly-zipper is at the helical interface. a) "MacKenzie plot" summarizing the effect of all mutations of ADCK3-TM measured in TOXCAT. The color coding of the GxxxG motifs in the sequence corresponds to **Figure 5.1**. The data has been subdivided in three categories as in the legend. The raw TOXCAT data is shown in supplementary **Figure S5.1**. A calculated average disruption score for each position is displayed at the bottom of the scheme. b) The same average disruption plotted numerically (0 = as TW; 3 = disruptive). The mutagenesis reveals two positions that are essential for self-association, G223 and G227, which are the last two position of ADCK3's Gly-zipper (red).

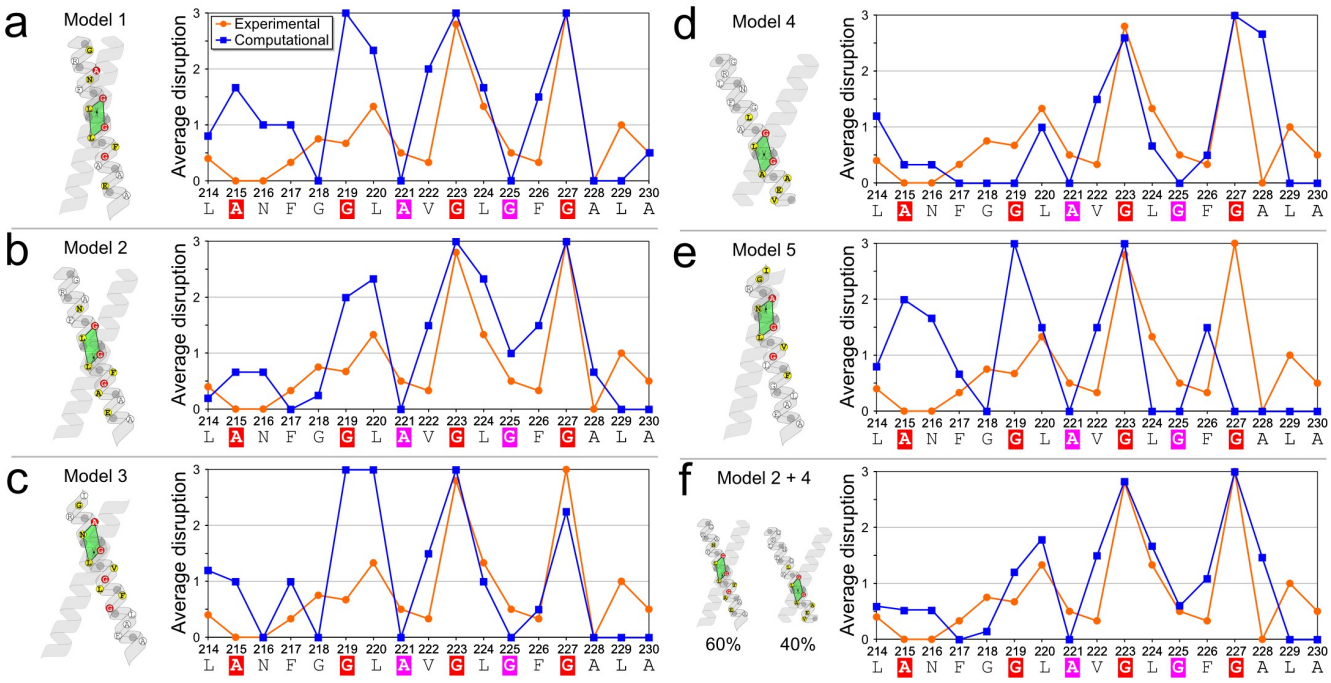

Figure 5.6. Computational mutagenesis identifies compatible models. Comparison of the mutagenesis obtained in TOXCAT (same as **Figure 5.5b**) with the computational mutagenesis performed on the five CATM models (panels a-e). The comparison suggest that Model 2 is the best fit to the experimental data, followed by Model 4. A linear combination of Model 2 (60%) and Model 4 (40%) produces an excellent fit to the data, suggesting that the TM of ADCK3 may be in equilibrium between at least two conformations in the TOXCAT system.

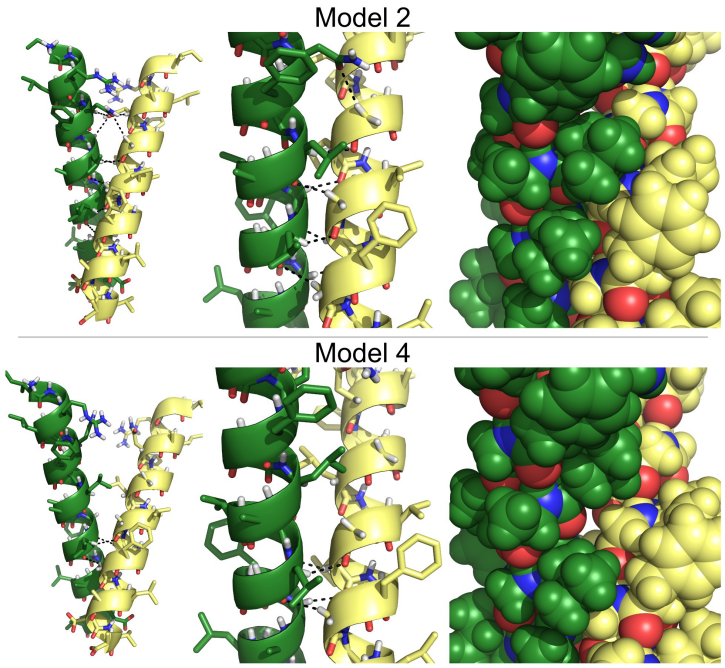

Figure 5.7. Structural Models 2 and 4. Comparison of the structures of CATM Models 2 and 4 for ADCK3. From left to right, entire TM helix, detail of the interface, and same conformation in full atom spheres. Model 2 has lower energy, a larger number of hydrogen bonds (12 in Model 2 versus 4 in Model 4) and more extended and complementary packing.

Table 5.1 Prediction of the transmembrane domain of the ADCK3 homologs

Name	Sequence	ΔG_{Oct}[1]	ΔG_{App}[2]	TMPRED[3]	Phobius[4]	TMHMM[5]	ΔG predictor[6]	MemBrain[7]	E(z)[8]
ADCK3	LANFGGLAVGLGFGALA	−0.28	+2.11	Yes	50%	No	Yes (+1.80)	Possible (70%)	No
ADCK4	LANFGGLAVGLGLGVLA	−0.78	+1.91	Yes	90%	40%	Yes (+1.69)	Yes (80%)	No

[1]Wimley-White octanol scale (kcal/mol)(Wimley et al. 1996)
[2]Biological hydrophobicity scale (kcal/mol)(Hessa et al. 2007; Hessa et al. 2005)
[3]TMPRED(Tusnády & Simon 1998; Tusnády & Simon 2001) at http://www.ch.embnet.org/software/TMPRED_form.html
[4]Phobius(Käll et al. 2004; Käll et al. 2007) at http://phobius.sbc.su.se
[5]TMHMM(Krogh et al. 2001) at http://www.cbs.dtu.dk/services/TMHMM-2.0
[6]ΔG predictior(Hessa et al. 2007) at http://dgpred.cbr.su.se (in parethesis the ΔG_{App} for the predicted TM segment, kcal/mol)
[7]MemBrain(Shen & Chou 2008; Yang et al. 2013) at http://www.csbio.sjtu.edu.cn/bioinf/MemBrain
[8]E(z) potential(Senes et al. 2007) at http://ez.degradolab.org/ez/original

Supplementary Information

Supplementary Table S5.1, summary of CATM Model 1 of ADCK3

Model 1		
Total CATM score	−59.8	
Van der Waals component	−43.3	
Hydrogen Bonding component	−16.6	
Quadrant of closest approach	G219-L224	
d (inter-helical distance)	6.6 Å	
θ (crossing angle)	−27.1 º	
Z' (crossing point, axial shift)	4.2 Å	
ω' (crossing point, axial rotation)	51.9 º	
Number of inter-helical H-bonds	12	
Donor	**Acceptor**	**Distance**
B 216 Asn HA	A 215 Ala O	3.25251
B 219 Gly HA1	A 216 Asn OD1	2.51865
B 219 Gly HA1	A 216 Asn O	2.94603
B 220 Leu HA	A 219 Gly O	2.37817
B 223 Gly HA1	A 220 Leu O	3.03996
B 224 Leu HA	A 223 Gly O	3.37371
A 216 Asn HA	B 215 Ala O	3.25251
A 219 Gly HA1	B 216 Asn OD1	2.51865
A 219 Gly HA1	B 216 Asn O	2.94603
A 220 Leu HA	B 219 Gly O	2.37817
A 223 Gly HA1	B 220 Leu O	3.03996
A 224 Leu HA	B 223 Gly O	3.37371

Supplementary Table S5.2, summary of CATM Model 2 of ADCK3

Model 2		
Total CATM score	−50.8	
Van der Waals component	−28.3	
Hydrogen Bonding component	−22.4	
Quadrant of closest approach	G219-L224	
d (inter-helical distance)	6.3 Å	
θ (crossing angle)	−42.2 º	
Z' (crossing point, axial shift)	0.6 Å	
ω' (crossing point, axial rotation)	42.8 º	
Number of inter-helical H-bonds	12	
Donor	**Acceptor**	**Distance**
B 216 Asn HA	A 216 Asn OD1	3.04807
B 219 Gly HA1	A 216 Asn OD1	3.13004
B 220 Leu HA	A 219 Gly O	2.83268
B 223 Gly HA1	A 220 Leu O	2.41331
B 224 Leu HA	A 223 Gly O	2.34205
B 227 Gly HA1	A 224 Leu O	3.11619
A 216 Asn HA	B 216 Asn OD1	3.04807
A 219 Gly HA1	B 216 Asn OD1	3.13004
A 220 Leu HA	B 219 Gly O	2.83268
A 223 Gly HA1	B 220 Leu O	2.41331
A 224 Leu HA	B 223 Gly O	2.34205
A 227 Gly HA1	B 224 Leu O	3.11619

Supplementary Table S5.3, summary of CATM Model 3 of ADCK3

Model 3		
Total CATM score	−47.7	
Van der Waals component	−32.2	
Hydrogen Bonding component	−15.5	
Quadrant of closest approach	A215-L220	
d (inter-helical distance)	6.3 Å	
θ (crossing angle)	−44.0 º	
Z' (crossing point, axial shift)	0.9 Å	
ω' (crossing point, axial rotation)	46.1 º	
Number of inter-helical H-bonds	10	
Donor	**Acceptor**	**Distance**
B 216 Asn HA	A 215 Ala O	2.75854
B 219 Gly HA2	A 216 Asn OD1	3.03411
B 219 Gly HA1	A 216 Asn O	2.35013
B 220 Leu HA	A 219 Gly O	2.40005
B 223 Gly HA1	A 220 Leu O	3.32438
A 216 Asn HA	B 215 Ala O	2.75854
A 219 Gly HA2	B 216 Asn OD1	3.03411
A 219 Gly HA1	B 216 Asn O	2.35013
A 220 Leu HA	B 219 Gly O	2.40005
A 223 Gly HA1	B 220 Leu O	3.32438

Supplementary Table S5.4, summary of CATM Model 4 of ADCK3

Model 4		
Total CATM score	−31.4	
Van der Waals component	−23.3	
Hydrogen Bonding component	−8.0	
Quadrant of closest approach	G223-A227	
d (inter-helical distance)	6.7 Å	
θ (crossing angle)	−49.9 º	
Z’ (crossing point, axial shift)	2.8 Å	
ω’ (crossing point, axial rotation)	47.0 º	
Number of inter-helical H-bonds	4	
Donor	**Acceptor**	**Distance**
B 224 Leu HA	A 223 Gly O	2.73165
B 227 Gly HA1	A 224 Leu O	2.65991
A 224 Leu HA	B 223 Gly O	2.73165
A 227 Gly HA1	B 224 Leu O	2.65991

Supplementary Table S5.5, summary of CATM Model 5 of ADCK3

Model 5		
Total CATM score	−29.6	
Van der Waals component	−17.9	
Hydrogen Bonding component	−11.7	
Quadrant of closest approach	A215-L220	
d (inter-helical distance)	6.9 Å	
θ (crossing angle)	−25.0 º	
Z' (crossing point, axial shift)	4.8 Å	
ω' (crossing point, axial rotation)	50.3 º	
Number of inter-helical H-bonds	6	
Donor	**Acceptor**	**Distance**
B 216 Asn HA	A 215 Ala O	2.69118
B 216 Asn HD21	A 215 Ala O	2.1257
B 219 Gly HA1	A 216 Asn O	3.42358
A 216 Asn HA	B 215 Ala O	2.69118
A 216 Asn HD21	B 215 Ala O	2.1257
A 219 Gly HA1	B 216 Asn O	3.42358

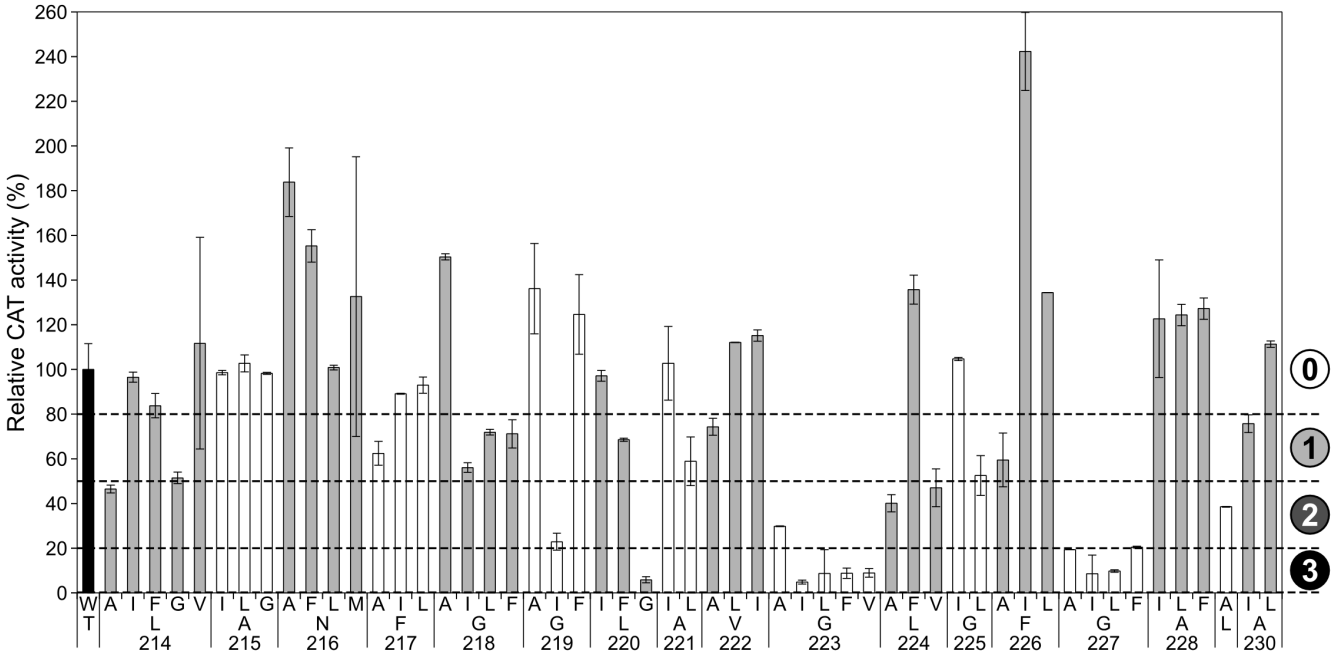

Figure S5.1 Mutagenesis of the TM helix of ADCK3. The figure shows the TOXCAT result for each of the point mutants of the TM domain of ADCK3 schematically summarized in **Figure 5.5**. The CAT activity (left axis) is normalized to that of the wild type sequence, shown in black. The mutations at each position are visually grouped by color. Each mutation has been categorized relative to the wild type activity (back bar) as “WT-like” (0: >80% of WT), “Mild” (1: 50-80%), “Severe” (2: 20-50%) or “Disruptive” (3: 0-20%), as indicated on the right axis and by the dashed lines.

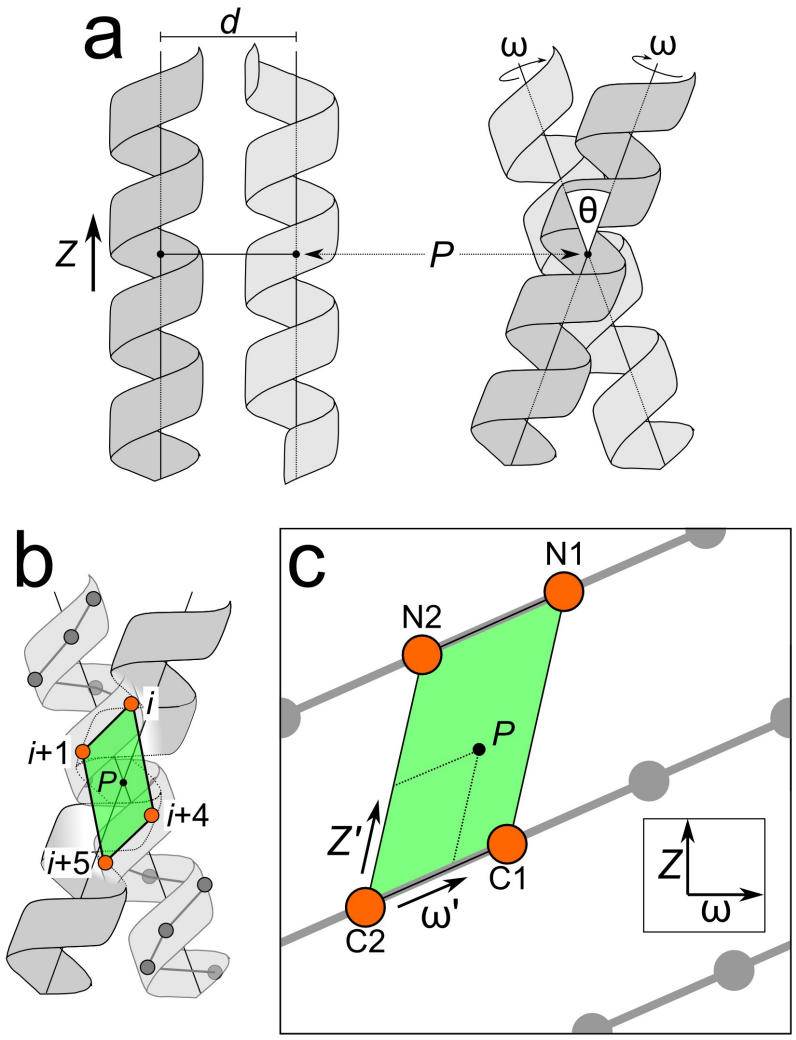

Figure S5.2. Definition of 4 parameters that define the geometry of a symmetrical dimer. a) *d*: inter-helical distance; θ: crossing angle; ω: rotation of the helix around its axis; *Z*: vertical position of the point of closest approach between the two helical axes (the crossing point *P*). b) The coordinates can be redefined by expressing them as a function of the unit cell (green) on the helical lattice that contains the point of closest approach *P*. The four interfacial positions that surround the the point of closest approach are designated as N1 (relative position *i*), N2 (*i*+1), C1(*i*+4) and C2 (*i*+5). The principal axes are the rotation along the helical screw (ω') and the vector between C2 and C2 (*Z*')(Mueller et al. 2014).

Supplementary Text ST5.1, sequence alignment of ADCK3 homologs

The sequence logo of **Figure 5.2c** was created using homologous sequence of ADCK3 obtained with Blast(Altschul et al. 1997) (http://blast.ncbi.nlm.nih.gov), which queried with the sequence of human ADCK3 and standard parameters. The top 400 hits were aligned using ClustalW(Goujon et al. 2010) (http://www.ebi.ac.uk/Tools/msa/clustalw2). The web logo was produced using WebLogo (http://weblogo.berkeley.edu)(Crooks et al. 2004). The identifiers of the sequence used in the alignment are the following:

gi|556101431|gb|ESO90083.1| hypothetical protein LOTGIDRAFT_218121 [Lottia gigantea]
gi|524869263|ref|XP_005091427.1| PREDICTED: chaperone activity of bc1 complex-like, mitochondrial-like isoform X1 [Aplysia californica]
gi|405957185|gb|EKC23415.1| Chaperone activity of bc1 complex-like, mitochondrial [Crassostrea gigas]
gi|340375939|ref|XP_003386491.1| PREDICTED: chaperone activity of bc1 complex-like, mitochondrial-like [Amphimedon queenslandica]
gi|32565180|ref|NP_498014.2| Protein COQ-8 [Caenorhabditis elegans]
gi|341896229|gb|EGT52164.1| CBN-COQ-8 protein [Caenorhabditis brenneri]
gi|268574088|ref|XP_002642021.1| C. briggsae CBR-COQ-8 protein [Caenorhabditis briggsae]
gi|308487612|ref|XP_003106001.1| CRE-COQ-8 protein [Caenorhabditis remanei]
gi|560117677|emb|CDJ97685.1| ABC-1 domain containing protein [Haemonchus contortus]
gi|560123355|emb|CDJ92014.1| ABC-1 domain containing protein [Haemonchus contortus]
gi|568281227|gb|ETN74063.1| ABC1 family protein [Necator americanus]
gi|170572278|ref|XP_001892048.1| chaperone-activity of bc1 complex-like, mitochondrial [Brugia malayi]
gi|393904834|gb|EJD73810.1| atypical/ABC1/ABC1-A protein kinase [Loa loa]
gi|541042808|gb|ERG81884.1| ubiquinone biosynthesis protein coq-8 [Ascaris suum]
gi|339240355|ref|XP_003376103.1| ubiquinone biosynthesis protein coq-8 [Trichinella spiralis]
gi|555930212|emb|CDJ07330.1| ABC domain containing protein kinase [Hymenolepis microstoma]
gi|556521987|emb|CDJ25289.1| ABC domain containing protein kinase [Echinococcus granulosus]
gi|256074523|ref|XP_002573574.1| ABC transporter [Schistosoma mansoni]
gi|18859849|ref|NP_572836.1| CG32649 [Drosophila melanogaster]
gi|195352724|ref|XP_002042861.1| GM11527 [Drosophila sechellia]
gi|194895760|ref|XP_001978335.1| GG19534 [Drosophila erecta]
gi|195478070|ref|XP_002100397.1| GE16192 [Drosophila yakuba]
gi|194764011|ref|XP_001964125.1| GF20885 [Drosophila ananassae]
gi|125980843|ref|XP_001354442.1| GA17042 [Drosophila pseudoobscura pseudoobscura]
gi|195173652|ref|XP_002027601.1| GL22961 [Drosophila persimilis]
gi|195133048|ref|XP_002010951.1| GI16276 [Drosophila mojavensis]
gi|195397037|ref|XP_002057135.1| GJ16920 [Drosophila virilis]
gi|195059807|ref|XP_001995703.1| GH17620 [Drosophila grimshawi]
gi|195425895|ref|XP_002061196.1| GK10272 [Drosophila willistoni]
gi|498984706|ref|XP_004530431.1| PREDICTED: chaperone activity of bc1 complex-like, mitochondrial-like isoform X1 [Ceratitis capitata]
gi|498984710|ref|XP_004530432.1| PREDICTED: chaperone activity of bc1 complex-like, mitochondrial-like isoform X2 [Ceratitis capitata]
gi|557776089|ref|XP_005187688.1| PREDICTED: chaperone activity of bc1 complex-like, mitochondrial-like isoform X1 [Musca domestica]
gi|557776091|ref|XP_005187689.1| PREDICTED: chaperone activity of bc1 complex-like, mitochondrial-like isoform X2 [Musca domestica]
gi|157103279|ref|XP_001647906.1| hypothetical protein AaeL_AAEL000003 [Aedes aegypti]
gi|170063784|ref|XP_001867254.1| ubiquinone biosynthesis protein coq-8 [Culex quinquefasciatus]
gi|347968821|ref|XP_311995.4| AGAP002906-PA [Anopheles gambiae str. PEST]
gi|568251291|gb|ETN60854.1| ubiquinone biosynthesis protein coq-8 [Anopheles darlingi]
gi|189236501|ref|XP_001815964.1| PREDICTED: similar to GA17042-PA [Tribolium castaneum]
gi|270005327|gb|EFA01775.1| hypothetical protein TcasGA2_TC007376 [Tribolium castaneum]
gi|478262769|gb|ENN81291.1| hypothetical protein YQE_02295, partial [Dendroctonus ponderosae]
gi|546675371|gb|ERL86581.1| hypothetical protein D910_03988 [Dendroctonus ponderosae]
gi|357627323|gb|EHJ77059.1| hypothetical protein KGM_21488 [Danaus plexippus]
gi|512933841|ref|XP_004932891.1| PREDICTED: chaperone activity of bc1 complex-like, mitochondrial-like [Bombyx mori]
gi|322798371|gb|EFZ20095.1| hypothetical protein SINV_02598 [Solenopsis invicta]
gi|332021879|gb|EGI62215.1| Chaperone activity of bc1 complex-like, mitochondrial [Acromyrmex echinatior]
gi|307167954|gb|EFN61320.1| Uncharacterized aarF domain-containing protein kinase 4 [Camponotus floridanus]
gi|307194680|gb|EFN76939.1| Uncharacterized aarF domain-containing protein kinase 4 [Harpegnathos saltator]
gi|328782774|ref|XP_624948.3| PREDICTED: uncharacterized aarF domain-containing protein kinase 4 isoform X5 [Apis mellifera]
gi|571571172|ref|XP_006563062.1| PREDICTED: uncharacterized aarF domain-containing protein kinase 4 isoform X4 [Apis mellifera]
gi|572301426|ref|XP_006616772.1| PREDICTED: uncharacterized aarF domain-containing protein kinase 4-like [Apis dorsata]
gi|380021104|ref|XP_003694414.1| PREDICTED: chaperone activity of bc1 complex-like, mitochondrial-like [Apis florea]
gi|340725065|ref|XP_003400895.1| PREDICTED: chaperone activity of bc1 complex-like, mitochondrial-like [Bombus terrestris]
gi|350398351|ref|XP_003485168.1| PREDICTED: chaperone activity of bc1 complex-like, mitochondrial-like [Bombus impatiens]
gi|383865801|ref|XP_003708361.1| PREDICTED: chaperone activity of bc1 complex-like, mitochondrial-like [Megachile rotundata]

gi|345483054|ref|XP_001605712.2| PREDICTED: chaperone activity of bc1 complex-like, mitochondrial-like [Nasonia vitripennis]
gi|193584682|ref|XP_001951205.1| PREDICTED: chaperone activity of bc1 complex-like, mitochondrial-like [Acyrthosiphon pisum]
gi|156379799|ref|XP_001631643.1| predicted protein [Nematostella vectensis]
gi|241651014|ref|XP_002411257.1| conserved hypothetical protein [Ixodes scapularis]
gi|196007476|ref|XP_002113604.1| hypothetical protein TRIADDRAFT_26675 [Trichoplax adhaerens]
gi|321478972|gb|EFX89928.1| hypothetical protein DAPPUDRAFT_300027 [Daphnia pulex]
gi|391343550|ref|XP_003746072.1| PREDICTED: uncharacterized protein LOC100906274 [Metaseiulus occidentalis]
gi|449665263|ref|XP_002161433.2| PREDICTED: chaperone activity of bc1 complex-like, mitochondrial-like [Hydra vulgaris]
gi|22760302|dbj|BAC11143.1| unnamed protein product [Homo sapiens]
gi|34147522|ref|NP_064632.2| chaperone activity of bc1 complex-like, mitochondrial [Homo sapiens]
gi|120538499|gb|AAI29931.1| CABC1 protein [Homo sapiens]
gi|332812087|ref|XP_514248.3| PREDICTED: aarF domain containing kinase 3 isoform 2 [Pan troglodytes]
gi|410034536|ref|XP_003949756.1| PREDICTED: aarF domain containing kinase 3 [Pan troglodytes]
gi|395728943|ref|XP_003775463.1| PREDICTED: LOW QUALITY PROTEIN: chaperone activity of bc1 complex-like, mitochondrial [Pongo abelii]
gi|426333991|ref|XP_004028547.1| PREDICTED: chaperone activity of bc1 complex-like, mitochondrial [Gorilla gorilla gorilla]
gi|397487825|ref|XP_003814979.1| PREDICTED: chaperone activity of bc1 complex-like, mitochondrial isoform 1 [Pan paniscus]
gi|52546036|emb|CAH56132.1| hypothetical protein [Homo sapiens]
gi|397487827|ref|XP_003814980.1| PREDICTED: chaperone activity of bc1 complex-like, mitochondrial isoform 2 [Pan paniscus]
gi|402857025|ref|XP_003893074.1| PREDICTED: chaperone activity of bc1 complex-like, mitochondrial isoform 1 [Papio anubis]
gi|402857027|ref|XP_003893075.1| PREDICTED: chaperone activity of bc1 complex-like, mitochondrial isoform 2 [Papio anubis]
gi|384475947|ref|NP_001245119.1| chaperone activity of bc1 complex-like, mitochondrial [Macaca mulatta]
gi|194375033|dbj|BAG62629.1| unnamed protein product [Homo sapiens]
gi|296230259|ref|XP_002760620.1| PREDICTED: chaperone activity of bc1 complex-like, mitochondrial [Callithrix jacchus]
gi|403277369|ref|XP_003930337.1| PREDICTED: chaperone activity of bc1 complex-like, mitochondrial [Saimiri boliviensis boliviensis]
gi|193786848|dbj|BAG52171.1| unnamed protein product [Homo sapiens]
gi|348577083|ref|XP_003474314.1| PREDICTED: chaperone activity of bc1 complex-like, mitochondrial [Cavia porcellus]
gi|533118786|ref|XP_005374854.1| PREDICTED: chaperone activity of bc1 complex-like, mitochondrial [Chinchilla lanigera]
gi|507627177|ref|XP_004626878.1| PREDICTED: chaperone activity of bc1 complex-like, mitochondrial [Octodon degus]
gi|351707065|gb|EHB09984.1| Chaperone activity of bc1 complex-like, mitochondrial [Heterocephalus glaber]
gi|512883071|ref|XP_004895646.1| PREDICTED: chaperone activity of bc1 complex-like, mitochondrial isoform X1 [Heterocephalus glaber]
gi|512983100|ref|XP_004853533.1| PREDICTED: chaperone activity of bc1 complex-like, mitochondrial isoform X1 [Heterocephalus glaber]
gi|512983104|ref|XP_004853535.1| PREDICTED: chaperone activity of bc1 complex-like, mitochondrial isoform X3 [Heterocephalus glaber]
gi|478530930|ref|XP_004439621.1| PREDICTED: chaperone activity of bc1 complex-like, mitochondrial [Ceratotherium simum simum]
gi|562857623|ref|XP_006157308.1| PREDICTED: chaperone activity of bc1 complex-like, mitochondrial [Tupaia chinensis]
gi|532081710|ref|XP_005326605.1| PREDICTED: chaperone activity of bc1 complex-like, mitochondrial isoform X1 [Ictidomys tridecemlineatus]
gi|291402048|ref|XP_002717679.1| PREDICTED: chaperone activity of bc1 complex-like, mitochondrial-like [Oryctolagus cuniculus]
gi|504132582|ref|XP_004578904.1| PREDICTED: chaperone activity of bc1 complex-like, mitochondrial [Ochotona princeps]
gi|395852655|ref|XP_003798850.1| PREDICTED: chaperone activity of bc1 complex-like, mitochondrial [Otolemur garnettii]
gi|344278579|ref|XP_003411071.1| PREDICTED: chaperone activity of bc1 complex-like, mitochondrial-like [Loxodonta africana]
gi|471370985|ref|XP_004376003.1| PREDICTED: chaperone activity of bc1 complex-like, mitochondrial [Trichechus manatus latirostris]
gi|507634746|ref|XP_004700024.1| PREDICTED: chaperone activity of bc1 complex-like, mitochondrial [Echinops telfairi]
gi|586481609|ref|XP_006871324.1| PREDICTED: chaperone activity of bc1 complex-like, mitochondrial [Chrysochloris asiatica]
gi|586562148|ref|XP_006914332.1| PREDICTED: chaperone activity of bc1 complex-like, mitochondrial [Pteropus alecto]
gi|507971753|ref|XP_004690821.1| PREDICTED: chaperone activity of bc1 complex-like, mitochondrial [Condylura cristata]
gi|26380702|dbj|BAB29459.2| unnamed protein product [Mus musculus]
gi|70778882|ref|NP_075830.2| chaperone activity of bc1 complex-like, mitochondrial [Mus musculus]
gi|148681213|gb|EDL13160.1| chaperone, ABC1 activity of bc1 complex like (S. pombe) [Mus musculus]
gi|568911100|ref|XP_006497026.1| PREDICTED: aarF domain containing kinase 3 isoform X4 [Mus musculus]
gi|354490267|ref|XP_003507280.1| PREDICTED: chaperone activity of bc1 complex-like, mitochondrial-like [Cricetulus griseus]
gi|537166611|gb|ERE73576.1| chaperone activity of bc1 complex-like protein [Cricetulus griseus]
gi|524956468|ref|XP_005078200.1| PREDICTED: chaperone activity of bc1 complex-like, mitochondrial [Mesocricetus auratus]
gi|61557218|ref|NP_001013203.1| chaperone activity of bc1 complex-like, mitochondrial [Rattus norvegicus]
gi|532010464|ref|XP_005349032.1| PREDICTED: chaperone activity of bc1 complex-like, mitochondrial [Microtus ochrogaster]
gi|507538935|ref|XP_004653481.1| PREDICTED: chaperone activity of bc1 complex-like, mitochondrial [Jaculus jaculus]
gi|505789979|ref|XP_004605582.1| PREDICTED: chaperone activity of bc1 complex-like, mitochondrial [Sorex araneus]
gi|114051798|ref|NP_001039884.1| chaperone activity of bc1 complex-like, mitochondrial [Bos taurus]
gi|555962731|ref|XP_005893453.1| PREDICTED: chaperone activity of bc1 complex-like, mitochondrial [Bos mutus]
gi|426239559|ref|XP_004013687.1| PREDICTED: LOW QUALITY PROTEIN: chaperone activity of bc1 complex-like, mitochondrial [Ovis aries]
gi|556740431|ref|XP_005965760.1| PREDICTED: LOW QUALITY PROTEIN: chaperone activity of bc1 complex-like, mitochondrial-like [Pantholops hodgsonii]
gi|548498106|ref|XP_005690657.1| PREDICTED: chaperone activity of bc1 complex-like, mitochondrial [Capra hircus]
gi|466014904|ref|XP_004271020.1| PREDICTED: chaperone activity of bc1 complex-like, mitochondrial [Orcinus orca]
gi|470647744|ref|XP_004327582.1| PREDICTED: LOW QUALITY PROTEIN: chaperone activity of bc1 complex-like, mitochondrial [Tursiops truncatus]
gi|545852349|ref|XP_003130598.4| PREDICTED: chaperone activity of bc1 complex-like, mitochondrial isoform 1, partial [Sus scrofa]
gi|560923968|ref|XP_006188176.1| PREDICTED: chaperone activity of bc1 complex-like, mitochondrial [Camelus ferus]
gi|560952717|ref|XP_006198884.1| PREDICTED: chaperone activity of bc1 complex-like, mitochondrial [Vicugna pacos]
gi|530668235|gb|EQB78536.1| chaperone activity of bc1 complex-like, mitochondrial [Camelus ferus]
gi|281348093|gb|EFB23677.1| hypothetical protein PANDA_015361 [Ailuropoda melanoleuca]
gi|301780770|ref|XP_002925802.1| PREDICTED: chaperone activity of bc1 complex-like, mitochondrial-like [Ailuropoda melanoleuca]

gi|511873470|ref|XP_004756948.1| PREDICTED: chaperone activity of bc1 complex-like, mitochondrial [Mustela putorius furo]
gi|511962401|ref|XP_004799377.1| PREDICTED: chaperone activity of bc1 complex-like, mitochondrial isoform X1 [Mustela putorius furo]
gi|511962403|ref|XP_004799378.1| PREDICTED: chaperone activity of bc1 complex-like, mitochondrial isoform X2 [Mustela putorius furo]
gi|511962405|ref|XP_004799379.1| PREDICTED: chaperone activity of bc1 complex-like, mitochondrial isoform X3 [Mustela putorius furo]
gi|472347789|ref|XP_004393611.1| PREDICTED: chaperone activity of bc1 complex-like, mitochondrial [Odobenus rosmarus divergens]
gi|585182226|ref|XP_006742744.1| PREDICTED: chaperone activity of bc1 complex-like, mitochondrial [Leptonychotes weddellii]
gi|587017724|ref|XP_006942676.1| PREDICTED: aarF domain containing kinase 3 [Felis catus]
gi|545506130|ref|XP_005623029.1| PREDICTED: aarF domain containing kinase 3 [Canis lupus familiaris]
gi|554576731|ref|XP_005880198.1| PREDICTED: chaperone activity of bc1 complex-like, mitochondrial isoform X1 [Myotis brandtii]
gi|584071606|ref|XP_006756105.1| PREDICTED: chaperone activity of bc1 complex-like, mitochondrial [Myotis davidii]
gi|432113956|gb|ELK36021.1| Chaperone activity of bc1 complex-like, mitochondrial [Myotis davidii]
gi|126307154|ref|XP_001377083.1| PREDICTED: chaperone activity of bc1 complex-like, mitochondrial-like [Monodelphis domestica]
gi|395531486|ref|XP_003767809.1| PREDICTED: chaperone activity of bc1 complex-like, mitochondrial [Sarcophilus harrisii]
gi|149641637|ref|XP_001513165.1| PREDICTED: chaperone activity of bc1 complex-like, mitochondrial-like [Ornithorhynchus anatinus]
gi|313661454|ref|NP_001186342.1| chaperone activity of bc1 complex-like, mitochondrial [Gallus gallus]
gi|326914963|ref|XP_003203792.1| PREDICTED: chaperone activity of bc1 complex-like, mitochondrial-like [Meleagris gallopavo]
gi|529444353|ref|XP_005241891.1| PREDICTED: chaperone activity of bc1 complex-like, mitochondrial [Falco peregrinus]
gi|541956581|ref|XP_005434055.1| PREDICTED: chaperone activity of bc1 complex-like, mitochondrial [Falco cherrug]
gi|543732775|ref|XP_005507410.1| PREDICTED: chaperone activity of bc1 complex-like, mitochondrial isoform X1 [Columba livia]
gi|543732777|ref|XP_005507411.1| PREDICTED: chaperone activity of bc1 complex-like, mitochondrial isoform X2 [Columba livia]
gi|449276751|gb|EMC85172.1| Chaperone activity of bc1 complex-like, mitochondrial, partial [Columba livia]
gi|514758667|ref|XP_005022606.1| PREDICTED: chaperone activity of bc1 complex-like, mitochondrial [Anas platyrhynchos]
gi|524990363|ref|XP_005043064.1| PREDICTED: chaperone activity of bc1 complex-like, mitochondrial isoform X1 [Ficedula albicollis]
gi|524990367|ref|XP_005043066.1| PREDICTED: chaperone activity of bc1 complex-like, mitochondrial isoform X3 [Ficedula albicollis]
gi|524990365|ref|XP_005043065.1| PREDICTED: chaperone activity of bc1 complex-like, mitochondrial isoform X2 [Ficedula albicollis]
gi|542159593|ref|XP_005488529.1| PREDICTED: chaperone activity of bc1 complex-like, mitochondrial [Zonotrichia albicollis]
gi|543277692|ref|XP_005427071.1| PREDICTED: chaperone activity of bc1 complex-like, mitochondrial [Geospiza fortis]
gi|543358942|ref|XP_005523340.1| PREDICTED: chaperone activity of bc1 complex-like, mitochondrial [Pseudopodoces humilis]
gi|449495964|ref|XP_002194924.2| PREDICTED: chaperone activity of bc1 complex-like, mitochondrial [Taeniopygia guttata]
gi|527267587|ref|XP_005151915.1| PREDICTED: chaperone activity of bc1 complex-like, mitochondrial [Melopsittacus undulatus]
gi|465951733|gb|EMP24538.1| Chaperone activity of bc1 complex-like protein [Chelonia mydas]
gi|530591945|ref|XP_005289615.1| PREDICTED: chaperone activity of bc1 complex-like, mitochondrial-like [Chrysemys picta bellii]
gi|558139018|ref|XP_006118119.1| PREDICTED: chaperone activity of bc1 complex-like, mitochondrial [Pelodiscus sinensis]
gi|557262176|ref|XP_006016618.1| PREDICTED: chaperone activity of bc1 complex-like, mitochondrial [Alligator sinensis]
gi|564253057|ref|XP_006265537.1| PREDICTED: chaperone activity of bc1 complex-like, mitochondrial [Alligator mississippiensis]
gi|327262641|ref|XP_003216132.1| PREDICTED: chaperone activity of bc1 complex-like, mitochondrial-like [Anolis carolinensis]
gi|565315927|gb|ETE67702.1| Chaperone activity of bc1 complex-like, mitochondrial [Ophiophagus hannah]
gi|147900195|ref|NP_001091311.1| aarF domain containing kinase 3 [Xenopus laevis]
gi|301618993|ref|XP_002938888.1| PREDICTED: aarF domain containing kinase 3 [Xenopus (Silurana) tropicalis]
gi|147899712|ref|NP_001088525.1| uncharacterized protein LOC495397 [Xenopus laevis]
gi|47219134|emb|CAG01797.1| unnamed protein product [Tetraodon nigroviridis]
gi|410916387|ref|XP_003971668.1| PREDICTED: chaperone activity of bc1 complex-like, mitochondrial-like [Takifugu rubripes]
gi|432946141|ref|XP_004083788.1| PREDICTED: chaperone activity of bc1 complex-like, mitochondrial-like [Oryzias latipes]
gi|551513801|ref|XP_005808412.1| PREDICTED: chaperone activity of bc1 complex-like, mitochondrial-like [Xiphophorus maculatus]
gi|498940545|ref|XP_004542084.1| PREDICTED: chaperone activity of bc1 complex-like, mitochondrial-like isoform X1 [Maylandia zebra]
gi|548345351|ref|XP_005725088.1| PREDICTED: chaperone activity of bc1 complex-like, mitochondrial-like isoform X1 [Pundamilia nyererei]
gi|583996053|ref|XP_006793141.1| PREDICTED: chaperone activity of bc1 complex-like, mitochondrial-like isoform X1 [Neolamprologus brichardi]
gi|583996055|ref|XP_006793142.1| PREDICTED: chaperone activity of bc1 complex-like, mitochondrial-like isoform X2 [Neolamprologus brichardi]
gi|554813655|ref|XP_005917659.1| PREDICTED: chaperone activity of bc1 complex-like, mitochondrial-like isoform X2 [Haplochromis burtoni]
gi|554813653|ref|XP_005917658.1| PREDICTED: chaperone activity of bc1 complex-like, mitochondrial-like isoform X1 [Haplochromis burtoni]
gi|498940549|ref|XP_004542085.1| PREDICTED: chaperone activity of bc1 complex-like, mitochondrial-like isoform X2 [Maylandia zebra]
gi|498940554|ref|XP_004542086.1| PREDICTED: chaperone activity of bc1 complex-like, mitochondrial-like isoform X3 [Maylandia zebra]
gi|548345353|ref|XP_005725089.1| PREDICTED: chaperone activity of bc1 complex-like, mitochondrial-like isoform X2 [Pundamilia nyererei]
gi|548345355|ref|XP_005725090.1| PREDICTED: chaperone activity of bc1 complex-like, mitochondrial-like isoform X3 [Pundamilia nyererei]
gi|542219606|ref|XP_005449721.1| PREDICTED: chaperone activity of bc1 complex-like, mitochondrial-like isoform X1 [Oreochromis niloticus]
gi|542219608|ref|XP_005449722.1| PREDICTED: chaperone activity of bc1 complex-like, mitochondrial-like isoform X2 [Oreochromis niloticus]
gi|75570792|sp|Q5RGU1.1|ADCK3_DANRE RecName: Full=Chaperone activity of bc1 complex-like, mitochondrial; Short=Chaperone-ABC1-like; AltName: Full=aarF domain-containing protein kinase 3; Flags: Precursor
gi|210147448|ref|NP_001002728.2| chaperone activity of bc1 complex-like, mitochondrial [Danio rerio]
gi|573875685|ref|XP_006626150.1| PREDICTED: chaperone activity of bc1 complex-like, mitochondrial-like [Lepisosteus oculatus]
gi|498932179|ref|XP_004540126.1| PREDICTED: chaperone activity of bc1 complex-like, mitochondrial-like [Maylandia zebra]
gi|548392780|ref|XP_005736748.1| PREDICTED: chaperone activity of bc1 complex-like, mitochondrial-like [Pundamilia nyererei]
gi|348510987|ref|XP_003443026.1| PREDICTED: chaperone activity of bc1 complex-like, mitochondrial-like [Oreochromis niloticus]
gi|554872385|ref|XP_005946136.1| PREDICTED: chaperone activity of bc1 complex-like, mitochondrial-like [Haplochromis burtoni]
gi|551495531|ref|XP_005799326.1| PREDICTED: chaperone activity of bc1 complex-like, mitochondrial-like [Xiphophorus maculatus]
gi|410930426|ref|XP_003978599.1| PREDICTED: chaperone activity of bc1 complex-like, mitochondrial-like [Takifugu rubripes]
gi|432954567|ref|XP_004085541.1| PREDICTED: chaperone activity of bc1 complex-like, mitochondrial-like [Oryzias latipes]

gi|326675425|ref|XP_002665174.2| PREDICTED: si:dkey-36g24.3 [Danio rerio]
gi|556954625|ref|XP_005988940.1| PREDICTED: chaperone activity of bc1 complex-like, mitochondrial isoform X1 [Latimeria chalumnae]
gi|556954628|ref|XP_005988941.1| PREDICTED: chaperone activity of bc1 complex-like, mitochondrial isoform X2 [Latimeria chalumnae]
gi|530642535|ref|XP_005307970.1| PREDICTED: chaperone activity of bc1 complex-like, mitochondrial-like isoform X1 [Chrysemys picta bellii]
gi|530642537|ref|XP_005307971.1| PREDICTED: chaperone activity of bc1 complex-like, mitochondrial-like isoform X2 [Chrysemys picta bellii]
gi|465954273|gb|EMP25824.1| Chaperone activity of bc1 complex-like protein [Chelonia mydas]
gi|558223105|ref|XP_006136616.1| PREDICTED: chaperone activity of bc1 complex-like, mitochondrial-like [Pelodiscus sinensis]
gi|61354508|gb|AAX41012.1| aarF domain containing kinase 4 [synthetic construct]
gi|217416386|ref|NP_001136027.1| aarF domain-containing protein kinase 4 isoform b [Homo sapiens]
gi|397482626|ref|XP_003812521.1| PREDICTED: uncharacterized aarF domain-containing protein kinase 4 isoform 2 [Pan paniscus]
gi|530417278|ref|XP_005259327.1| PREDICTED: uncharacterized aarF domain-containing protein kinase 4 isoform X1 [Homo sapiens]
gi|27363457|ref|NP_079152.3| aarF domain-containing protein kinase 4 isoform a [Homo sapiens]
gi|397482624|ref|XP_003812520.1| PREDICTED: uncharacterized aarF domain-containing protein kinase 4 isoform 1 [Pan paniscus]
gi|441653776|ref|XP_003270391.2| PREDICTED: uncharacterized aarF domain-containing protein kinase 4 isoform 1 [Nomascus leucogenys]
gi|297704826|ref|XP_002829281.1| PREDICTED: LOW QUALITY PROTEIN: uncharacterized aarF domain-containing protein kinase 4 [Pongo abelii]
gi|296233847|ref|XP_002762184.1| PREDICTED: uncharacterized aarF domain-containing protein kinase 4 isoform 1 [Callithrix jacchus]
gi|296233849|ref|XP_002762185.1| PREDICTED: uncharacterized aarF domain-containing protein kinase 4 isoform 2 [Callithrix jacchus]
gi|403305330|ref|XP_003943220.1| PREDICTED: uncharacterized aarF domain-containing protein kinase 4 [Saimiri boliviensis boliviensis]
gi|388454683|ref|NP_001252874.1| uncharacterized aarF domain-containing protein kinase 4 [Macaca mulatta]
gi|544511478|ref|XP_005589349.1| PREDICTED: uncharacterized aarF domain-containing protein kinase 4 isoform X1 [Macaca fascicularis]
gi|544511480|ref|XP_005589350.1| PREDICTED: uncharacterized aarF domain-containing protein kinase 4 isoform X2 [Macaca fascicularis]
gi|402905602|ref|XP_003915605.1| PREDICTED: uncharacterized aarF domain-containing protein kinase 4 isoform 2 [Papio anubis]
gi|402905600|ref|XP_003915604.1| PREDICTED: uncharacterized aarF domain-containing protein kinase 4 isoform 1 [Papio anubis]
gi|544511482|ref|XP_005589351.1| PREDICTED: uncharacterized aarF domain-containing protein kinase 4 isoform X3 [Macaca fascicularis]
gi|426388803|ref|XP_004060822.1| PREDICTED: LOW QUALITY PROTEIN: uncharacterized aarF domain-containing protein kinase 4 [Gorilla gorilla gorilla]
gi|301776655|ref|XP_002923742.1| PREDICTED: uncharacterized aarF domain-containing protein kinase 4-like isoform 1 [Ailuropoda melanoleuca]
gi|301776657|ref|XP_002923743.1| PREDICTED: uncharacterized aarF domain-containing protein kinase 4-like isoform 2 [Ailuropoda melanoleuca]
gi|281340735|gb|EFB16319.1| hypothetical protein PANDA_012945 [Ailuropoda melanoleuca]
gi|345785025|ref|XP_541612.3| PREDICTED: LOW QUALITY PROTEIN: uncharacterized aarF domain-containing protein kinase 4 [Canis lupus familiaris]
gi|472353458|ref|XP_004396399.1| PREDICTED: uncharacterized aarF domain-containing protein kinase 4 isoform 1 [Odobenus rosmarus divergens]
gi|472353460|ref|XP_004396400.1| PREDICTED: uncharacterized aarF domain-containing protein kinase 4 isoform 2 [Odobenus rosmarus divergens]
gi|585199774|ref|XP_006750848.1| PREDICTED: uncharacterized aarF domain-containing protein kinase 4 [Leptonychotes weddellii]
gi|511913667|ref|XP_004776163.1| PREDICTED: LOW QUALITY PROTEIN: uncharacterized aarF domain-containing protein kinase 4 [Mustela putorius furo]
gi|410983006|ref|XP_003997835.1| PREDICTED: LOW QUALITY PROTEIN: uncharacterized aarF domain-containing protein kinase 4 [Felis catus]
gi|478534964|ref|XP_004441612.1| PREDICTED: LOW QUALITY PROTEIN: uncharacterized aarF domain-containing protein kinase 4 [Ceratotherium simum simum]
gi|545175623|ref|XP_001499301.2| PREDICTED: LOW QUALITY PROTEIN: uncharacterized aarF domain-containing protein kinase 4 [Equus caballus]
gi|358416778|ref|XP_001790539.3| PREDICTED: uncharacterized aarF domain-containing protein kinase 4 isoform X1 [Bos taurus]
gi|528919554|ref|XP_005195382.1| PREDICTED: uncharacterized aarF domain-containing protein kinase 4 isoform X4 [Bos taurus]
gi|359075501|ref|XP_002695038.2| PREDICTED: uncharacterized aarF domain-containing protein kinase 4 isoform X1 [Bos taurus]
gi|528991909|ref|XP_005219173.1| PREDICTED: uncharacterized aarF domain-containing protein kinase 4 isoform X4 [Bos taurus]
gi|296477723|tpg|DAA19838.1| TPA: CG32649-like [Bos taurus]
gi|555957046|ref|XP_005890661.1| PREDICTED: uncharacterized aarF domain-containing protein kinase 4 isoform X1 [Bos mutus]
gi|440910287|gb|ELR60096.1| Putative aarF domain-containing protein kinase 4 [Bos mutus]
gi|555957048|ref|XP_005890662.1| PREDICTED: uncharacterized aarF domain-containing protein kinase 4 isoform X2 [Bos mutus]
gi|556735916|ref|XP_005963563.1| PREDICTED: uncharacterized aarF domain-containing protein kinase 4 isoform X1 [Pantholops hodgsonii]
gi|556735918|ref|XP_005963564.1| PREDICTED: uncharacterized aarF domain-containing protein kinase 4 isoform X2 [Pantholops hodgsonii]
gi|426242907|ref|XP_004015310.1| PREDICTED: LOW QUALITY PROTEIN: uncharacterized aarF domain-containing protein kinase 4 [Ovis aries]
gi|548504237|ref|XP_005692475.1| PREDICTED: uncharacterized aarF domain-containing protein kinase 4 [Capra hircus]
gi|560927453|ref|XP_006189892.1| PREDICTED: LOW QUALITY PROTEIN: uncharacterized aarF domain-containing protein kinase 4 [Camelus ferus]
gi|528757664|gb|EPY77323.1| aarF domain containing kinase 4-like protein [Camelus ferus]
gi|560985733|ref|XP_006215065.1| PREDICTED: LOW QUALITY PROTEIN: uncharacterized aarF domain-containing protein kinase 4 [Vicugna pacos]
gi|466016349|ref|XP_004271313.1| PREDICTED: LOW QUALITY PROTEIN: uncharacterized aarF domain-containing protein kinase 4 [Orcinus orca]
gi|470617903|ref|XP_004317662.1| PREDICTED: LOW QUALITY PROTEIN: uncharacterized aarF domain-containing protein kinase 4

[Tursiops truncatus]
gi|507980581|ref|XP_004693955.1| PREDICTED: LOW QUALITY PROTEIN: uncharacterized aarF domain-containing protein kinase 4 [Condylura cristata]
gi|586524116|ref|XP_006905482.1| PREDICTED: uncharacterized aarF domain-containing protein kinase 4 isoform X2 [Pteropus alecto]
gi|586524114|ref|XP_006905481.1| PREDICTED: uncharacterized aarF domain-containing protein kinase 4 isoform X1 [Pteropus alecto]
gi|521027530|gb|EPQ09318.1| Putative aarF domain-containing protein kinase 4 [Myotis brandtii]
gi|554548625|ref|XP_005868851.1| PREDICTED: uncharacterized aarF domain-containing protein kinase 4 isoform X6 [Myotis brandtii]
gi|554548615|ref|XP_005868846.1| PREDICTED: uncharacterized aarF domain-containing protein kinase 4 isoform X1 [Myotis brandtii]
gi|584078231|ref|XP_006759254.1| PREDICTED: uncharacterized aarF domain-containing protein kinase 4 isoform X1 [Myotis davidii]
gi|584078239|ref|XP_006759258.1| PREDICTED: uncharacterized aarF domain-containing protein kinase 4 isoform X5 [Myotis davidii]
gi|558187491|ref|XP_006102683.1| PREDICTED: uncharacterized aarF domain-containing protein kinase 4 isoform X1 [Myotis lucifugus]
gi|558187509|ref|XP_006102687.1| PREDICTED: uncharacterized aarF domain-containing protein kinase 4 isoform X5 [Myotis lucifugus]
gi|58865696|ref|NP_001012065.1| aarF domain-containing protein kinase 4 [Rattus norvegicus]
gi|149056534|gb|EDM07965.1| rCG53591 [Rattus norvegicus]
gi|148692246|gb|EDL24193.1| aarF domain containing kinase 4, isoform CRA_a [Mus musculus]
gi|148692247|gb|EDL24194.1| aarF domain containing kinase 4, isoform CRA_b [Mus musculus]
gi|81882352|sp|Q566J8.1|ADCK4_MOUSE RecName: Full=AarF domain-containing protein kinase 4
gi|124244100|ref|NP_598531.2| aarF domain-containing protein kinase 4 [Mus musculus]
gi|532057885|ref|XP_005371641.1| PREDICTED: uncharacterized aarF domain-containing protein kinase 4 [Microtus ochrogaster]
gi|507573610|ref|XP_004670390.1| PREDICTED: uncharacterized aarF domain-containing protein kinase 4 [Jaculus jaculus]
gi|533203123|ref|XP_005414084.1| PREDICTED: uncharacterized aarF domain-containing protein kinase 4 isoform X1 [Chinchilla lanigera]
gi|533203139|ref|XP_005414092.1| PREDICTED: uncharacterized aarF domain-containing protein kinase 4 isoform X9 [Chinchilla lanigera]
gi|533203127|ref|XP_005414086.1| PREDICTED: uncharacterized aarF domain-containing protein kinase 4 isoform X3 [Chinchilla lanigera]
gi|533203125|ref|XP_005414085.1| PREDICTED: uncharacterized aarF domain-containing protein kinase 4 isoform X2 [Chinchilla lanigera]
gi|533203129|ref|XP_005414087.1| PREDICTED: uncharacterized aarF domain-containing protein kinase 4 isoform X4 [Chinchilla lanigera]
gi|507713992|ref|XP_004648033.1| PREDICTED: uncharacterized aarF domain-containing protein kinase 4 [Octodon degus]
gi|348552480|ref|XP_003462055.1| PREDICTED: uncharacterized aarF domain-containing protein kinase 4 isoformX1 [Cavia porcellus]
gi|351715414|gb|EHB18333.1| hypothetical protein GW7_03562 [Heterocephalus glaber]
gi|512940021|ref|XP_004909014.1| PREDICTED: uncharacterized aarF domain-containing protein kinase 4 isoform X3 [Heterocephalus glaber]
gi|512939977|ref|XP_004909012.1| PREDICTED: uncharacterized aarF domain-containing protein kinase 4 isoform X1 [Heterocephalus glaber]
gi|512940005|ref|XP_004909013.1| PREDICTED: uncharacterized aarF domain-containing protein kinase 4 isoform X2 [Heterocephalus glaber]
gi|532101764|ref|XP_005336498.1| PREDICTED: uncharacterized aarF domain-containing protein kinase 4 isoform X1 [Ictidomys tridecemlineatus]
gi|532101766|ref|XP_005336499.1| PREDICTED: uncharacterized aarF domain-containing protein kinase 4 isoform X2 [Ictidomys tridecemlineatus]
gi|444732041|gb|ELW72365.1| Putative aarF domain-containing protein kinase 4 [Tupaia chinensis]
gi|562821230|ref|XP_006140531.1| PREDICTED: LOW QUALITY PROTEIN: uncharacterized aarF domain-containing protein kinase 4 [Tupaia chinensis]
gi|395859756|ref|XP_003802198.1| PREDICTED: LOW QUALITY PROTEIN: uncharacterized aarF domain-containing protein kinase 4 [Otolemur garnettii]
gi|344298217|ref|XP_003420790.1| PREDICTED: uncharacterized aarF domain-containing protein kinase 4 [Loxodonta africana]
gi|471418854|ref|XP_004390922.1| PREDICTED: uncharacterized aarF domain-containing protein kinase 4 [Trichechus manatus latirostris]
gi|586482135|ref|XP_006871583.1| PREDICTED: LOW QUALITY PROTEIN: uncharacterized aarF domain-containing protein kinase 4 [Chrysochloris asiatica]
gi|488534652|ref|XP_004459036.1| PREDICTED: uncharacterized aarF domain-containing protein kinase 4 isoform 1 [Dasypus novemcinctus]
gi|488534658|ref|XP_004459039.1| PREDICTED: uncharacterized aarF domain-containing protein kinase 4 isoform 4 [Dasypus novemcinctus]
gi|488534656|ref|XP_004459038.1| PREDICTED: uncharacterized aarF domain-containing protein kinase 4 isoform 3 [Dasypus novemcinctus]
gi|488534654|ref|XP_004459037.1| PREDICTED: uncharacterized aarF domain-containing protein kinase 4 isoform 2 [Dasypus novemcinctus]
gi|505854734|ref|XP_004620788.1| PREDICTED: uncharacterized aarF domain-containing protein kinase 4 [Sorex araneus]
gi|585714667|ref|XP_006901010.1| PREDICTED: uncharacterized aarF domain-containing protein kinase 4 [Elephantulus edwardii]
gi|291412188|ref|XP_002722364.1| PREDICTED: aarF domain containing kinase 4 [Oryctolagus cuniculus]
gi|504178057|ref|XP_004598133.1| PREDICTED: uncharacterized aarF domain-containing protein kinase 4 [Ochotona princeps]
gi|507680869|ref|XP_004710559.1| PREDICTED: LOW QUALITY PROTEIN: uncharacterized aarF domain-containing protein kinase 4 [Echinops telfairi]
gi|126329345|ref|XP_001371518.1| PREDICTED: uncharacterized aarF domain-containing protein kinase 4 [Monodelphis domestica]
gi|149517884|ref|XP_001517948.1| PREDICTED: uncharacterized aarF domain-containing protein kinase 4, partial [Ornithorhynchus anatinus]
gi|564259209|ref|XP_006268530.1| PREDICTED: uncharacterized aarF domain-containing protein kinase 4 [Alligator mississippiensis]
gi|47224869|emb|CAG06439.1| unnamed protein product [Tetraodon nigroviridis]
gi|410931113|ref|XP_003978940.1| PREDICTED: chaperone activity of bc1 complex-like, mitochondrial-like [Takifugu rubripes]
gi|499024141|ref|XP_004562829.1| PREDICTED: uncharacterized aarF domain-containing protein kinase 4-like isoform X1 [Maylandia zebra]
gi|499024143|ref|XP_004562830.1| PREDICTED: uncharacterized aarF domain-containing protein kinase 4-like isoform X2 [Maylandia zebra]
gi|554832150|ref|XP_005926629.1| PREDICTED: uncharacterized aarF domain-containing protein kinase 4-like isoform X1 [Haplochromis burtoni]

gi|554832152|ref|XP_005926630.1| PREDICTED: uncharacterized aarF domain-containing protein kinase 4-like isoform X2 [Haplochromis burtoni]
gi|542231740|ref|XP_005454356.1| PREDICTED: chaperone activity of bc1 complex-like, mitochondrial-like isoform X1 [Oreochromis niloticus]
gi|542231744|ref|XP_005454358.1| PREDICTED: chaperone activity of bc1 complex-like, mitochondrial-like isoform X3 [Oreochromis niloticus]
gi|542231742|ref|XP_005454357.1| PREDICTED: chaperone activity of bc1 complex-like, mitochondrial-like isoform X2 [Oreochromis niloticus]
gi|551506177|ref|XP_005804621.1| PREDICTED: chaperone activity of bc1 complex-like, mitochondrial-like [Xiphophorus maculatus]
gi|432891020|ref|XP_004075509.1| PREDICTED: chaperone activity of bc1 complex-like, mitochondrial-like [Oryzias latipes]
gi|125845977|ref|XP_001336310.1| PREDICTED: aarF domain containing kinase 3 [Danio rerio]
gi|573878944|ref|XP_006627695.1| PREDICTED: uncharacterized aarF domain-containing protein kinase 4-like [Lepisosteus oculatus]
gi|301618935|ref|XP_002938863.1| PREDICTED: uncharacterized aarF domain-containing protein kinase 4 isoform X1 [Xenopus (Silurana) tropicalis]
gi|512861086|ref|XP_004917145.1| PREDICTED: uncharacterized aarF domain-containing protein kinase 4 isoform X2 [Xenopus (Silurana) tropicalis]
gi|148237982|ref|NP_001087459.1| aarF domain containing kinase 4 [Xenopus laevis]
gi|327276355|ref|XP_003222935.1| PREDICTED: uncharacterized aarF domain-containing protein kinase 4-like [Anolis carolinensis]
gi|260803936|ref|XP_002596845.1| hypothetical protein BRAFLDRAFT_237511 [Branchiostoma floridae]
gi|390340728|ref|XP_791783.2| PREDICTED: chaperone activity of bc1 complex-like, mitochondrial-like [Strongylocentrotus purpuratus]
gi|443693751|gb|ELT95038.1| hypothetical protein CAPTEDRAFT_4776 [Capitella teleta]
gi|555698322|gb|ESO01555.1| hypothetical protein HELRODRAFT_185687 [Helobdella robusta]
gi|198433434|ref|XP_002126787.1| PREDICTED: Chaperone, ABC1 activity of bc1 complex like (S. pombe)-like [Ciona intestinalis]
gi|70984246|ref|XP_747640.1| molecular chaperone (ABC1) [Aspergillus fumigatus Af293]
gi|159122426|gb|EDP47547.1| molecular chaperone (ABC1), putative [Aspergillus fumigatus A1163]
gi|119467674|ref|XP_001257643.1| molecular chaperone (ABC1), putative [Neosartorya fischeri NRRL 181]
gi|121703680|ref|XP_001270104.1| molecular chaperone (ABC1), putative [Aspergillus clavatus NRRL 1]
gi|83771723|dbj|BAE61853.1| unnamed protein product [Aspergillus oryzae RIB40]
gi|317148885|ref|XP_001822986.2| molecular chaperone (ABC1) [Aspergillus oryzae RIB40]
gi|391872361|gb|EIT81488.1| ABC (ATP binding cassette) 1 protein [Aspergillus oryzae 3.042]
gi|115386302|ref|XP_001209692.1| protein ABC1, mitochondrial precursor [Aspergillus terreus NIH2624]
gi|134082149|emb|CAK42263.1| unnamed protein product [Aspergillus niger]
gi|317035315|ref|XP_001396633.2| molecular chaperone (ABC1) [Aspergillus niger CBS 513.88]
gi|350636116|gb|EHA24476.1| hypothetical protein ASPNIDRAFT_210041 [Aspergillus niger ATCC 1015]
gi|358369687|dbj|GAA86301.1| molecular chaperone [Aspergillus kawachii IFO 4308]
gi|255945845|ref|XP_002563690.1| Pc20g12040 [Penicillium chrysogenum Wisconsin 54-1255]
gi|584407182|emb|CDM37491.1| Protein kinase-like domain [Penicillium roqueforti]
gi|425773941|gb|EKV12266.1| Molecular chaperone (ABC1), putative [Penicillium digitatum PHI26]
gi|525582383|gb|EPS28633.1| hypothetical protein PDE_03579 [Penicillium oxalicum 114-2]
gi|557729936|dbj|GAD91447.1| molecular chaperone (ABC1), putative [Byssochlamys spectabilis No. 5]
gi|67540804|ref|XP_664176.1| hypothetical protein AN6572.2 [Aspergillus nidulans FGSC A4]
gi|212546311|ref|XP_002153309.1| molecular chaperone (ABC1), putative [Talaromyces marneffei ATCC 18224]
gi|242823783|ref|XP_002488129.1| molecular chaperone (ABC1), putative [Talaromyces stipitatus ATCC 10500]
gi|303322252|ref|XP_003071119.1| ABC1 family protein [Coccidioides posadasii C735 delta SOWgp]
gi|320034974|gb|EFW16916.1| hypothetical protein CPSG_06184 [Coccidioides posadasii str. Silveira]
gi|119196625|ref|XP_001248916.1| hypothetical protein CIMG_02687 [Coccidioides immitis RS]
gi|258569513|ref|XP_002543560.1| ABC1 [Uncinocarpus reesii 1704]
gi|296810398|ref|XP_002845537.1| ABC1 [Arthroderma otae CBS 113480]
gi|225554743|gb|EEH03038.1| ABC1 protein [Ajellomyces capsulatus G186AR]
gi|325095075|gb|EGC48385.1| molecular chaperone [Ajellomyces capsulatus H88]
gi|240276886|gb|EER40397.1| molecular chaperone [Ajellomyces capsulatus H143]
gi|154272561|ref|XP_001537133.1| hypothetical protein HCAG_08242 [Ajellomyces capsulatus NAm1]
gi|239613160|gb|EEQ90147.1| molecular chaperone [Ajellomyces dermatitidis ER-3]
gi|327354767|gb|EGE83624.1| molecular chaperone [Ajellomyces dermatitidis ATCC 18188]
gi|261190961|ref|XP_002621889.1| molecular chaperone [Ajellomyces dermatitidis SLH14081]
gi|531984034|gb|EQL34621.1| Atypical/ABC1/ABC1-A protein kinase [Ajellomyces dermatitidis ATCC 26199]
gi|225678532|gb|EEH16816.1| ubiquinone biosynthesis protein coq-8 [Paracoccidioides brasiliensis Pb03]
gi|295668939|ref|XP_002795018.1| molecular chaperone (ABC1) [Paracoccidioides sp. 'lutzii' Pb01]
gi|226294759|gb|EEH50179.1| molecular chaperone (ABC1) [Paracoccidioides brasiliensis Pb18]
gi|378728060|gb|EHY54519.1| aarF domain-containing kinase [Exophiala dermatitidis NIH/UT8656]
gi|565939386|gb|ETI28492.1| hypothetical protein G647_00941 [Cladophialophora carrionii CBS 160.54]
gi|568122948|gb|ETN45538.1| hypothetical protein HMPREF1541_09370 [Cyphellophora europaea CBS 101466]
gi|189190186|ref|XP_001931432.1| ubiquinone biosynthesis protein coq-8 [Pyrenophora tritici-repentis Pt-1C-BFP]
gi|330935611|ref|XP_003305048.1| hypothetical protein PTT_17791 [Pyrenophora teres f. teres 0-1]
gi|576923973|gb|EUC38086.1| hypothetical protein COCCADRAFT_22435 [Bipolaris zeicola 26-R-13]
gi|578492995|gb|EUN30391.1| hypothetical protein COCVIDRAFT_90496 [Bipolaris victoriae FI3]
gi|451854432|gb|EMD67725.1| hypothetical protein COCSADRAFT_179327 [Bipolaris sorokiniana ND90Pr]
gi|576933723|gb|EUC47246.1| hypothetical protein COCMIDRAFT_90666 [Bipolaris oryzae ATCC 44560]
gi|482812665|gb|EOA89384.1| hypothetical protein SETTUDRAFT_183445 [Setosphaeria turcica Et28A]
gi|526193171|gb|EPS35371.1| hypothetical protein H072_11228 [Dactylellina haptotyla CBS 200.50]
gi|549049527|emb|CCX11368.1| Similar to Protein ABC1 homolog, mitochondrial; acc. no. Q92338 [Pyronema omphalodes CBS 100304]
gi|85101761|ref|XP_961212.1| hypothetical protein NCU03823 [Neurospora crassa OR74A]
gi|336472939|gb|EGO61099.1| hypothetical protein NEUTE1DRAFT_76825 [Neurospora tetrasperma FGSC 2508]

gi|576046376|ref|XP_006697061.1| hypothetical protein CTHT_0067700 [Chaetomium thermophilum var. thermophilum DSM 1495]
gi|475667257|gb|EMT65046.1| Protein ABC1 like protein, mitochondrial [Fusarium oxysporum f. sp. cubense race 4]
gi|517313371|emb|CCT65584.1| probable abc1 protein precursor [Fusarium fujikuroi IMI 58289]
gi|500252321|gb|EON96167.1| putative abc1 family protein [Togninia minima UCRPA7]
gi|573057179|gb|ETS77054.1| hypothetical protein PFICI_10928 [Pestalotiopsis fici W106-1]
gi|346974573|gb|EGY18025.1| ABC1 protein [Verticillium dahliae VdLs.17]
gi|353244349|emb|CCA75757.1| related to ABC1-ubiquinol--cytochrome-c reductase complex assembly protein [Piriformospora indica DSM 11827]
gi|540383897|gb|AFR95375.2| Atypical/ABC1/ABC1-A protein kinase [Cryptococcus neoformans var. grubii H99]
gi|384494254|gb|EIE84745.1| hypothetical protein RO3G_09455 [Rhizopus delemar RA 99-880]
gi|511009067|gb|EPB90317.1| Atypical/ABC1/ABC1-A protein kinase [Mucor circinelloides f. circinelloides 1006PhL]
gi|3087737|emb|CAA04557.1| ABC1 protein [Arabidopsis thaliana]
gi|15234260|ref|NP_192075.1| ABC transporter 1 [Arabidopsis thaliana]
gi|297814165|ref|XP_002874966.1| ABC1 protein [Arabidopsis lyrata subsp. lyrata]
gi|565458552|ref|XP_006287275.1| hypothetical protein CARUB_v10000471mg [Capsella rubella]
gi|567161086|ref|XP_006396362.1| hypothetical protein EUTSA_v10028510mg [Eutrema salsugineum]
gi|225437742|ref|XP_002273486.1| PREDICTED: chaperone activity of bc1 complex-like, mitochondrial [Vitis vinifera]
gi|508703589|gb|EOX95485.1| Ubiquinone biosynthesis protein coq-8 [Theobroma cacao]
gi|462418300|gb|EMJ22749.1| hypothetical protein PRUPE_ppa002977mg [Prunus persica]
gi|255548205|ref|XP_002515159.1| Ubiquinone biosynthesis protein coq-8, putative [Ricinus communis]
gi|567904304|ref|XP_006444640.1| hypothetical protein CICLE_v10019335mg [Citrus clementina]
gi|356501819|ref|XP_003519721.1| PREDICTED: uncharacterized aarF domain-containing protein kinase 4-like isoform X1 [Glycine max]
gi|356533503|ref|XP_003535303.1| PREDICTED: chaperone activity of bc1 complex-like, mitochondrial-like isoform X1 [Glycine max]
gi|561018272|gb|ESW17076.1| hypothetical protein PHAVU_007G208100g [Phaseolus vulgaris]
gi|502117517|ref|XP_004495848.1| PREDICTED: chaperone activity of bc1 complex-like, mitochondrial-like [Cicer arietinum]
gi|449449246|ref|XP_004142376.1| PREDICTED: chaperone activity of bc1 complex-like, mitochondrial-like [Cucumis sativus]
gi|449487112|ref|XP_004157500.1| PREDICTED: chaperone activity of bc1 complex-like, mitochondrial-like [Cucumis sativus]
gi|527203960|gb|EPS70264.1| hypothetical protein M569_04492, partial [Genlisea aurea]
gi|460366560|ref|XP_004229149.1| PREDICTED: chaperone activity of bc1 complex-like, mitochondrial-like [Solanum lycopersicum]
gi|586684890|ref|XP_006841526.1| hypothetical protein AMTR_s00003p00150920 [Amborella trichopoda]
gi|242052821|ref|XP_002455556.1| hypothetical protein SORBIDRAFT_03g013060 [Sorghum bicolor]
gi|514777156|ref|XP_004968647.1| PREDICTED: chaperone activity of bc1 complex-like, mitochondrial-like [Setaria italica]
gi|302783410|ref|XP_002973478.1| hypothetical protein SELMODRAFT_99295 [Selaginella moellendorffii]
gi|302809972|ref|XP_002986678.1| hypothetical protein SELMODRAFT_42234 [Selaginella moellendorffii]
gi|159489070|ref|XP_001702520.1| ubiquinone biosynthesis protein [Chlamydomonas reinhardtii]
gi|545376077|ref|XP_005652152.1| ubiquinone biosynthesis protein, partial [Coccomyxa subellipsoidea C-169]
gi|299116986|emb|CBN75090.1| Protein required for ubiquinone (coenzyme Q) biosynthesis and for respiratory growth [Ectocarpus siliculosus]
gi|530737183|gb|EQC35425.1| aarF domain-containing kinase [Saprolegnia diclina VS20]

Supplementary References

Altschul, S.F. et al., 1997. Gapped BLAST and PSI-BLAST: a new generation of protein database search programs. *Nucleic acids research*, 25(17), pp.3389–3402.

Crooks, G.E. et al., 2004. WebLogo: a sequence logo generator. *Genome Research*, 14(6), pp.1188–1190.

Goujon, M. et al., 2010. A new bioinformatics analysis tools framework at EMBL-EBI. *Nucleic Acids Research*, 38(Web Server issue), pp.W695–699.

Mueller, B.K., Subramaniam, S. & Senes, A., 2014. A frequent, GxxxG-mediated, transmembrane association motif is optimized for the formation of interhelical Cα-H hydrogen bonds. *Proceedings of the National Academy of Sciences of the United States of America*, 111(10), pp.E888–895.

CHAPTER SIX

CONCLUSIONS

In our lab we are interested in understanding the biophysical and structural properties of integral membrane proteins and their interactions. Membrane proteins are overrepresented in the human genome and make up a considerable percentage of the current drug targets, but are still underrepresented in the structural database of proteins. In order to study these proteins, it is important to be able to achieve stable sample conditions that mimic their natural environment, the membrane bilayer. Biological membranes are made up of a complex variety of lipids, proteins and carbohydrates, which form dynamic structures enabling interactions between the macromolecules that are important to the membrane's functions. Since replicating the composition of the diverse bilayer environment is difficult, obtaining high resolution structural information for membrane proteins with traditional methods such as NMR and X-ray crystallography is still challenging. Thus, we employ a combination of biophysical, and biochemical techniques in combination with computational modeling to obtain information on these proteins. In particular, we focus on single-pass membrane proteins, or those that have a single transmembrane domain. Study of this structural class of membrane proteins not only serves as a tractable system to investigate, but also sheds light on the physical components of transmembrane helix-helix association.

One of the biological systems we are investigating is that of cell division in bacteria – one of the most fundamental and complex process of its survival. The process of cell division involves mechanisms responsible for constriction of the cell membrane, induction of membrane fusion, remodeling of the cell envelope, and synthesis of the new cell wall. All these events are known to be enabled by the bacterial divisome, a complex of membrane proteins that are localized to the cell septum at the time of cell division. The divisome proteins

have been identified and extensively analyzed *in vivo*, but not much is known about the structural organization of the membrane components of this complex. To embark on this investigation, we began by looking at two single-pass membrane proteins of the divisome, FtsB and FtsL, which are essential for cell division and have been shown to form a complex. We divided the proteins into their transmembrane and periplasmic components to understand the contributions of these domains to the stability of the complex. For most of my graduate work, I focused on the interactions between the transmembrane regions of these proteins.

The technique that I primarily used for this investigation is FRET. FRET enables a measure of the interaction strengths between two molecules by labeling the molecules with fluorophores that form a FRET pair. FRET can be used both in vitro and in vivo. While *in vivo* experiments allow analysis of the proteins in their native environment, *in vitro* experiments allow more control over the concentrations of samples used, enabling more accurate biophysical analyses of the interactions. For my work, I used FRET *in vitro* to study the FtsB-FtsL complex. Use of this technique for membrane proteins involves synthesis of the proteins, labeling them with fluorophores, purifying them using analytical separation techniques such as HPLC, quantifying the protein stocks accurately, resuspending them in artificial lipid bilayers and measuring their FRET spectra. Synthesizing these proteins can be done using overexpression in bacteria or chemical synthesis, but since the transmembrane regions of these proteins are usually hydrophobic and often prove toxic to bacteria, I used solid phase peptide synthesis to obtain the peptides. Working with these 'difficult peptides' required extensive optimization in each of the steps mentioned above, which I have documented in Chapter 2.

Using FRET I demonstrated that the FtsB transmembrane domain self-associates, and

that FtsB and FtsL form a higher order complex in artificial lipid bilayers. I also showed that the FtsB-FtsL complex is made up of a 1:1 stoichiometry of the two proteins, which indicates the formation of a tetramer or a higher oligomeric complex. This work is detailed in Chapter 3. Future work on the investigation of the exact number of FtsB and FtsL subunits is ongoing using analytical ultracentrifugation and single molecule fluorescence microscopy, which I have described in Chapter 4. Along with the biophysical investigation of the transmembrane regions of these proteins, simultaneous work on the periplasmic regions is also ongoing in our lab. A first structural report of the periplasmic region of FtsB is reported in Appendix I, which shows that it forms a coiled coil dimer when fused to Gp7, a soluble globular protein from bacteriophage Φ29 that nucleates the helix and stabilizes the coiled coil. Moreover, *in vivo* experiments with mutants of FtsB and FtsL are being tested for their effect on cell-division in wild-type knock-out strains. Together, all this work on FtsB and FtsL serves as the first structural investigation of the membrane region of the protein complex that enables cell-division in bacteria.

Another aspect of studying single-pass membrane proteins is that it enables studying the nature of interactions between transmembrane helices. To do this our lab utilizes a strategy based on analyzing frequently occurring interaction motifs in transmembrane helices. Using this strategy, my colleagues developed a computational program based on the simultaneous optimization of Cα-H hydrogen bonding between the backbone atoms and side chain packing. This program called CATM was tested against known structures of transmembrane dimers and showed near atomic precision in predicting their structures. CATM was then used to predict the homo-dimeric structure of ADCK3, a human mitochondrial kinase important for coenzyme Q biosynthesis, which is predicted to have a functionally

important transmembrane region. Using a genetic screening assay, TOXCAT, which measures the relative strength of TM helix self association in bacterial membrane, I experimentally performed large scale mutagenesis on the ADCK3 TM domain, and found that the interaction interface obtained matches with the structural prediction of the protein dimer by CATM. This report served as a first experimental validation of the CATM program in addition to shedding light on the interaction motifs of the ADCK3 transmembrane region, and is detailed in Chapter 5.

On the whole, this PhD thesis showcases how *in vitro*, *in vivo* and *in silico* methods can be used in tandem to study membrane proteins, an important class of proteins that are difficult to study experimentally. Moreover, the use of FRET as a very useful technique to study membrane protein interactions has been highlighted not just in its utility in my work, but also in the membrane protein research community, as reviewed in Chapter 1. My hope is that the documentation of this work helps researchers in the field in different ways; ranging from understanding the intricacies of using FRET to study membrane proteins, to gaining perspective about the wide applicability of different approaches in tandem, toward understanding the organization of these difficult-to-study but biologically important class of proteins.

APPENDIX I

Structural organization of FtsB, a transmembrane protein of the bacterial divisome

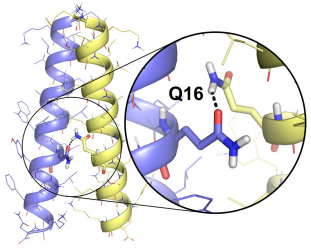

Based on:

LaPointe L.M., Taylor, K.C., Subramaniam S., Khadria A, Rayment I and Senes A, 2013. Structural organization of FtsB, a transmembrane protein of the bacterial divisome. *Biochemistry*, 52(15), pp.2574–2585.

Abbreviations:

TM: transmembrane

Abstract

We report the first structural analysis of an integral membrane protein of the bacterial divisome. FtsB is a single-pass membrane protein with a periplasmic coiled coil. Its heterologous association with its partner FtsL represents an essential event for the recruitment of the late components to the division site. Using a combination of mutagenesis, computational modeling and X-ray crystallography, we determined that FtsB self-associates and we investigated its structural organization. We found that the transmembrane domain of FtsB homo-oligomerizes through an evolutionarily conserved interaction interface where a polar residue (Gln 16) plays a critical role through the formation of an inter-helical hydrogen bond. The crystal structure of the periplasmic domain, solved as a fusion with Gp7, shows that 30 juxta-membrane amino acids of FtsB form a canonical coiled coil. The presence of conserved Gly residue in the linker region suggests that flexibility between the transmembrane and coiled coil domains is functionally important. We hypothesize that the transmembrane helices of FtsB form a stable dimeric core for its association with FtsL into a higher-order oligomer, and that FtsL is required to stabilize the periplasmic domain of FtsB, leading to the formation of a complex that is competent for binding to FtsQ, and to their consequent recruitment to the divisome. The study provides an experimentally validated structural model and identifies point mutations that disrupt association, thereby establishing important groundwork for the functional characterization of FtsB *in vivo*.

Cell division is one of the most fundamental processes in the life of bacteria. In gram-negative, bacteria division requires a complex and coordinated remodeling of the three-layer cell envelope, and therefore mechanisms must exist to sort the duplicated chromosome, to provide constrictive force, to synthesize the septal cell wall and, finally, to induce membrane fusion. These events are enabled by a multi-protein complex called the divisome. The assembly of the divisome begins with the formation of a ring-like structure at the site of division (the Z-ring), where the polymeric FtsZ likely provides constrictive force and forms a scaffold for the recruitment of the complex(Adams & Errington 2009; Mingorance et al. 2010; Erickson et al. 2010). In *Escherichia coli* the recruitment of the essential proteins follows a strikingly linear hierarchy, illustrated in **Figure 1a**(Goehring & Beckwith 2005). The cytoplasmic side of the ring is formed by the early components: FtsA, a membrane-associated actin family member that forms protofilaments(Szwedziak et al. 2012; Shiomi & Margolin 2007); ZipA, a single-pass membrane protein that contributes to FtsZ tethering along with FtsA(Hale et al. 2000; Liu et al. 1999); and FtsK, a DNA translocase that is essential for unlinking chromosome dimers after homologous recombination(Sherratt et al. 2010). In contrast, the late proteins perform functions related to the reconstruction of the cell-wall: FtsW is a transporter of cell-wall precursors across the membrane(Mohammadi et al. 2011; Fraipont et al. 2011); FtsI is important for the cross-linking of the cell wall during division(Nguyen-Distèche et al. 1998); and FtsN is necessary for the recruitment of non-essential septal components, the murein hydrolase AmiC(Bernhardt & de Boer 2003; Heidrich et al. 2001), and the Tol-Pal complex required for proper invagination during constriction(Gerding et al. 2007).

The early and late components of the divisome are linked by a trio of single pass transmembrane (TM) proteins: FtsQ, FtsB, and FtsL. The ability of FtsB and FtsL to recruit the late divisome elements suggests that they have a structural role as a scaffold in the assembly of the divisome(Gonzalez & Beckwith 2009), and it has been proposed that they are involved in Z-ring stabilization(Geissler & Margolin 2005). FtsB and FtsL may also be involved in a regulatory checkpoint of division because the depletion of FtsB from *E. coli* cells results in the disappearance of FtsL(Buddelmeijer et al. 2002). The cellular instability of FtsL was also observed in *B. subtilis(Daniel et al. 1998; Daniel & Errington 2000; Daniel et al. 2006)*, where $FtsL_B$ is rapidly degraded by the intramembrane protease RasP unless it is

stabilized by its interaction with the FtsB homologue (DivIC)(Bramkamp et al. 2006). These observations led to an unconfirmed hypothesis that active proteolysis of FtsL may be a regulatory factor in the timing of bacterial cell division(Wadenpohl & Bramkamp 2010).

While the precise function of FtsB and FtsL is not well understood, substantial evidence indicates that they physically interact with each other. As highlighted in **Figure 1a**, FtsB and FtsL are mutually dependent for their recruitment at the division site, and both proteins depend on the localization of FtsQ(Buddelmeijer et al. 2002; Ghigo et al. 1999). A similar picture has been reported in *Bacillus subtilis*, where the localization of the homologues of $FtsL_B$ and DivIC depends on the FtsQ homologue (DivIB) at the temperature at which DivIB is essential(Daniel & Errington 2000; Katis et al. 2000). There is strong evidence that FtsB and FtsL form a stable sub-complex *in vivo.* A complex comprising FtsB, FtsL, and FtsQ was isolated from *E. coli* by co-immunoprecipitation(Buddelmeijer & Beckwith 2004). The physical interaction of the *E. coli* and *B. subtilis* proteins was also confirmed by two-hybrid analysis(Daniel et al. 2006; Karimova et al. 2005; Robichon et al. 2011). Further evidence of a stable interaction between FtsB and FtsL was obtained with a series of artificial septal targeting experiments(Goehring et al. 2005; Goehring et al. 2006; Robichon et al. 2008; Rowland et al. 2010; Gonzalez & Beckwith 2009; Gonzalez et al. 2010) that demonstrated that FtsL and FtsB interact with each other and can recruit the downstream proteins even when FtsQ has been depleted from the cell(Goehring et al. 2006). Moreover, the *B. subtilis* homologues $FtsL_B$ and DivIC form a complex when co-expressed in *E. coli* despite the fact that they are unlikely to interact with the significantly divergent *E. coli* division proteins(Robichon et al. 2008).

The domain organization of FtsB and FtsL **(Figure 1b)** suggests that they may interact through an extended helical structure encompassing the membrane and periplasmic regions. Both proteins contain a TM domain and a juxta-membrane coiled coil, in addition to a small (FtsL) or minimimal (FtsB) cytoplasimic N-terminal tail. The TM and coiled coil regions of FtsB are necessary and sufficient for its interaction with FtsL(Gonzalez & Beckwith 2009), and similarly, the TM and coiled coil regions of FtsL are both essential for its interaction with FtsB(Buddelmeijer & Beckwith 2004). A low resolution model of the soluble domains of the *Streptococcus pneumoniae* homologues of FtsB, FtsL and FtsQ was proposed by Masson et al.(Masson et al. 2009), based on a combination of NMR, small angle neutron and X-ray

scattering, and surface plasmon resonance. In this study the TM domains were truncated and replaced by a soluble coiled coil pair(Masson et al. 2009; Noirclerc-Savoye et al. 2005). More recently, a bioinformatic analysis of the soluble domains of FtsB, FtsL and FtsQ suggested two alternative models with 1:1:1 or 2:2:2 oligomeric stoichiometries(Villanelo et al. 2011). However, no structural information was available regarding the organization of the important TM region.

In an effort toward understanding the structural organization and precise oligomeric state of the FtsB-FtsL complex, we investigated the self-association propensities of both TM and soluble regions of the two individual proteins. We hypothesized that if the FtsB-FtsL complex is larger than a dimer, one or both proteins could potentially self-associate and be studied in isolation. Indeed, we found that FtsB homo-oligomerizes. Here we present a structural analysis obtained with a combination of extensive mutagenesis, computational modeling and X-ray crystallography. The results provide a theoretical scaffold for the biophysical characterization of the FtsB-FtsL heterologous complex, and offer several structure-based hypotheses that can be tested in the context of cell division by functional studies *in vivo*.

Materials and Methods

Vectors and strains

All oligonucleotides were purchased in desalted form from Integrated DNA Technologies and used without purification. The expression vectors pccKAN, pccGpA-wt, and pccGpA-G83I, and *malE* deficient *Escherichia coli* strain MM39 were kindly provided by Dr. Donald M. Engelman(Russ & Engelman 1999). Genes encoding the TM domains of FtsB and FtsL were cloned into the NheI-BamHI restriction sites of the pccKAN vector resulting in the following protein sequences: FtsB "...NRASLALTLLLLAILVWLQYSLWFGILIN..."; FtsL "...NRASFGKLPLCLFICIILTAVTVVTTAGILIN...". All mutagenesis was done with the QuikChange kit (Stratagene).

The periplasmic segment of FtsB was obtained from the *E. coli* genome (K12 strain) by PCR using PfuUltra II Fusion DNA polymerases (Stratagene), and cloned into a pET31b vector containing the fusion protein Gp7, using a modified QuikChange protocol that includes the use of PfuUltra II Fusion DNA polymerase, 1 min annealing time, 2 min/kb extension time at 65 ˚C, 50 ng of template and 100–150 ng of the first round PCR product, in the presence of 4% DMSO(Chen et al. 2000). All constructs generated throughout the studies were sequence-verified over the entire ORF insert and at least 50 bp upstream and downstream of the ORF. The resulting plasmids containing Gp7-FtsB fusions were transformed into BL21-DE3 cells for overexpression and further analyses.

Expression of Chimeric Proteins in MM39 cells and MalE complementation assay

The TOXCAT constructs were transformed into MM39 cells. A freshly streaked colony was inoculated into 3 mL of LB broth containing 100 μg/mL ampicillin and grown overnight at 37 ˚C. Overnight cultures were inoculated into 3 mL of LB broth at a ratio of 1:1000 and grown to an OD_{420} of approximately 1 (OD_{600} of 0.6) at 37 ˚C. After recording the optical density, 1 mL of cells was spun down for 10 min at 17000*g* and resuspended in 500 mL of sonication buffer (25 mM Tris-HCl, 2 mM EDTA, pH 8.0). Cells were lysed by probe sonication at medium power for 10 seconds over ice, and an aliquot of 50 μL was removed from each sample and stored in SDS-PAGE loading buffer for immunoblotting. The lysates were then cleared by centrifugation and the supernatant was kept on ice for chloramphenicol acetyltransferase (CAT) activity assay. To confirm for proper membrane insertion of the TOXCAT constructs,

overnight cultures were plated on M9 minimal medium plates containing 0.4% maltose as the only carbon source and grown at 37 ˚C for 48 hours(Russ & Engelman 1999). The variants that did not grow in these conditions were not considered in the study.

Chloramphenicol Acetyltransferase (CAT) spectrophotometric assay

CAT activity was measured as described(Shaw 1975; Sulistijo & Mackenzie 2009). 1 mL of buffer containing 0.1 mM acetyl coA, 0.4 mg/mL 5,5'-dithiobis-(2-nitrobenzoic acid), and 0.1 M Tris-HCl pH 7.8 was mixed with 40 µL of cleared cell lysates and the absorbance at 412 nm was measured for two minutes to establish basal activity rate. After addition of 40 µL of 2.5 mM chloramphenicol in 10% ethanol, the absorbance was measured for an additional two minutes to determine CAT activity. The basal CAT activity was subtracted and the value was normalized by the cell density measured as OD_{420}. All measurements were determined at least in duplicate and the experiments were repeated at least twice.

Quantification of expression by immunoblotting

Protein expression was confirmed by immunoblotting. The cell lysates (10 µL) were loaded onto a NuPAGE 4-12% Bis-Tris SDS-PAGE gel (Invitrogen) and then transferred to PVDF membranes (VWR) for 1 hour at 100 millivolts. Blots were blocked using 5% Bovine serum albumin (US Biologicals) in TBS-Tween buffer (50 mM Tris, 150 mM NaCl, 0.05% Tween 20) for two hours at 4 ˚C, incubated with biotinylated anti-Maltose Binding Protein antibodies (Vector labs), followed by peroxidase-conjugated streptavidin (Jackson ImmunoResearch). Blots were developed with the Pierce ECL Western Blotting Substrate Kit and chemiluminescence was measured using an ImageQuant LAS 4000 (GE Healthsciences).

Expression of chimeric proteins in BL21-DE3 cells for E. coli overexpression and Ni-NTA purification

The Gp7-FtsB chimerae, with an added C-terminal six-His tag preceded by the recognition site for TEV protease, were expressed in *E. coli* BL21-DE3 cells using a modified pET31b vector. A single colony was grown at 37 ˚C in 50 mL overnight and then inoculated into 4L of LB broth. Cells were grown to an OD_{600} of 0.8-1.0 before addition of 1 mM IPTG to induce over-expression which was carried out for 18 hours at 18 ˚C. The cell pellets were washed and stored at -80 ˚C until purification. All Gp7 fusion proteins were purified using an identical protocol. Typically, 8-12 g of frozen cell pellets were mixed with 10 mL lysis buffer (50 mM

NaCl, 5 mM β-mercaptoethanol, 0.5 mg/mL lysozyme, 50 mM HEPES pH 8.0, 1 mM phenylmethylsulfonyl fluoride) per gram of cell pellet and lysed by sonication. Lysates were cleared using centrifugation at 45000*g* for 30 min (JA 25.5 rotor). Cleared lysates were loaded onto 5 mL of Ni-NTA resin, washed extensively with Buffer A (300 mM NaCl, 1 mM β-mercaptoethanol, 20 mM imidazole, 25 mM HEPES, pH 8.0), and eluted with Buffer B (same as Buffer A, but with 300 mM imidazole). The eluted fractions were mixed with TEV protease at a molar ratio of ~1:40 and dialyzed at 4 ˚C overnight against Buffer C (10 mM HEPES, 100 mM NaCl, 0.5 mM TCEP, 0.1 mM EDTA pH 8.0). The TEV protease was prepared as described(Blommel & Fox 2007). The dialysate was repurified on Ni-NTA, this time by collecting fractions that elute during washes with lower imidazole (Buffer A). The pure fractions were pooled and dialyzed against Buffer C again and concentrated to ~10 mg/mL using an Ultracel - 10K (Millipore), clarified by centrifugation at 5000*g* and finally flash frozen as 30 µL droplets in liquid nitrogen and stored at -80 ˚C.

Circular dichroism (CD)

The purified Gp7-FtsB constructs were diluted to 0.2-0.4 mg/mL for CD analysis. CD measurements were carried out on an Aviv 202SF spectropolarimeter. Samples were measured in 1 mM Hepes pH 8, 10 mM NaCl, and 0.1 mM TCEP. The thermostability studies were performed under the same buffer conditions with a temperature ramp of 3 ˚C/min, and the ellipticity was monitored at 222 nm and 208 nm.

Crystallization of Gp7-FstB

Gp7-FtsB was screened for initial crystallization conditions by vapor diffusion at 20 ˚C with a 144-condition sparse matrix screen developed in the Rayment laboratory. Crystals of Gp7-FtsB were grown by vapor diffusion at 20 ˚C from a 1:1 (v/v) mixture of protein at 10 mg/mL with 100 mM Bis-Tris, 5 mM gamma-caprolactone, 2.1 M ammonium sulfate, 0.6 M malonate, 5% glycerol, pH 6.5. After one day hexagonal crystals measuring 0.1 x 0.1 x 0.5 mm were observed. The crystals were soaked in mother liquor for 24 hours subsequent to flash freezing in liquid nitrogen. Gp7-FtsB crystallized in the space group $P6_1$ with unit cell dimensions of a = 87.6 Å, b = 87.6 Å, and c = 185.1 Å where two Gp7-FtsB dimers were present in the asymmetric unit.

Data collection and structure determination for Gp7-FtsB

X-ray data for Gp7-FtsB were collected at 100 K on the Structural Biology Center beam line 19ID at the Advanced Photon Source in Argonne, IL. Diffraction data were integrated and scaled with HKL3000(Otwinowski & Minor 1997). A molecular replacement solution was obtained using residues 2 – 48 of Gp7 (PDB entry 1NO4)(Morais et al. 2003) as a search model in the program Molrep(Vagin & Teplyakov 2000). The electron density was improved with the program Parrot and the initial model was built using Buccaneer(Cowtan 2008; Cowtan 2010). Final Models were generated with alternate cycles of manual model building and least-squares refinements using the programs Coot(Emsley & Cowtan 2004) and Refmac(Murshudov et al. 1999).

Computational modeling

The TM oligomer of FtsB was modeled with programs written in house and distributed with the MSL molecular modeling libraries v. 1.1(Kulp et al. 2012), available at at http://msl-libraries.org. This was performed on helices in which all amino acids were converted to Ala except Gln 16, Tyr 17 and Ser 18. The *predictHelixOligomer* program creates standard helices and performs a global rigid search altering the inter-helical separation, the crossing angle, the crossing point and the axial orientation of the helices. To impose the formation of an inter-helical hydrogen bond involving Gln 16, the conformational space was pre-screened prior to the analysis to exclude the region of space that were incompatible with the program *filterOligomerByConstraint*. The backbone was kept rigid during the procedure while the side chains were optimized using a greedy trials method implemented in MSL(Xiang & Honig 2001; Kulp et al. 2012). Side chain mobility was modeled using the Energy-Based conformer library applied at the 90% level(Subramaniam & Senes 2012). The models were evaluated using a van der Waals function with CHARMM 22 parameters and the SCWRL hydrogen bond function implemented in MSL. The models were sorted by their energies. All low-energy models were visually inspected to verify that they did not include poorly packed solutions containing cavities. The computational mutagenesis was performed on all low-energy models by applying the same mutation studied experimentally in the context of a fixed backbone, followed by side chain optimization. The relative energy of each mutant was calculated as

$$\Delta E_{mut} = (E_{mut,dimer} - E_{mut,monomer}) - (E_{WT,dimer} - E_{WT,monomer})$$

where $E_{WT,dimer}$ and $E_{mut,dimer}$ are the energies of the wild type and mutant sequence in the dimeric state, and $E_{WT,monomer}$ and $E_{mut,monomer}$ are the energies of the wild type and mutant sequence in a side chain optimized monomeric state with the same sequence. The effect of each mutation was classified in four categories analogously to the experimental mutagenesis using the following criterion: category 0, "WT-like", $\Delta E_{mut} < 2$ kcal/mol; category 1, "Mild", $2 \leq \Delta E_{mut} < 4$; category 2, "Severe", $4 \leq \Delta E_{mut} < 8$; category 3, "Disruptive", $\Delta E_{mut} \geq 8$. The numerical category values were averaged to calculate the position dependent average disruption value reported in **Figure 5**.

Creation of TM + coiled coil model

The computational model of the TM domain and the coiled coil region were connected together using fragments from the PDB database. To do this, protein fragments of the pattern *hhx*G*xx*G*xhh* (where *x* is any amino acid, and *h* is any amino acid in a helical conformation) were extracted from high resolution X-ray structures deposited in the PDB database with a resolution of 2 Å or better. The MSL program *connectWithFragments* takes these fragments and aligns the helical end residues with the corresponding residues in the coiled coil domain and then the modeled TM domain. Only the N, C, CA and O atoms were considered for the alignment and the fragments with the lowest R.M.S.D. were selected. The side chains on the fragment were replaced with the one corresponding to the FtsB sequence and their conformation was optimized using a greedy trials method.

FtsB sequence alignment and consensus sequence

The alignment was obtained by entering the sequence of E. coli FtsB as the query in BLAST (http://blast.ncbi.nlm.nih.gov) using the blastp algorithm with default settings. The resulting 464 sequences were aligned with the multiple alignment facility in BLAST (COBALT). The prevalent amino acid at each position in the sequence was used to determine a consensus sequence if it was present in at least 30% of the sequences.

Accession numbers

Coordinates and structure factors of Gp7-FtsB have been deposited in the Protein Data Bank with PDB ID code 4IFF.

Results and Discussion

The transmembrane domain of FtsB self-associates

To determine if the TM domains of FtsB and FtsL from *E. coli* self-associate, we analyzed them with TOXCAT, a widely used biological assay for TM association(Russ & Engelman 1999). The assay is based on a chimeric construct in which the TM domain of interest is fused to the ToxR transcriptional activator domain from *Vibrio cholera* **(Figure 2*a*)**. Oligomerization, driven by the TM helices, results in the expression of the reporter gene chloramphenicol acetyltransferase (CAT). The expression level of CAT (measured enzymatically) is compared to that of a stable dimer, Glycophorin A (GpA), as a standard. While TOXCAT is applicable to membrane proteins of any origin (GpA for example is a human protein), it is significant that in the case of FtsB and FtsL the analysis is performed in their native *E. coli* membrane. This fact also raised an initial concern that the TOXCAT constructs could potentially interfere with the cell division process. Fortunately this concern was unfounded as the cells grew and divided normally.

The results of the TOXCAT analysis of FtsB and FtsL are shown in **Figure 2b**. The CAT activity of both constructs is above background, although the association of FtsL appears to be weak (19% of the GpA signal). The activity of FtsB is approximately half of the GpA signal (48%), indicating that the homo-oligomerization of its TM domain is rather stable.

The transmembrane self-association of FtsB is mediated by a critical polar amino acid

To investigate what amino acids are important for the self-association of FtsB and FtsL, we systematically mutated each position and monitored the effects on association. The expectation is that the changes at interfacial positions would perturb oligomerization more than the changes at positions that are lipid exposed, as commonly observed (for example(Adams et al. 1995; Fleming & Engelman 2001a; Jenei et al. 2011; Lemmon et al. 1992; Li et al. 2004)). We applied an initial scanning mutation strategy using both Ala (small) and Ile (large) substitutions, and then expanded the mutagenesis to include a larger variety of hydrophobic amino acids.

Figure 3 shows the TOXCAT data for the 57 single amino acid variants tested for FtsB. All variants displayed similar levels of TOXCAT construct expression, as verified by Western blot analysis (data not shown). While a majority of the variants have a CAT activity level

comparable to the wild type constructs, there are a number of mutations that display drastically reduced activity. Conversely, several constructs with significantly increased activity were also observed. To obtain an estimate of the overall sensitivity of each position, we have applied a simple classification scheme for the variants' phenotypes using four categories (dashed lines in **Figure 3)**, labeled as “WT-like” (>80% of wild type CAT activity), “Mild” (50-80%), “Severe” (20-50%) and “Disruptive” (0-20%). We then averaged the scores to obtain a position specific disruption index. Position-based averaging reduces some of the natural variability of the biological assay and the method has been reliable in identifying the most sensitive positions at the helix-helix binding interface(Sulistijo et al. 2003; Li et al. 2004; Adams et al. 1995). The data is schematically represented in **Figure 4*a***.

When the average disruption is projected on a helical wheel diagram **(Figure 4*b*)** it becomes evident that the sensitive mutations cluster on one helical face defined by positions T5, L6, L8, L9, L12, L15, Q16, L19 and W20. When the average disruption is fit to a sine function to analyze its periodicity **(Figure 4*c*)**, we obtained a value of 3.5 amino acids per turn, which suggests that the helices of the FtsB oligomer interact with a left-handed crossing angle. Interestingly, the variants with enhanced CAT activity (A10, W14, Y17, W20 and F21) are primarily located on the opposite face relative to the disruptive positions. Therefore, it seems unlikely that these variants enhance stability by direct participation to the interaction interface.

We attempted a similar mutagenesis analysis for FtsL. While a number of mutations that appear to be disruptive were identified, the disruption pattern does not clearly map to a helical interface as in the case of FtsB, confirming that that the weak self-association of FtsL observed in TOXCAT is unlikely to be specific in nature.

FtsB self-association is mediated by inter-helical hydrogen bonding

Among the positions of the TM domain of FtsB that are sensitive to mutation, Gln 16 is of particular interest. Polar amino acids, such as Gln, Asn, Glu, Asp, Lys, Arg and His, are not frequent in TM domains, which are primarily composed by hydrophobic residues(Senes et al. 2000; Senes et al. 2007). When present, however, polar residues can stabilize the association of TM helices through the formation of hydrogen bonds, which are enhanced in an apolar environment(Senes et al. 2004; Bowie 2011). While the energetic contribution of

hydrogen bonding to membrane protein folding appears to be on average rather modest (~1 kcal/mol)(Bowie 2011; Joh et al. 2008), polar amino acids can be important for the association of model peptides(Choma et al. 2000; Zhou et al. 2000) and of biological systems(Fleming & Engelman 2001b; Stanley & Fleming 2007; Li et al. 2006; Lawrie et al. 2010, p.3; Sulistijo & Mackenzie 2009, p.3). When present, polar amino acids are also likely to play an important structural or functional role, and it has been observed that phenotypic alterations and diseases are likely to result from mutations that reverse the polarity of an amino acid in membrane proteins(Partridge et al. 2002; Partridge et al. 2004).

When Gln 16 is substituted by hydrophobic amino acids (Ala, Phe and Val), the oligomerization of FtsB appears to be severely reduced (Figs. 3 and 4). Even when the Gln was replaced by a non-polar amino acid with similar size and flexibility (Met) the CAT activity decreased to 22% of WT. Conversely, when position 16 is substituted by Asn, which has the same amide terminal moiety of Gln, the variant retains most of the activity (67%). This result confirms that hydrogen bond formation is likely to play a major role in stabilizing the TM oligomer. Two side chains that could potentially hydrogen bond with Gln 16 across the interface are Tyr 17 and Ser 18. However, the removal of their hydroxyl groups (Y17F and S18A variants) did not appear to reduce oligomerization. This observation suggests that Gln 16 is likely to donate to a carbonyl oxygen atom from the backbone or to form a hydrogen bond with itself (from the opposing helix), a hypothesis that we structurally investigated using computational modeling, as presented in the next section.

Computational model of a FtsB left-handed homo-dimer

Molecular modeling can interpret the wealth of information contained in large scale mutagenesis and synthesize it into an often highly accurate structural hypothesis(Adams et al. 1995; Fleming & Engelman 2001a; Jenei et al. 2011; Lemmon et al. 1994). The modeling of the TM domain of FtsB was performed with a search protocol implemented with the molecular software library developed in this laboratory (MSL)(Kulp et al. 2012). The program generates helices in standard conformation and systematically varies their relative orientation to explore conformational space. In this calculation we imposed the formation of a symmetrical oligomer and also required that Gln 16 forms an inter-helical hydrogen bond in the structure. The calculation produced two well packed dimeric low-energy solutions (Fig 5). In one solution (Model 1, panel *a*) Gln 16 is hydrogen bonded non-symmetrically with Gln 16 on the opposite

side. In Model 2 (panel *b*) the side chain is hydrogen bonded symmetrically to the carbonyl oxygen of Val 13. The two models are closely related (1.5Å RMSD), having a similar left-handed crossing angle and inter-helical distance, and differing by a relative rotation of approximately 60˚ applied around the helical axis. To identify which solution was most compatible with the experimental data, we applied *in silico* the same set of mutations that were experimentally tested, and computed an analogous average disruption. The theoretical and experimental disruption patterns are compared in **Figure 5*c* and *d***. Model 2 is in reasonable agreement with the data overall, but its periodicity appears be slightly off-phase with respect to the experimental data, and the match becomes poor toward the C-terminal end of the helix (panel *d*). Model 1 (panel *c*) is in excellent agreement with the experimental data, and therefore we propose it as the most likely structural interpretation. Model 1 is illustrated in more detail in **Figure 6** where the specific orientation of the side chains at the dimer interface is shown and the contacts are described.

Gln 16 and the interfacial amino acids of the transmembrane domain of FtsB are evolutionarily conserved

To investigate if the interfacial amino acids, and Gln 16 in particular, are evolutionarily important, we performed a multi-sequence alignment of related FtsB sequences obtained using BLAST(Altschul et al. 1990; Altschul et al. 1997) and computed a consensus. A condensed version of the alignment is shown in **Figure 7**. The TM region of FtsB appears to be relatively well conserved across a broad group of gamma and beta proteobacteria. Most importantly, the pattern of conservation (shaded columns) corresponds remarkably well to the positions that have the highest sensitivity to mutagenesis (indicated by a dot). The average amino acid identity conservation of the sensitive positions is 68%, compared to 42% of the other positions. The most conserved positions is Trp 20, which is found in over 95% of the sequences. The key Gln 16 is also almost invariable (91% of the sequences). Interestingly, its most frequent substitution is His (4%), another polar amino acid. These observation supports the hypothesis that the structural organization of the TM domain of FtsB is evolutionarily conserved and therefore must be of biological importance for cell division.

The X-ray crystal structure of the periplasmic region of FtsB reveals a canonical coiled coil

After determining the organization of the TM domain of FtsB, we were interested in establishing if the periplasmic coiled coil region is also compatible with the formation of a homo-dimer. We approached this question by using X-ray crystallography. Unlike TM helices, which are stabilized by the hydrophobic environment, the soluble coiled coils tend to be unstable in isolation(Masson et al. 2009). For this reason we adopted a fusion strategy, replacing the TM region with a soluble globular protein (bacteriophange Φ29 Gp7) which nucleates the helix and stabilizes the coiled coil. This strategy has been demonstrated to greatly improve the solubility and crystallization propensity of coiled coil domains(Frye et al. 2010; Klenchin et al. 2011).

A Gp7 fusion construct encompassing amino acids 28-63 of FtsB (Gp7-FtsB$_{CC}$) crystallized readily and its structure was solved at a 2.3 Å, with two dimeric molecules in the asymmetric unit. The structure of the Gp7-FtsB$_{CC}$ dimer is shown in **Figure 8**, where the Gp7 moiety is highlighted in gray and the FtsB component in blue. This region of FtsB adopts a canonical coiled coil conformation. As expected, the two Asn residue that are present at "*a"* heptad positions (Asn 43 and 50) form a hydrogen bond across the interface with their corresponding residues on the other chain **(Figure 8b)**. The coil is straight for one of the dimers (chains A-B) but it exhibits a slight kink in the second (near Val 36 on chain C-D). The overall RMSD between the two dimers is 1.74Å but it decreases to 0.41Å and 0.81Å when the pre- and post-kink segments are aligned separately, therefore the kink is presumably due to the effect of crystal packing.

The structure demonstrates that, like the TM domain, the coiled coil region of FtsB can also assume a homo-dimeric form. The structure also determines that the coiled coil region of FtsB can extend at least to position 60. It is not clear whether the coiled coil would extend further, at least in the absence of FtsL. Gonzales and Beckwith determined that a C-terminal truncation of FtsB starting position 55 is still sufficient to interact with FtsL(Gonzalez & Beckwith 2009). CD analysis of a longer constructs that encompassed 7 heptad repeats (positions 28-77) revealed that it is poorly helical. A Gp7-FtsB$_{CC}$ construct that contains the entire soluble region of FtsB is also only moderately helical.

Flexibility may be important between the transmembrane and coiled coil region of FtsB

There is a gap of six amino acids (positions 22-27) between the computational model of the TM domain and the X-ray structural model of the periplasmic coiled coil, raising the question of how these two regions are connected. The simplest hypothesis would be that the two domains form a seamless helical structure that transverses the TM region and extends into the periplasm. Our geometric analysis, however, revealed that the two models cannot be connected by a simple fusion of their helices. While the crossing angle and inter-helical distance of the two domains match each other, the orientation of the helices around their main axes is not compatible. The interface of the TM region is rotated around the helical axis by approximately 100˚ with respect to the interface that would result from a natural extension of the coiled coil.

The analysis of the sequence alignment **(Figure 7)** also supports the hypothesis that a helical break is likely present in the linker region between the domains. The alignment reveals that two Gly residue at positions 22 and 25 are highly conserved (highlighted cyan). Gly 22 is present in 93% of the sequences. Gly 25 is less ubiquitous (63% of the sequences) but a third Gly is frequently present at position 24 (47%). Interestingly, the other amino acids that are prevalent at positions 24 and 25 are Ser and Asn, two residues that have a relatively high propensity for random-coil regions(Costantini et al. 2006). The data suggests that the linker requires either flexibility or adopts a backbone conformation that would be inaccessible to non-Gly amino acids, or perhaps both. According to this view, we mined the structural database for protein fragments that contained two Gly residues with the correct spacing (G*xx*G) to find candidate linkers for the two models. We extracted all *x*G*xx*G*x* fragments existing in high-resolution structures from the PDB, where *x* is any amino acid. We also imposed a constraint that two additional residues at each side of the fragment must assume a helical conformation (thus the pattern becomes *hhx*G*xx*G*xhh*, where *h* is any amino acid in helical conformation). These helical amino acids were geometrically aligned with the ends of the TM and coiled coil structure. With this procedure we were able to identify the low-energy solution that connects the two models illustrated in **Figure 9**.

Is FtsL required to stabilize the periplasmic domain of FtsB?

While the model of the linker region in **Figure 9** is hypothetical, it raises the question of

whether the Gly-rich segment could effectively nucleate and stabilize the juxta-membrane coiled coil. The question is even more compelling when it is considered that the Gp7-FtsB$_{CC}$ construct has low thermal stability. Although the fusion protein crystallizes readily and is helical at low temperature, it reversibly unfolds quite rapidly and it appears to be completely unfolded at 40 ˚C. Longer constructs, including one that extends to the entire soluble region of FtsB, showed lower helicity and even lower stability. The relatively low stability of the coiled coil, however, is not surprising when it is considered that the structure includes a large number of polar amino acids (Q35, N43, N50) at the buried "*a*" and "*d*" positions, which are generally occupied by hydrophobic amino acids(Harbury et al. 1993; Grigoryan & Keating 2008). These sequence features appear conserved in the sequence alignment **(Figure 7)**. Therefore it is possible that association with FtsL may be required for the stabilization of the periplasmic region of FtsB. The fact that the periplasmic domain of FtsB may be partially unfolded could also account for some of the cellular instability of FtsB, which is rapidly degraded in the absence of FtsL(Gonzalez & Beckwith 2009).

On the basis of our analysis, we hypothesize that a FtsB transmembrane homo-dimer forms an initial core that laterally recruits FtsL into a higher-order oligomer **(Figure 10)**, likely a tetramer as proposed also by a recent bioinformatic analysis of the soluble domains(Villanelo et al. 2011). Given the presence of several Thr residues in the TM helix of FtsL, an interesting possibility is that its lateral association could augment the membrane-embedded polar network by forming additional hydrogen bonds with the donor or acceptor groups that are left unsatisfied on Gln 16 **(Figure 5a)**. The formation of the heterologous complex and the folding of the periplasmic domains may be a determinant for making FtsB competent for binding to the periplasmic domain of FtsQ(Gonzalez & Beckwith 2009), which is required for their septal localization and the recruitment of the late proteins.

Conclusions

In this article we have presented the first structural analysis of an integral membrane protein of the bacterial divisome. We demonstrate that the TM helix of FtsB self-associates in *E. coli* membranes. The interaction is mediated by an inter-helical hydrogen bond formed by a critical polar residue embedded in the middle of the hydrophobic region. We also report the structure of the juxta-membrane domain of FtsB which forms a canonical coiled coil. The two domains are connected by a linker that is likely flexible. While the present study does not experimentally establish the precise oligomeric state of FtsB directly, the mutagenesis, modeling and crystallographic data are consistent with the formation of a homo-dimer.

By defining the protein-protein interaction interface of FtsB and providing an experimentally validated structural model, the present work suggests the hypothesis that FtsB and FtsL assemble into a higher-order oligomer and sets the stage for the biophysical analysis of their heterologous complex. This study also establishes important groundwork for biological studies *in vivo* that will address whether the self-association of FtsB is essential for division and, specifically, whether the structural features identified here – the TM interaction interface, the Gly-rich linker and the stability of the coiled coil – are important for the localization of FtsB, for its association with FtsL, and for the recruitment of the other downstream proteins to the divisome.

Acknowledgements

We are grateful to Dr. Darrell McCaslin of the Biophysical Instrumentation Facility of the Department of Biochemistry for assistance in the collection of the CD data. We thank Dr. Engelman and Miriam Alonso for providing the TOXCAT plasmids. We are grateful to Ben Mueller for useful discussion and assistance with TOXCAT, and to Dr. Vadim Klenchin for assistance with the QuikChange method. We thank Dr. Gevorg Gregorian for helpful discussion. IR and KCT were supported by funds from the NIH GM083987. Use of the Structural Biology ID19 beamline Argonne National Laboratory Advanced Photon Source was supported by the U.S. Department of Energy, Office of Energy Research, under Contract No. W-31-109-ENG-38.

References

Adams, D.W. & Errington, J., 2009. Bacterial cell division: assembly, maintenance and disassembly of the Z ring. *Nature reviews. Microbiology*, 7(9), pp.642–653.

Adams, P.D. et al., 1995. Computational searching and mutagenesis suggest a structure for the pentameric transmembrane domain of phospholamban. *Nature Structural Biology*, 2(2), pp.154–162.

Altschul, S.F. et al., 1990. Basic local alignment search tool. *Journal of molecular biology*, 215(3), pp.403–410.

Altschul, S.F. et al., 1997. Gapped BLAST and PSI-BLAST: a new generation of protein database search programs. *Nucleic acids research*, 25(17), pp.3389–3402.

Bernhardt, T.G. & de Boer, P.A.J., 2003. The Escherichia coli amidase AmiC is a periplasmic septal ring component exported via the twin-arginine transport pathway. *Molecular microbiology*, 48(5), pp.1171–1182.

Blommel, P.G. & Fox, B.G., 2007. A combined approach to improving large-scale production of tobacco etch virus protease. *Protein expression and purification*, 55(1), pp.53–68.

Bowie, J.U., 2011. Membrane protein folding: how important are hydrogen bonds? *Current Opinion in Structural Biology*, 21(1), pp.42–49.

Bramkamp, M. et al., 2006. Regulated intramembrane proteolysis of FtsL protein and the control of cell division in Bacillus subtilis. *Molecular Microbiology*, 62(2), pp.580–591.

Buddelmeijer, N. et al., 2002. YgbQ, a cell division protein in Escherichia coli and Vibrio cholerae, localizes in codependent fashion with FtsL to the division site. *Proceedings of the National Academy of Sciences of the United States of America*, 99(9), pp.6316–6321.

Buddelmeijer, N. & Beckwith, J., 2004. A complex of the Escherichia coli cell division proteins FtsL, FtsB and FtsQ forms independently of its localization to the septal region. *Molecular Microbiology*, 52(5), pp.1315–1327.

Chen, G.J. et al., 2000. Restriction site-free insertion of PCR products directionally into vectors. *BioTechniques*, 28(3), pp.498–500, 504–505.

Choma, C. et al., 2000. Asparagine-mediated self-association of a model transmembrane helix. *Nature structural biology*, 7(2), pp.161–6.

Costantini, S., Colonna, G. & Facchiano, A.M., 2006. Amino acid propensities for secondary structures are influenced by the protein structural class. *Biochemical and biophysical research communications*, 342(2), pp.441–451.

Cowtan, K., 2008. Fitting molecular fragments into electron density. *Acta crystallographica. Section D, Biological crystallography*, 64(Pt 1), pp.83–89.

Cowtan, K., 2010. Recent developments in classical density modification. *Acta crystallographica. Section D, Biological crystallography*, 66(Pt 4), pp.470–478.

Daniel, R.A. et al., 1998. Characterization of the essential cell division gene ftsL(yIID) of Bacillus subtilis and its role in the assembly of the division apparatus. *Molecular Microbiology*, 29(2), pp.593–604.

Daniel, R.A. et al., 2006. Multiple interactions between the transmembrane division proteins of Bacillus subtilis and the role of FtsL instability in divisome assembly. *Journal of Bacteriology*, 188(21), pp.7396–404.

Daniel, R.A. & Errington, J., 2000. Intrinsic instability of the essential cell division protein FtsL of Bacillus subtilis and a role for DivIB protein in FtsL turnover. *Molecular Microbiology*, 36(2), pp.278–289.

Emsley, P. & Cowtan, K., 2004. Coot: model-building tools for molecular graphics. *Acta crystallographica. Section D, Biological crystallography*, 60(Pt 12 Pt 1), pp.2126–2132.

Erickson, H.P., Anderson, D.E. & Osawa, M., 2010. FtsZ in bacterial cytokinesis: cytoskeleton and force generator all in one. *Microbiology and molecular biology reviews: MMBR*, 74(4), pp.504–528.

Fleming, K.G. & Engelman, D.M., 2001a. Computation and mutagenesis suggest a right-handed structure for the synaptobrevin transmembrane dimer. *Proteins*, 45(4), pp.313–317.

Fleming, K.G. & Engelman, D.M., 2001b. Specificity in transmembrane helix-helix interactions can define a hierarchy of stability for sequence variants. *Proceedings of the National Academy of Sciences of the United States of America*, 98(25), pp.14340–14344.

Fraipont, C. et al., 2011. The integral membrane FtsW protein and peptidoglycan synthase PBP3 form a subcomplex in Escherichia coli. *Microbiology (Reading, England)*, 157(Pt 1), pp.251–259.

Frye, J., Klenchin, V.A. & Rayment, I., 2010. Structure of the tropomyosin overlap complex from chicken smooth muscle: insight into the diversity of N-terminal recognition. *Biochemistry*, 49(23), pp.4908–4920.

Geissler, B. & Margolin, W., 2005. Evidence for functional overlap among multiple bacterial cell division proteins: compensating for the loss of FtsK. *Molecular Microbiology*, 58(2), pp.596–612.

Gerding, M.A. et al., 2007. The trans-envelope Tol-Pal complex is part of the cell division machinery and required for proper outer-membrane invagination during cell constriction in E. coli. *Molecular microbiology*, 63(4), pp.1008–1025.

Ghigo, J.M. et al., 1999. Localization of FtsL to the Escherichia coli septal ring. *Molecular Microbiology*, 31(2), pp.725–737.

Goehring, N.W. & Beckwith, J., 2005. Diverse Paths to Midcell: Assembly of the Bacterial Cell Division Machinery. *Current Biology*, 15(13), pp.R514–R526.

Goehring, N.W., Gonzalez, M.D. & Beckwith, J., 2006. Premature targeting of cell division proteins to midcell reveals hierarchies of protein interactions involved in divisome assembly. *Molecular Microbiology*, 61(1), pp.33–45.

Goehring, N.W., Gueiros-Filho, F. & Beckwith, J., 2005. Premature targeting of a cell division protein to midcell allows dissection of divisome assembly in Escherichia coli. *Genes & Development*, 19(1), pp.127–137.

Gonzalez, M.D. et al., 2010. Multiple interaction domains in FtsL, a protein component of the widely conserved bacterial FtsLBQ cell division complex. *Journal of bacteriology*, 192(11), pp.2757–2768.

Gonzalez, M.D. & Beckwith, J., 2009. Divisome Under Construction: Distinct Domains of the Small Membrane Protein FtsB Are Necessary for Interaction with Multiple Cell Division Proteins. *Journal of Bacteriology*, 191(8), pp.2815–2825.

Grigoryan, G. & Keating, A.E., 2008. Structural specificity in coiled-coil interactions. *Current Opinion in Structural Biology*, 18(4), pp.477–483.

Hale, C.A., Rhee, A.C. & de Boer, P.A., 2000. ZipA-induced bundling of FtsZ polymers mediated by an interaction between C-terminal domains. *Journal of bacteriology*, 182(18), pp.5153–5166.

Harbury, P.B. et al., 1993. A switch between two-, three-, and four-stranded coiled coils in GCN4 leucine zipper mutants. *Science (New York, N.Y.)*, 262(5138), pp.1401–1407.

Heidrich, C. et al., 2001. Involvement of N-acetylmuramyl-L-alanine amidases in cell separation and antibiotic-induced autolysis of Escherichia coli. *Molecular microbiology*, 41(1), pp.167–178.

Jenei, Z.A. et al., 2011. Packing of transmembrane domain 2 of carnitine palmitoyltransferase-1A affects oligomerization and malonyl-CoA sensitivity of the mitochondrial outer membrane protein. *FASEB journal: official publication of the Federation of American Societies for Experimental Biology*, 25(12), pp.4522–4530.

Joh, N.H. et al., 2008. Modest stabilization by most hydrogen-bonded side-chain interactions in membrane proteins. *Nature*, 453(7199), pp.1266–1270.

Karimova, G., Dautin, N. & Ladant, D., 2005. Interaction network among Escherichia coli membrane proteins involved in cell division as revealed by bacterial two-hybrid analysis. *Journal of Bacteriology*, 187(7), pp.2233–2243.

Katis, V.L., Wake, R.G. & Harry, E.J., 2000. Septal localization of the membrane-bound division proteins of Bacillus subtilis DivIB and DivIC is codependent only at high temperatures and requires FtsZ. *Journal of bacteriology*, 182(12), pp.3607–3611.

Klenchin, V.A. et al., 2011. Structure-function analysis of the C-terminal domain of CNM67, a core component of the Saccharomyces cerevisiae spindle pole body. *The Journal of Biological Chemistry*, 286(20), pp.18240–18250.

Kulp, D.W. et al., 2012. Structural informatics, modeling, and design with an open-source Molecular Software Library (MSL). *Journal of computational chemistry*, 33(20), pp.1645–1661.

Lawrie, C.M., Sulistijo, E.S. & MacKenzie, K.R., 2010. Intermonomer hydrogen bonds enhance GxxxG-driven dimerization of the BNIP3 transmembrane domain: roles for sequence context in helix-helix association in membranes. *Journal of Molecular Biology*, 396(4), pp.924–936.

Lemmon, M.A. et al., 1994. A dimerization motif for transmembrane alpha-helices. *Nature structural biology*, 1(3), pp.157–163.

Lemmon, M.A. et al., 1992. Sequence specificity in the dimerization of transmembrane alpha-helices. *Biochemistry*, 31(51), pp.12719–25.

Li, E., You, M. & Hristova, K., 2006. FGFR3 dimer stabilization due to a single amino acid pathogenic mutation. *Journal of molecular biology*, 356(3), pp.600–612.

Li, R. et al., 2004. Dimerization of the transmembrane domain of Integrin alphaIIb subunit in cell membranes. *The Journal of Biological Chemistry*, 279(25), pp.26666–26673.

Liu, Z., Mukherjee, A. & Lutkenhaus, J., 1999. Recruitment of ZipA to the division site by interaction with FtsZ. *Molecular microbiology*, 31(6), pp.1853–1861.

Masson, S. et al., 2009. Central domain of DivIB caps the C-terminal regions of the FtsL/DivIC coiled-coil rod. *The Journal of Biological Chemistry*, 284(40), pp.27687–27700.

Mingorance, J. et al., 2010. Strong FtsZ is with the force: mechanisms to constrict bacteria. *Trends in Microbiology*, 18(8), pp.348–356.

Mohammadi, T. et al., 2011. Identification of FtsW as a transporter of lipid-linked cell wall precursors across the membrane. *The EMBO journal*, 30(8), pp.1425–1432.

Morais, M.C. et al., 2003. Bacteriophage phi29 scaffolding protein gp7 before and after prohead assembly. *Nature structural biology*, 10(7), pp.572–576.

Murshudov, G.N. et al., 1999. Efficient anisotropic refinement of macromolecular structures using FFT. *Acta crystallographica. Section D, Biological crystallography*, 55(Pt 1), pp.247–255.

Nguyen-Distèche, M. et al., 1998. The structure and function of Escherichia coli penicillin-binding protein 3. *Cellular and molecular life sciences: CMLS*, 54(4), pp.309–316.

Noirclerc-Savoye, M. et al., 2005. In vitro reconstitution of a trimeric complex of DivIB, DivIC and FtsL, and their transient co-localization at the division site in Streptococcus pneumoniae. *Molecular Microbiology*, 55(2), pp.413–424.

Otwinowski, Z. & Minor, W., 1997. [20] Processing of X-ray diffraction data collected in oscillation mode. In J. Charles W. Carter, ed. *Methods in Enzymology*. Academic Press, pp. 307–326. Available at: http://www.sciencedirect.com/science/article/pii/S007668799776066X [Accessed September 26, 2012].

Partridge, A.W., Therien, A.G. & Deber, C.M., 2004. Missense mutations in transmembrane domains of proteins: phenotypic propensity of polar residues for human disease. *Proteins*, 54(4), pp.648–656.

Partridge, A.W., Therien, A.G. & Deber, C.M., 2002. Polar mutations in membrane proteins as a biophysical basis for disease. *Biopolymers*, 66(5), pp.350–358.

Robichon, C. et al., 2008. Artificial septal targeting of Bacillus subtilis cell division proteins in Escherichia coli: an interspecies approach to the study of protein-protein interactions in multiprotein complexes. *Journal of Bacteriology*, 190(18), pp.6048–6059.

Robichon, C. et al., 2011. Role of leucine zipper motifs in association of the Escherichia coli cell division proteins FtsL and FtsB. *Journal of bacteriology*, 193(18), pp.4988–4992.

Rowland, S.L. et al., 2010. Evidence from Artificial Septal Targeting and Site-Directed Mutagenesis that Residues in the Extracytoplasmic {beta} Domain of DivIB Mediate Its Interaction with the Divisomal Transpeptidase PBP 2B. *Journal of Bacteriology*, 192(23), pp.6116–6125.

Russ, W.P. & Engelman, D.M., 1999. TOXCAT: A Measure of Transmembrane Helix Association in a Biological Membrane. *Proceedings of the National Academy of Sciences*, 96(3), pp.863–868.

Senes, A. et al., 2007. E(z), a depth-dependent potential for assessing the energies of insertion of amino acid side-chains into membranes: derivation and applications to determining the orientation of transmembrane and interfacial helices. *Journal of Molecular Biology*, 366(2), pp.436–448.

Senes, A., Engel, D.E. & DeGrado, W.F., 2004. Folding of helical membrane proteins: the role of polar, GxxxG-like and proline motifs. *Current Opinion in Structural Biology*, 14(4), pp.465–479.

Senes, A., Gerstein, M. & Engelman, D.M., 2000. Statistical analysis of amino acid patterns in transmembrane helices: the GxxxG motif occurs frequently and in association with beta-branched residues at neighboring positions. *Journal of molecular biology*, 296(3), pp.921–36.

Shaw, W.V., 1975. Chloramphenicol acetyltransferase from chloramphenicol-resistant bacteria. *Methods in Enzymology*, 43, pp.737–755.

Sherratt, D.J. et al., 2010. The Escherichia coli DNA translocase FtsK. *Biochemical Society transactions*, 38(2), pp.395–398.

Shiomi, D. & Margolin, W., 2007. Dimerization or oligomerization of the actin-like FtsA protein enhances the integrity of the cytokinetic Z ring. *Molecular microbiology*, 66(6), pp.1396–1415.

Stanley, A.M. & Fleming, K.G., 2007. The role of a hydrogen bonding network in the transmembrane beta-barrel OMPLA. *Journal of molecular biology*, 370(5), pp.912–924.

Subramaniam, S. & Senes, A., 2012. An energy-based conformer library for side chain optimization: Improved prediction and adjustable sampling. *Proteins*, 80(9), pp.2218–2234.

Sulistijo, E.S., Jaszewski, T.M. & MacKenzie, K.R., 2003. Sequence-specific dimerization of the transmembrane domain of the "BH3-only" protein BNIP3 in membranes and detergent. *The Journal of Biological Chemistry*, 278(51), pp.51950–51956.

Sulistijo, E.S. & Mackenzie, K.R., 2009. Structural basis for dimerization of the BNIP3 transmembrane domain. *Biochemistry*, 48(23), pp.5106–5120.

Szwedziak, P. et al., 2012. FtsA forms actin-like protofilaments. *The EMBO journal*, 31(10), pp.2249–2260.

Vagin, A. & Teplyakov, A., 2000. An approach to multi-copy search in molecular replacement. *Acta crystallographica. Section D, Biological crystallography*, 56(Pt 12), pp.1622–1624.

Villanelo, F. et al., 2011. A model for the Escherichia coli FtsB/FtsL/FtsQ cell division complex. *BMC structural biology*, 11, p.28.

Wadenpohl, I. & Bramkamp, M., 2010. DivIC Stabilizes FtsL Against RasP Cleavage. *Journal of Bacteriology*, 192(19), pp.5260–5263.

Xiang, Z. & Honig, B., 2001. Extending the accuracy limits of prediction for side-chain conformations. *Journal of Molecular Biology*, 311(2), pp.421–430.

Zhou, F.X. et al., 2000. Interhelical hydrogen bonding drives strong interactions in membrane proteins. *Nature structural biology*, 7(2), pp.154–60.

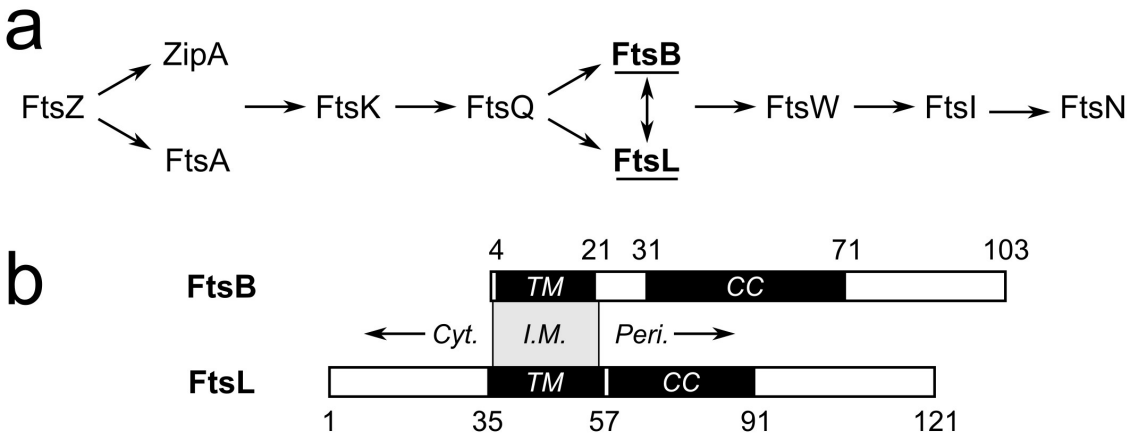

Figure 1. The recruitment hierarchy of the divisome and the predicted topology of FtsB and FtsL. a) In *E. coli* the recruitment of the divisome to the division site follows a strict hierarchical dependency(Goehring & Beckwith 2005). A functional FtsZ is required for the recruitment of FtsA and ZipA, which in turn are required for the recruitment of FtsK, and so on. FtsB and FtsL are co-dependent for their recruitment and both depend on FtsQ. b) Putative domain topology of FtsB and FtsL, as annotated in UniProt. Their interaction is presumed to be mediated by their single transmembrane domain (*TM*) and a juxta-membrane coiled coil region (*CC*). The start and end positions of the predicted *TM* and *CC* domains are indicated. *Cyt.* = cytoplasm. *I.M.* = Inner Membrane. *Peri.* = Periplasm.

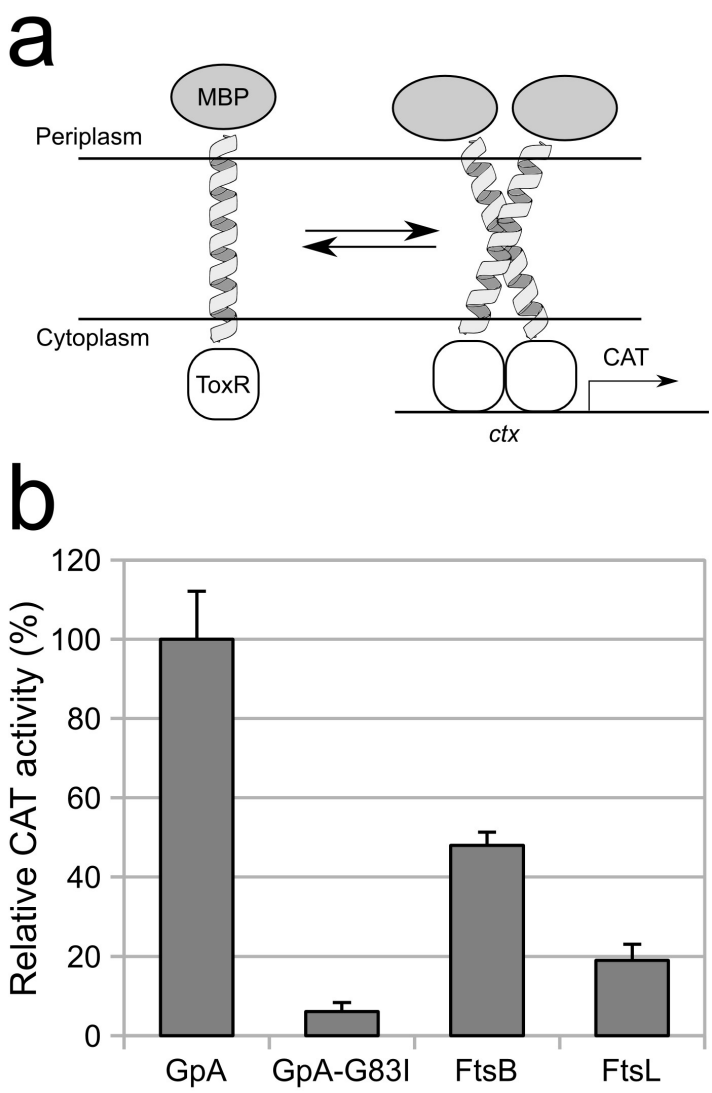

Figure 2. FtsB and FtsL self-associate in TOXCAT. a) TOXCAT is an *in vivo* assay based on a construct in which the transmembrane domain under investigation is fused to the ToxR transcriptional activator of *V. cholerae*. Transmembrane association results in the expression of a reporter gene in *E. coli* cells, which can be quantified. b) TOXCAT assay of FtsB and FtsL transmembrane domains. FtsB shows half of the activity of the strong transmembrane dimer of Glycophorin A (GpA). The activity of FtsL is above baseline but low, indicating a weak propensity to homo-oligomerize. The monomeric G83I mutant of GpA is used as a negative control. Data reported as average and standard deviation over four replicate experiments.

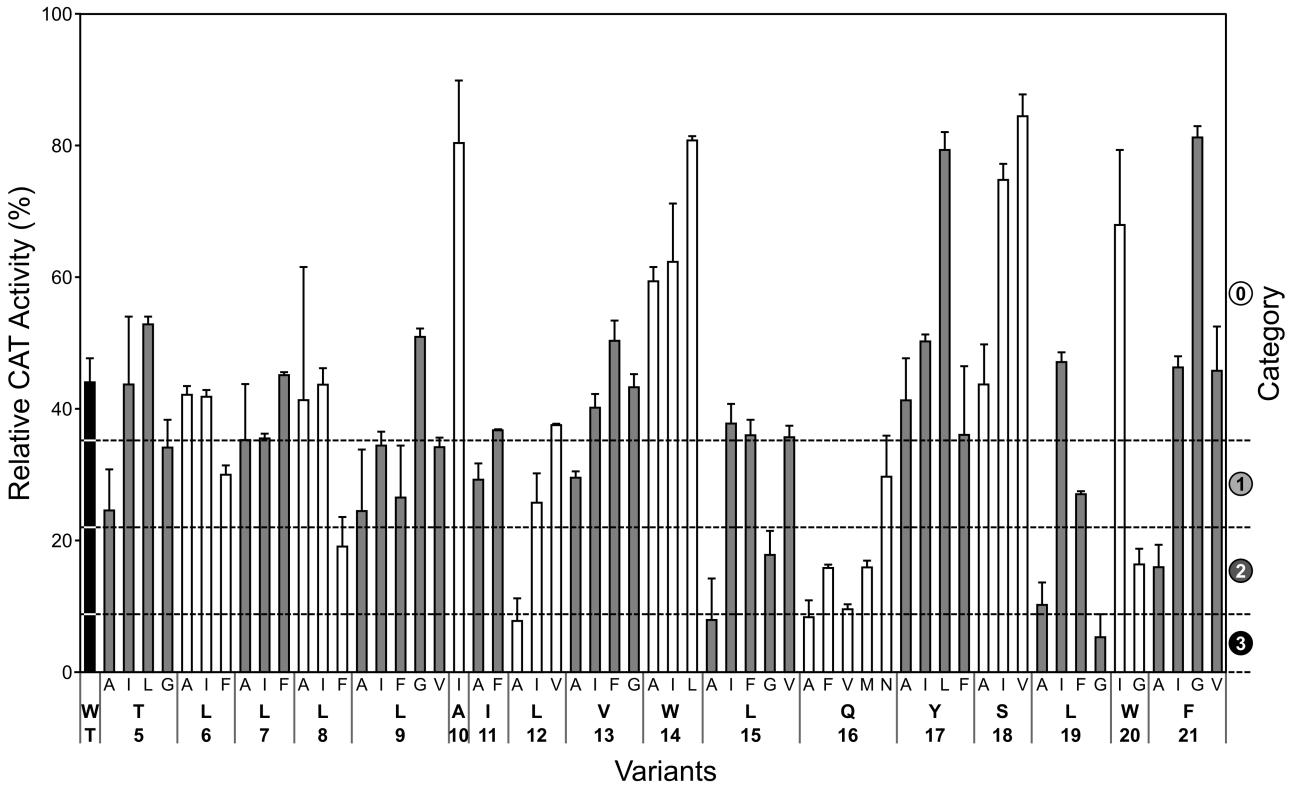

Figure 3. Mutagenesis of the transmembrane helix of FtsB. The figure shows the 57 point mutants of the TM domain of FtsB (residues 5-21) analyzed in TOXCAT. The CAT activity (left axis) is normalized to that of the GpA construct, as in **Figure 2**. The activity of the wild type FtsB construct is in black. The mutations at each position are visually grouped by color. Each mutation has been categorized relative to the wild type FtsB TOXCAT activity (back bar) as “WT-like” (0: >80% of WT), “Mild” (1: 50-80%), “Severe” (2: 20-50%) or “Disruptive” (3: 0-20%), as indicated on the right axis and by the dashed lines. The TOXCAT data for all 57 variants is summarized using the above category scheme in **Figure 4**.

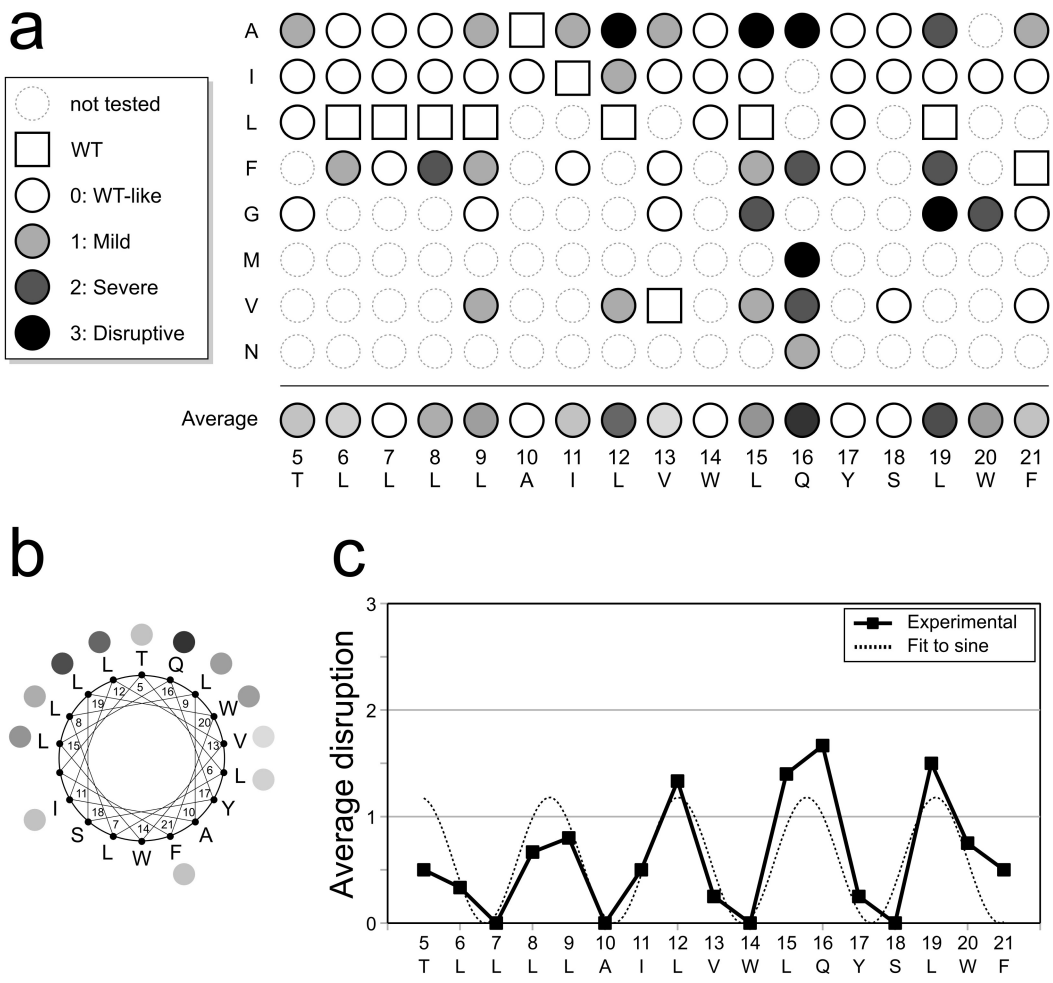

Figure 4. Position specific "average disruption" identifies a helical interface and an essential polar residue. a) The scheme summarizes the effect of all mutations of FtsB-TM measured in TOXCAT. The data has been categorized as explained in **Figure 2**. An average disruption score is displayed at the bottom of the scheme. While Gln 16 is the most sensitive position, the introduction of an Asn side chain restores association almost entirely, indicating that a hydrogen bond is important for the association. b) Diagram mapping the average disruption score to a helical wheel. The disruption pattern clusters on one helical face defined by positions T5, L6, L8, L9, L12, L15, Q16, L19 and W20. c) Fit of the average disruption index to a sine function. The estimated periodicity is approximately 3.5 amino acid per turn, which corresponds to a helical interaction with a left-handed crossing angle (dotted line).

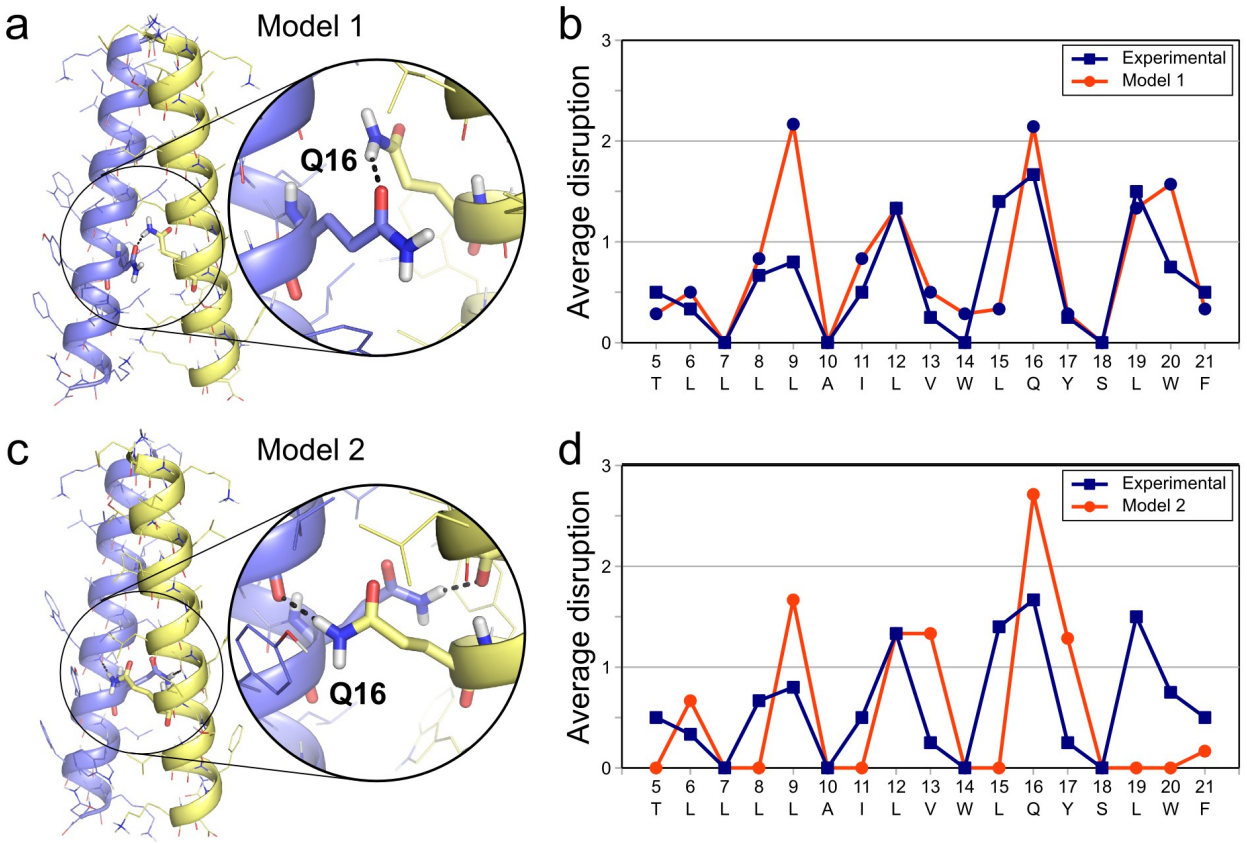

Figure 5. Molecular model of the FtsB transmembrane dimer. Modeling identified two well packed low-energy structures in which Gln 16 forms an inter-helical hydrogen bond (panels a and c). Model 1 and 2 are closely related (Cα RMSD of 1.5Å), with a left-handed crossing angle (25˚ and 20˚, respectively) and an inter-helical distance of 10.1Å. In Model 1 the side chains of Gln 16 interact with a non-symmetrical hydrogen bond. The helices of Model 2 are rotated axially by about 60˚ with respect to Model 1. The side chains of Gln 16 interact symmetically with the carbonyl oxygen of Val 13. Panels b and d compare the average disruption index for the computational mutagenesis applied to the models to the average disruption observed experimentally. Model 1 shows an excellent agreement with the experimental data, which is better than Model 2, particularly in the C-terminal side of the transmembrane domain.

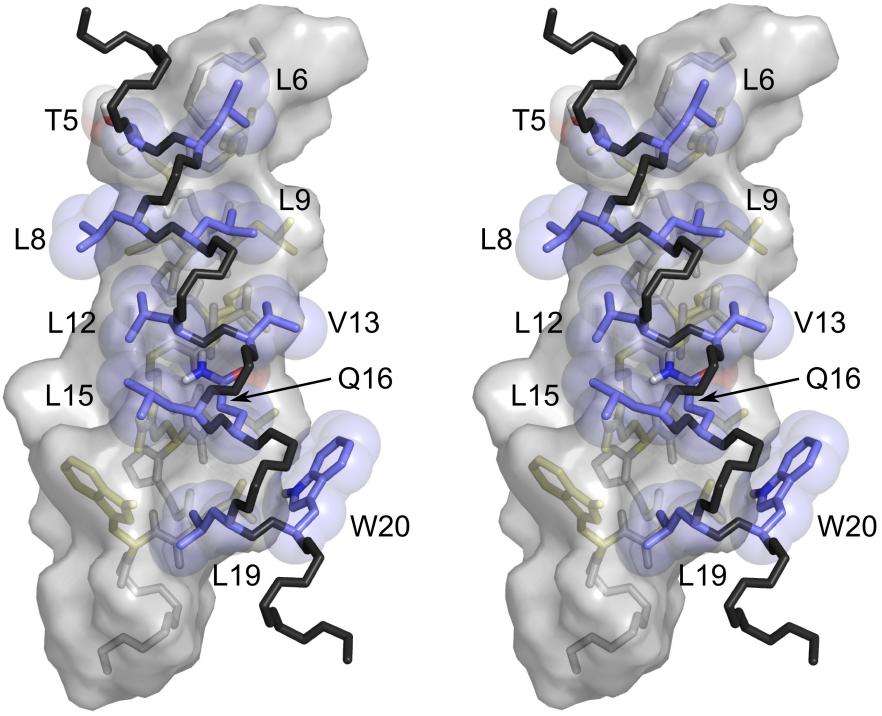

Figure 6. Computational model of FtsB-TM (Model 1). Stereo representation of the side chain interactions across the interface. The interacting positions on the opposite chains are shown in sticks to highlight the arrangement and packing of the side chains. The van der Waals sphere of the side chains of the monomer in the foreground (blue) and the surface of the monomer in the background are also displayed with transparency. L15 and L19 interact against a ridge formed by W20. L12 and V13 pack against each other across the interface, and so do the L8/L9 and the T5/L6 pairs.

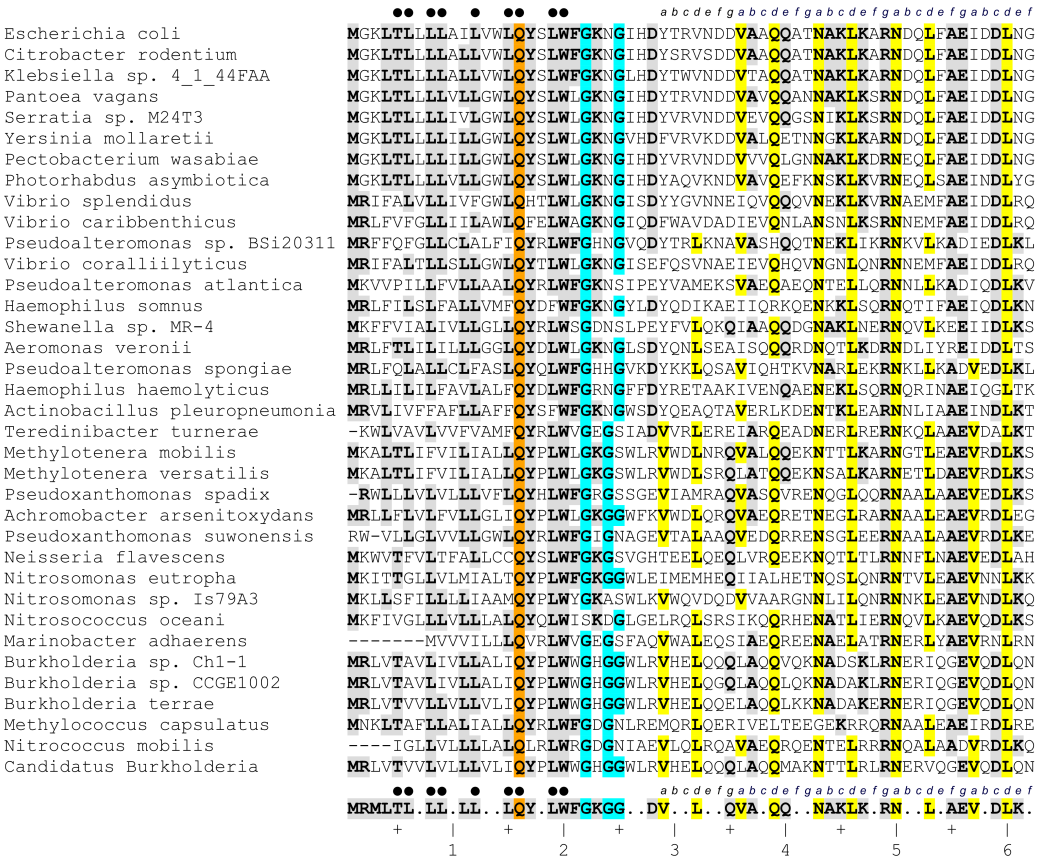

Figure 7. Sequence alignment of FtsB indicates that the interfacial positions are evolutionary conserved. Partial representation of a sequence alignment of FtsB. FtsB is relatively well conserved among a diverse group of beta and gamma proteobacteria. The amino acids that are present in at least 30% of sequence at each position are shown in bold and shaded. These amino acids are also highlighted in the consensus sequence at the bottom of the alignment. The positions that are involved at the FtsB dimer interface **(Figure 5)** are marked with a full circle (●). A remarkable match between conservation and the interfacial positions is evident. In particular, positions Q16 (highlighted in orange), L20 and W21 are almost invariable. The heptad repeat designation (positions *a* to *g*) of the coiled coil region is also given, and the conserved amino acid at the interfacial *a* and *d* positions are highlighted in yellow. In cyan are highlighted three conserved Gly amino acids (positions 22, 24 and 25) that are likely to confer flexibility to the linker region between the transmembrane domain and the coiled coil region.

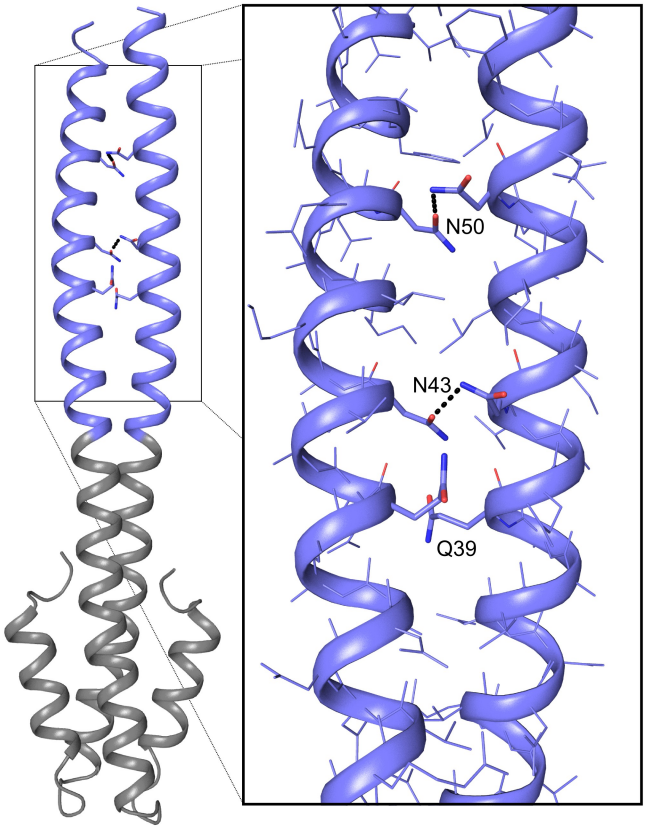

Figure 8. X-ray crystal structure of a Gp7-FtsB$_{cc}$ fusion protein. Ribbon representation of one of the two dimeric molecules in the asymmetric unit. This molecule forms a straight canonical coiled coil. The second molecule in the asymmetric unit exhibits a slight bend, possibly as a result of crystal packing. The N-terminal Gp7 unit which replaces the transmembrane domain is highlighted in gray, and the FtsB sequence in blue. The inset highlights a number of polar amino acids that are present at the interface in "*d*" (Q39) and "*a*" (N43 and N50) positions.

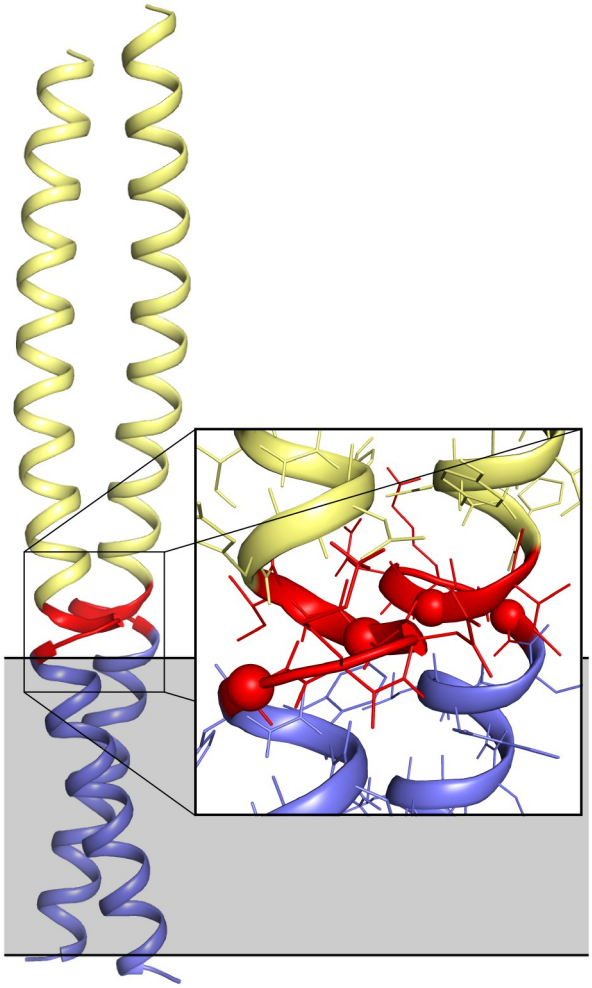

Figure 9. A theoretical model of a FtsB dimer that encompasses the transmembrane and coiled coil domains. The crystal structure of the coiled coil region of FtsB (yellow) and the computational Model 1 of the transmembrane domain (blue) were stitched together using a fragment based approach (see Methods). The resulting theoretical model includes a hinge between the coiled coil and the transmembrane helix where the helix unfolds (red). This hinge corresponds to conserved a Gly rich region in the sequence alignment (G21 and G25, spheres), suggesting that a flexible connection may be functionally important.

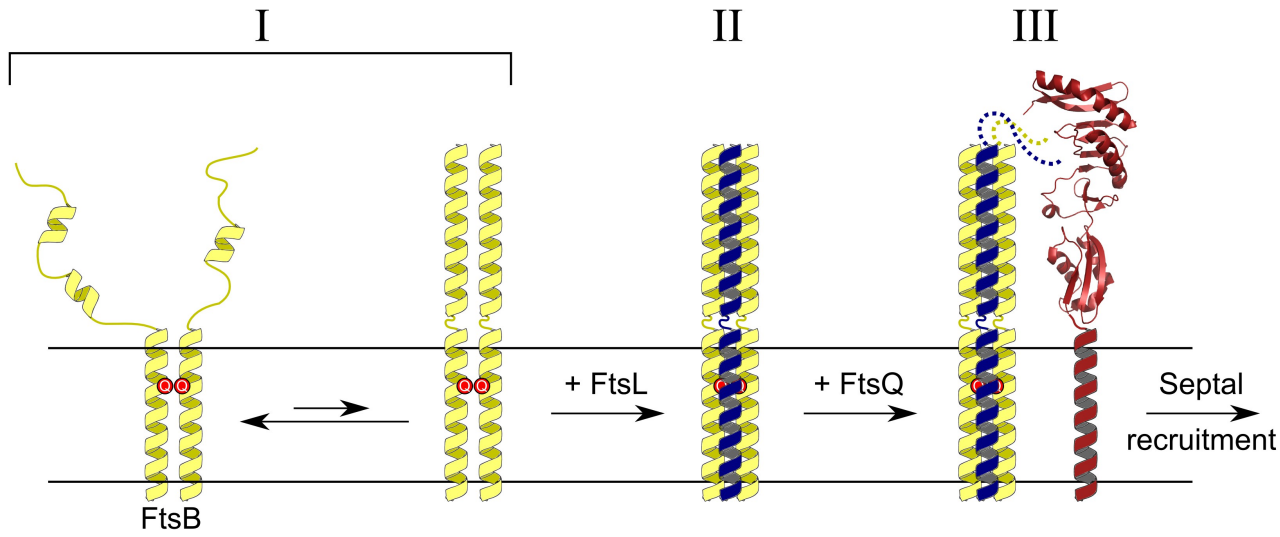

Figure 10. A functional hypothesis for the formation of FtsB/FtsL complex and its recruitment to the divisome. The transmembrane domain of FtsB self-associates in *E. coli* membranes, driven by an inter-helical hydrogen bond (Gln 16, represented by a red circle) but the coiled coil region is likely to be marginally stable or unstable (I). This finding raises the hypothesis that the interaction with FtsL is required to stabilize the periplasmic domain. It is likely that FtsL (blue) laterally associates with a pre-existing FtsB dimer (II). Alternatively, FtsL may compete with the self-association of FtsB to form an FtsB/FtsL hetero-dimer (not represented). Once the periplasmic domain is folded, the C-terminal tails of the FtsB/FtsL complex (dotted lines) would bind to FtsQ (red) and the proteins would subsequently be recruited to the division septum (III).

APPENDIX II

The FRETting tendency of bacterial proteins

I feel fortunate to be able to contribute my scientific work to the broader society through this platform of expression. I would like to thank the efforts of the Wisconsin Initiative for Science Literacy (WISL) and the AAAS-sponsored Dance your PhD contest for providing us the microphone to reach the wider public.

Note: Please visit http://www.news.wisc.edu/22449 for a video containing a depiction of the following work in the form of an interpretive dance. The video provides a visual to go along with the methodologies used in my work, which I have described in this chapter.

Introduction

What is the problem to be targeted?

Most of the research in biological sciences these days tackles a problem. And for us, humans, a biological problem means a disease. The word disease can be broken into dis–ease, which means something within us is not at ease. There is a reason for the state of dis-ease, and our job as scientists, is to research, or find the root cause of that dis-eased state, and try to rectify it. We are aware of the various kinds of dis-eases that bother us in our lives – the smaller kind such as cold and flu, and the ones that don't have a cure, such as cancer. The reason cold and flu aren't life threatening anymore is because the root causes of those dis-eased states have been identified and tackled. For cancer, the search continues...

One example of a dis-ease is a bacterial infection. Bacteria are micro-organisms that are present everywhere – in our houses, in our food and even inside us. Based on the type of bacteria, there are those that are harmful to us, and those that we can tolerate. Some bacteria reside in our gut, some are present in yogurt and so on. But there are others that cause problems or 'infections' such as the one that causes the commonly occurring 'strep throat'. In the case of an infection, bacteria enter our body through some form (food, air, contact with another living organism), decide to mark their territory in one part of the body, and start feeding on us and multiplying. One bacterium takes the nutrients it needs from our body, grows in size, and then splits into two new bacteria. The two new bacteria will then take up more nutrients, grow in size, split into two more to make four bacteria. This way there will be more and more bacteria in our system, feeding on us, and making us sick. One rod-shaped bacterium is 1 micrometer in size, so you can imagine, that in a 1 cm x 1cm area on your body, there can be 10,000 x 10,000 = 10^8 bacteria at work!

Our body has a natural defense mechanism which usually works very well to fight off and kill these unwanted organisms. But each individual is made differently, and based on the strength of the individual's fighting machinery or 'immune system', they can either ward off a bacterial invasion, or get 'infected'. In such cases, doctors prescribe us 'antibiotics'. These medications are designed such that they will attack only the bacteria and not us humans. So when we consume these antibiotics, they target the bacteria, prevent them from carrying out the processes they need, to grow and survive, and the bacteria eventually die. Infection cured. There is a catch, however. These bacteria are smart, and once they get an idea of how the drug is designed to attack them, they slowly modify themselves such that the drug doesn't work on them anymore! And we get what we know today as a superbug! Bacteria that are 'antibiotic resistant'. For bacteria to modify themselves, all they need is familiarity with the drug. The more frequently we use antibiotics, the more familiar they become, and the more resistance these bacteria develop to them. *The CDC (Center for Disease Control and Prevention) generated a threat report in 2013, showcasing an alarming number of over two million illnesses and about twenty three thousand deaths caused by infections due to antibiotic resistant bacteria in the United States alone*. So how do we tackle this serious problem?

How do we target this problem?

One way is to prevent overuse of antibiotics. This is difficult because a lot of antibiotics in the market are broad-spectrum, which means they can treat different kinds of bacteria. When we take in an antibiotic, it may kill a certain type of bacteria, but at the same time present itself to another type of bacteria for familiarization, and make that bacteria modify itself and be resistant to it. Next time if the same antibiotic is used on an infection by this

modified bacteria, it may no longer be effective, and the infection would take over. Antibiotics work by entering the inside of the bacterium, and affecting some of its very basic cellular processes; which it requires to fully function and live. ***Before going into further detail, let us zoom in a bit to understand this better.***

As we have all heard, the most basic unit of life is a cell. A cell is what carries out all the process required for life. Multiple cells of a certain type club together to form different organs in our body. Our lungs are made of cells that help us breathe, our heart is made of cells that can help circulate blood, blood itself is made up of different kinds of cells like red blood cells, white blood cells, and so on. Zooming in further, we are now looking at the inside of the cell. Imagine a factory, with thousands of processes simultaneously going on. There are millions of people carrying out their jobs in a concerted fashion. Some are carrying cargo from one end of the factory to another, some are building the architecture of the factory, some are welcoming newer people into the factory who have just arrived after being fully trained to work, some are managing poor workers and eliminating them. Each of these processes are necessary for the proper functioning of the factory, and the concerted effort of all these people is what makes that possible. These 'people', inside a cell are known as 'proteins'. Proteins are of various kinds and carry out various cellular processes. Some proteins are involved in the synthesis of other proteins as well as synthesis of protein precursors. Without these essential proteins, the cell will not function, and eventually die.

The antibiotics for bacterial infections in the market work by attacking some proteins inside the cell that are required for synthesis of other proteins and protein precursors. The reason such antibiotics are available is because these processes of protein synthesis etc. are very well understood, and thus drugs to alter these processes have been designed. But as

described earlier, the problem of antibiotic resistance is growing.

Now, unlike humans that are made up of millions of cells, a bacterium is made of just one cell. The cell itself is the bacterium. As I mentioned earlier, it carries out all its cellular processes, grows, and then splits into two new cells. The process of splitting into two new cells is called cell-division. Some proteins carry out the cellular processes needed for the cell to function and grow, and some proteins are needed for cell-division. These proteins required for cell division of the bacteria are not really present inside the cell, but are part of an outer layer of the cell called the cell-membrane that separates a cell from its outside environment. **Thus, these proteins are called membrane-proteins**. When the cell is ready to divide, these membrane proteins all come together in the middle region of the cell membrane, interact with each other, and start deforming the cell there so that it can prepare to split in two.

Designing drugs that target the membrane proteins that carry out cell division, can be another approach to tackle bacterial infection. But the reason this approach is not fully used, is because the process of cell division is still not very well understood. The different kinds of membrane proteins involved in the process are known, and we also know that these membrane proteins come together in the cell membrane and interact in some way to enable cell division. It has also been studied and shown previously that in the absence of membrane proteins, cell division cannot occur. But exactly which proteins are partnering with each other and forming what sort of a structure, a set-up that is important to know in order to design drugs, is still not well understood. Further, we don't know exactly how these proteins communicate with each other as well.

Thus, the focus of my work is to better understand the process of cell division in bacteria by studying the membrane protein interactions, in an effort to target the problem of antibiotic resistance.

The specific question

To begin understanding the complex interactions of the membrane proteins involved in bacterial cell division, we started looking at the interactions between two such proteins, FtsB and FtsL. We know from previous research that FtsB and FtsL do form a complex, meaning, they are interaction partners. It has also been shown by other research groups that the two proteins are essential for each other's viability in the cell membrane, and that upon interaction, they can recruit the remaining proteins needed for completion of the cell division process. But exactly how they interact with each other, that is, which parts of the two proteins are involved in interaction, is not known.

Now, if we take a look at the architecture of these two proteins, both have a component that is embedded in the cell membrane, and a component that is present right outside the cell membrane (called the periplasmic region). In order to start mapping the interaction regions, we decided to divide them into individual components (membrane region and periplasmic region), and investigate which regions are required for the two proteins to interact. For my PhD, I have focused on the membrane regions of FtsB and FtsL in order to understand the role of the membrane region of these proteins in the FtsB-FtsL interaction, and thereby in bacterial cell division.

The technique used

To study proteins or, for that matter, any molecular component of a cell, there are three broad approaches scientists use in our field – *in vivo, in vitro* and *in silico*. *In vivo* refers to studying the molecules in their native environment, that is, inside a cell or inside an organism,

such as the studies performed on mice. In this approach we employ techniques like microscopy and fluorescence methods where the molecules are genetically modified to be tagged or labeled with fluorescent molecules so that their behavior in their native environment can be monitored from the outside. The advantages are that we are observing the molecules in their natural state along with their natural components, but the disadvantages are that we cannot alter the environment too much to observe its effects on the molecule in question. *In vitro* on the other hand refers to taking the molecule in isolation and studying it. Here the disadvantage is that we don't look at the molecule in its native state, but we have more control over the modifications on the molecule and the environment, and can obtain more physical parameters. A third approach is *in silico*, or computational analysis. *In silico* analyses observe the molecule's parameters computationally, and can perform complicated modifications to the molecule in much lesser time to observe its theoretical effect. Computational modeling of biomolecules has been a tremendous breakthrough in aiding and complementing experimental research in the biological sciences. A comprehensive analysis of any biological system employs a concerted effort of all three approaches.

In my work, I have focused on studying the interactions between the membrane components of the two cell division proteins FtsB and FtsL using an *in vitro* approach. To do so, I first chemically synthesized the two proteins using a chemical synthesis technique. In this technique, the building blocks of the proteins are added stepwise in a certain sequence that is characteristic to the identity of the protein. Each protein is synthesized in this manner until they mimic the natural composition of their membrane component. Once the synthesis is completed, the proteins are chemically labeled, or tagged with fluorophores (molecules that are fluorescent upon shining with light) at their ends. Since fluorescent molecules have a specific color, or a specific behavior under light, tagging the proteins with fluorophores allows

me to visualize their behavior. Once the labeling is achieved, the reaction is subject to a purification procedure that separates the labeled proteins from the unlabeled proteins, allowing me to perform the experiments with pure labeled proteins. Finally, using the pure labeled FtsB and FtsL proteins, I carry out the experiment that enables me to look at the interactions between these proteins, and to do this experiment, **I use a method known as – FRET**.

FRET stands for Förster Resonance Energy Transfer. In this technique, one fluorophore transfers its energy to another fluorophore if the two are in close proximity to each other. These two fluorophores are called a FRET pair, and need to be chosen based on their behavior under light. For example, if we look at the spectrum of visible light going from low to high wavelengths, it actually is split between different lights in the form of VIBGYOR, or Violet-Indigo-Blue-Green-Yellow-Orange-Red. So when a blue fluorophore is excited by shining light of an adjacent lower wavelength on it, such as Indigo,, it will exhibit blue fluorescence. Similarly when a green fluorophore is excited by shining blue light on it, it will exhibit green fluorescence. This means that for the green fluorophore to be excited, it requires light energy corresponding to blue light. Now, if the blue and green fluorophores are in close proximity to each other, then if we shine indigo light on them, the blue fluorophore will get excited; but instead of exhibiting its blue fluorescence, it will transfer that energy to the green fluorophore which is of the right energy to excite it, and we will observe green fluorescence instead. This phenomenon of energy transfer between two fluorophores in close proximity is called FRET. Thus, FRET can be used to study interactions between two proteins. If the two proteins are attached to, or labeled with fluorophores that form a FRET pair, then we will observe FRET in the form of green fluorescence if there are interactions that exist between the proteins.

FtsB and FtsL are membrane proteins, and in my work I used FRET to study the

interactions between their membrane components. This means that to understand the natural interaction tendencies of these two proteins, I needed to study them in an environment that is close to the composition of the cell membrane. Now, the cell membrane's composition is very diverse – it is made up of different kinds of molecules comprising various sizes and properties, but the most important characteristic of the membrane is that it is 'hydrophobic', or water repelling. It is made of molecules that are lipidic, or 'greasy'. Thus, the proteins that reside in this part of the cell are also greasy in composition and do not dissolve in water. This makes studying membrane proteins complicated, because unlike proteins that are present inside the cell (which has a high percentage of water), membrane proteins cannot be studied in water-based solvents *in vitro*. Therefore, to study membrane proteins using FRET or any other technique *in vitro,* we first need to dissolve them in artificial lipid environments like detergent based solutions, or small artificial membranes that try and mimic the natural membrane environment. This provides a habitat close to their natural state, and allows us to study the proteins with the assumption that their behavior in the natural cell membrane is similar to the artificial lipid membranes we synthesize.

So, once I synthesized, labeled and purified the FtsB and FtsL membrane proteins, I added them to artificial membranes and performed my FRET experiment. In one reaction, I had FtsB labeled with blue fluorophores only. I excited them with indigo light, and observed blue fluorescence. This told me that the fluorophores are behaving well in the artificial set up. In another reaction, I took FtsL labeled with green fluorophores only. Again I excited them with indigo light, and observed nothing. This was as expected, because indigo light doesn't have the exact energy/wavelength to excite a green fluorophore. In a third reaction, I mixed the two proteins – blue labeled FtsB and green labeled FtsL. Now when I excited this reaction with indigo light, I expected to observe one of two things – either blue fluorescence only, indicating

that I am exciting the blue FtsB proteins and they are not transferring their energy to green, or lesser blue fluorescence compared to my first reaction, and an additional green fluorescence. The second situation would arise if a green fluorophore will be in proximity to the blue fluorophore, indicating that FtsB and FtsL are close to each other, and thus interacting. I performed these experiments in very dilute conditions such that any FRET observed was only due to specific interactions between FtsB and FtsL proteins and not just due to a crowded environment with proteins 'bumping into each other'. The extent of the interaction could be estimated by the amount of decrease in blue fluorescence observed, compared to the first reaction with blue-FtsB alone. With this experiment, I found that FtsB and FtsL did exhibit the second situation of FRET with appearance of green light and decrease of blue light indicating that they have a very high tendency to interact through their membrane components alone.

Conclusions

In our lab, we study interactions between membrane proteins using various techniques. For my dissertation, I focused on studying the membrane components of two proteins FtsB and FtsL that are required for cell-division in bacteria. Using a technique known as FRET, I observed that the two proteins contain a membrane component that drives their interaction to form a FtsB-FtsL complex. In addition, I also observed that FtsB alone has a tendency to form a 'dimer', or a pair with another molecule of itself. This led us to believe that there must exist some sort of competition between one FtsB molecule and one FtsL molecule to pair up with the other FtsB molecule. On performing FRET studies on the different combinations of these proteins, I found that these two proteins probably interact in a manner where the interaction complex is not just made of two proteins but contain a higher number of each of the proteins. I found that the number of FtsB and FtsL molecules in that complex has

to be equal, and thus we think that the way these two proteins interact is that FtsB alone forms a complex with two or more molecules of itself, and then two or more FtsL molecules 'dock' on the FtsB complex to form a higher complex.

Whether this complex is made of two molecules of each protein or a higher number of molecules of each protein, is still unknown. But what we gather from this piece of information is that during the process of cell division in bacteria, these two proteins form a big interacting complex. We also know from previous research that other proteins needed for cell-division interact separately with FtsB and FtsL. Thus we think that by forming a big FtsB-FtsL complex, these two proteins bring other cell-division proteins together in the membrane and facilitate cell division.

Membrane proteins are hard to study because maintaining them in their native state and designing artificial cell membrane-like media to keep them 'happy and healthy' is quite a challenge. Information on the FtsB-FtsL complex is only one piece of the puzzle as to how cell-division in bacteria works, but it is the first piece of information on the interaction characteristics of the membrane components of these proteins, and is a start! As a research group, we continue to work on the different components of all these proteins separately. Using various techniques and approaches, we aim to slowly put the pieces of the puzzle together toward the bigger goal of understanding how bacteria divide and multiply, so that they can be manipulated in order to tackle the ever growing medical problems of bacterial infections and antibiotic resistance.